

Some pages of this thesis may have been removed for copyright restrictions.

If you have discovered material in Aston Research Explorer which is unlawful e.g. breaches copyright, (either yours or that of a third party) or any other law, including but not limited to those relating to patent, trademark, confidentiality, data protection, obscenity, defamation, libel, then please read our [Takedown policy](#) and contact the service immediately (openaccess@aston.ac.uk)

Investigation of Metabolic Dysfunction in Alzheimer's Patient
iPSC-derived Neuron and Astrocytic Cells

Sarah Y A S Al-Qattan
Doctor of Philosophy

Aston University
October 2019

©Sarah Y A S Al-Qattan, 2019

Sarah Y A S Al-Qattan asserts her moral right to be identified as the
author of this thesis

This copy of the thesis has been supplied on condition that anyone who consults it is understood to recognise that its copyright belongs to its author and that no quotation from the thesis and no information derived from it may be published without appropriate permission or acknowledgement.

Aston University

Investigation of Metabolic Dysfunction in Alzheimer's Patient iPSC-derived
Neuron and Astrocytic Cells

Sarah Y A S Al-Qattan

Doctor of Philosophy

October 2019

Thesis Summary

Alzheimer's disease (AD) is the most common cause of dementia, affecting an estimated 44 million people worldwide. Currently, there are no methods available for the definitive diagnosis or treatment of AD before the onset of the overt clinical features of the disease. AD is associated with the formation of amyloid plaques and NFTs formed as a result of the accumulation of A β and abnormally folded tau proteins. Metabolic dysfunction has been recognised as a preclinical pathogenic event preceding obvious clinical onset of AD by decades. The aim of this project was to determine if metabolic dysfunction correlates with exposure to A β peptides. Our hypothesis is that early metabolic dysfunction occurs in AD before the onset of symptoms, and is related to excessive production of toxic A β species. Neurons and astrocytes were differentiated from hiPSC-derived NPCs; 'healthy' and familial AD (fAD) patients. 'Healthy' cells were exposed to synthetic A β 1-42 oligomers and then glucose uptake and glycogen storage was determined. Exposure to synthetic A β 1-42 induced a significant reduction in glucose uptake in 'healthy' hiPSC-derived astrocytes and neurons as well as primary human astrocytes (HA). A significant reduction in glycogen storage was also recorded for the 'healthy' hiPSC-derived astrocytes, but not in HA. To determine if neurons and astrocytes from fAD patient-derived hiPSC demonstrated metabolic dysfunction, glucose uptake and glycogen storage was determined in these cells. Human fAD patient iPSC-derived astrocytes and neurons demonstrated increased A β production compared to 'healthy' controls. These cultures also demonstrated reduced glucose uptake. However, the conditioned media from the fAD cultures failed to induce metabolic dysfunction in 'healthy' control cells. These results provide evidence of early metabolic dysfunction in human fAD, and provide an important step in understanding the role of A β early in the progression of AD.

Keywords: Alzheimer's disease, Amyloid, iPSCs, Neurons, Astrocytes, Metabolism.

Acknowledgment

In the Name of God, the Most Gracious and the Most Merciful. All praises to God and all thanks to God. There is no power nor strength except with God. All praise be to God for the countless bounties bestowed upon me in life and glory be to God for giving me the opportunity to complete this thesis through these bounties.

I would like to acknowledge and give thanks to the humanitarian leader His Highness Sheikh Sabah Al-Ahmad Al-Jaber Al-Sabah, Amir of the State of Kuwait. I would like to thank my country Kuwait (a special mention to Ministry of Health) for allowing me this opportunity, I am very grateful and honoured for the scholarship.

I must make a special mention to my Mother. My Mother who is my everything. I do not even know where to begin, words cannot express how much she means to me or do justice to her status, and I could never repay my Mother. All the love, patience, support, prayers, tears and sacrifices she has made, I am where I am today because of her. 'My Lord! Bestow on them Your Mercy, as they did bring me up when I was small' (17:24).

I would also like to show appreciation to my family and friends without whom I would not have been able to complete my PhD. Their continuous support and encouragement throughout the journey has made my experience easier and more beautiful. My sisters often visiting me; supporting me and inspiring me, they are my best friends. And my brothers, always trusting me and reassuring me, they are my strength. My family has been with me every step of the way.

I would also like to express my sincere gratitude to my supervisor Dr Eric Hill for the continuous support of my PhD study and related research. I thank him for his patience, motivation, and vast knowledge. His supervision and guidance helped me in all the time of research and writing of this thesis. I could not have imagined having a better advisor and mentor for my PhD study. I would also like to mention a thanks to my associate supervisor Dr James Brown.

Finally, I would like to mention a little about myself. I would never have thought I would be capable of completing a PhD. I always knew it would be very difficult as it required a lot of sacrifice and hard work. I had to leave home for a new country, leave behind my family and friends, learn to live on my own and adapt to a new life and unknown surroundings. This all has not been easy and I have had many moments in this journey where I have thought about giving up, leaving everything behind and just going home. I can now look back and be very proud that I have endured all of this and that I never gave up, I have achieved and completed my PhD, even though it cause me to have many grey hair.

Shukran Jazeelan. Thank you.

Table of Contents

Title Page	1
Thesis Summary.....	2
Acknowledgment	3
Table of Contents	5
List of Figures.....	12
List of Tables.....	15
Abbreviations.....	16
Chapter 1: Introduction	19
1.1 The Overview and Prevalence of Alzheimer’s Disease.....	19
1.2 History of AD.....	19
1.3 Symptoms of AD	20
1.4 Epidemiology and Risk Factors	22
1.5 Clinical Variants.....	22
1.6 Genetics of AD	23
1.7 Aetiology and Pathogenesis of AD	24
1.7.1 Tau Hypothesis	24
1.7.2 Amyloid Cascade Hypothesis	25
1.7.2.1 Amyloid Processing	26
1.7.2.2 The Role of A β	29
1.7.2.3 Links between the Amyloid Hypothesis and Tau Pathology	30
1.8 Therapeutic Targets	31
1.9 Hypometabolism in AD	33
1.9.1 Mitochondrial Dysfunction in AD.....	39
1.9.2 Dysregulation of Insulin Signalling	39
1.10 Human Brain	40
1.11 Neurons and Astrocytes.....	41
1.12 Normal Brain Energy ‘Metabolism’	41

1.13 Studying AD: The Models	44
1.14 Human iPSCs.....	45
1.14.1 Generation and Differentiation of Human iPSC-derived Neuronal and Astrocytic Cells	45
1.14.2 Human iPSC Models of AD.....	47
1.14.3 Characterisation of Neural Lineage Cells	48
1.15 Hypothesis	51
Chapter 2: Characteristic of Healthy Human iPSC-derived NPCs Cell Line.....	52
2.1 Introduction.....	52
2.1.1 Astrocyte Metabolism	53
2.1.2 Astrocytic Differentiation of Human iPSCs	54
2.1.3 Neuronal Differentiation of Human iPSCs.....	55
2.1.4 Aims and Objectives of the Study	57
2.2 Materials and Methods	58
2.2.1 Expansion of 'Healthy' Control Human iPSC-derived NPCs.....	58
2.2.2 Generation and Characterisation of Human Brain Neural Lineage Cells from iPSC-derived NPCs.....	60
2.2.2.1 Spontaneous Neuronal Differentiation Method.....	60
2.2.2.2 Synchronous Neuronal Differentiation Method	60
2.2.2.3 Astrocytic Cells Differentiation and Maturation Methods	63
2.2.2.3.1 Astrocytic Cells Differentiation Method	63
2.2.2.3.2 Astrocytic Cells Maturation Method	63
2.2.3 Cultures and Expansion of Cell Lines and Primary Human Cultures	66
2.2.3.1 Human Primary Astrocytic Cells.....	66
2.2.3.2 C2C12 Cell Line	66
2.2.3.3 SH-SY5Y Cell Line	67
2.2.4 Histochemical Staining Assays.....	67
2.2.4.1 Glycogen Staining.....	67
2.2.4.2 Immunohistochemical Staining.....	68
2.2.4.3 Synaptic Marker Staining	68

2.2.4.4 Co-Staining	69
2.2.5 Microscopes, Images Capture and Slides Storage.....	69
2.2.6 Determination of Glycogen Content Levels	72
2.2.6.1 Samples Preparation	72
2.2.6.2 Glycogen Assay Protocol	72
2.2.7 Glycogen Breakdown Assays	73
2.2.7.1 Astrocytic Cells Cultures Preparation	73
2.2.7.2 Hypoglycaemic Conditions Assay	74
2.2.7.3 Pharmacological Treatment.....	74
2.2.7.4 Glutamate Treatment.....	74
2.2.8 Determination of Protein Levels.....	74
2.2.9 Quantification and Statistical Analysis.....	74
2.3 Results	76
2.3.1 Characterisation and Generation of ‘Healthy’ Human Brain Neural Cells from iPSC-derived NPCs	76
2.3.1.1 Characterisation of ‘Healthy’ Human iPSC-derived NPCs	76
2.3.1.2 Characterisation and Differentiation of ‘Healthy’ Human iPSC-derived NPCs Control Cell Line	76
2.3.1.2.1 Spontaneous Differentiation Method.....	76
2.3.1.2.2 Synchronous Differentiation Method	77
2.3.1.2.3 Characterisation of Human iPSC-derived Astrocytic Cells	77
2.3.2 Characterisation of Human Primary Astrocytic Cells	88
2.3.3 Determination of Glycogen Content Levels	90
2.3.4 Glycogen Breakdown Assays	91
2.3.4.1 Hypoglycaemic Conditions Assay.....	91
2.3.4.2 Pharmacological Treatment	93
2.3.4.3 Glutamate Treatment	95
2.4 Discussion.....	99
2.5 Conclusion	103

Chapter 3: Treatment of Healthy Human iPSC-derived Neurons and Astrocytes and Primary Astrocytes with Synthetic Aβ1-42 Oligomers	104
3.1 Introduction.....	104
3.1.1 Astrocytes	104
3.1.2 Astrocyte-Neuron Metabolic Coupling.....	105
3.1.3 Effects of A β on Metabolism.....	107
3.1.4 Aims and Objectives of the Study	108
3.2 Materials and Methods.....	109
3.2.1 Preparation of Synthetic A β 1-42 Oligomers	109
3.2.2 Electrophoresis Studies.....	109
3.2.2.1 SDS-PAGE Gel Electrophoresis	109
3.2.2.2 Western Blotting	110
3.2.3 Treatment of Human Primary Astrocytes and iPSC-derived Neurons and Astrocytic Cells with Synthetic A β 1-42 Oligomers	111
3.2.4 Cell Viability and Cytotoxicity Studies	111
3.2.4.1 MTT Assay	112
3.2.4.2 Cell Nucleus Count Assay	112
3.2.5 Determination the Effects on Carbohydrate Levels	113
3.2.5.1 Determination the Effects on Glucose Uptake Levels.....	113
3.2.5.2 Determination the Effects on Glycogen Content Levels	113
3.2.6 Cell Lysis	113
3.2.7 Determination of Protein Levels	114
3.2.8 Quantification and Statistical Analysis.....	114
3.3 Results	115
3.3.1 Synthetic A β 1-42 Oligomers Examination.....	115
3.3.2 Electrophoresis Studies	115
3.3.2.1 SDS-PAGE Gel.....	115
3.3.2.2 Western Blotting	115
3.3.3 Cell Viability and Cytotoxicity Studies	117
3.3.3.1 MTT Assay	117

3.3.3.2 Cell Nucleus Count Assay	121
3.3.4 Synthetic A β 1-42 Oligomers Treatment and Effects on Carbohydrate Levels	122
3.3.4.1 Determination the Effects on Glucose Uptake Levels.....	122
3.3.4.2 Determination of Effects on Glycogen Content Levels	125
3.4 Discussion.....	126
3.5 Conclusion.....	130
Chapter 4: Characteristic of Human Familial AD patient Cell Line and Aβ Release ...	131
4.1 Introduction.....	131
4.1.1 Familial AD	131
4.1.2 Genetic Mutations in fAD	131
4.1.3 Presenilin Proteins.....	132
4.1.4 A β	133
4.1.5 The Role of Astrocytes in A β Release.....	134
4.1.6 Aims and Objectives	135
4.2 Materials and Methods	136
4.2.1 Generation and Characterisation of Human fAD Patient iPSC-derived NPCs	136
4.2.1.1 Neural Cells Differentiation Methods.....	136
4.2.2 ICC Staining	137
4.2.3 Microscopes, Images Capture and Slides Storage.....	137
4.2.4 Characterisation of Amyloid Release Profile	137
4.2.4.1 Sample Preparation	137
4.2.4.2 Collection of Conditioned Medium.....	137
4.2.4.3 Enzyme-linked Immunoabsorbant Assay (ELISA).....	138
4.2.5 Determination of Carbohydrate Levels.....	138
4.2.5.1 Determination of Glucose Uptake Levels	138
4.2.5.2 Determination of Glycogen Content Levels.....	138
4.2.6 Cell Lysis	139
4.2.7 Determination of Protein Levels	139
4.2.8 Quantification and Statistical Analysis.....	139

4.3 Results	140
4.3.1 Generation and Differentiation of Human Brain Neural Lineage Cells from fAD Patient iPSCs-derived NPCs	140
4.3.2 Characterisation of A β Profile Release from fAD Patient-derived iPSCs Using ELISA Analysis.....	149
4.3.3 Determination of Carbohydrate Levels	154
4.3.3.1 Determination of Glucose Uptake Levels	154
4.3.3.2 Determination of Glycogen Content Levels	157
4.4 Discussion	158
4.4.1 Differentiation of fAD Patient-derived hiPSCs to Neurons and Astrocytes.....	158
4.4.2 A β Production by fAD Patient hiPSC-derived Neurons and Astrocytes	159
4.4.3 Metabolic Dysfunction in fAD Patient-derived Neurons and Astrocytes.....	160
4.5 Conclusion.....	162
Chapter 5: Optimising Production of Human Aβ Derived from fAD Patient iPSCs	163
5.1 Introduction.....	163
5.2 Materials and Methods	164
5.2.1 Preparation of Concentrated Secretomes (Amicons-Concentration)	164
5.2.2 Immunodepletion Assay.....	164
5.2.3 ELISA Analysis	165
5.2.4 Electrophoresis Studies	165
5.2.4.1 SDS-PAGE Gel.....	165
5.2.4.2 Western Blotting Analysis	165
5.2.5 Treatment with Human fAD Patient-derived A β and Determination the Effects on Carbohydrate Levels	167
5.2.5.1 Preparation of Treatment	167
5.2.5.2 Determination the Effects on Glucose Uptake Level	167
5.2.5.3 Determination the Effects on Glycogen Content Levels	167
5.2.6 Determination of Protein Levels	167
5.2.7 Quantification and Statistical Analysis.....	168
5.3 Results	169

5.3.1 Immunodepletion Experiment	169
5.3.2 SDS-PAGE Gel Electrophoresis	169
5.3.3 Western Blotting Analysis	170
5.3.4 ELISA Analysis	170
5.3.5 Treatment of Healthy hiPSC-derived Astrocytic Cells with fAD Patient-derived Secretomes and Effects on Carbohydrate Levels	172
5.3.5.1 Determination the Effects on Glucose Uptake Levels.....	172
5.3.5.2 Determination the Effects on Glycogen Content Levels	173
5.4 Discussion	174
Chapter 6: Final Conclusions and Future Directions	175
6.1 Final Conclusions	175
6.2 Future Directions	178
6.2.1 Neural Induction Method.....	178
6.2.2 2D vs 3D Culture	180
List of References.....	182
Appendices.....	213

List of Figures

Figure 1.1 Healthy human brain and Alzheimer's disease patient brain	21
Figure 1.2 APP processing	28
Figure 1.3 FDG-PET image demonstrates brain cerebral hypometabolism.....	35
Figure 1.4 The effects of A β on key enzymes involved in energy metabolism	38
Figure 1.5 Transport and utilisation of glucose by brain cells	43
Figure 1.6 Generation of various brain cell types from hiPSC	49
Figure 1.7 Effects of A β on brain cells metabolism	50
Figure 2.1 Differentiation of cortical neuronal cells from hiPSC-derived NPCs.....	62
Figure 2.2 Differentiation and maturation of astrocytes from hiPSC-derived NPCs	65
Figure 2.3 Chemical equation of glycogen	73
Figure 2.4 hiPSC-Derived NPCs from 'healthy' cell line	79
Figure 2.5 Development of neural cells from 'healthy' hiPSC-derived NPCs at day 10	80
Figure 2.6 Development of neural cells from 'healthy' hiPSC-derived NPCs at day 20	81
Figure 2.7 Development of neural cells from 'healthy' hiPSC-derived NPCs at day 30	82
Figure 2.8 Development of neural cells from 'healthy' hiPSC-derived NPCs at day 40	83
Figure 2.9 Synaptic markers of hiPSC-derived neural cells at day 30	84
Figure 2.10 Synaptic markers of hiPSC-derived neural cells at day 40	84
Figure 2.11 hiPSC-derived astrocytic progenitor from line ax0018.....	85
Figure 2.12 hiPSC-derived astrocytic cells from line ax0018	86
Figure 2.13 Presence of glycogen in hiPSC-derived astrocytic cells from line ax0018	87
Figure 2.14 Human primary astrocyte cells.....	89
Figure 2.15 Determination of glycogen content level of different cell lines	90
Figure 2.16 Glycogen breakdown in astrocytic cells: hypoglycaemia	92
Figure 2.17 Glycogen breakdown in astrocytic cells: using dbcAMP and Isoproterenol ...	94
Figure 2.18 Glycogen breakdown in astrocytic cells: using Glutamate and Ouabain.....	96
Figure 2.19 Glycogen breakdown in astrocytic cells: using Glutamate and TBOA	97

Figure 2.20 Summary of the development of hiPSC-derived NPCs into neural cells.....	98
Figure 3.1 SDS-PAGE gel and western blotting of synthetic A β 1-42.....	116
Figure 3.2 Cell viability of astrocytes treated with synthetic A β 1-42 oligomers of ax0018-derived astrocytic cells and HA.....	119
Figure 3.3 Cell viability of neural cells treated with synthetic A β 1-42 oligomers for 'healthy' neuronal cells of ax0018 derived from SP and SY differentiation methods	120
Figure 3.4 Quantitation of cell number of live and dead cells using cell nucleus count assay	121
Figure 3.5 Effect of synthetic A β 1-42 treatment on astrocytic cells glucose uptake.....	123
Figure 3.6 Effect of synthetic A β 1-42 treatment on neuronal cells glucose uptake.....	124
Figure 3.7 Effect of synthetic A β 1-42 treatment on astrocytic glycogen content levels...	125
Figure 4.1 hiPSC-Derived NPCs from fAD cell line	142
Figure 4.2 Development of neural cells from fAD hiPSC-derived NPCs at day 10	143
Figure 4.3 Development of neural cells from fAD hiPSC-derived NPCs at day 20	144
Figure 4.4 Development of neural cells from fAD hiPSC-derived NPCs at day 30	145
Figure 4.5 Development of neural cells from fAD hiPSC-derived NPCs at day 40	146
Figure 4.6 Synaptic markers of fAD patient hiPSC-derived neural cells	147
Figure 4.7 hiPSC-derived astrocytic cells from fAD patient	148
Figure 4.8 Quantification of total A β peptides secretion of neuronal cells derived from fAD patient and 'healthy' control	151
Figure 4.9 Quantification of A β peptide secretion of neuronal cells from spontaneous and synchronous differentiation methods	152
Figure 4.10 Quantification of A β peptide profile released from astrocytic cells.....	153
Figure 4.11 Glucose uptake by fAD patient and 'healthy' control neuronal cells.....	155
Figure 4.12 Glucose uptake by fAD patient and 'healthy' control astrocytic cells	156
Figure 4.13 Glycogen content level of fAD patient and 'healthy' control astrocytic cells.	157
Figure 5.1 Diagrammatic overview of concentrated CM preparation	166
Figure 5.2 SDS-PAGE gel of concentrated secretomes from CM	169
Figure 5.3 Western blotting of concentrated secretomes from CM.....	170
Figure 5.4 A β prolife in the concentrated secretomes and immunodepleted samples	171

Figure 5.5 Effects of fAD-derived concentrated secretome treatment on astrocytic glucose uptake	172
Figure 5.6 Effect of fAD-derived concentrated secretome treatment on astrocytic glycogen content levels	173

List of Tables

Table 2.1 Description of 'healthy' hiPSC-derived NPCs cell line	59
Table 2.2 List of antibody markers for ICC staining.....	70
Table 4.1 Description of fAD patient hiPSC-derived NPCs cell line.....	136

Abbreviations

AD	Alzheimer's disease
ADM	Astrocyte differentiation medium
AKt	Serine/threonine-specific protein kinas
AM	Astrocyte medium
AMG	Amyloglucosidase enzyme
AMM	Astrocyte maturation medium
ANLS	Astrocyte-neuron lactate shuttle
APOE4	Apolipoprotein E 4
APP	Amyloid precursor protein
ATP	Adenosine triphosphate
A β	Beta amyloid
BACE1	Beta-secretase 1
BACE1	β -site APP cleaving enzyme-1
BCA	Bicinchoninic acid
BMP	Bone morphogenetic protein
BMP	Bone Morphogenetic Protein
BSA	Bovine serum albumin
CM	Conditioned medium
CNS	Central nervous system
CSF	Cerebrospinal fluid
CTNF	Ciliary neurotrophic factor
DAB	1,4-dideoxy-1,4-imino-d-arabinitol
DAPT	Gamma-secretase inhibitor
dbcAMP	Dibutyl cyclic adenosine monophosphate
DLL1	Delta like canonical notch ligand 1
DMEM	Dulbecco's modified eagle's medium
DMSO	Dimethyl sulfoxide
D-PBS	Dulbecco's phosphate buffered saline
Drp1	Dynamin-1-like protein
ELISA	Enzyme-linked immunosorbent assay
fAD	Familial Alzheimer's disease
FDG-PET	Fluorodeoxyglucose positron emission tomography
FGF	Fibroblast growth factor
FGF8	Fibroblast growth factor 8

Fis1	Fission mitochondrial 1
GABA	Gamma-amino butyric acid
GFAP	Glial fibrillary acidic protein
GLP-1	Glucagon-like peptide-1
GLUT	Glucose transporter
GSK-3	Glycogen synthase kinase 3
GSMs	γ -Secretase modulators
HES1	Hes Family BHLH Transcription Factor 1
hiPSC	Human Induced pluripotent stem cells
HK	Hexokinase enzyme
ICC	Immunocytochemistry staining
IGF-1	Insulin agonists insulin-like growth factor-1
IL-6	Interleukin 6 cytokine
JAK/STAT	Janus kinase/signal transducer and activator of transcription
JNK	C-Jun N-terminal kinase
KDGH	α -keto-glutarate dehydrogenase
Klf4	Krüppel-like factor 4
KRH	Krebs'–Ringer HEPES buffer
LDH	Lactate dehydrogenase
LTP	Long-term potentiation
MAP2	Microtubule-associated proteins 2
MAPK	Mitogen-activated protein kinase
MCT	Monocarboxylate transporter
NAD+	Nicotinamide adenine dinucleotide
NADH	Nicotinamide adenine dinucleotide
NFTs	Neurofibrillary tangles
NMDA	N-methyl-D-aspartate receptor
NMR	Nuclear magnetic resonance analysis
NPCs	Neural progenitor/precursor cells
NSAIDs	Non-steroidal anti-inflammatory drugs
Oct4	Octamer-binding transcription factor 4
PAS	Periodic Acid-Schiff
Pax6	Paired box protein 6
PDHC	Pyruvate dehydrogenase complex
PFA	Paraformaldehyde
PI3K	Phosphoinositide-3-kinase
PI3K-AKT	Phosphatidylinositol-3-kinase and protein kinase B

PLO	Poly-L-Orinthine
PSEN1	Presenilin 1
PSEN2	Presenilin 2
RA	Retinoic acid
RIPA	Radioimmunoprecipitation assay
ROCK	Rho associated protein Kinase inhibitor
ROS	Reactive oxygen species
S100 β	S100 Calcium Binding Protein β
sAD	Sporadic Alzheimer's disease
sAPP α	Soluble amyloid precursor protein alpha
SDS-PAGE	Sodium dodecyl sulfate polyacrylamide gel electrophoresis
SHH	Sonic Hedgehog signalling molecule
Sox2	(sex determining region Y)-box 2
SP	Spontaneous differentiation method
SY	Synchronous differentiation method
TBOA	DL-threo- β -Benzyloxyaspartic acid
TBS	Tris-buffered saline
TCA	Tricarboxylic acid cycle
TEMED	Tetramethylethylene-diamine
TM-2	Transmembrane domain 2
TNF α	Tumour necrosis factor alpha
TUJ1	Neuron-specific Class III β -tubulin
VEGF	Vascular endothelial growth factor

Chapter 1: Introduction

1.1 The Overview and Prevalence of Alzheimer's Disease

Alzheimer's disease (AD) is the most common cause of dementia worldwide. It is a chronic neurodegenerative disease characterised by a gradual degeneration of neurons in the brain due to a combination of genetic factors and environmental factors related to lifestyle and diet. The disease presents mainly with behavioural changes, manifesting as confusion, decline in memory, mental capacity, challenging behaviours and social withdrawal over time. It has significant effects on the quality of life of affected individuals, and often affects their ability to perform usual activities of daily living like personal care, meal preparations and shopping.

AD is the most common cause of dementia, affecting an estimated 44 million people worldwide and being responsible for 60 - 70% of cases of dementia (World Health Organization, 2015). It presents with anterograde amnesia (loss of recent memory and inability to retain new information) in the early stages, and progresses to retrograde amnesia (long-term memory loss) as the disease advances, presenting as inability to recognise long term relatives and family. Increasing age is a well-known risk factor associated with the disease, however, it can also occur in younger individuals.

1.2 History of AD

The name 'Alzheimer's disease' was described as an eponym in a textbook written by Kraepelin in 1910 (Hoff and Hippus, 1989). The disease was named after Alois Alzheimer, who first described the pathological hallmarks of the disease (neurofibrillary tangles and amyloid plaques) in 1907, after performing an autopsy on a 55 years old woman who had severe progressive behavioural and cognitive changes prior to her death. He presented the disease at a meeting of Southwest German Psychiatrists in Tübingen in 1906, and published a short paper in 1907 and a more detailed one in 1911 (Alzheimer, 1907). Prior to her death, the patient named Auguste Deter, had severe cognitive deficits characterised by unpredictable and unusual behaviours, confusion, delusions, and aphasia. He noted on the autopsy that the woman had a severe atrophy of her brain cortex and internal components. He later described neuritic plaques in the cortex, which were made up of collections of dystrophic neuronal processes surrounding a special substance. He named these neuritic plaques miliary foci (Alzheimer *et al.*, 1995). The 'special substance' was isolated in 1984 as oligopeptides

containing mostly 40 or 42 amino acids (Glennner and Wong, 1984). These oligopeptides are now known as amyloid beta peptides ($A\beta$), while the miliary foci are now known as amyloid plaques. He also described the presence of intracellular aggregates which he named neurofibrillary tangles. These lesions are now known to be composed of aggregates of hyperphosphorylated tau protein. Since the observations made by Alzheimer and his colleagues in the early twentieth century, very little progress was made in gaining a better understanding into the natural history of the disease for several decades, until 1968 when a direct relationship was established, linking the existence of amyloid plaques with the occurrence of dementia (Blessed *et al.*, 1968).

1.3 Symptoms of AD

AD patients experience different symptoms depending on the stage of the disease, as well as other lifestyle factors that may influence each individual. The disease usually spans over several years to decades, and the symptoms are often become progressively worse with time, although the rate of progression differs with each individual. It often presents in the early stages as confusing behaviours manifesting as a result of memory loss. For example, asking for a meal just after just having eaten, or not remembering an appointment that was recently organised. As the disease progresses, more symptoms occur, including reduction in problem-solving capabilities, communication, incontinence and increased frequency of physical health problems (Aarsland *et al.*, 1996). At later stages, there are severe limitations to normal bodily functions like walking and swallowing leading to the affected individual being bed-bound, completely withdrawn socially and unable to care for themselves in the terminal stages. At these stages, there is severe generalised atrophy of the brain due to extensive neuronal and brain mass loss (Fig. 1.1).

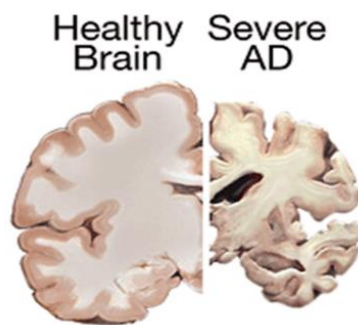


Figure 1.1: Representative diagrammatic overview of AD patient brain (right) with neural cell loss leading to shrinkage in the AD brain compared to healthy human brain (left). Obtained from National Institute of Aging (NIA) website.

1.4 Epidemiology and Risk Factors

About 767,000 people were affected by dementia in the UK in 2016 (Ahmadi-Abhari *et al.*, 2017), and it was reported to cost the UK economy about £24.2 billion yearly as at 2015. The vast majority of this cost (83%) was attributed to the cost of physical care, while healthcare costs accounted for the remainder (Wittenberg *et al.*, 2019). Higher costs were reported for those with moderate and severe dementia, rising from £24,400 for mild dementia to £46,050 for severe dementia. The number of individuals affected by dementia in England and Wales is expected to rise up to 1.9 million by 2040 (Ahmadi-Abhari *et al.*, 2017). AD, is the most common cause of dementia, affecting 5.4% of the population and commonly occurs in people over 65 years (Ferri *et al.*, 2005, Ferri *et al.*, 2010). The most prominent risk factor is increasing age, with the highest risk around 80 years (Di Carlo *et al.*, 2002, Bermejo-Pareja *et al.*, 2008). More women than men are affected by the disease (Di Carlo *et al.*, 2002), with a incidence of 14.3 and 17.0 per 1000 person years in men and 17.0 per 1000 person years in women aged 50 or more as at 2010. It affects Caucasians more than other races (Burns and Iliffe, 2009). Other risk factors include family history, head injury, genetic predisposition (Ward *et al.*, 2012), as well as vascular and metabolic disorders like hypertension, diabetes, coronary heart disease, dyslipidaemias, obesity, atherosclerosis and smoking (Burns and Iliffe, 2009, Blennow *et al.*, 2006). With an increasing elderly population, the prevalence of AD is expected to double every 20 years with an estimated 81 million people to be affected by dementia worldwide by 2040 (Ferri *et al.*, 2010).

1.5 Clinical Variants

There are two clinical subtypes of AD. Early-onset AD is an uncommon form of the disease which occurs before the age of 65 years. It accounts for about 4% of AD cases (Prince *et al.*, 2014) and is linked to mutations in key genes. It is caused by mutations in presenilin 1 (PSEN1), presenilin 2 (PSEN2) and amyloid precursor protein (APP) genes, that represent key proteins in A β protein metabolism (Blennow *et al.*, 2006). PSEN1 and PSEN2 mutations are the most commonly found mutations, and they present at around 50 years of age (Prince *et al.*, 2014). These are the most aggressive forms of the disease, leading to death of most patients in their 60s. PSEN1 and PSEN2 are core components of the presenilin complex, a group of transmembrane proteins which are important in the regulation of several cellular enzymes. They regulate the proteolytic activities of the gamma and beta secretase enzymes, which are responsible for the production of A β from APP.

The sporadic form of the disease is more common, with no currently identified cause. It is believed to have a multifactorial origin involving increasing age, environmental and genetic factors (Blennow *et al.*, 2006). The major genetic factor associated with the sporadic form is the presence of the apolipoprotein E ϵ 4 (APOE4) allele, with a higher risk in the homozygous state. Despite the association of APOE4 with the sporadic form of AD, it has been difficult to determine the mechanism by which it promotes disease formation. The normal function of APOE is as a brain cholesterol transporter and is important in maintenance of membrane integrity and neuronal function. APOE4 is defective at cholesterol transport, and its presence may result in a reduced repair capability in the neuron (Blennow *et al.*, 2006). However, the normal APOE promotes A β accumulation and plaque formation (Holtzman *et al.*, 2000), making it difficult to identify a clear mechanism of involvement in the disease process. In addition, meta-analyses of genome-wide association studies have revealed 22 genetic susceptibility foci for late-onset AD (Lambert *et al.*, 2013, Seshadri *et al.*, 2010).

1.6 Genetics of AD

AD is a disease with very strong genetic links; the familial form of the disease, although rare, is caused by genetic mutations that can be passed down generations in an autosomal dominant fashion. The sporadic form of the disease, although with less strong familial tendencies, is also characterised by the presence of the APOE4 allele which can also be passed down generations, increasing the risk of progeny developing the disease. While APOE4 has been the traditionally recognised genetic link with sporadic AD, recent studies have revealed other significant genetic loci that play important roles in the pathogenesis of sporadic AD, especially those with a high predilection for microglia (Efthymiou and Goate, 2017, Dos Santos *et al.*, 2017). Genome-wide studies (GWAS) have identified a particularly important genetic variant which exerts a significant role in AD pathogenesis (Benitez and Cruchaga, 2013, Guerreiro *et al.*, 2013). This triggering receptor expressed on myeloid cells-2 (TREM2) is a rare gene variant which has a high expression in the microglia, and exerts important effects on microglial function, metabolism and survival (Benitez and Cruchaga, 2013, Guerreiro *et al.*, 2013). TREM2 is believed to exert influence of microglial metabolism and survival through inhibition of apoptosis by activating the p13K/AKTmTOR pathway which leads to increased cellular energy generation, and by activating the Wnt/b-catenin signalling, which then facilitates proliferation of microglia (Reviewed in Zheng *et al.*, 2018). The PSEN1, PSEN2 and APP genes are the hallmarks of familial AD (fAD). Genetic mutations associated with the familial form of the disease affect either APP itself or enzymes involved in the processing of amyloid such as PSEN1 and PSEN2, result in increased A β production and

aggregation (Bertram and Tanzi, 2008).

The strong genetic links of AD is also expressed in patients with Down syndrome, who are known to start accumulating A β plaques and neurofibrillary tangles (NFTs) from as early as 8 years of age (Leverenz and Raskind, 1998), and have established pathologic features of AD by the age of 40 (Mann and Esiri, 1989). The strong association between AD and Down's syndrome is likely explained by the fact that the APP gene is located on chromosome 21, the chromosome that is in excess in people with Down syndrome. The prevalence of AD in Down syndrome patients above 50 years of age is estimated at 4 - 55% (Head *et al.*, 2012), and 15 - 77% over the age of 60 (Prasher and Filer, 1995, Zigman *et al.*, 1996).

1.7 Aetiology and Pathogenesis of AD

Despite years of research and progress in the understanding of AD, its aetiology remains unknown. Several hypotheses have been postulated on the origin of the disease and how the disease progresses. The inter-relationship of these different pathologic courses remains a focus of discourse amongst researchers. The two most prominent hypotheses are the amyloid hypothesis and the tau hypothesis. These are based on the two pathological hallmarks of the disease: amyloid aggregates and NFTs.

1.7.1 Tau Hypothesis

The 'tau hypothesis' suggests that the occurrence of dementia in AD patients is due to the presence of neurofibrillary tangles, which are aggregates of abnormally hyperphosphorylated tau protein. Tau protein is a cytoskeletal (microtubule) stabilising protein. Its normal function is to support anterograde axonal transport in neurons (Santa-Maria *et al.*, 2007). In AD, it becomes hyperphosphorylated due to abnormal metabolism, causing it to aggregate and polymerise, resulting in the formation of neurofibrillary tangles and disruption of the neuronal microtubular transport mechanisms. Abnormal tau deposition has been reported to be spatially divided into six stages depending on the location of the brain in which deposition is detectable temporally. These stages are known as the Braak staging first developed in 1991 (Braak and Braak, 1991), and the modified Braak staging (Braak *et al.*, 2006). The first stage of tau deposition was reported to begin in the entorhinal and transentorhinal cortex which are responsible for memory formation, time perception and spatial orientation (Solodkin *et al.*,

2014). At stage 2, tau deposition becomes detectable in the hippocampus which also plays a major role in learning and memory (Solodkin *et al.*, 2014). The third and fourth stages involve tau deposition in the temporal cortex before spreading to the other cortical regions at stage four. The fifth and sixth stages involve deposition in the visual association and primary visual cortex respectively (Braak *et al.*, 2006).

The cause of abnormal tau formation is not clear, but it has been suggested that abnormal tau formation may be induced by the presence of A β deposits or toxic A β oligomers, providing a link between the amyloid and the tau hypotheses. However, this relationship remains controversial, as other studies have found temporal and spatial differences in the occurrence of A β peptides and plaques, as well as tau and tangle formation (Mudher and Lovestone, 2002). However, the fact that tau mutations do not result in AD (Houlden *et al.*, 1999) gives more credence to the amyloid hypothesis. Indeed, tau protein mutations lead to clinically different neurodegenerative disorders like progressive supranuclear palsy and frontotemporal dementia (Ballatore, Lee and Trojanowski, 2007). Furthermore, there is evidence that the spread of AD in the brain may be due to the prion-like property to tau (Holmes *et al.*, 2014).

1.7.2 Amyloid Cascade Hypothesis

The amyloid hypothesis states that the formation of amyloid plaques is the central pathogenic event of the disease (Hardy and Allsop, 1991). Amyloid plaques are made up of A β peptides. These 39 - 43 amino acid peptides are formed as a result of abnormal sequential proteolytic cleavage of APP. APP is a transmembrane protein important for neuronal growth and survival. Amyloidogenic processing of APP by β - and γ -secretase generates A β peptides containing 36 - 43 amino acids, of which A β 1-40 and A β 1-42 (containing 40 and 42 amino acids, respectively) are the most common. Non-amyloidogenic processing of APP by γ - and α -secretase cleaves within the APP sequence, precluding A β production, and generating a large soluble ectodomain of APP called sAPP α (Figure 1.2). Interestingly, sAPP α has opposing actions to A β , promoting neuronal plasticity and survival as well as protection against neurotoxicity, thus preventing the occurrence of AD (Furukawa *et al.*, 1996, Mattson, 1997). The sAPP α has also been shown to play important roles in neural stem cell proliferation and central nervous system (CNS) differentiation (Ohsawa *et al.*, 1999, Caille *et al.*, 2004). Jonsson *et al.* (2012) reported that a rare APP gene mutation (A673T) results in a 40% reduction in amyloidogenic processing of APP *in vitro*, and prevents the occurrence of AD, and prevents cognitive decline.

1.7.2.1 Amyloid Processing

The process of Ab generation begins from the processing of the transmembrane APP protein by the β -secretase enzyme (O'Brien and Wong, 2011). The β -secretase enzyme is an aspartyl transmembrane protease which is made up of a β -site APP-cleaving enzyme 1 (BACE1) which is the functional unit of the β -secretase complex, and a homologous protease called BACE2 (Reviewed in Vassar, 2004). Classically, BACE1 cleaves the luminal portion of APP, leaving the C-terminal fragment (CTF β) within the membrane, and releasing the soluble ectodomain (sAPP α). The CTF β then becomes the substrate for the γ -secretase enzyme, which then results in the generation of A β species (Fernandez *et al.*, 2016).

The γ -secretase enzyme is a large integral membrane aspartyl protease complex, which is made up of four intramembrane subunits which include the presenilins as the catalytic components (Edbauer *et al.*, 2003). The other components of the γ -secretase complex include the presenilin enhancer 2 (Pen-2), nicastrin and the anterior pharynx-defective1 (Aph1) (Chiang *et al.*, 2010, Kimberly *et al.*, 2003, Crystal *et al.*, 2003). Pen-2 also has two transmembrane components which has both the carboxyl and amino terminals on the luminal side of the cellular membrane (Crystal *et al.*, 2003). The γ -secretase active site shows a varied substrate cleavage sites, but is sequestered from the hydrophobic membrane side, requiring substrates to first bind to an external component of the complex before gaining access to the active site (Komilova *et al.*, 2005).

Neither the β - nor the γ -secretase show specificity of cleavage sites in their respective substrates (APP or CTF β , respectively). BACE1 cleavage could occur at the Asp+1 residue of the sequence, leading to the classic C99 terminal fragment of A β , or the Glu11 position, leading to the N-terminally truncated form of A β (Sato *et al.*, 2003). The γ -secretase enzyme in turn, cleaves the transmembrane domain (TMD) in successive cleavages, beginning with an endoproteolytic cut at the ϵ -sites (Leu 49 or Thr48), releasing the APP intracellular domain (AICD) and generating A β 48 or A β 49, which is then followed by successive C-terminal cleavages within the membrane at every three residues (ζ and then γ sites) to produce shorter forms of A β which are then secreted (Funamoto *et al.*, 2004, Takami *et al.*, 2009, Fernandez *et al.*, 2016). This leads to two major forms of A β depending on the initial cleavage site (tripeptide hypothesis): A β 49 \rightarrow 46 \rightarrow 43 \rightarrow 40 for Leu49 ϵ -site, and A β 48 \rightarrow 45 \rightarrow 42 \rightarrow 38 for Thr48 ϵ -site initial cleavages respectively (Takami *et al.*, 2009). Mutations in the genes coding for the APP, PSEN1 or PSEN2 all result in altered A β processing and production. For example,

the London mutation (V717I) in the APP gene increases BACE1 activity and alters the γ -secretase active site, leading to increased generation of A β 1-42 and A β 1-38 (Muratore *et al.*, 2014). Similarly PSEN1 mutations, which are the most common genetic causes of fAD, also result in A β species of varying lengths and structure, mostly resulting in C- or N-terminally truncated A β peptides (Sherrington *et al.*, 1995, Cruts *et al.*, 2012). Generally, presenilin gene mutations are believed to reduce C-terminal cleavage activity, leading to accumulation of longer A β fragments (Reviewed in Arber *et al.*, 2019, Chavez-Gutierrez *et al.*, 2012).

Amyloid plaques are made up of β -sheet-rich aggregates of insoluble amyloid oligomers. Soluble oligomers are A β forms which are peptides of varying amino acid lengths, the most common of which is the A β 1-42 (Reviewed in Selkoe and Hardy, 2016). These oligomers remain soluble in aqueous buffer after high speed centrifugation and have been shown to be the most cytotoxic species that are thought to induce neuronal dysfunction early in the disease process (Wang *et al.*, 2002, Lesne *et al.*, 2006).

Amyloid oligomers are believed to induce neurodegeneration by initiating neuronal apoptosis (Turner *et al.*, 2003). These toxic amyloid oligomers are believed to induce apoptosis by disrupting the cell's calcium homeostasis, and causing oxidative stress (Mattson, 2004). Animal studies have shown that the removal of A β through passive immunisation with anti-A β antibodies reduces brain amyloid deposits, and improves cognitive function (Wilcock and Colton, 2008). However, human clinical trials have yielded mixed results, with some trials showing that short term administration of immunoglobulins to AD patients prevented cognitive decline, or improves cognition (Dodel *et al.*, 2004, Relkin *et al.*, 2009). However, other trials produced desirable effects in a small minority of participants, but resulted in immune cell activation, and sterile encephalitis, resulting in abandonment of some studies (Gilman *et al.*, 2005, Orgogozo *et al.*, 2003).

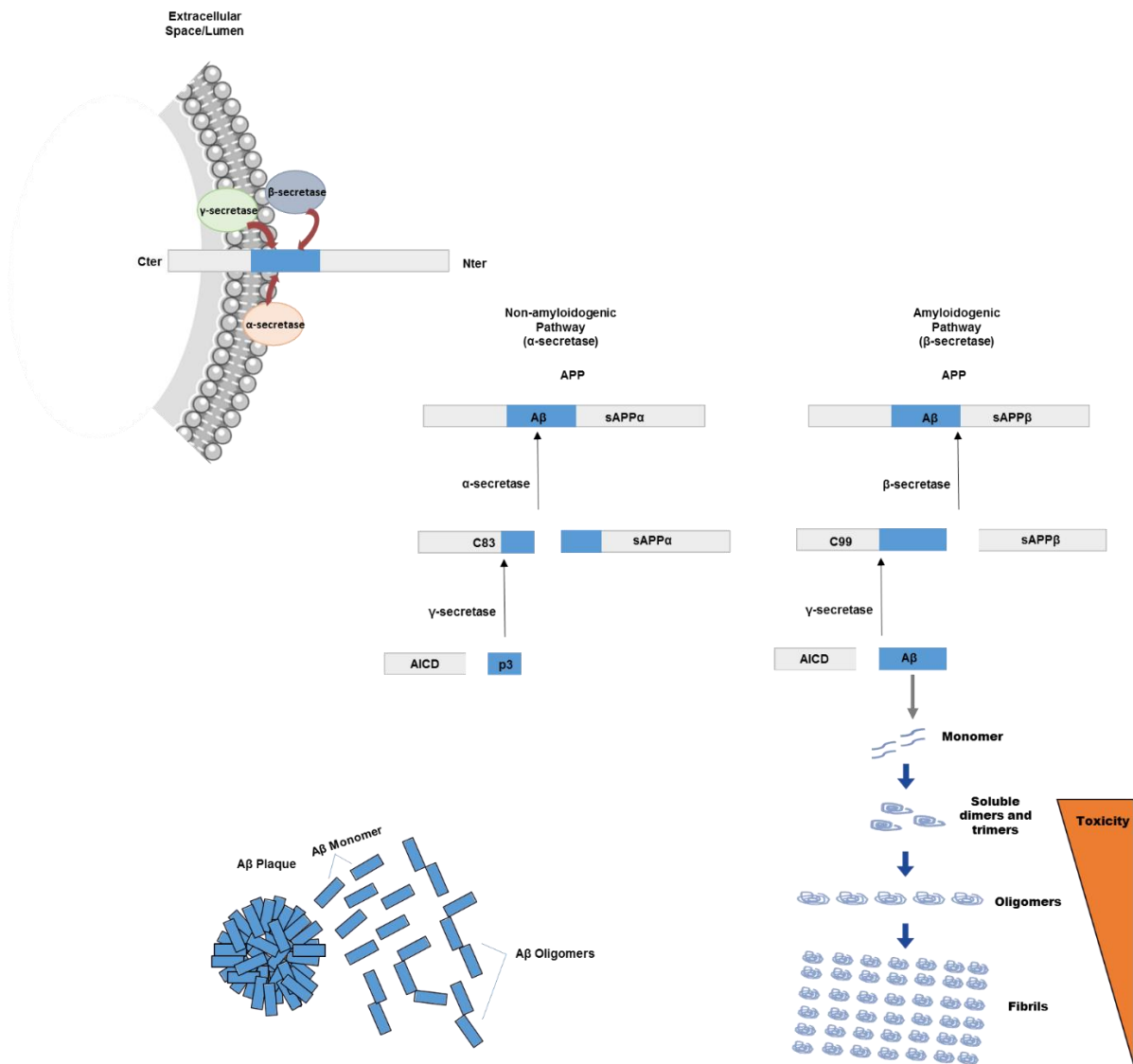


Figure 1.2: Representative diagrammatic presentation of the sequential processing of APP to via the amyloidogenic and non-amyloidogenic pathways to generate Aβ peptides, sAPPα and sAPPβ, respectively. The toxic Aβ exist in multiple assembly states: monomers, oligomers, fibrils and larger amorphous aggregates; Aβ plaque.

1.7.2.2 The Role of A β

It is a well-established fact that amyloid peptides are produced in excessive amounts in the AD brain, with resultant neurotoxic effects. However, A β is produced in small quantities in the normal human brain, especially during synaptic activity, although it produces no adverse clinical events at these concentrations. It has been proposed that because amyloid production in the normal brain is directly influenced by synaptic activity (Cirrito *et al.*, 2003), amyloid peptides could play modulatory roles in synaptic activity (Plant *et al.*, 2003). It has also been suggested that low levels of A β could work as an antioxidant and chelator because of its affinity for free metals like iron, copper and zinc (Atwood *et al.*, 1998). Furthermore, Garcia-Osta and Alberini (2009), showed that at physiological concentrations, soluble amyloid peptides potentiate memory and acquisition of new knowledge. It has thus been suggested that at physiological concentrations, amyloid peptides may play important opposite roles in neuronal growth, synaptic transmission, antioxidant defence and cell survival; giving it opposing roles at physiological and pathological concentrations. The location of accumulation of A β in cells may also be important in the pathogenic process of AD.

A β is generated at multiple cellular sites in neural cells, including the endoplasmic reticulum, the endo-lysosomal and vesicular systems, the Golgi apparatus, mitochondria and cytosol. These are sites where the APP and β - and γ -secretases are present in considerable amounts (LaFerla *et al.*, 2007). There are several isoforms of the A β peptide named based on the number of amino acids in their peptide chains. The most common are the A β 1-40 (90%) and A β 1-42 (10%). A β 1-42 is the most toxic form, most likely to aggregate and is the most abundant form in the fAD (Selkoe, 2000). The higher aggregative property of the A β 1-42 is believed to be due to the presence of two extra hydrophobic amino acids (Kim and Hecht, 2006).

In AD, A β peptides accumulate at cellular locations where they do not exist in normal individuals - the late endosomes and lysosomes. This is believed to be due to oxidative stress-induced activation of autophagy and a resultant lysosomal membrane damage, with release of lysosomal enzymes into the cytosol (Ditaranto *et al.*, 2001). Indeed, Zheng *et al.* (2009) demonstrated that oxidative stress in neuronal cells induces accumulation of A β fibrils and macroautophagy, and is believed to be responsible for progressive disruption of neuronal synaptic transmission, leading to progressive synaptic loss which may be responsible for the cognitive changes observed in AD (Cleary *et al.*, 2005, Townsend *et al.*, 2006).

Furthermore, A β peptides have been shown to accumulate early on before the onset of clinical features in brain cells of affected individuals, with a predilection for the mitochondrial membranes and the synaptic ends (Oddo *et al.*, 2003, Knobloch *et al.*, 2007). Post-mortem examinations of the brains of AD patients showed that the degree of accumulation was positively correlated to age (Gouras *et al.*, 2000). Studies on transgenic mouse lines have produced similar results (Oddo *et al.*, 2003, Manczak *et al.*, 2006).

In contrast to the spatial pattern of tau deposition as described above (section 1.7.1), amyloid deposition is divided into five phases as described by Thal *et al.* (2002). They reported the first phase of amyloid deposition being detectable in the temporal lobe (particularly) and other neocortical areas (frontal, parietal and occipital lobes). At the second phase, amyloid deposition was noted to spread into the allocortical regions (hippocampus, amygdala, olfactory regions and the entorhinal cortex). At phases 3 and 4, the deposition was observable in the subcortical regions (hypothalamus, striatum and other nuclei of the diencephalon), and the brainstem nuclei respectively before reaching the cerebellum at the fifth phase (Thal *et al.*, 2002).

There appears to be a clinicopathological correlation in the temporal pattern of amyloid deposition and the occurrence of clinical symptoms of AD, as problems with the functions of the earliest sites of amyloid deposition correlate with the earliest symptoms of AD, including difficulty with learning new information, difficulties with planning and organisation as well as difficulties with complex tasks are often the earliest symptoms of AD (Albert *et al.*, 2011). The later stages of the disease, characterized by psychiatric symptoms, severe behavioural problems (aggression, disinhibition, incontinence) (Burns, 2009), also correlate with dysfunction of the subcortical regions and the brainstem nuclei. There is also a temporal clinicopathologic correlation with the areas of the brain affected by hypometabolism as described later (section 1.9).

1.7.2.3 Links between the Amyloid Hypothesis and Tau Pathology

Despite the apparent strength and evidence of support for the amyloid hypothesis in the pathogenesis of AD, therapeutic approaches targeting amyloid processing have largely been unsuccessful as highlighted in section 1.8. This has led to increased examination of possible links between the two main hypotheses being the central pathway to the development of the

disease, and the possibly therapeutic strategy that needs to be developed. It has been suggested that increased amyloid generation and deposition could be the trigger and potential facilitator for the pathogenic cascade of AD, while tau would be the main executor of the main pathologic events (Reviewed in Stancu *et al.*, 2014). For example studies on some murine models have shown that downregulation of tau prevented the typical behavioural and cellular neurodegenerative changes in these models (Morris *et al.*, 2011, Roberson *et al.*, 2011, Jin *et al.*, 2011). In vitro studies have revealed A β induction of tau-mediated neurodegeneration, although the signalling mechanisms and the exact A β species responsible are yet to be identified. These were believed to be induced by A β -mediated tau protein kinase/glycogen synthase activation, increased phosphorylation, loss of microtubule binding (De Felice *et al.*, 2008, Ma *et al.*, 2009, Takashima *et al.*, 1993, Robertson *et al.*, 2011). It has also been revealed that at the molecular level, A β fibrils induce tau deposition in mouse neurons and human neuroblastoma cells (Shin *et al.*, 2019). In vitro studies in triple transgenic AD model of mice (APP, PSEN2 and tau) has also shown an age-dependent synergistic induction of mitochondrial dysfunction by tau and A β (Rhein *et al.*, 2009).

Despite developments in our understanding of the pathogenesis of the disease the development of successful new treatments has been lacking.

1.8 Therapeutic Targets

Several therapeutic options have been developed for treatment of AD, but despite several decades of research, no definitive treatment is currently available. Current therapies involve preserving cognitive function and slowing down the progression of cognitive decline. This includes a combination of lifestyle modifications (nutritional changes, stopping smoking, physical activity, etc.) and pharmacological therapeutic agents. These agents include the acetylcholinesterase inhibitors like galantamine, rivastigmine and donepezil which are used for mild to moderate dementia, as well as memantine, an *N*-methyl-D-aspartate receptor antagonist which is used for moderate to severe dementia. However, these agents are unable to reverse any functional deficit loss that has occurred, and are unable to ultimately prevent the progressive decline that occurs in AD (Reviewed in De Strooper *et al.*, 2010).

Because amyloid accumulation is a central pathological event in the pathogenesis of AD, the possibility of blocking amyloid processing and production has been identified as a potential therapeutic target for treatment of AD. Indeed, γ -secretase inhibitors have been developed as

therapeutic agents, and currently have the greatest potential for a therapeutic cure for AD (Hahn *et al.*, 2011). However, severe and extensive toxicity has precluded such therapies reaching fruition. γ -Secretase inhibitors that have been trialled clinically for mild to moderate AD include avagacestat (phase II) and semagacestat (phase III), but these trials were terminated because of a lack of efficacy, and an unexpected worsening of cognitive function as compared to placebo (Coric *et al.*, 2012, Coric *et al.*, 2015, Doody *et al.*, 2013). This lack of efficacy and cognitive deterioration was believed to be due to the diverse important functions of the γ -secretase enzyme which are mediated by Notch signalling and current inability to induce selectivity of potential therapeutic agents to only inhibit amyloidogenic functions of the γ -secretase enzyme at generating toxic amyloid species. This has led to the development of small modulators of the γ -secretase enzyme, called γ -secretase modulators (GSMs) (Weggen *et al.*, 2001). These small molecule modulators are reported to alter γ -secretase function towards generating shorter amyloid peptides that are less toxic and less prone to aggregation. They are also reported to alter the amyloidogenic properties of the γ -secretase enzyme without any significant effects on the Notch signalling activities of the enzyme (Leuchtenberger *et al.*, 2006, Okochi *et al.*, 2006).

The GSMs are currently the most promising chemotherapeutic agents for a definitive treatment of AD. They are members of the non-steroidal anti-inflammatory drugs (NSAIDs). They were discovered following reports of preventive properties of NSAIDs against AD in patients (McGeer *et al.*, 1996, Anthony *et al.*, 2000). They have been reported to decrease A β ₁₋₄₂ levels by as much as 80% (Weggen *et al.*, 2001). These effects are believed to occur independent of cyclo-oxygenase inhibition, and the mechanisms are yet to be fully explained. However, common NSAIDs like ibuprofen and indomethacin are currently unable to produce clinically significant reduction in AD prevalence or progression due to low penetration of the blood brain barrier (BBB) and low potency at current pharmacological levels (Leuchtenberger *et al.*, 2006).

Ongoing clinical trials also include β -secretase 1 (BACE1) inhibitors which aim to also reduce the production of A β by blocking the initial cleavage of APP by BACE1. However, like the γ -secretase inhibitors, this also blocks very important physiological functions, and results in intolerable side effect profiles (Carroll and Li, 2016). Indeed, mouse studies involving BACE inhibition revealed defects in neurogenesis, neuronal network formation, myelination and muscle spindle formation. They also exhibited defective spine formation, pigmentation and impaired pancreatic beta cell function (Esterhazy *et al.*, 2011, Filser *et al.*, 2015, Zhu *et al.*,

2018). Several β -secretase inhibitors have been trialled for clinical use, but there are only two agents currently undergoing phase III clinical trials - Elenbecestat and CNP520, with other trials being terminated mainly due to intolerable side effects (Panza *et al.*, 2019).

Other therapeutic strategies currently being trialled include Anti-A β immunotherapies that aim to induce clearance of A β , one of which is currently undergoing a phase II trial (CAD 106) (Vandenberghe *et al.*, 2016). Previous trials on A β immunotherapies resulted in significant reduction in A β levels, but no significant clinical improvement, and also resulted in potentially catastrophic side effects like meningoencephalitis (Gilman *et al.*, 2005). Tau-targeting therapies have also been trialled, but severe toxicity has led to abandonment of most of these trials (Panza *et al.*, 2019). Cell therapies are also a potential strategy at providing cure for AD, but no cell therapies currently have approval (Alipour *et al.*, 2019). They also have several procedural, mechanistic and ethical hurdles to cross before they can become an acceptable mode of therapy. First, the correct cells have to be produced, and then a method fashioned to incorporate these newly cultured neural cells into the existing neuronal networks in the affected portions of the brains of affected individuals (Fang *et al.*, 2018).

It is clear that most of the therapeutic ventures at definitive management of AD have yielded unsatisfactory results, or very little clinical benefits in the face of potentially severe side effects. This begs a new approach at understanding the pathogenesis of the disease, and at identifying potentially exploitable upstream and downstream therapeutic targets in the development of the overt neurotoxicity that characterises the disease. One such mechanism could involve the downstream metabolic effects of A β in inducing neurotoxicity.

1.9 Hypometabolism in AD

As with other neurodegenerative diseases, hypometabolism is a feature of well-established and advanced AD. However, a number of studies have shown that metabolic dysfunction predates the appearance of recognisable structural changes and cognitive deficits in AD patients by at least a decade (Mosconi *et al.*, 2008b). Small *et al.* (2000) and Silverman *et al.* (2001) have shown that cognitively normal carriers of the APOE4 allele exhibit decreased glucose metabolism. This provides a promising opportunity for early detection, and possible prevention of AD before the onset of the neuropathologic events heralding the disease. Affected neurons in AD patients are known to demonstrate decreased protein synthesis,

reduced glucose uptake and reduced glycogen turnover amongst other metabolic abnormalities (Mosconi *et al.*, 2008a).

The regions of the brain affected by hypometabolism appear to correlate with the corresponding functional deficits seen at different stages of the course of the disease (Fig.1.3). The parieto-temporal regions, responsible for memory and new learning are the first parts of the brain to be affected by hypometabolism, followed by the frontal association areas which are involved with the planning of movements and expression of emotional behaviours (Wolfe *et al.*, 1995). Reduction in glucose uptake is believed to be due to several factors, including mitochondrial toxicity from the accumulation of A β , and results in oxidative stress from the generation of reactive oxygen species (ROS) (Chen and Yan, 2006).

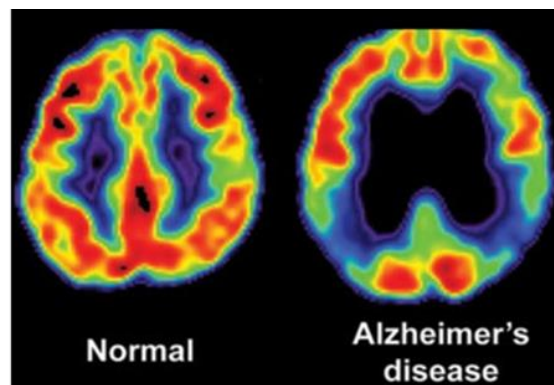


Figure 1.3: Fluorodeoxyglucose-positron emission tomography image (FDG-PET) demonstrating brain cerebral hypometabolism and severe reduction in glucose utilisation in AD patient brain in comparison to normal brain metabolism and utilisation of glucose (Mosconi *et al.*, 2008a and 2008b).

Although they produce very different clinical features in affected patients, AD and diabetes mellitus are characterised by metabolic dysfunction in the brain, and share many pathological similarities including impaired glucose metabolism and insulin resistance (Bomfim *et al.*, 2012, Ozes *et al.*, 2001). Furthermore, patients with diabetes have been shown to have a two-fold increase in risk of developing AD compared to non-diabetic individuals (Ott *et al.*, 1999). This has led some authors to postulate that AD represents a 'type 3 diabetes mellitus' (Steen *et al.*, 2005).

Impaired insulin signalling also appears to play a significant role in the pathogenesis of AD. This is evidenced by positive changes in experiments involving alterations in the insulin signalling pathway. For example, the administration of insulin and glucose has been shown to produce a transient improvement in the memory of AD patients (Craft *et al.*, 2000). In animal models, administration of the insulin agonists insulin-like growth factor-1 (IGF-1) and glucagon-like peptide-1 (GLP-1) causes a reversal of signalling abnormalities and produce positive effects on markers of neurodegeneration (Bomfim *et al.*, 2012, Bassil *et al.*, 2014). IGF-1 is a strong modulator of the phosphatidylinositol-3-kinase and protein kinase B (PI3K-Akt) pathway, which is very important for metabolism and growth, and it is believed that IGF-1 plays a very important role in neurogenesis, neurite outgrowth and synaptic transfer and maintenance of neuronal connections (Hansson *et al.*, 1986, Cheng *et al.*, 2003).

Several key enzymes involved in the Krebs's cycle have been found to be dysfunctional in AD patients (Fig.1.4), including α -keto-glutarate dehydrogenase (KDGH), which is the rate-limiting enzyme for the Krebs's cycle (Gibson *et al.*, 1998). Other affected enzymes include pyruvate dehydrogenase complex (PDHC), succinate dehydrogenase complex II, and isocitrate dehydrogenase (Perry *et al.*, 1980, Bubber *et al.*, 2005). Studies have reported AD-induced reductions in KDGH activity which clinically correlate with the degree of dementia without evidence of general mitochondrial failure (Gibson *et al.*, 2000). Similarly, the consequences of reduced Krebs's cycle enzyme functions also precede reductions in ATP production. For example, the reduction of mitochondrial membrane potential induced by KDGH inhibition is preceded by release of cytochrome C and activation of apoptotic pathways (Huang *et al.*, 2003). In addition, the inhibition of PDHC or KDGH results in reduced acetylcholine production before causing reduction in ATP levels (Gibson and Blass, 1976). Moreover, reduction in the activities of PDHC or KDGH result in decreased neurotransmitter production (including glutamate and gamma-amino butyric acid (GABA) derived from the Krebs's cycle), increased production of ROS, reduction in ability of the brain to prevent oxidative damage, and promotes neurodegeneration (Klivenyi *et al.*, 2004).

Furthermore, enzymes of the electron transport chain have also been shown to be affected in AD patients (Aksenov *et al.*, 1999). The effects of accumulation of A β in mitochondria are believed to be exerted in part by its interaction with A β -binding alcohol dehydrogenase (ABAD) (Chen and Yan, 2006). In AD, mitochondrial dysfunction occurs because of oxidative stress occurring as a result of accumulation of A β within the mitochondria and disruption of the electron transport chain (Manczak *et al.*, 2006), A β binding to mitochondrial proteins, a resultant increase in ROS and decreased ATP production (Reddy and Beal, 2008).

Oxidative stress is a crucial cause of brain metabolic dysfunction in AD. This is because the brain shows a high susceptibility to oxidative stress, owing to its high oxygen demand, high lipid content, and relatively poor mechanisms to prevent damage from oxidants and free radicals. The presence of increased oxidative stress as an important pathogenic component of AD is indicated by the presence of increased accumulation of free iron stores in different parts of the brain in AD (Thompson *et al.*, 1988), increased lipid peroxidation and decreased polyunsaturated fatty acids in the AD brain (Subbarao *et al.*, 1990) and the presence of increased free radicals in NFTs and amyloid plaques (Hensley *et al.*, 1994).

It has been suggested that A β fibrils induce oxidative stress by several mechanisms, including the release of free radicals. For example, Mattson *et al.* (1995) demonstrated H₂O₂ accumulation in cultured hippocampal neurons and in cultures of neuroblastoma cells. While Butterfield *et al.* (1994) demonstrated A β induced lipid peroxidation in synaptic ends.

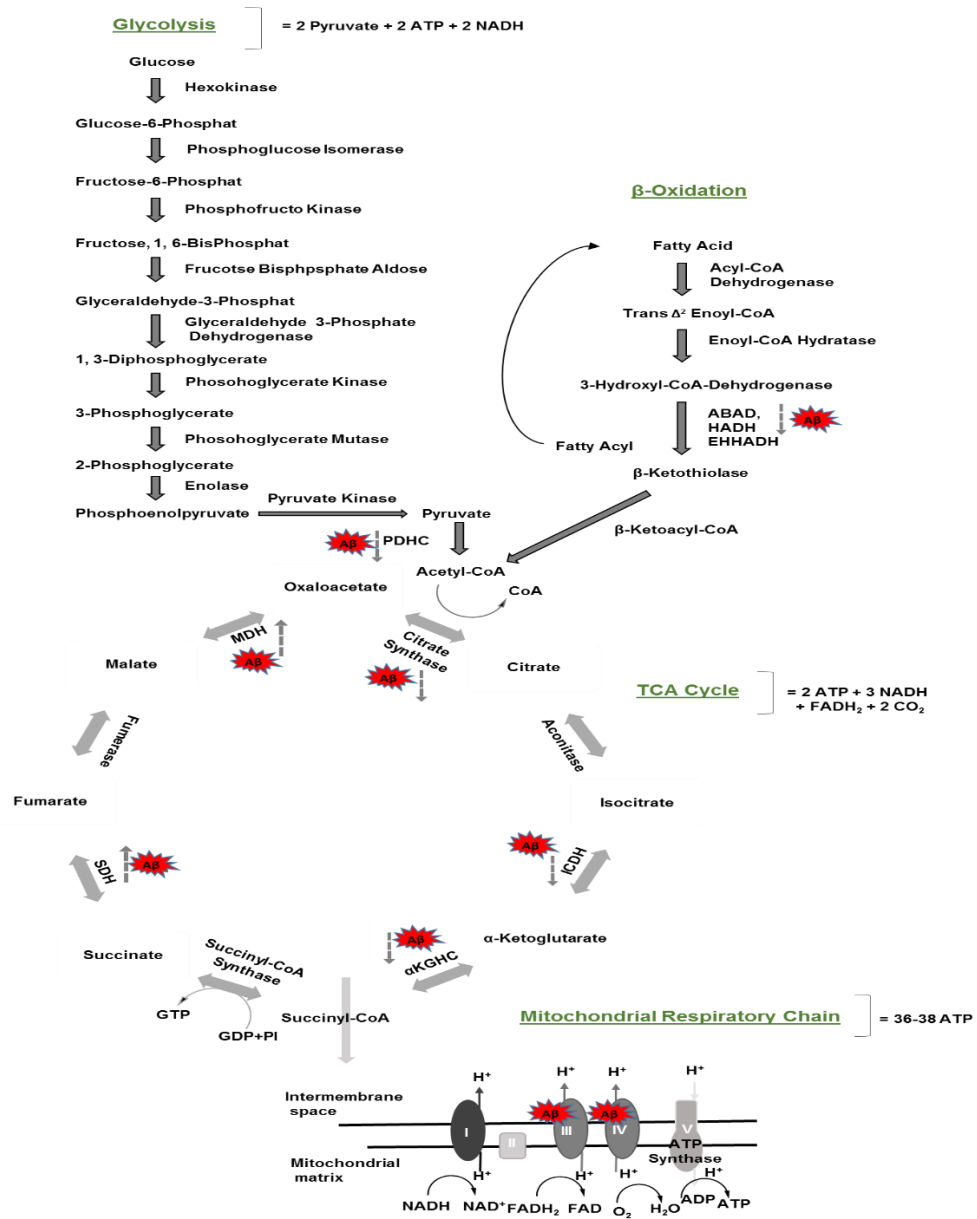


Figure 1.4: Representative overview of the effects of Aβ on key enzymes involved in energy metabolism. This diagram shows the metabolism of glucose and fatty acids (the latter are converted into acetyl-CoA upon entry into the mitochondria). Aβ exerts its toxicity at many points within energy metabolism. In the TCA cycle, the activity of PDHC is decreased reducing the conversion of pyruvate to acetyl-CoA (Bubber *et al.*, 2005, Yao *et al.*, 2009). Citrate synthase, ICDH and αKGHC are all decrease in response to Aβ treatment. Both MDH and SDH are increased after Aβ treatment (Casley *et al.*, 2002a, Casley *et al.*, 2002b, Bubber *et al.*, 2005). ABAD activity is decreased upon Aβ binding therefore affecting fatty acid metabolism (Yan *et al.*, 1997, Lustbader *et al.*, 2004, Muirhead, 2010). Within the respiratory chain both complexes III and IV are decreased by the increased presence of Aβ (Caspersen *et al.*, 2005, Manczak *et al.*, 2006, Yao *et al.*, 2009).

1.9.1 Mitochondrial Dysfunction in AD

Mitochondrial dysfunction is a core component of hypometabolism in AD. Bell *et al.* (2018) showed that fibroblasts derived from both fAD and sporadic AD (sAD) displayed reduced mitochondrial numbers with perinuclear clustering. Similarly, Hirai *et al.* (2001) found evidence of increased oxidative damage to AD mitochondria when they conducted analyses of AD and normal human deceased brain specimens, where they reported the increased presence of deformed mitochondria and mitochondrial degradation products in the AD specimens.

The mechanism of mitochondrial dysfunction in AD remains to be determined, although studies have revealed several postulates. Studies have shown that increased free radical production by A β peptides induced mitochondrial degradation by activating the mitochondrial fission proteins dynamin-1-like protein (Drp1) and fission mitochondrial 1 (Fis1) (Barsoum *et al.*, 2006). Furthermore, A β has also been shown to induce mitochondrial membrane dysfunction, by blocking entry of crucial proteins into the mitochondria, thereby causing oxygen and glucose deprivation, reduced antioxidant capabilities and deformation of the mitochondria (Sirk *et al.*, 2007). Other studies have also reported that the A β -induced mitochondrial membrane dysfunction occurs via calcium ion modulated opening of the permeability transition pores, and this is believed to play a key role in apoptosis (Moreira *et al.*, 2001, Koo *et al.*, 1990).

1.9.2 Dysregulation of Insulin Signalling

A β oligomers induce insulin resistance via several mechanisms. Oligomers have been shown to significantly impair neuronal response to insulin. This is done by rapidly inducing redistribution of insulin receptors from dendrites into the cytoplasm by driving calcium into dendrites via N-methyl-D-aspartate (NMDA) receptors. A β oligomers also inhibit downstream insulin activity by inducing tumour necrosis factor alpha (TNF α) secretion, which in turn causes C-Jun N-terminal kinase (JNK) stimulated suppression of PI3-kinase and serine/threonine-specific protein kinase (AKt) (Bomfim *et al.*, 2012, Ozes *et al.*, 2001).

Derangement in astrocyte function has also been suggested as an early event in the course of AD, and with a resultant reduction in anti-oxidant abilities. Neurons are continually exposed to oxidative stress due to their high level of oxidative metabolism (Abramov *et al.*, 2004). AD

patients have been shown to have significant reductions in glutathione levels, indicative of reduced capacity to protect against oxidative stress.

It has now become more apparent that the events indicating the presence of AD in patients are preceded by cellular toxicity, and loss induced by possibly prolonged periods of exposure to A β oligomers and abnormal tau proteins. It is thus important to examine the affected cell types, as well as the metabolic and molecular changes occurring before the appearance of overt disease. All cell types in the brain, predominantly the neurons and glial cells are affected in AD.

1.10 Human Brain

The brain is made up of the cerebral hemispheres, the brainstem (mid brain and pons) and the cerebellum. The brain is very active metabolically, and has about 750ml of blood flowing through per minute. This accounts for about 15% of the cardiac output. It is made up of the cortex, which is composed of cell bodies and synapses, making up the grey matter on the outside, and the white matter, which is made up mainly of axonal tracts on the inside (Lodish H, 2000). There are also subcortical grey matter which include the nuclei, thalamus, putamen etc. Microscopically, the brain is made up of multiple cell types mainly classified into nerve cells (neurons) and glial cells (astrocytes, microglia, oligodendrocytes and ependymal cells).

The brain makes up 2% of the human body weight, but takes up a quarter of the body's glucose, as well as a fifth of the body's total oxygen consumption (Magistretti and Pellerin, 1996). Glucose is the main energy substrate for the brain under normal physiologic conditions. Although brain cells have been shown to utilise energy substrates like mannose, lactate and pyruvate in vitro (Magistretti and Pellerin, 2000). However, these substrates are not normally utilised physiologically, either because of absence from the blood in normal people (mannose) or because they cannot penetrate the BBB (pyruvate) (Magistretti and Pellerin, 2000). The only other energy sources utilised by the human brain are lactate (Gallagher *et al.*, 2009) and ketones, which the brain utilises at times of starvation or during diabetic crises (Magistretti and Pellerin, 2000).

In order to understand the impact of hypometabolism on the brain the interaction between different brain cell types should be considered.

1.11 Neurons and Astrocytes

Neurons and the glial cells are the basic elements of the CNS. The human brain is the most complex organ in the body, reported to contain about 100 billion neural cells that communicate with each other and transmit electrochemical signals via synapses at which the different neurons connected by their axons (Herculano-Houzel, 2009). There are different types of cells in the brain, and each type performs a different function.

Neurons are the primary cells involved in electrical impulse transmission. All neurons have an excitable membrane, made possible by energy-dependent ion pumps which create a voltage gradient of Na⁺ and K⁺ ions across the intracellular and extracellular portions of the membrane, and calcium ion gradients at the synaptic ends of the membranes (Nowakowski, 2006).

Astrocytes are glial cells which were originally believed to simply support neuronal function. They are now recognised as a complex and functionally diverse group of cells that demonstrate important roles during development, normal function. They modulate synaptic function, aid neuronal metabolism, nutrition and electrolyte balance. During development, they associate with multiple synapses and coordinate the development of functional neuronal networks and synapses using both contact-mediated (Barker *et al.*, 2008, Hama *et al.*, 2004, Elmariah *et al.*, 2005) and secreted signals (Clarke and Barres, 2013). Astrocytes also promote the maturation of synaptic transmission in *in vitro* co-cultures (Rempe *et al.*, 2007, Tang *et al.*, 2013, Hartley *et al.*, 1999). Astrocyte processes wrap around multiple synapses to modulate synaptic transmission (Carmignoto, 2000). In addition, they serve as a bridge between capillaries and the neuronal cells. The involvement of astrocytes in the modulation of neuronal activity and signalling has been reported in animal models (Allaman *et al.*, 2010). They are believed to form intimate relations with neuronal signalling by forming 'tripartite synapses' (Volterra and Meldolesi, 2005). The physical and physiological relationship between neurons and astrocytes is very crucial for neuronal function, and the metabolic coupling between neurons and astrocytes is an essential component of normal brain metabolism.

1.12 Normal Brain Energy 'Metabolism'

There are spatial and cellular differences in the method of glucose utilisation in the adult brain for energy production. On a cellular level, astrocytes mainly utilise glucose through glycolysis, whilst neurons predominantly utilise the oxidative phosphorylation process of the Krebs's cycle.

The close physical and physiological relationship between astrocytes and neurons allows for a functional metabolic system coupling of synaptic activity and energy delivery, which has been termed the astrocyte-neuron lactate shuttle (ANLS) (Magistretti and Pellerin, 2000). Glutamate stimulates glucose uptake and lactate production via glycolysis in astrocytes. This lactate can then be used by neurons via the Krebs' cycle for adenosine triphosphate (ATP) generation (Magistretti, 2000, Tarczyluk *et al.*, 2013) (Fig. 1.5). Astrocytes play a very significant role in normal brain metabolism. They are the sole stores of glycogen in the brain, and they are important for maintenance of potassium ion homeostasis as well neurotransmitter reuptake (Peters *et al.*, 2005). The spatial positioning of astrocytes is crucial to their function; their processes are wrapped around the synaptic ends, while their end-feet surround capillaries, providing a cellular conduit for transport of substances between intraparenchymal blood vessels and the neurons (Magistretti and Pellerin, 2000). Astrocytes are also connected to one another via gap junctions, creating a syncytium, which plays a vital role in spatial buffering of K⁺ ions released as a result of neuronal activity, as well as other metabolic functions. Astrocytes also take up glutamate released from neurons into the synaptic cleft and recycle it to produce glutamine for reuse as a transmitter by the neurons and as an energy source (Giaume *et al.*, 2010). Since astrocytes play a very important role in normal metabolism, it is important to understand the crucial roles they play in the metabolic changes that occur during the pathogenesis of neurodegenerative conditions such as AD. It is thus important to examine the models for studying the metabolic changes that occur during the developmental stages of the disease.

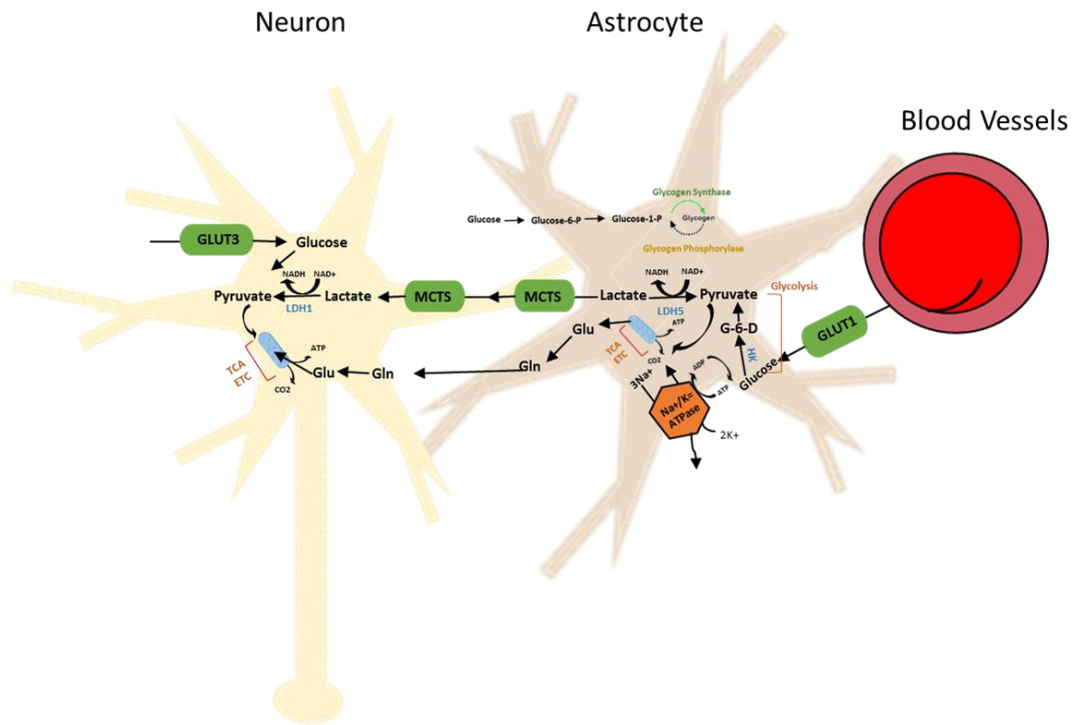


Figure 1.5: Representative overview of the transport and utilisation of glucose by cells. Glucose enters the cells through the glucose transporters (GLUTs), is phosphorylated by hexokinase enzyme to produce glucose-6-phosphate (G6P), which is then metabolized through glycolysis, producing to two molecules each of pyruvate, ATP and NADH. Pyruvate is then reduced by pyruvate dehydrogenase to produce lactate, which is transported to the neurons via monocarboxylase transporters to be metabolized through oxidative phosphorylation and the electron transport chain, producing ATP and CO₂ - ANLS. Astrocytes also participate in the recycling of synaptic glutamate via the glutamate-glutamine cycle. Glutamate (Glu) released from the synaptic ends is converted to glutamine (Gln) by glutamine synthetase (GS) and shuttled to neurons, where it is converted back to glutamate by glutaminases. Reproduced by the hypothesis of Magistretti and Pellerin, 2000.

1.13 Studying AD: The Models

While advancements in brain imaging have provided increased understanding of AD at a macroscopic level, one obstinate peculiarity of AD is that it can only be diagnosed by histology, usually post-mortem. This makes it very difficult to study the early stages of the disease and the preclinical stages at a cellular level before appearance of overt clinical features of AD. To overcome this issue many studies utilise animal models to study the disease. However, there are severe limitations to the use of animal models, chief being the significant differences in the structure and physiology between different animal models and man. This results in highly variable and unpredictable results depending on the animal model used. Furthermore, some animal models of AD do not develop the major features of the disease observed in man, such as neuronal loss. *In vivo* animal models studying changes in brain glucose metabolism have yielded conflicting results depending on the animal model used. These studies have tested models overexpressing APP (Nicolakakis *et al.*, 2008, Luo *et al.*, 2012, Poisnel *et al.*, 2012) and Tau (Nicholson *et al.*, 2010) mutations with mixed results without consistency in pattern of effects seen in the various animal models.

Several authors have also used human cell lines created from transformed cells derived from tumours such as gliomas, pheochromocytomas and neuroblastomas in studies on AD. The drawback of these models however, is that the cells are derived from tumour cells which differ from the naturally occurring cell types being studied cells, and their metabolism may show varying degrees of difference from what happens in the normal physiological environment. They also show a very high degree of homogeneity which is far removed from the heterogenic behaviours of primary human cells, both *in vitro* and *in vivo*. The homogeneity of tumour cell lines in culture is an advantage with producing consistent results, and understanding of pathways, but it may fail to properly represent the behaviours and responses of primary cells, which may differ, and may have important downstream effects on the response to drug therapies for example.

In order to overcome the limitations of animal models and tumour cell lines, novel cellular models using disease-specific human cells could provide a more realistic and robust understanding of the early preclinical cellular and molecular events heralding the pathogenesis of metabolic dysfunction in AD. As such, human stem cell-derived models are currently being developed for *in vitro* studies. Recent work in our laboratory has produced important insights into A β -induced metabolic dysfunction using the NT2.D1 stem cell derived neurons (Tarczyluk *et al.*, 2015). There is a need to build up on these results by observing the

occurrence of hypometabolism in cells that produce disease-associated forms of APP and A β at physiological levels. This is currently the best opportunity of observing the natural occurrence of these preclinical pathogenic processes in fAD. This is possible due to recent advancements in the development of human derived induced pluripotent stem cells (hiPSCs) that offer the opportunity to study this disease with greater accuracy than has previously been possible. It potentially gives the opportunity to model the disease process in living tissue.

1.14 Human iPSCs

Human iPSCs are pluripotent stem cells derived from adult mature cells and are capable of giving rise to differentiated progeny from the three germ layers, and would retain the genetic make-up of the parent source. They were first produced through the work of Yamanaka and Takahashi (2006), when they produced pluripotent stem cells from fully differentiated adult stem cells by introducing four transcription factors octamer-binding transcription factor 4 (Oct4) (Pou5f1), SRY (sex determining region Y)-box 2 (sox2), c-Myc, and Krüppel-like factor 4 (Klf4). Traditionally, neuronal cells for research were produced from animal cells or immortalised cell lines derived from human cancers. However, hiPSC-derived neuronal cells have the advantage of being able to produce physiologically relevant neural cell types, and could produce results that are more closely related to what occurs in the normal human brain. Disease-specific cells (fAD patient-derived cortical neural cells in this situation) offer a previously underexplored opportunity to observe the development of pathogenic processes such as metabolic dysfunction that precede the appearance of overt disease. These can be compared with cortical neural cells derived from normal individuals as controls.

1.14.1 Generation and Differentiation of Human iPSC-derived Neuronal and Astrocytic Cells

The development of human neural cells culture derived from AD patients has been made possible by the development of iPSC (Yamanaka and Takahashi, 2006). Furthermore, the development of protocols to produce neural cell types has also supported the production of *in vitro* brain neural cell cultures (Chambers et al., 2009, Shi et al., 2012a). Such methods have enabled the development of AD models and have demonstrated the production of mixed populations of GFAP-positive astrocytic glial cells and microtubule-associated proteins (MAP2-positive) neurons derived from AD patient hiPSCs (Anderson *et al.*, 2015).

Although the process to differentiate neurons and astrocytes is complex, it is important to briefly explore important components the differentiation process as they may bear significant effects on understanding of the disease process and exploitable therapeutic targets. The differentiation process involves induction of the pluripotent iPSC into the multipotent neural precursor cell (NPC), which can then be induced to differentiate into mature astrocytes or neurons (Fig. 1.6). The NPC is the committed multipotent progenitor of neuronal and glial cells which is capable of self-renewal or differentiation into mature neurons or glial cells. It plays a very crucial role in embryonic development of the nervous system, and in adult life, it is located in certain parts of the brain, including the dentate gyrus of the hippocampus where it is responsible for memory and the learning process (Zhao *et al.*, 2008), as well as the sub-ventricular zone of the lateral ventricles (Ming and Song, 2011).

The differentiation of NPCs into neuronal or astrocyte lineage is determined by a complex interplay of external and internal chemical stimuli. This complex biochemical interplay of signals interplay includes fibroblast growth factor (FGF) and vascular endothelial growth factor (VEGF) which facilitate NPC proliferation, while bone morphogenetic protein (BMP) signalling promotes astrocytic differentiation, a mechanism that is often blocked by noggin, a SMAD (BMP signalling cytokine) inhibitor when neuronal differentiation is the goal (Chambers *et al.*, 2009). Notch signalling also plays a significant role in neuronal differentiation (Reviewed in Ladrán *et al.*, 2013). In addition, inhibition of glycogen synthase kinase 3 (GSK-3 β) and activation of sonic hedgehog signalling molecule (SHH), retinoic acid (RA) and fibroblast growth factor 8 (FGF8) have been shown to promote neuronal differentiation (Xi *et al.*, 2012, Karumbayaram *et al.*, 2009). Conversely, astrocytic differentiation of NPCs is enhanced by the Notch signalling activation, neuregulin (an EGF-like ligand), BMP signalling and ciliary neurotrophic factor (CNTF), an Interleukin 6 cytokine (IL-6) which inhibits neuronal differentiation and promotes astrocytic differentiation by downstream activation of Janus kinase/signal transducer and activator of transcription signalling (JAK/STAT) (Bonni *et al.*, 1997).

Furthermore, astrocytes also play a significant role in the differentiation process, as astrocyte-mediated wntless-related integration site signalling (WNT) modulates differentiation and replication of NPCs, they produce cholesterol and extracellular matrix proteins which exert a strong influence on synaptogenesis, and their spatial location with respect to intracranial blood vessels allows them modulate the release of factors from blood vessels and ependymal cells (Reviewed in Ladrán *et al.*, 2013).

1.14.2 Human iPSC Models of AD

The development of the iPSC offered a unique opportunity, and enhanced the potential to generate disease-specific cells that could be utilised to study complex neurodegenerative diseases like AD. Historically, the challenges faced with the generation of such disease-specific cells include the prolonged differentiation timelines as well as difficulties with generating pure cultures of functional cell types. The challenges have now mostly been significantly tackled or at least mitigated (with respect to previous efforts) by an explosive number of studies into developing representative models for the disease (Reviewed in Penney *et al.*, 2019).

Efforts at developing iPSC models of AD have mirrored the natural process and stages of neurogenesis (induction, neural fate determination and differentiation) (Reviewed in Arber *et al.*, 2017), with intense focus on signalling determinants that speed up the differentiation process, and increase the specificity of the final cell types produced (Zhang *et al.*, 2013, Sheltoiuki *et al.*, 2013, Bardy *et al.*, 2015, Di Lullo *et al.*, 2017). Two dimensional models remain the most widely used models for studying AD pathogenesis, and typically involves the use of adherent neuronal cultures to study the AD pathological changes at the cellular level (Reviewed in Arber *et al.*, 2017). These models utilise alternations of signalling pathways to induce a neural fate (by double SMAD inhibition) (Chambers *et al.*, 2009), and then a Wnt mediated cortical differentiation which can be manipulated to specific cellular fates by inhibition of SHH signalling and alterations of retinoid signalling (Li *et al.*, 2009, Van de Leemput *et al.*, 2014, Shi *et al.*, 2012, Nicholas *et al.*, 2013, also reviewed in Arber *et al.*, 2017). These two dimensional models however struggle to recapitulate the complex spatial interactions that may be important in the pathogenic process of AD. Three dimensional models have also been developed with the aim of tackling these deficits of the 2D models. They involve the use of scaffolds or the use of organoid cultures. These allow for observation of the temporal trends of A β and tau deposition that mirrors the occurrence *in vivo* (Choi *et al.*, 2014, Gonzalez *et al.*, 2018). However, these models exhibit a higher degree of heterogeneity and variability in results (Qain *et al.*, 2016), with a resultant reduction in reproducibility, and reliability of the results.

Human iPSC models have also developed further with producing specific disease-specific cells for AD research which can be matched to age, disease type, as well as brain regions which can be studied for the earliest pathologic features of the disease. Numerous iPSC cell lines have now been developed for fAD, which carry the various disease causing mutations which are now in widespread use for studying the pathology of the early-onset form of the

disease. This availability of newer forms of technology like the CRISPR/Cas9 has also made the understanding of these processes easier, as they can be used to generate disease-causing mutations in iPSCs (Maeder *et al.*, 2013, Paquet *et al.*, 2016).

1.14.3 Characterisation of Neural Lineage Cells

The NPC is marked by positivity to sox2, paired box protein (pax6) and nestin (Reviewed in Ladrán *et al.*, 2013). During the maturation process, cortical neurons are marked by positive expression of neuron-specific Class III β -tubulin (TUJ1) as well as specific cortical markers such as CTIP2 and MAP2 (Anderson *et al.*, 2015), while astrocytes show positive expression of S100 Calcium Binding Protein β (S100 β) and Glial fibrillary acidic protein (GFAP) (Fig. 1.6).

The metabolic changes that occur in early AD will likely be key to understanding the disease and developing newer diagnostic methods, and novel approaches for tackling the disease for definitive cure. To understand these early metabolic changes, appropriate approaches should involve the use of patient-specific cells for understanding the natural history and metabolic course of the disease (Fig. 1.7). This is part of what this project hoped to achieve.

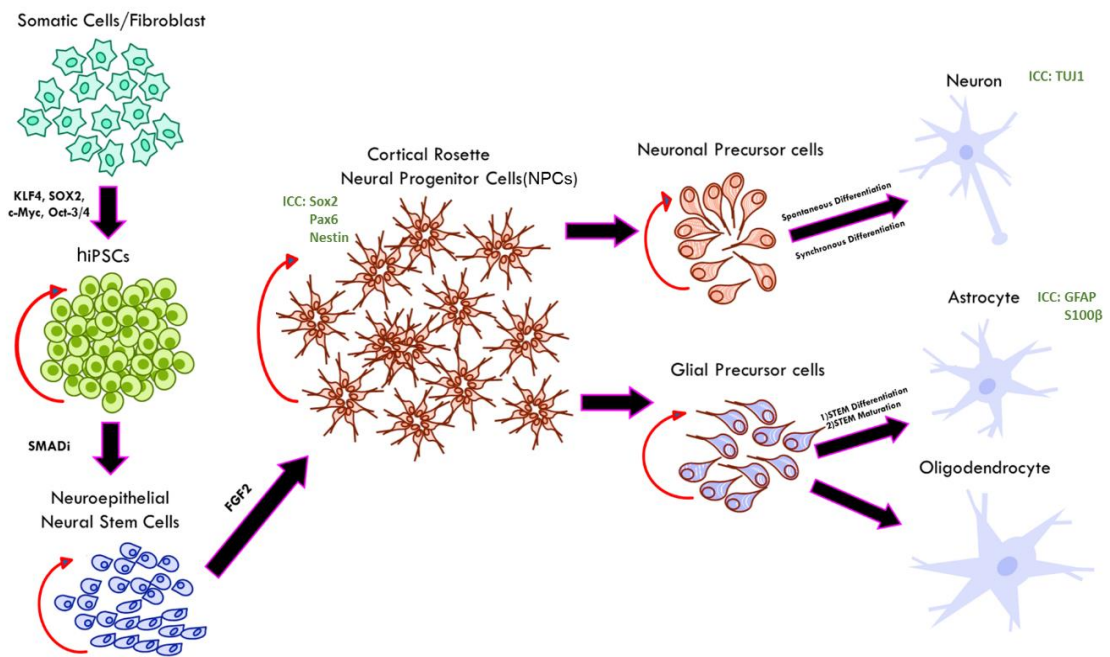


Figure 1.6: Diagrammatic presentation of the process of generation of various brain cell types from hiPSCs via the neural progenitor cells.

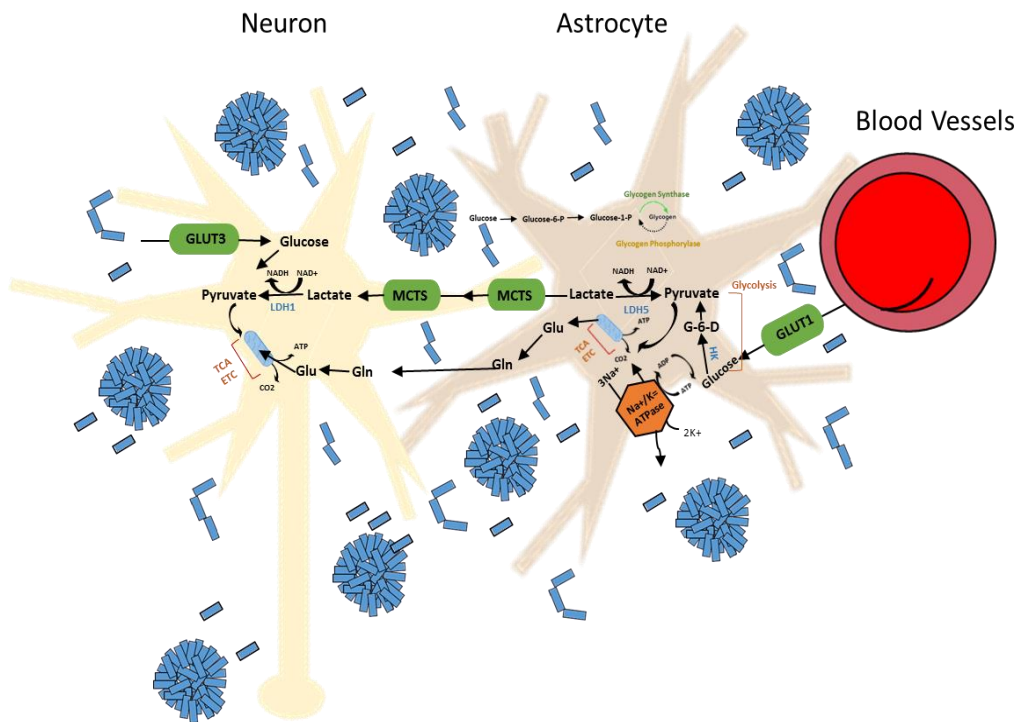


Figure 1.7 Schematic representation of potential sites of toxic effects of various amyloid species (A β oligomers, A β fibrils, A β plaques) on brain cells metabolism.

1.15 Hypothesis

The main hypothesis of this project is that fAD patient-derived hiPSC neurons and astrocytes will show abnormal metabolic properties compared to neurons and astrocytes derived from hiPSCs produced from 'healthy' controls. A second hypothesis is that synthetic A β oligomers will induce metabolic dysfunction in human primary astrocytes and 'healthy' hiPSC-derived astrocytes and neurons.

The aim of this project is to:

- Differentiate NPCs differentiated from 'healthy' human and fAD patient-derived iPSCs from the stage to astrocytes and neurons, and then to compare the efficiency of differentiation using morphology and immunohistochemical staining.
- Assess metabolic dysfunction in the form of glucose uptake and astrocytic glycogen levels in human primary astrocytes and 'healthy' patient hiPSC-derived astrocytes and neurons as a result of exposure to synthetic A β 1-42 oligomers.
- Assess the production of A β peptides in both fAD patient-derived and control neurons and astrocytes using ELISA at defined time points during the differentiation process.
- Explore the occurrence of metabolic dysfunction in fAD patient hiPSC-derived neurons and astrocytes, as measured by neuronal glucose uptake and astrocytic glycogen levels.
- Determine if metabolic dysfunction correlates with the presence of disease specific A β peptides using immunodepletion studies.

Chapter 2: Characteristic of Healthy Human iPSC-derived NPCs Cell Line

2.1 Introduction

Until recent advances in neural cell culture techniques, diseases like AD have been hitherto impossible to re-create and study in an *in vitro* setting. Whilst post-mortem has provided valuable information it is virtually impossible to study living human brain tissue. The ability to study diseases like AD before the onset of overt clinical signs and symptoms may be the key to identifying modifiable therapeutic targets and management options. Studying the human brain for pre-clinical changes before the onset of AD has hitherto been impossible for several reasons, including the non-representative nature of animal studies and the need to recapitulate the complex spatial and functional characteristics of the human brain. The development of human iPSCs has now made it possible to overcome some of these challenges. It is now possible to develop hiPSCs from both 'healthy' and AD patients, and then differentiate these into neural cells, with the aim of studying pre-clinical disease mechanisms at the cellular level.

In order to be able to carry out studies on human brain cells in the *in vitro* setting, the first step would be to successfully differentiate pluripotent hiPSC into fully mature neural cells, especially those of cortical origin, and then to ensure that these differentiated cells mirror the naturally derived neural cells structurally and functionally, and are able to recapitulate natural processes as it occurs in the human brain. It is thus important to explore the process of differentiation of hiPSC-derived NPCs into neurons and astrocytes and to characterise them morphologically, by immunohistochemistry staining, and metabolic function, including response to known neurometabolic modulators. These cells have important roles in the pathologic process in AD because neurons are the major electrical impulse transmitters, and the astrocytic cells are the major glial cells of the human brain. They have also been reported to have very important complex interactions with each other, and together, they make up the most important cells within the human brain. They are together responsible for essential components of the information processing functions of the human brain. Furthermore, they are the cells predominantly affected in the disease. Indeed, the early neurodegenerative changes and neuronal losses in AD mainly affects the cerebral cholinergic and glutamatergic neurons and surrounding glial cells (Hampel *et al.*, 2018). It thus bears relevance to utilise these cell types as a study focus for the disease process.

2.1.1 Astrocyte Metabolism

Astrocytes are indispensable metabolic components of brain growth, function, metabolism and survival. They are the sole cellular stores of glycogen in the brain, and provide crucial supplies of lactate for neuronal function and survival. They also play significant roles in synaptic formation and transmission (section 1.11). Their role in neuronal metabolism, survival and in synaptic function highlights the need for their inclusion in cellular models of brain function/dysfunction.

Astrocytes mainly utilise glucose via glycolysis, resulting in the generation of lactate which can then be transmitted to neurons for energy metabolism via the Krebs's cycle (Hu and Wilson, 1997, Galeffi *et al.*, 2007) (Fig. 1.4 and 1.5). The uptake of glucose is modulated by several factors including availability of glucose in the surrounding, presence of neuroregulators like glutamate, adrenergic agonists, and metabolic hormones like glucagon and insulin (Hertz *et al.*, 2007, Dienel and Hertz, 2001). They also play crucial roles in potassium and calcium ion buffering during neurotransmission as well as uptake of neurotransmitters released into the synaptic clefts (Peters *et al.*, 2005). Although astrocytes are the primary stores of glycogen in the brain, they have significantly lower stores of glycogen than the liver or muscle cells, hence prolonged starvation or glucose deprivation would have catastrophic consequences for neuronal function and survival (Brown *et al.*, 2005, Gruetter, 2003).

The astrocytic glycogen stores, although very little compared to other body stores, are very crucial to reserving function during starvation conditions and at times of intense neural energy consumption, where the lactate supplies from astrocytic glycogen breakdown have been shown to maintain neuronal survival and function for at least 20 minutes (Brown and Ransom, 2007). Besides from the glucose concentration in the immediate environment and extant energy demands, other factors also affect the rate at which glycogen is metabolised by astrocytes. These include neurotransmitters and other neuroregulators listed above which also affect the glucose uptake.

The process of glycogen formation and breakdown, like other metabolic processes, is enzyme dependent. The rate-limiting enzyme for glycogen formation is the glycogen synthase enzyme, while the rate-limiting enzyme for glycogen breakdown is glycogen phosphorylase (Brown and Ransom, 2007). In the process of glycogen formation, glucose is transported into the astrocyte cells via the glucose transporter (GLUT1) after passing through the endothelial cells from the blood vessels. This glucose is then supplied with a phosphate unit by hexokinase to produce glucose-6-phosphate (G-6-P), essentially making it 'heavy' and preventing it from leaving the

cell. G-6-P is converted by phosphoglucomutase to glucose-1-phosphate (G-1-P) which is then conjugated with uridine triphosphate glucose (UDP-glc) by UDP glucose phosphorylase (Fig. 1.5). Glycogen has a protein skeleton called glycogenin, onto which UDP-glc units are added by glycogen synthase, through the formation of α -1,4-glycosidic bonds, resulting in the release of the UDP units. To create a complex, rather than linear molecular structure, α -1,6-glycosidic bonds are added at every 8th - 10th glycosyl units by amylo-(α -1,4- α -1,6)-transglycosylase, creating a branching structure.

The process of releasing glucose units from the glycogen molecule requires several enzymes, the first of which is glycogen phosphorylase which cleaves off G1P units by breaking the α -1,4-glycosidic bonds, and then Oligo- (α -1,4- α -1,4)-glucantransferase and amylo- α -(1,6)-glucosidase translocates the three outermost glycosyl units to another non-reducing end of the molecule for further glycogen synthase cleavages of G1P units. The last units on the α -1-6 bond branches are removed as glucose units by amylo- α -(1,6)-glucosidase.

Hypometabolism has been reported as an early feature of AD (Mosconi et al., 2008a), and is suspected to be the central pathogenic event leading up to brain cell loss as seen in established AD. One of the mechanisms suspected to be involved in the pathogenesis of early AD is impaired insulin signalling which leads to impaired uptake of glucose and altered glycogen turnover (Frölich *et al.*, 1998, Ratzmann and Hampel, 1980). As glycogen turnover and glucose uptake in astrocytes are directly related to insulin signalling and nutrient availability, assessing either would be a representative method of assessing metabolic function in neural cells. It is important to ensure that crucial metabolic processes in hiPSC-derived astrocytes mirror those of naturally derived human primary astrocytes. To our knowledge, no studies have investigated the glycogen turnover under defined conditions to confirm metabolic conformity between in these cells.

2.1.2 Astrocytic Differentiation of Human iPSCs

The process of differentiation of hiPSC-derived NPCs to astrocytes and neurons has been briefly described in chapter 1 (section 1.14.1). This chapter briefly examines the differentiation process *in vitro*. Astrocytes are complex and heterogeneous, in their developmental origins (Hall *et al.*, 2003, Hochstim *et al.*, 2008).

Astrocyte differentiation is believed to occur through two pathways during foetal development and postnatally (Shaltouki *et al.*, 2013). The first pathway, the prominent pathway, is believed

to mostly occur during early neurogenesis, involving the development of a CD44+ve intermediate before astrocytes are differentiated from neural stem cells. The second pathway, the indirect pathway, is believed to occur in the adult brain and in response to injury, when glial cell precursors produce astrocyte precursors that mature astrocytes after downregulation of A2B5 and NG2 immunoreactivity. The development of astrocytes in the *in vitro* setting has also shown similar developmental heterogeneity in response to environmental cues (Krencik *et al.*, 2011). Previous protocols for the generation of human astrocytes from pluripotent stem cells have been complex and time-consuming, involving over six months of culture. Further studies by Shaltouki *et al.* (2013) showed that Neuregulin, Notch signalling, hairy enhancer of split (HES) and nuclear factor 1A (NF1A) pathways are important in the differentiation process, and could significantly shorten the duration of differentiation and maturation of the neural precursors into astrocytes (Shaltouki *et al.*, 2013).

The astrocytes differentiation method used in this study involves the differentiation and maturation protocols developed by STEMCELL Technologies Inc., UK.

2.1.3 Neuronal Differentiation of Human iPSCs

The neural differentiation of hiPSCs was conventionally carried out by co-culture with stromal cells, or by embryoid body formation (Denham and Dottori, 2011). However, more advanced methods have been developed to enable researchers to generate particular groups of brain cells including cortical (Shi *et al.*, 2012a), dopaminergic (Yan *et al.*, 2005) and cholinergic neurons (Karumbayaram *et al.*, 2009). Some authors have successfully generated functional cortical neuronal models of fAD which exhibited the typical features of fAD including the production of insoluble intracellular and extracellular A β 1-42 aggregates as well as the presence of hyperphosphorylated tau (Shi *et al.*, 2012a, Shi *et al.*, 2012b, Kondo *et al.*, 2013).

A protocol to differentiate hiPSCs into cortical neuronal cells was developed by Shi *et al.* (2012a). This method involves the inhibition of SMAD signalling (Chambers *et al.*, 2009), and then improving the efficiency of differentiation by replacing noggin with dorsomorphin, a small-molecule inhibitor of SMAD signalling (Kim *et al.*, 2010). The role of Notch signalling inhibition in determining a neuronal fate for NPCs occurs through the suppression of HES Family BHLH Transcription Factor 1 (HES1) which then results in upregulation of neurogenic genes like the Delta like canonical Notch ligand 1 (Dll1) and Neurogenin 2 (Shimojo, Ohtsuka and Kageyama, 2008, Ladrán *et al.*, 2013).

The protocols used for this study were adapted from methods described by Shi *et al.* (2012a and 2012b), who described two methods of differentiating pluripotent cells into cortical neurons. The first is spontaneous differentiation method, a 40-day three-step process involving differentiation of hiPSCs into cortical NPCs, production of cortical projection neurons and then maturation for development of functional action potentials (Shi *et al.*, 2012a). The second is synchronous differentiation method, which is essentially similar to spontaneous differentiation, but with the use of a γ -secretase inhibitor (DAPT) to induce rapid differentiation (Shi *et al.*, 2012b). These methods were adapted for this project, using cortical NPCs obtained from Axol Biosciences (Cambridge, UK).

2.1.4 Aims and Objectives of the Study

The aim of this chapter was to provide specific comparisons of neural cell differentiation methods to generate neural cells (neurons and astrocytes) from human iPSC-derived NPCs cell line derived from 'healthy' individual, and to characterise them morphologically by immunohistochemical staining. In addition, the differentiated hiPSC-derived astrocytic cells were compared morphologically and histochemically with human primary astrocytes, and then assessed for their ability to break down glycogen stores in response to hypoglycaemic conditions and pharmacological treatments (neuromodulators and glutamate).

2.2 Materials and Methods

2.2.1 Expansion of 'Healthy' Control Human iPSC-derived NPCs

Human NPCs derived from iPSCs were obtained from Axol Bioscience. Details of cell line is provided in table 2.1. The ax0018 'healthy' cell line a cell line used as control. The 'healthy' hiPSC-derived NPCs were cultured and expanded according to a protocol modified from the manufacturer's instructions.

These cell lines were expanded over three passages. Cells were expanded in Axol Neural maintenance basal medium (Axol Bioscience, UK) in 6-well plates (Corning®, USA). The plates were pre-coated with 0.2mg/ml poly-L-Orinthine stock (0.01% PLO) (Sigma-Aldrich, UK), which was diluted in sterile distilled water and incubated for two hours at 37°C, and then washed twice with sterile distilled water. Plates were then coated with 7.5µg/ml laminin (Sigma-Aldrich, UK), which was diluted in sterile distilled water and incubated overnight at 37°C. Before cell seeding, the wells were washed once with Dulbecco's phosphate buffered saline (D-PBS) (Sigma-Aldrich, UK). At 70 - 90% confluency, cells were passaged by washing once with 1ml D-PBS, and then the cells dissociated with 1ml Accutase (Sigma-Aldrich, UK) at 37°C for 5 minutes. The cells were transferred into a 15ml sterile conical tube with 4ml Axol Neural maintenance basal medium or Dulbecco's modified eagle's medium (DMEM) (Sigma-Aldrich, UK) and centrifuged for 5 minutes at 200 x g. The pellet was re-suspended in 1ml plating-XF medium or 50µM Rho associated protein Kinase inhibitor (ROCK) (Abcam, UK) in Axol Neural maintenance basal medium. The cell count was performed using trypan blue and a haemocytometer, and then the cells were plated at a density of 5×10^4 - 20×10^4 cells/cm². After plating, the cells were incubated at 37°C in a humidified atmosphere of 5% CO₂. After overnight incubation, the medium was replaced with pre-warmed Axol neural maintenance basal medium supplemented with 10ng/ml FGF2 (Axol Bioscience, UK) every 2 - 3 days.

Cell Name	ax0018
Cell Type	hiPSC-derived NPCs Healthy Control Line
Starting material	Dermal fibroblast
Mutation	None
Karyotype	Normal
Donor Age	74 years old
Donor Gender	Male

Table 2.1: Description of hiPSC-derived NPCs cell line from ‘healthy’ human control donor.

2.2.2 Generation and Characterisation of Human Brain Neural Lineage Cells from iPSC-derived NPCs

The 'healthy' human cell line (ax0018) was differentiated into neuronal subtypes and astrocytic cells according to different differentiation methods (section 2.2.2.1, 2.2.2.2 and 2.2.2.3, respectively) and were evaluated by immunocytochemistry staining (ICC) (section 2.2.4). The NPCs derived from 'healthy' hiPSCs were differentiated using two neural differentiation protocols (section 2.2.2.1 and 2.2.2.2) to produce cerebral cortical neuronal cells over 40 days using spontaneous and synchronous differentiation methods. All protocols were adapted from Axol Bioscience.

2.2.2.1 Spontaneous Neuronal Differentiation Method

This method was used to generate a mixed population of cerebral cortical neurons and astrocytes (Fig. 2.1A). Human iPSC-derived NPCs were differentiated using the spontaneous differentiation method (SP); this medium formulation was based on Shi *et al.* (2012a). Briefly, expanded cells were cultured on a pre-coated 12-well plate (Corning®, USA) with PLO/Laminin, and pre-coated 16mm glass coverslips coated with PLO/Laminin at a density of 7×10^4 cells/cm² (section 2.2.1). After 24 hours of plating, cells were treated with pre-warmed Axol Neural maintenance basal medium without supplementation (10ng/ml FGF2). The cultured cells were replaced every 2 - 3 days with pre-warmed Axol Neural maintenance basal medium over 40 days. Differentiated neuronal cells were assessed using ICC staining (section 2.2.4).

2.2.2.2 Synchronous Neuronal Differentiation Method

This method was used to generate an enriched cerebral cortical neurons (Fig. 2.1B). Human iPSC-derived NPCs were differentiated using synchronous differentiation (SY) using medium formulation based on Shi *et al.* (2012b) containing 10µM DAPT (γ-secretase inhibitor) (Abcam, UK). Expanded cells (section 2.2.1) were replated on a pre-coated in 12-well plate and pre-coated 16mm glass coverslips coated with PLO/Laminin at a density of 7×10^4 cells/cm². After 24 hours of plating, cells were treated with pre-warmed Axol Neural maintenance basal medium supplemented with 10µM DAPT for a maximum 5 days (medium was replaced twice). Media was then replaced with pre-warmed Axol Neural maintenance basal medium without

supplementation. The medium was replaced every 2 - 3 days over 40 days. Differentiated neuronal cells were assessed using ICC staining (section 2.2.4).

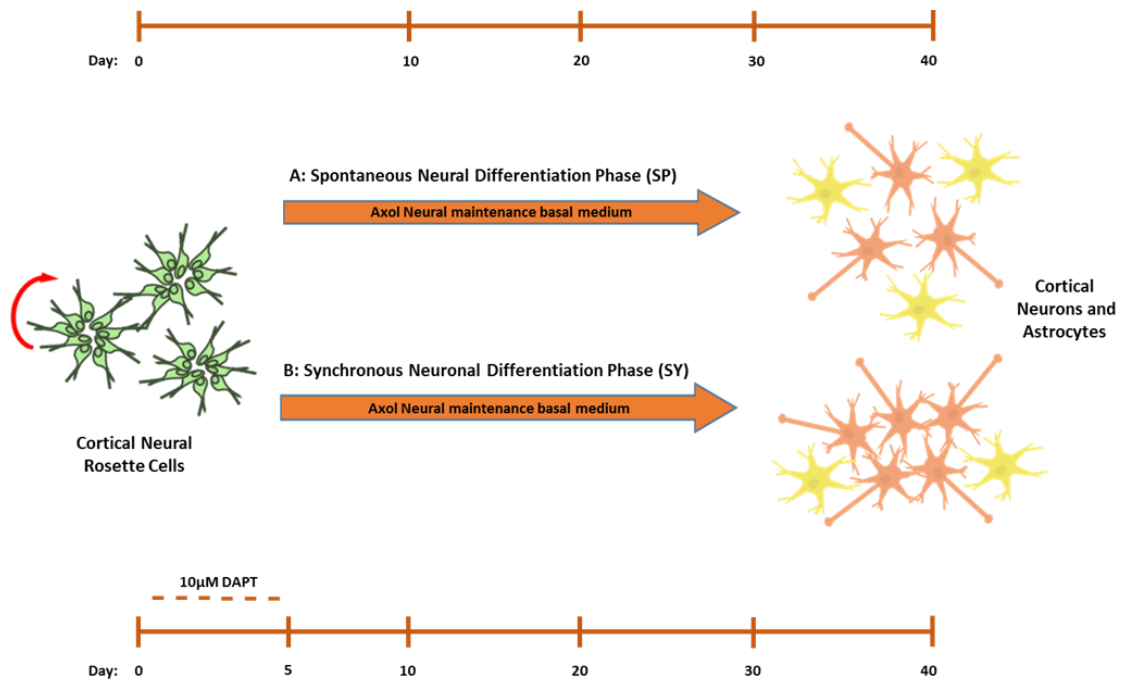


Figure 2.1: Diagrammatic overview of generation and differentiation of cortical neuronal cells from hiPSC-derived NPCs over a period of 40 days. NPCs were differentiated using two differentiation methods: (A) spontaneous neural differentiation method to generate a mixture cells of both neurons and astrocytes. (B) Synchronous neuronal differentiation method using 10µM DAPT for 5 days to produce a culture containing predominantly neurons.

2.2.2.3 Astrocytic Cells Differentiation and Maturation Methods

Human iPSC-derived NPCs of ax0018 cell line was differentiated into astrocytic cells using two-step process using astrocyte differentiation kit and astrocyte maturation kit obtained from STEMCELL Technologies. The first step was used to generate lineage-restricted astrocyte precursor cells using STEMdiff™ differentiation kits for 21 days. The second step was used to generate mature astrocytic cells from astrocytic precursor cells using STEMdiff™ maturation kits for over 14 days. NPCs were cultured and differentiated according to manufacturer's protocol (section 2.2.1). The protocol includes multiple passaging steps to eradicate the neuronal cells to promote the enrichment of astrocytic cells in culture. Astrocytic precursor cells and the mature astrocytic cells were characterised and confirmed using ICC staining (section 2.2.4).

2.2.2.3.1 Astrocytic Cells Differentiation Method

Human iPSC-derived NPCs were seeded onto pre-coated 6-well plates with PLO/Laminin at densities ranging from 4×10^4 - 6×10^4 cells/cm² in Axol Neural maintenance basal medium and incubated overnight at 37°C and 5% CO₂. Next day, the medium was replaced with pre-warmed complete STEMdiff™ astrocyte differentiation medium (ADM) for 21 days, and a full medium was changed every other day. Cells were passaged at approximately 90 - 95% confluency or weekly (Fig. 2.2) by washing once with 1ml D-PBS, and then the cells dissociated with 1ml Accutase at 37°C and 5% CO₂ for 5 minutes. The cells were transferred into a 15ml sterile conical tube with 4ml DMEM and centrifuged for 5 minutes at speed of 200 x g. The pellet was re-suspended in 1ml complete STEMdiff™ ADM, and then the cells were plated at a density of 1×10^5 cells/cm². On day 21, the generated astrocytic precursors expanded. Additionally, the astrocytic precursor cells at day 21 were frozen for long-term storage in liquid nitrogen containers using cryopreservation method. Astrocytic precursor cells pellet 2×10^6 cells/ml (2M cells) was re-suspended with 1ml of STEMdiff™ ADM containing 10% dimethyl sulfoxide (DMSO) (Sigma-Aldrich, UK), and stored at -80°C overnight, and then transferred to liquid nitrogen container.

2.2.2.3.2 Astrocytic Cells Maturation Method

For astrocyte maturation, the astrocytic progenitor cells were plated in pre-coated 6-well plates with PLO/Laminin at a density of 1.5×10^5 cells/cm² in complete STEMdiff™ astrocyte

maturation medium (AMM) and incubated overnight at 37°C and 5% CO₂. Cells were fuelled by pre-warmed complete STEMdiff™ AMM every other day. The cells were passaged weekly or at approximately 90 - 95% confluency and seeded at the same cell density for 14 days (Fig. 2.2). At day 35 - 40 astrocytic cells were transferred to astrocytes medium (AM), at which stage they could be cultured and expanded or cryopreserved, by re-suspending the astrocytic cell pellets 2×10^6 cell/ml (2M cells) in 1ml of STEMdiff™ AMM or AM containing 10% DMSO (section 2.2.2.3.1).

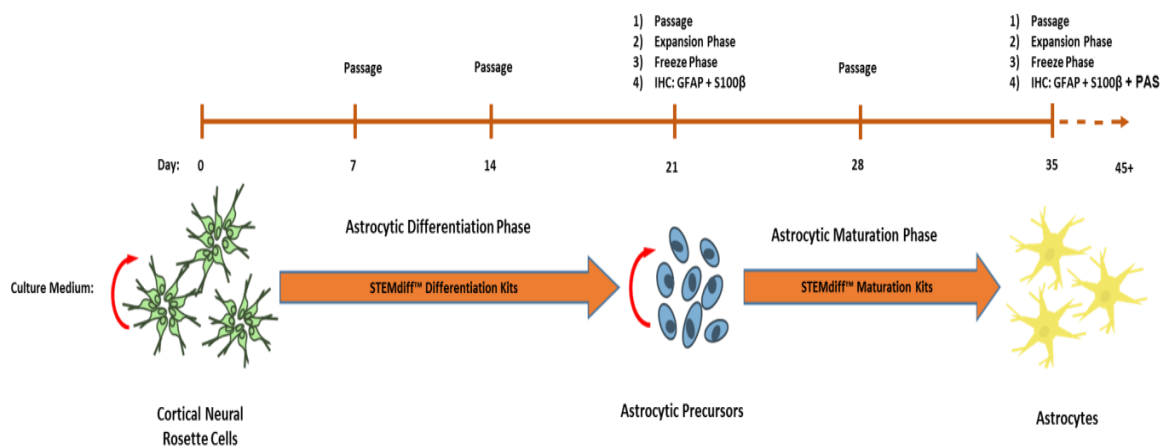


Figure 2.2: Diagrammatic overview of differentiation and maturation methods to generate enriched astrocytes over 45 days. A two-step protocol was utilised for generation of astrocytic cells from hiPSC-derived NPCs. Astrocytic differentiation phase: cultured the cortical hiPSC-derived NPCs with STEMdiff™ differentiation kits for 21 days to generate astrocytic precursor cells. Astrocytic maturation phase: cultured the astrocytic precursor cells with STEMdiff™ maturation kits for over 14 days to produce mature astrocytic cells. The cells were passaged 4 - 5 times during the differentiation and maturation periods (~7 days between passages).

2.2.3 Cultures and Expansion of Cell Lines and Primary Human Cultures

2.2.3.1 Human Primary Astrocytic Cells

Human primary astrocytic cells (HA) were obtained from ScienCell Research Laboratories (California, USA). HA cells were cultured in AM containing basal astrocyte medium supplemented with 2% foetal bovine serum, 1% Astrocyte growth supplement, 10,000U/ml penicillin and 10,000µg/ml streptomycin (all from ScienCell Research Laboratories, California, USA). The HA were culture-expanded in pre-coated 75cm³ cell culture flask (Corning®, USA) using 3ml of 0.1mg/ml poly-D-Lysine hydrobromide (Sigma-Aldrich, UK) and incubated overnight at 37°C). The cells were passaged after reaching 70 - 90% confluency; cells were passaged by washing the cells once with 5ml D-PBS, and then incubated with 3ml 1X Trypsin-EDTA (Sigma-Aldrich, UK) at 37°C for 5 minutes. 7ml of AM was added to the flask and transferred into a 15ml sterile conical tube and centrifuged for 5 minutes at speed of 200 x g. The supernatant was discarded, and pellet was re-suspended in 1ml of AM and the cell count was performed using trypan blue solution (Sigma-Aldrich, UK) and a haemocytometer (Counting Chamber) (Weber Scientific International LTD, UK). Before seeding the cells, the pre-coated 75cm³ culture flask was washed twice with 5ml sterile distilled water. HA cells were plated in 75cm³ cell culture flask at a density of 5 x10⁶ cell/ml (5M cells) or 1:5 diluted in AM. After plating, the cells were maintained by incubation at 37°C in a humidified atmosphere of 5% CO₂. The medium was replaced with pre-warmed AM every 2 days. These cells were expanded through 10 passages according to the manufacturer's instructions.

2.2.3.2 C2C12 Cell Line

The C2C12 cell line was used to detect the presence of glycogen stores as positive control using glycogen storage assay (section 2.2.6). C2C12 cells are a myoblast cell line and were established from normal adult C3H mouse leg muscle. The C2C12 cell line was supplied by European collection of authenticated cell cultures (ECACC). The myoblast cells were cultured in DMEM–high glucose containing 4.5g/L glucose with Glutamax (Invitrogen, Paisley, UK), supplemented with 2mM L-Glutamine, 100U/ml Penicillin and 100µg/ml Streptomycin and 10% (v/v) FBS. Cells were culture-expanded in 75cm³ cell culture flask and passaged after reaching 70% confluency or every 2 days (to avoid spontaneous differentiation). Afterwards, cells were passaged by washing twice with 5ml D-PBS. Cells were then dissociated with 1X Trypsin-EDTA and then incubated for 5 - 10 minutes at 37°C. The cells were transferred into

a 15ml sterile conical tube with 9ml DMEM and centrifuged for 5 minutes at 200 x g. The pellet was re-suspended in 1ml supplemented DMEM. Cells were plated at a density of 1×10^5 cells/cm² of surface area of 12-well culture plates for glycogen storage assay (section 2.2.6.1). After plating, the cells were maintained by incubation at 37°C in a humidified atmosphere of 5% CO₂. The Medium was replaced with pre-warmed complete medium every two days.

2.2.3.3 SH-SY5Y Cell Line

The SH-SY5Y cell line was used in glycogen storage assay (section 2.2.6) as a negative control as these cells do not store glycogen. The SH-SY5Y cell line is a neuroblastoma of a thrice cloned sub line of the neuroepithelioma cell line, SK-N-SH (Ross *et al.*, 1983). The parental cell line was derived from a bone marrow biopsy in 1970 from a young girl with metastatic neuroblastoma. SHSY5Y cells were cultured and expanded in RPMI-1640 medium (Sigma-Aldrich, UK), supplemented with 100U/ml Penicillin and 100µg/ml Streptomycin and 10% FBS. Cells were culture-expanded in 75cm³ cell culture flask and passaged after reaching 80 - 90% confluency. Cells were passaged by washing the cell once with 5ml D-PBS, and then the cells dissociated with 1X Trypsin-EDTA and then incubated for 5 minutes at 37°C. Afterwards, cells were transferred into a 15ml sterile conical tube with 9ml DMEM and centrifuged for 5 minutes at 200 x g. The pellet was re-suspended in 1ml complete DMEM. Cells were then plated at a density of 1×10^5 cells/cm² of surface area of culture vessel of 12-well culture plates for glycogen assay (section 2.2.6.1). After plating, the cells were maintained by incubation at 37°C in a humidified atmosphere of 5% CO₂. The medium was replaced with pre-warmed supplemented RPMI-1640 medium every two days.

2.2.4 Histochemical Staining Assays

2.2.4.1 Glycogen Staining

To define and confirm the existence of cytosolic localisation of glycogen in HA cells, astrocytic cells derived from hiPSCs were demonstrated using Periodic Acid-Schiff (PAS) protocol (Rosenberg and Dichter, 1985). This method was used for staining and detecting macromolecules such as glycogen stored in human astrocytes. Cells grown on 16mm glass coverslips (section 2.2.2.3.2 and 2.2.3.1) were washed twice with ice-cold D-PBS, and then fixed with methanol for 5 minutes at room temperature. Subsequently, the coverslips were rinsed 3 times with 70% (v/v) ethanol for 5 minutes, and then 1ml of 1% Periodic acid (w/v)

(dissolved in 70% ethanol) was added to the cells and incubated for 30 minutes at room temperature. Next, the cells were washed 3 times with 70% ethanol and stained with 500µl of 0.5% (w/v) basic fuchsin (Sigma-Aldrich, UK) for one hour at room temperature. The 0.5% basic fuchsin stock was prepared by dissolving in acid ethanol (80% ethanol, 19% distilled water and 1% concentrated HCl). After incubation, the cells were rinsed three times with 70% Ethanol and the coverslips were mounted on glass slide with mounting medium with DAPI (Vectashield, UK) and incubated overnight in dark at room temperature.

2.2.4.2 Immunohistochemical Staining

The immunocytochemical staining was used to confirm and characterise cells. For ICC all the cells were cultured on 16mm glass coverslips (section, 2.2.1, 2.2.2 and 2.2.3.1). The cells were washed twice with ice-cold D-PBS, and then fixed in 4% paraformaldehyde (PFA) (Sigma-Aldrich, UK) for 15 - 30 minutes at room temperature. Next, cells were rinsed twice with D-PBS and the fixed cells were preserved with 0.05% (v/v) Sodium azide (Sigma-Aldrich, UK) for later staining. The fixed cells were incubated at room temperature for one hour in blocking buffer (0.2% Triton X-100 (Sigma-Aldrich, UK), 2% (w/v) Bovine serum albumin (BSA) (Sigma-Aldrich, UK) in D-PBS for permeabilization. After incubation, blocking buffer was replaced with the appropriated primary antibodies diluted in blocking buffer (Table 2.2) and incubated for 2 hours at room temperature on gyro-rocker or overnight incubation at 4°C. Following incubation, the cells were washed 3 times with blocking buffer for 5 minutes each. Subsequently, the cells were incubated with diluted secondary antibodies in blocking buffer (Table 2.2) and covered with foil for one hour at room temperature on a gyro-rocker (Stuart®, UK). Coverslips were then washed 3 times with blocking buffer for 5 minutes each, and then washed twice with D-PBS. The coverslips were counterstained on the slide using a drop of mounting medium containing DAPI (Vectashield, UK) and incubated overnight in dark at room temperature.

2.2.4.3 Synaptic Marker Staining

To assess the presence of synaptic markers within the neuronal culture (section 2.2.2.1) cells were stained with synaptic marker staining method. Cells cultured on 16mm glass coverslips were washed twice with ice-cold D-PBS, and then fixed by 4% PFA for 15 - 30 minutes at room temperature. Next, cells were rinsed twice with D-PBS and the fixed cells were stained immediately or preserved with 0.05% Sodium Azide (Sigma-Aldrich, UK) for later staining. The

fixed cells were washed three times with 50mM Ammonium Chloride (Sigma-Aldrich, UK). Next, 1ml of Ammonium Chloride solution was added and incubated for 5 minutes. After aspiration of Ammonium Chloride solution, 1ml of 0.1% Saponin (Sigma-Aldrich, UK) in D-PBS was added and incubated for 10 minutes. Afterwards, the saponin solution was removed, and 1ml of blocking buffer (D-PBS containing 3% BSA and 0.1% saponin) was added and incubated for 30 minutes. Subsequently, the primary antibody was diluted in blocking buffer (Table 2.2). 200µl of primary antibody solution was added to the top of a piece of parafilm (Bemis, USA) on wet 3MM CHR Whatman chromatography paper (Whatman International LTD, UK) and then coverslips were placed upside down on primary antibody solution and incubated for 1 hour at room temperature. After incubation, the coverslips were transferred back to the 12-well plate and washed twice with 0.1% saponin in D-PBS. Subsequently, the cells were incubated for 10 minutes with blocking buffer. 200µl of secondary antibody diluted in blocking buffer (Table 2.2) was then added to the cells and incubated for 1 hour at room temperature. After incubation, the cells were washed twice with 0.1% saponin in D-PBS, and then washed twice with D-PBS. The stained coverslips were mounted on slides by a drop of mounting medium containing DAPI and incubated overnight in dark at room temperature.

2.2.4.4 Co-Staining

HA cells and the astrocytes derived from hiPSC-derived NPCs from the healthy cell lines were co-stained for glycogen staining protocol (section 2.2.4.1), and then astrocytic marker S100β protocol (section 2.2.4.2). The coverslips were counterstained and mounted on the slide with DAPI and incubated overnight at room temperature.

2.2.5 Microscopes, Images Capture and Slides Storage

Cell images were captured using EVOS XL Core microscope (Life Technologies, UK) for phase contrast images, and Leica SP2 fluorescent microscope (Leica Microsystems, UK) for ICC staining images with 10x, 20x ("dry" objective lens magnification) and 63x (Immersion oil with objective lens) and Leica Application Suite X (LAS X) software, version 3.02. All the fluorescent slides were stored in the dark slide box at 4°C.

Marker	Expression	Primary Antibody		Secondary Antibody	
		Type/Species	Conc. Dilution	Type/Species	Conc. Dilution
Anti-Beta III Tubulin Antibody ab7751 (TUJ1) (Abcam) Cat. No. ab7751	General neuronal marker	Monoclonal Mouse	1:500	Donkey Anti mouse Rhodamine (Red) (Jackson ImmunoResearch) Lot no. 127016	1:1000
Pax6 (Biolegend) Cat. No 901301	Human neural progenitor development marker	Polyclonal Rabbit	1:300	Goat Anti Rabbit FITC (Green) (Jackson immunoResearch) Lot no. 112581	1:250
Sox2 (R&D system) Cat. No. MAB2018	Human stem cells marker	Monoclonal Mouse	1:100	Donkey Anti mouse Rhodamine	1:250
GFAP (Millipore) Cat. No mab360	Astrocytes Marker	Mouse	1:250	Donkey Anti mouse Rhodamine	1:200
S100 β (Dako) Lot. No. 00095194	Mature Astrocytes Marker	Rabbit	1:250	Goat Anti Rabbit FITC	1:200
Synaptophysin (Abcam) Cat. No. ab68851	Presynaptic terminals marker	Rabbit	1:1000	Goat Anti Rabbit FITC	1:500

PSD95 (Abcam) Cat. No. ab2723	Glutamatergic neurons, postsynaptic marker	Mouse	1:1000	Donkey Anti mouse Rhodamine	1:500
Nestin	Neural stem cell intermediate filament	Monoclonal Mouse	1:100	Donkey Anti mouse Rhodamine	1:250

Table 2.2: Table listing the different primary and secondary antibody markers used for ICC staining and synaptic markers staining for identification of NPCs and neural cells: neurons and astrocytes.

2.2.6 Determination of Glycogen Content Levels

2.2.6.1 Samples Preparation

Astrocytic cells were prepared and cultured with AM, and seeded at a density of 1×10^5 cells/cm² into pre-coated 12-well plates (triplicate wells) (section 2.2.2.3 and 2.2.3.1). The cells were ready and implemented after 2 days in culture, and washed three times with ice-cold D-PBS. Subsequently, 200µl of ice-cold D-PBS was added on the cells and scraped using cell scraper (Fisher Scientific, UK) and then transferred into 1.5ml microcentrifuge tubes (3 wells pooled) and sonicated using Ultrasonic processor (JENCONS Scientific LTD, UK) for 30 seconds with all the tubes kept on ice. 100µl of homogenised samples were removed as lysate for further analysis to measure the protein content using BCA assay (section 2.2.8). The homogenised samples were heated at 70°C using a heat block for 10 minutes. Afterwards, the samples were centrifuged for 3 minutes at 4°C at 13,000rpm, and then the supernatant were transferred into 1.5ml sterile microcentrifuge tube and stored at -80°C for glycogen stores analysis.

2.2.6.2 Glycogen Assay Protocol

The homogenised samples were diluted into 1:2 with D-PBS, and the diluted samples were mixed with 0.1M acetate buffer at a pH of 4.6. The diluted sample was divided equally into two separated microfuge tubes one tube was used to measure the amount of glycogen and the second tube for measuring the free glucose in the homogenised sample to subtract the readings. Next, an equal volume 1mg/ml Amyloglucosidase enzyme stock (AMG.S) (Sigma-Aldrich, UK), which was prepared by adding 75µl of Amyloglucosidase enzyme reagent (AMG) in 1ml of acetate buffer with a pH of 4.6. Afterwards, all the samples were incubated at 57.5°C on a heat block for 2 hours. After incubation, 30µl of sample was transferred into a 96-well plate and added 100µl of using Hexokinase enzyme reagent (HK) from glucose assay kit (Sigma-Aldrich, UK), and then mixed and incubated at room temperature for 15 minutes (Fig. 2.3). The absorbance was read at 370nm using Thermo multiscan EX 96-well plate reader (Thermofisher, UK). The protein content levels in the cell lysate samples were also determined using BCA assay to normalise the glycogen values (section 2.2.8). This method allowed us to measure the amount of glycogen levels in homogenised samples as well as the free glucose and glucose-6-phosphate.

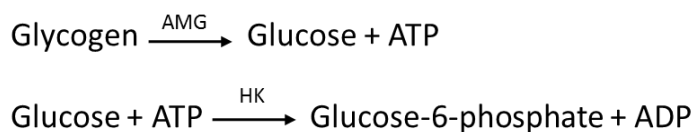


Figure 2.3: Chemical equation demonstrating the glycogen under glycogen assay analysis using AMG and HK enzymes.

2.2.7 Glycogen Breakdown Assays

The glycogen breakdown was investigated under hypoglycaemic conditions, and in response to pharmacological treatments to assess the maturity and functionality of the HA and the astrocytic cells derived from ax0018 cell line. These cells were assessed for their ability to build up and breakdown glycogen in response to physiological cues such as hypoglycaemia: 1,4-dideoxy-1,4-imino-d-arabinitol (DAB) (Sigma-Aldrich, UK) or drugs including: Dibutyryl cyclic adenosine monophosphate (dbcAMP) (Tocris, UK), Isoproterenol (Tocris, UK), Ouabain (Tocris, UK) and DL-threob-benzyloxyaspartic acid (TBOA) (Tocris, UK).

2.2.7.1 Astrocytic Cell Culture Preparation

The HA cells and the astrocytic cells derived from hiPSC-derived NPCs line (ax0018) were prepared as described in section 2.2.3.1 and 2.2.2.3, respectively. The astrocytic cells were plated at a density of 1×10^5 cells/cm² on a 12-well plate in triplicate wells (3 wells pooled) (three independent cultures). After 2 days of plating, the cells were washed once with D-PBS and then treated with either DAB, dbcAMP, Isoproterenol, Ouabain and TBOA in Krebs'-Ringer HEPES buffer (KRH) according to the following experiments. The KRH buffer was made with a pH of 7.4, and was composed of 115mM sodium chloride, 5mM potassium chloride, 1mM magnesium chloride, 24mM sodium bicarbonate, 2.5mM calcium chloride dehydrate, 25mM HEPES (Sigma-Aldrich, UK), prepared in 0.5L distilled water. The KRH buffer was sterile filtered through 0.2µm filter (Fisher Scientific, UK) and stored at 4°C. The glycogen content was determined using glycogen assay (section 2.2.6), and protein content was determined using BCA assay (section 2.2.8). The same procedure was utilised for the following treatments.

2.2.7.2 Hypoglycaemic Conditions Assay

The astrocytic cells were exposed to 10 μ M DAB in KRH buffer without glucose for starvation conditions. Cells were incubated for 0, 60 and 180 minutes at 37°C in a humidified atmosphere of 5% CO₂.

2.2.7.3 Pharmacological Treatment

Astrocytic cells were treated with 1mM dbcAMP and 100 μ M Isoproterenol independently in KRH buffer supplemented with 5mM glucose, and then incubated for 0 and 180 minutes at 37°C in a humidified atmosphere of 5% CO₂.

2.2.7.4 Glutamate Treatment

To determine the effects of glutamate on astrocytes, cells were treated with 100 μ M Ouabain and 100 μ M TBOA in KRH buffer supplemented with 1mM L-Glutamic Acid (Sigma-Aldrich, UK) and 5mM glucose, and then incubated for 0, 60, 18 and 360 minutes at 37°C in a humidified atmosphere of 5% CO₂.

2.2.8 Determination of Protein Levels

Cell lysates were analysed using Bicinchoninic acid (BCA) assay Kit according to the manufacturer's instructions (Thermofisher, UK). Briefly, 25 μ l of BSA standard and cell lysate samples were added to a 96-well plate with 200 μ l of BCA working reagent (50:1 ratio of reagent A:B) and incubated for 30 minutes at 37°C. The absorbance was read at 590nm using Thermo multiscan EX 96-well plate reader (Thermofisher, UK).

2.2.9 Quantification and Statistical Analysis

All quantification and statistical analyses were done using Excel software 2013 (Windows 7) and GraphPad Prism 7 software (Version 7.00, GraphPad Software Inc., California USA). Data values were determined by variance ANOVA (One-way ANOVA or two-way ANOVA) with Dunnett's multiple comparisons test or Tukey's multiple comparisons. All values represent mean \pm SD, n=3 (each 'n' represents data replicate from an independent culture). Significant

comparisons were labelled in figures as ($P < 0.05$ (*), $P < 0.01$ (**), $P < 0.001$ (***) and $P < 0.0001$ (****)). The data for glucose assay and glycogen assay were normalised using the BCA values (Total cellular protein) before utilising them for creation of graphs. The quantification of hiPSC-derived neural cell subpopulations were performed and counted using software of ImageJ. The neural cells were counted with automated counting of the images (3 fields for each image). Firstly, the image was converted to greyscale before proceeding; Edit>Options>Conversions, then use Image>Type>16-bit to convert to greyscale. Secondly, use Image>Adjust>Threshold - then highlight all the area to be counted. Then, for merged particles; Process>Binary>Waters and cut them apart by adding a one pixel or more thick line. Lastly, to count use Analyze>Analyze Particles.

2.3 Results

2.3.1 Characterisation and Generation of ‘Healthy’ Human Brain Neural Cells from iPSC-derived NPCs

The neural cells derived the using spontaneous and synchronous differentiation neuronal methods (section 2.2.2.1 and 2.2.2.2) and astrocytic cells differentiation methods (section 2.2.2.3) were characterised by their morphology and by ICC staining for neuronal and astrocytic markers at different days of cell cultures. The ax0018 cell line was first characterised morphologically at the start of the differentiation process (section 2.3.1.1). The morphological and ICC staining findings for the different days of differentiation are presented separately in section 2.3.1.2. The cultures yielded mixed populations of astrocytes and neurons. The neuronal cells were also examined for synaptic markers to confirm synaptic formation and activity.

2.3.1.1 Characterisation of ‘Healthy’ Human iPSC-derived NPCs

The NPCs derived from ‘healthy’ hiPSC control line ax0018 (Fig. 2.4) were positively identified at day zero using ICC staining for the neural precursor cell markers sox2, pax6 and nestin (an intermediate filament protein and NPCs marker), after 2 passages. Cortical neural rosettes are morphologically identifiable structures in cultures under phase contrast microscopy (Fig. 2.4A). Human iPSC-derived NPCs were differentiated into cortical neurons using spontaneous and synchronous differentiation methods over a period of 40 days. Additionally, the NPCs were differentiated into astrocytes using differentiation and maturation methods and cultured for up to 5 weeks.

2.3.1.2 Characterisation and Differentiation of ‘Healthy’ Human iPSC-derived NPCs Control Cell Line

2.3.1.2.1 Spontaneous Differentiation Method

Human iPSC-derived NPCs from control cell lines ax0018 cell line was differentiated using the spontaneous differentiation method (section 2.2.2.1) to produce mature mixed cerebral

cortical neurons and astrocytes cultures over a 40 day period. The phase contrast images of neural cells demonstrate extensive neurite outgrowth which started to appear from days 10 and 20 (Fig. 2.5A and 2.6A), forming denser neural networks by days 30 and 40 (Fig. 2.7A and 2.8A). Cortical neurons were identified using ICC staining at days 10, 20, 30 and 40 by positive expression of the TUJ1 general neuronal marker (Fig. 2.5B, 2.6B, 2.7B and 2.8B, respectively). Spontaneous differentiation method also resulted in the differentiation of the cells into S100 β -positive astrocytes at days 10, 20, 30 and 40 (Fig. 2.5C, 2.6C, 2.7C and 2.8C, respectively). There was no detectable pre-synaptic marker synaptophysin or post-synaptic marker PSD-95 (postsynaptic density protein 95) at days 10 and 20 (data not shown). However, synaptic markers were detected at days 30 and 40 using synaptophysin (Fig. 2.9A and 2.10A, respectively) and PSD-95 (Fig. 2.9B and 2.10B, respectively).

2.3.1.2.2 Synchronous Differentiation Method

Human iPSC-derived NPCs from control cell lines ax0018 cell line was cultured using the synchronous differentiation method which involved treating the cells with 10 μ M DAPT for 5 days (section 2.2.2.2) to produce cerebral cortical neuronal cell population within 40 days. The phase contrast images of neuronal cells demonstrated extensive neurite outgrowths and morphology by day 10 (Fig. 2.5B), with typical extensive neurite networks by days 20, 30 and 40 (Fig. 2.6B, 2.7B and 2.8B, respectively). The NPCs were differentiated into TUJ1-positive expressing cortical neuronal networks and the networks became denser over time from day 10 to 40 of culture (Fig. 2.5D, 2.6D, 2.7D and 2.8D, respectively). Synchronous differentiation method also led to the successful differentiation of the cells into S100 β -positive astrocytes at days 10, 20, 30 and 40 (Fig. 2.5F, 2.6F, 2.7F and 2.8F, respectively). Likewise, synaptophysin and PSD-95 expression were not detectable at days 10 and 20 (data not shown). Whereas, at days 30 and 40 synaptic markers were detected by positive expression of synaptophysin (Fig. 2.9D and 2.10D) and PSD-95 (Fig. 2.9E and 2.10E).

2.3.1.2.3 Characterisation of Human iPSC-derived Astrocytic Cells

Mature astrocytic cells were produced from 'healthy' control hiPSC-derived NPCs cell line (ax0018). The human cortical neural rosettes were differentiated into mature astrocytes by employing a sequential two-phase methods; using astrocyte differentiation protocol to generate astrocytic progenitors for 3 weeks (section 2.2.2.3.1). This was followed by the

astrocyte maturation protocol over a period of 2 weeks to yield mature astrocytic cells (section 2.2.2.3.2).

Astrocytes derived from ax0018 cell line were identified and stained using ICC staining using the astrocytic markers after day 21 in astrocyte differentiation medium. The morphology of the astrocyte progenitors was assessed via phase-contrast images (Fig. 2.11A). The hiPSC-derived astrocyte progenitors positively expressed the astrocytic markers GFAP and S100 β (Fig. 2.11B and C, respectively).

Phase-contrast images of astrocytes in culture of both control lines after 45+ days in astrocyte maturation medium displayed the stellate morphology (Fig. 2.12A). The mature astrocytes and neural progenitors positively stained for GFAP (Fig. 2.12B), whereas mature astrocytes were primarily S100 β positive (Fig. 2.12C). Astrocytic culture of line ax0018 expressed a low number of neuronal lineage marker TUJ1-positive (Fig. 2.12F). The cell cultures of the ax0018 cell line showed positive staining for GFAP 42.02%, S100 β 53.15% and TUJ1 3.50% (Fig. 2.12).

Human iPSC-derived astrocytic cells also stained positively for glycogen using PAS staining (Fig. 2.13A and B). The glycogen in astrocyte cells were found to co-localised within the cytoplasm of cells that also stained positively for S100 β (Fig. 2.13C). To definitively identify glycogen in astrocytic cells, cell lysates were analysed using a glycogen assay to determine the amount of glycogen content level in the astrocytic cells (section 2.3.3).

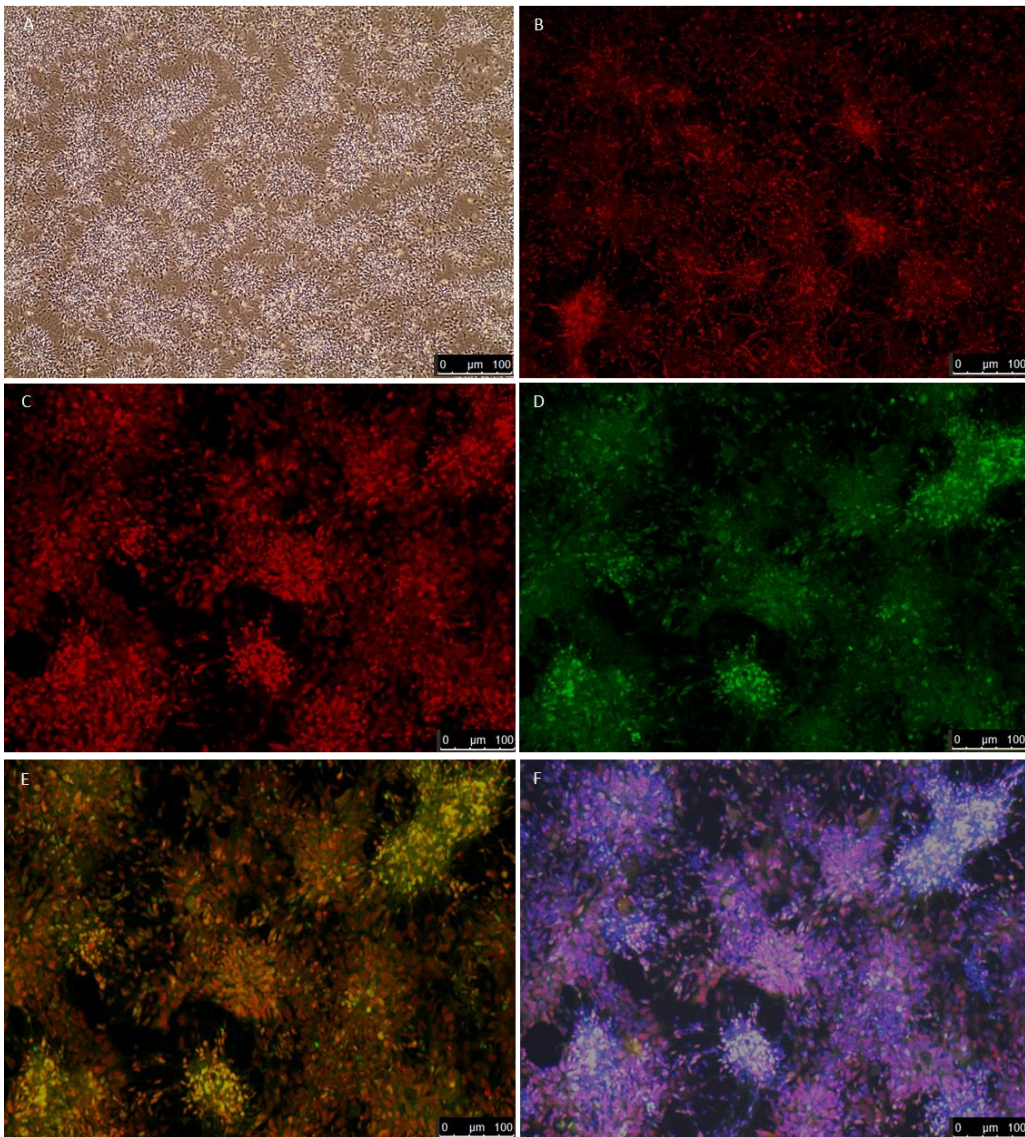


Figure 2.4: Representative images of 'healthy' hiPSC-derived NPCs from cell line ax0018 using ICC staining. A phase contrast image demonstrating the neural rosettes feature of human healthy control NPCs (A). The NPCs were stained for neural precursor cells antibodies against nestin (red, B), sox2+ (red, C) and pax6+ (green, D). Merged image showing co-expression of both pax6+ and sox2+ (E). Cells were counterstained with DAPI+ (blue, F). Cells were stained at passage number 2, n=3. Scale bars: 100μM.

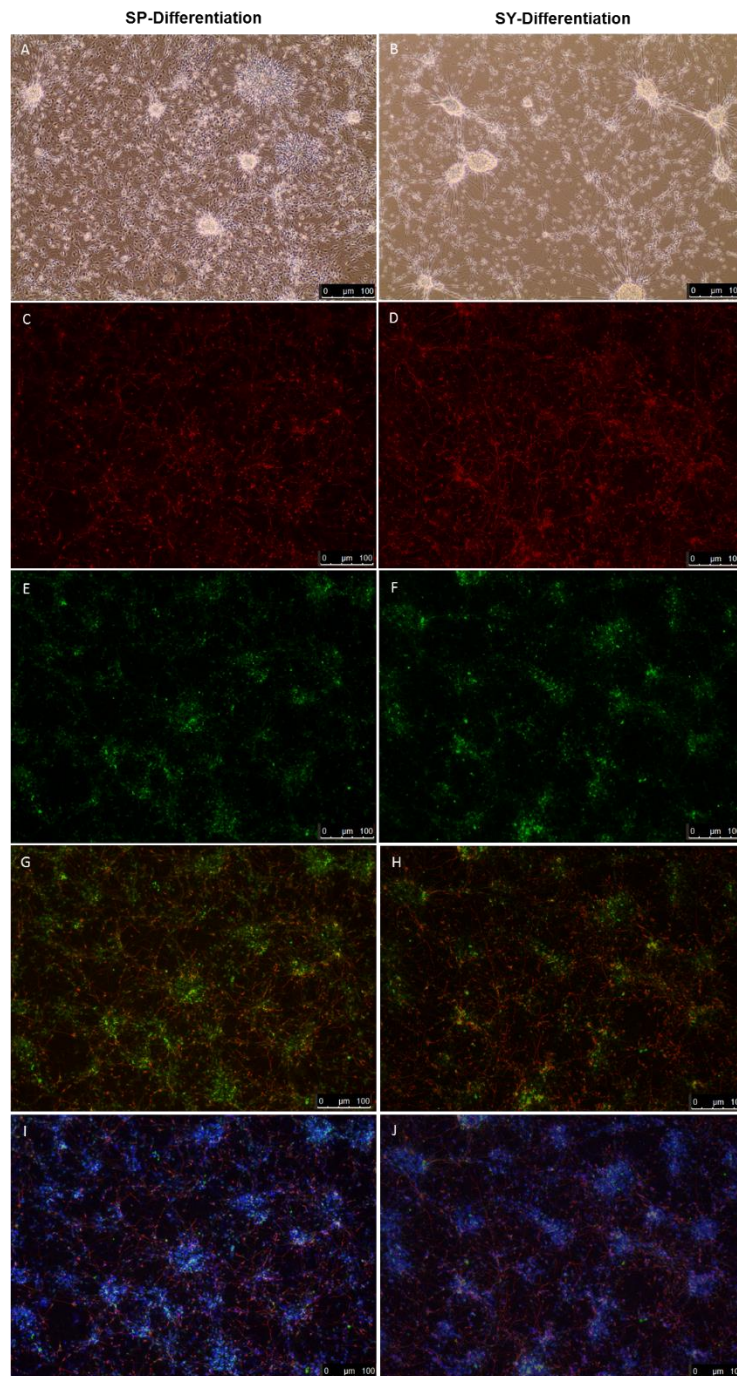


Figure 2.5: Representative images presenting the development of neural cells from 'healthy' hiPSC-derived NPCs of ax0018 cell line following cultures in spontaneous and synchronous differentiation methods at day 10. A and B showing phase contrast images of differentiation cells. Immunofluorescent images showing neuronal cells that was confirmed using a TUJ1+ marker of positive neurons (red, C and D). Astrocytes were identified using S100 β + marker (green, E and F). Merged image showing expression of both TUJ1+ and S100 β + (G and H). Nuclei were counter stained with DAPI+ (blue, I and J). n=3. Scale bars: 100 μ M.

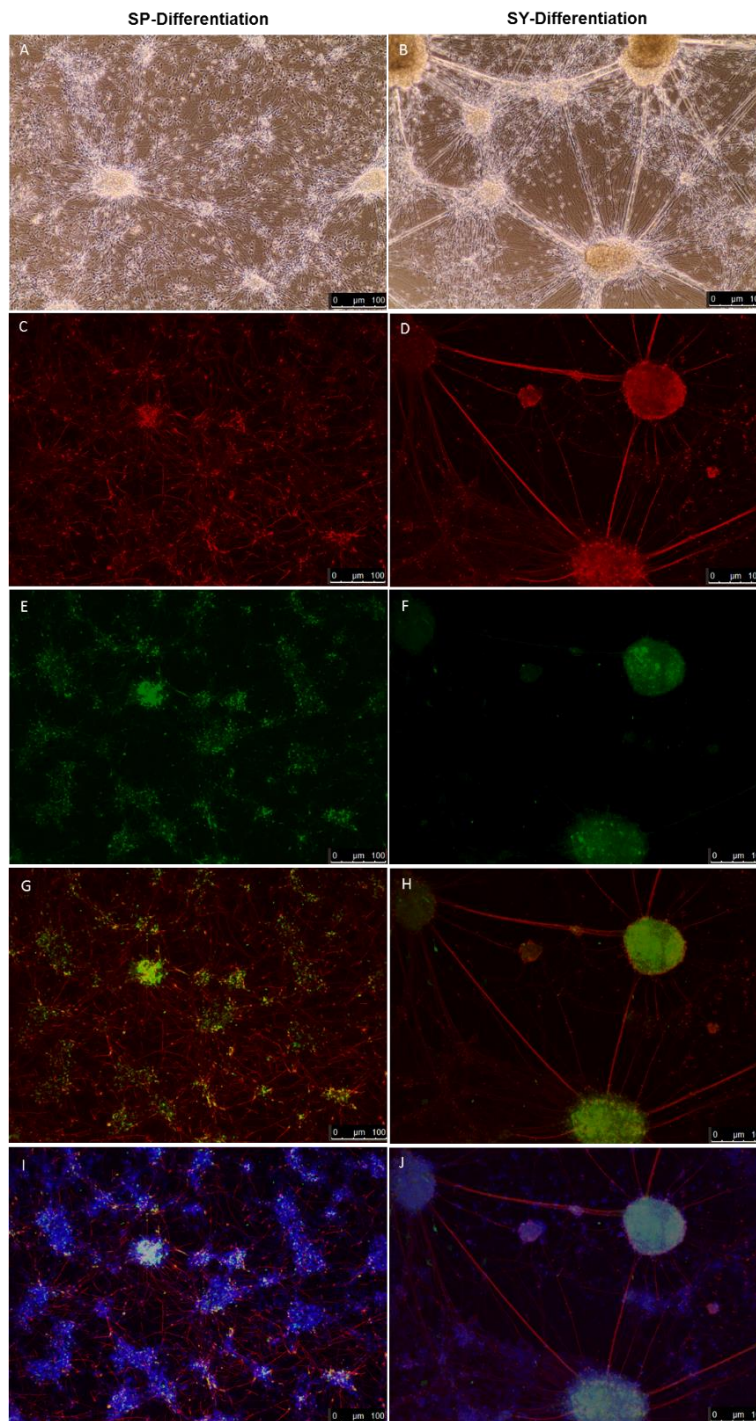


Figure 2.6: Representative images showing the development of neural cells from ‘healthy’ hiPSC-derived NPCs of cell line ax0018 in spontaneous and synchronous differentiation methods at day 20. A and B showing phase contrast images of the differentiating cells. Immunofluorescent images presenting neuronal cells that was confirmed using a TUJ1+ (red, C and D). Astrocytic cells were identified using S100 β + marker (green, E and F). Merged image showing co-expression of both TUJ1+ and S100 β + (G and H). Nuclei were counter stained with DAPI+ (blue, I and J). n=3. Scale bars: 100 μ M.

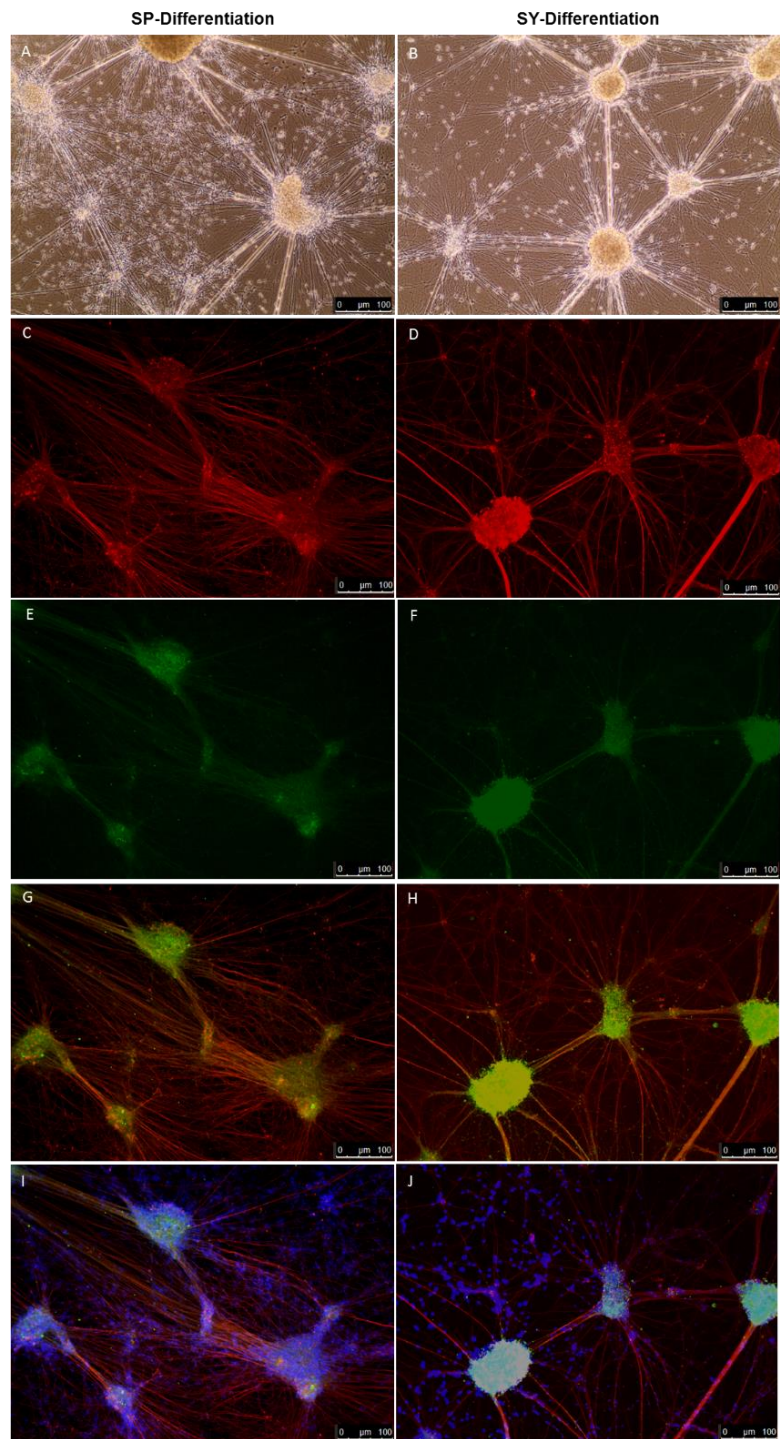


Figure 2.7: Representative images showing the development of neural cells at day 30 in spontaneous and synchronous differentiation cultures from line ax0018 of 'healthy' hiPSC-derived NPCs. A and B showing phase contrast images of neural cells in network of the differentiation cells. Immunofluorescent images presenting a network neuronal cells that was confirmed using a TUJ1+ (red, C and D). Astrocytic cells were identified using S100 β + marker (green, E and F). Merged image showing co-expression of both TUJ1+ and S100 β + (G and H). Nuclei were counter-stained with DAPI+ (blue, I and J). n=3. Scale bars: 100 μ M.

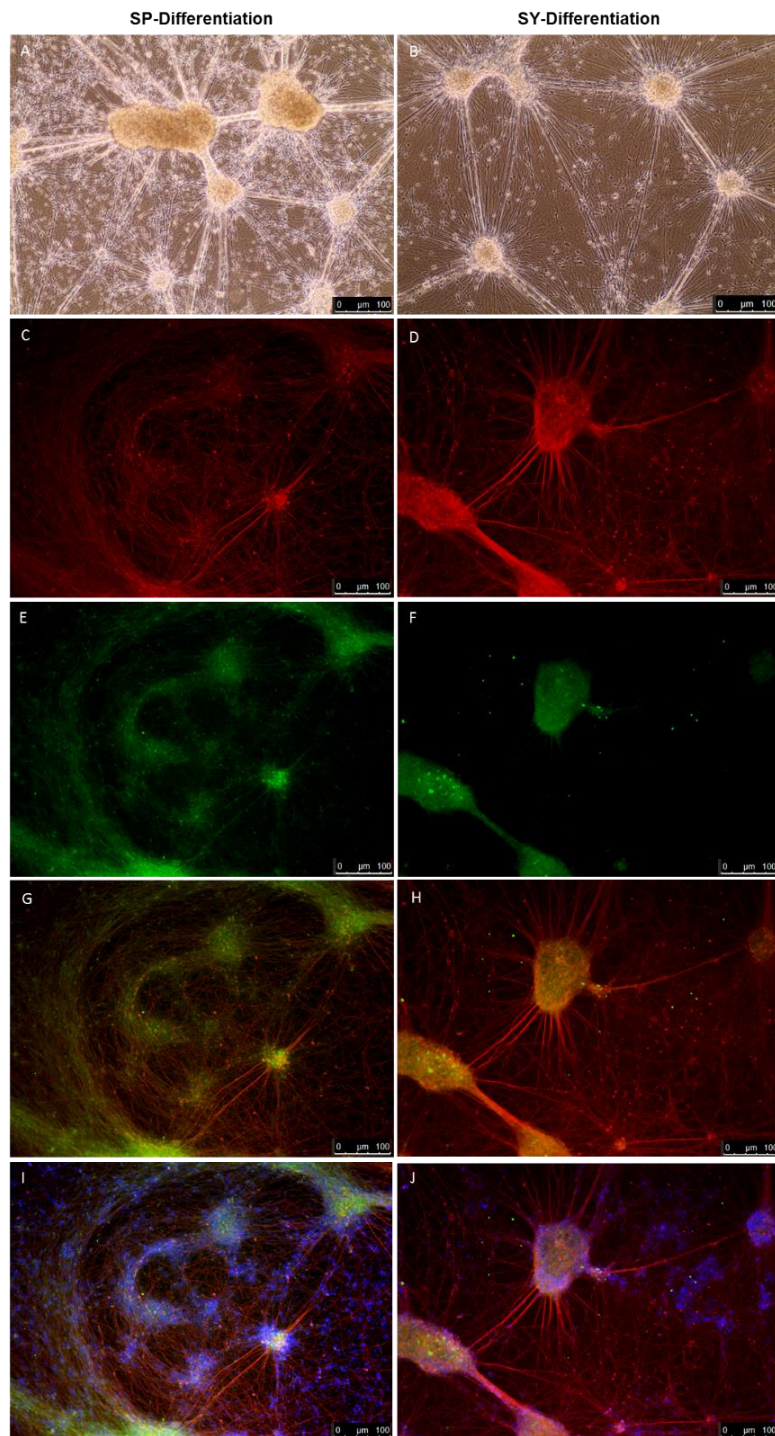


Figure 2.8: Representative images illustrating the development of neural cells at day 40 in spontaneous and synchronous differentiation cultures from line ax0018 of 'healthy' hiPSC-derived NPCs. A and B showing phase contrast images of neural cells in network of the differentiation cells. Immunofluorescent images showing a network neuronal cells that was confirmed using a TUJ1+ (red, C and D). Astrocytes were identified using S100 β + marker (green, E and F). Merged image showing co-expression of both TUJ1+ and S100 β + (G and H). Nuclei were counter stained with DAPI+ (blue, I and J). n=3. Scale bars: 100 μ M.

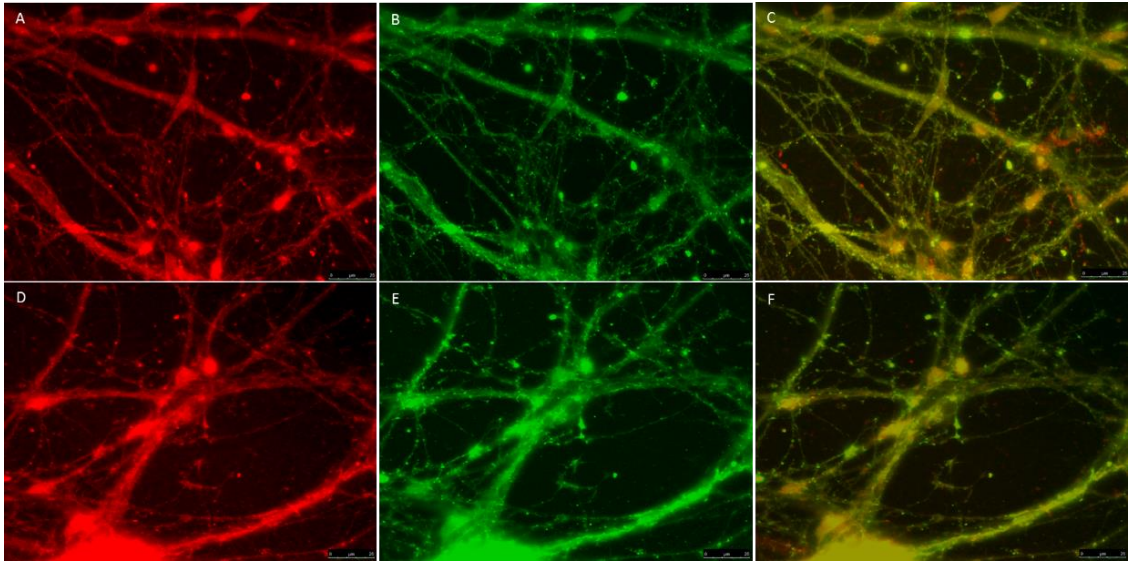


Figure 2.9: Immunofluorescent images of synaptic markers expression in neural cells derived from hiPSC-derived NPCs of line ax0018 using SP-differentiation (A-C) and SY-differentiation (D-F) at day 30. Synaptic formation is confirmed by positivity of synaptophysin+ (red, A and D) and PSD95+ (green, B and E). Merged image showing expression of both synaptic markers (C and F). n=3. Scale bars: 25 μ M.

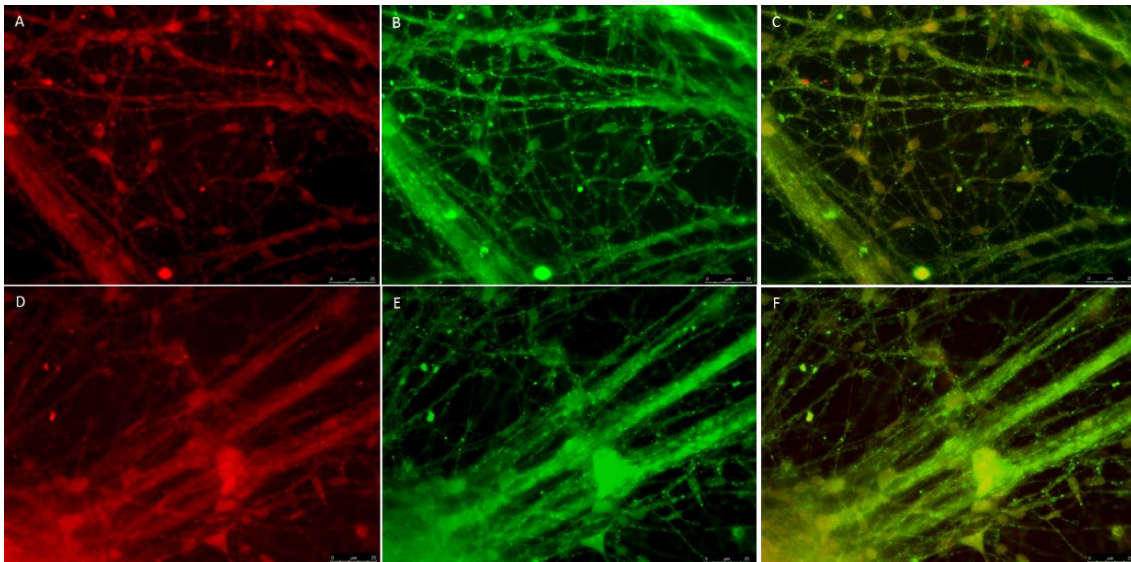


Figure 2.10: Immunofluorescent images of synaptic markers expression in neural cells derived from hiPSC-derived NPCs of line ax0018 using SP-differentiation (A-C) and SY-differentiation (D-F) at day 40. Synaptic formation is confirmed by positivity of synaptophysin+ (red, A and D) and PSD95+ (green, B and E). Merged image showing expression of both synaptic markers (C and F). n=3. Scale bars: 25 μ M.

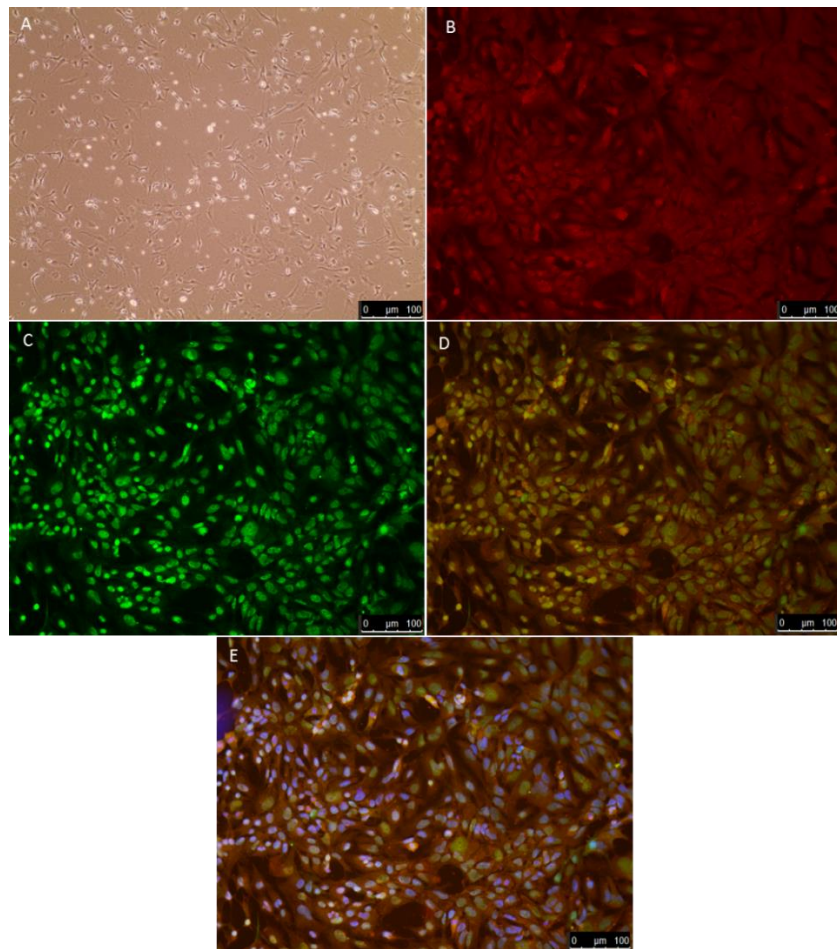


Figure 2.11: Representative images showing ICC staining of hiPSC-derived astrocytic progenitor cells at day 21. The ax0018 cells were cultured using ADM and AMM differentiation methods. (A) Shows a phase contrast image of the differentiating astrocyte precursor cells. Immunofluorescent images confirming early astrocytic differentiation using GFAP+ (red, B). The developing astrocyte cells were also identified using S100 β + marker (green, C). Merged image showing expression of both GFAP+ and S100 β + (D). Nuclei were counter stained with DAPI+ (blue, E). n=3. Scale bars: 100 μ M.

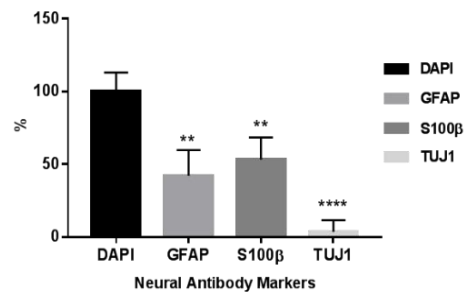
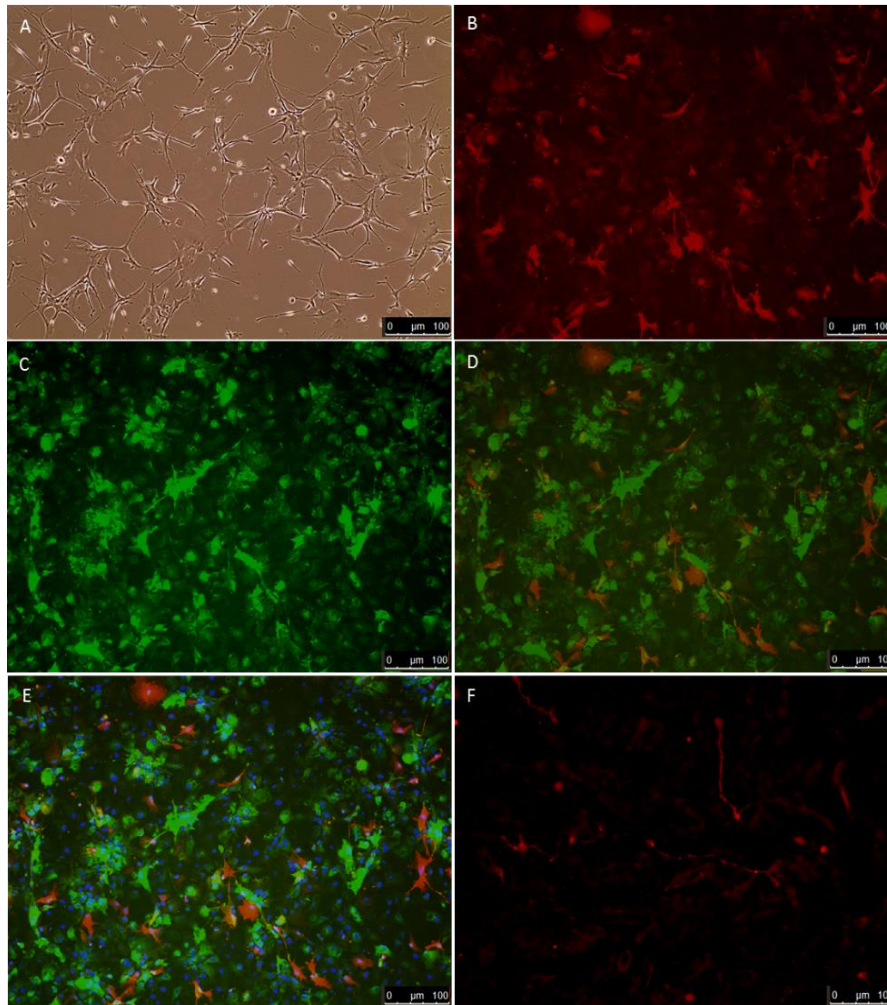


Figure 2.12: Representative images showing ICC staining of hiPSC-derived astrocytic cells from line ax0018 at day 45+. The cells were cultured using the astrocytes differentiation and maturation protocols. (A) Shows a phase contrast image of the astrocyte cells. Immunofluorescent images of astrocytic markers GFAP+ (red, B), S100β+ (green, C) and TUJ1+ neuronal marker (F). Merged image showing expression of both GFAP+ and S100β+ (D). Nuclei were counter stained with DAPI+ (blue, E). Scale bars: 100μM. The graph shows the quantification of cell-types using ImageJ analysis of neural cell populations produced at this stage of differentiation, $n=3$, $P<0.0001$ (****) and $P<0.01$ (**). The statistical analysis was done using One-way ANOVA, Dunnett's post-test.

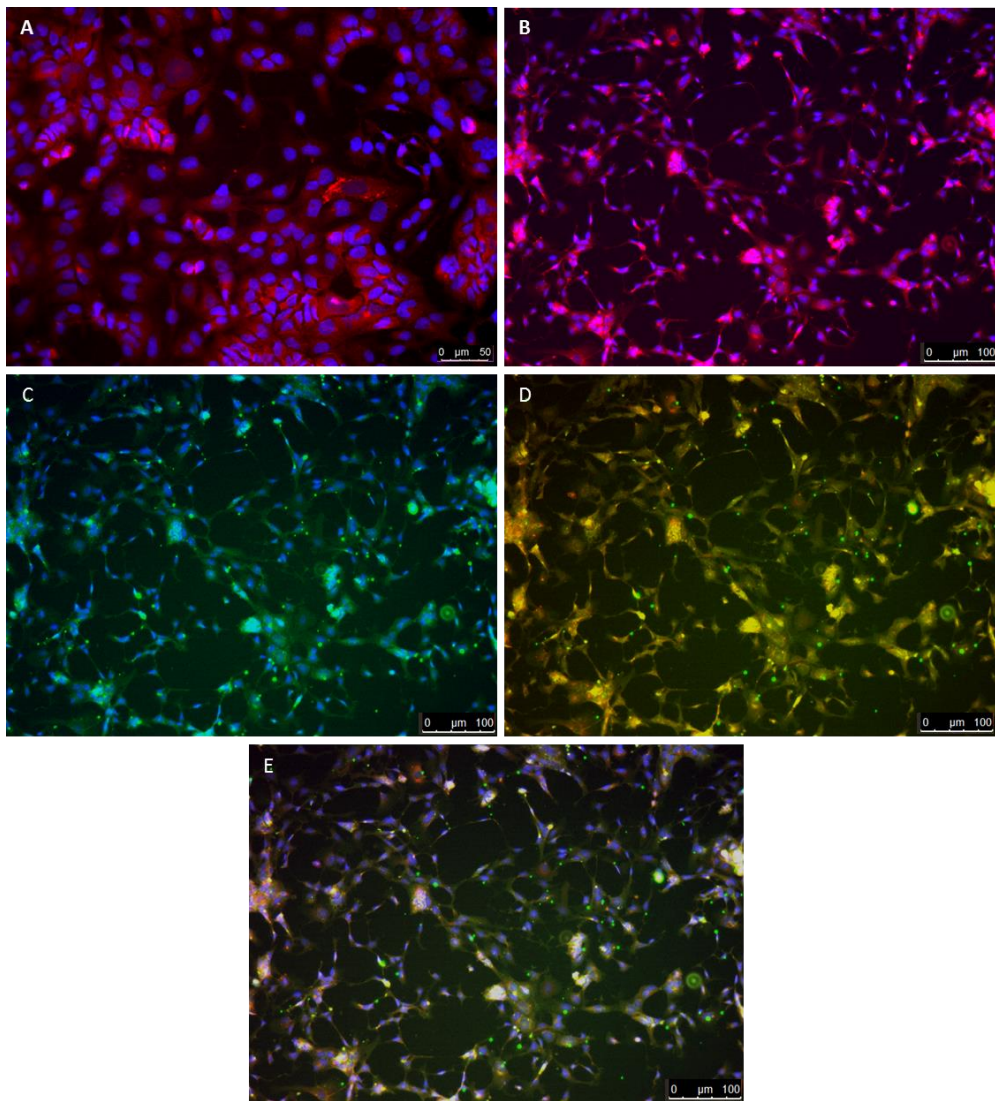


Figure 2.13: Representative images of hiPSC-derived astrocytic cells from line ax0018 at day 45+. PAS staining confirmed the presence of glycogen in astrocytes cells (red) (A and B). Cells were counterstained with DAPI+ (blue). Merged image showing expression of co-staining: S100 β + and PAS+ staining (C). Merged image showing expression of S100 β +, PAS+ staining and DAPI+ (D). n=3. Scale bars: 100 μ M and 50 μ M (A).

2.3.2 Characterisation of Human Primary Astrocytic Cells

HA were assessed microscopically to identify their characteristic morphology (section 2.2.3.1). The cells took up the typical stellate morphology on phase contrast (Fig. 2.14A). The cells were stained using ICC staining using the astrocytic markers S100 β and GFAP. GFAP is an intermediate filament (astrocyte cytoskeleton) that is expressed in astrocytes and astrocytic progenitor cells, whereas S100 β is a calcium binding protein (found mainly in the cytosol of astrocytes) that is primarily expressed by mature astrocytes and astrocytic progenitor cells. These are common markers used to identify astrocytes. The cells stained positively for GFAP and S100 β markers (Fig. 2.14B, C and D, respectively). The astrocyte cells also stained positively for the presence glycogen stores with PAS staining (Fig. 2.14E), and S100 β co-staining (Fig. 2.14F). Glycogen assays were carried out to definitively confirm glycogen stores in astrocytic cells and provide quantitative analyses (section 2.3.3).

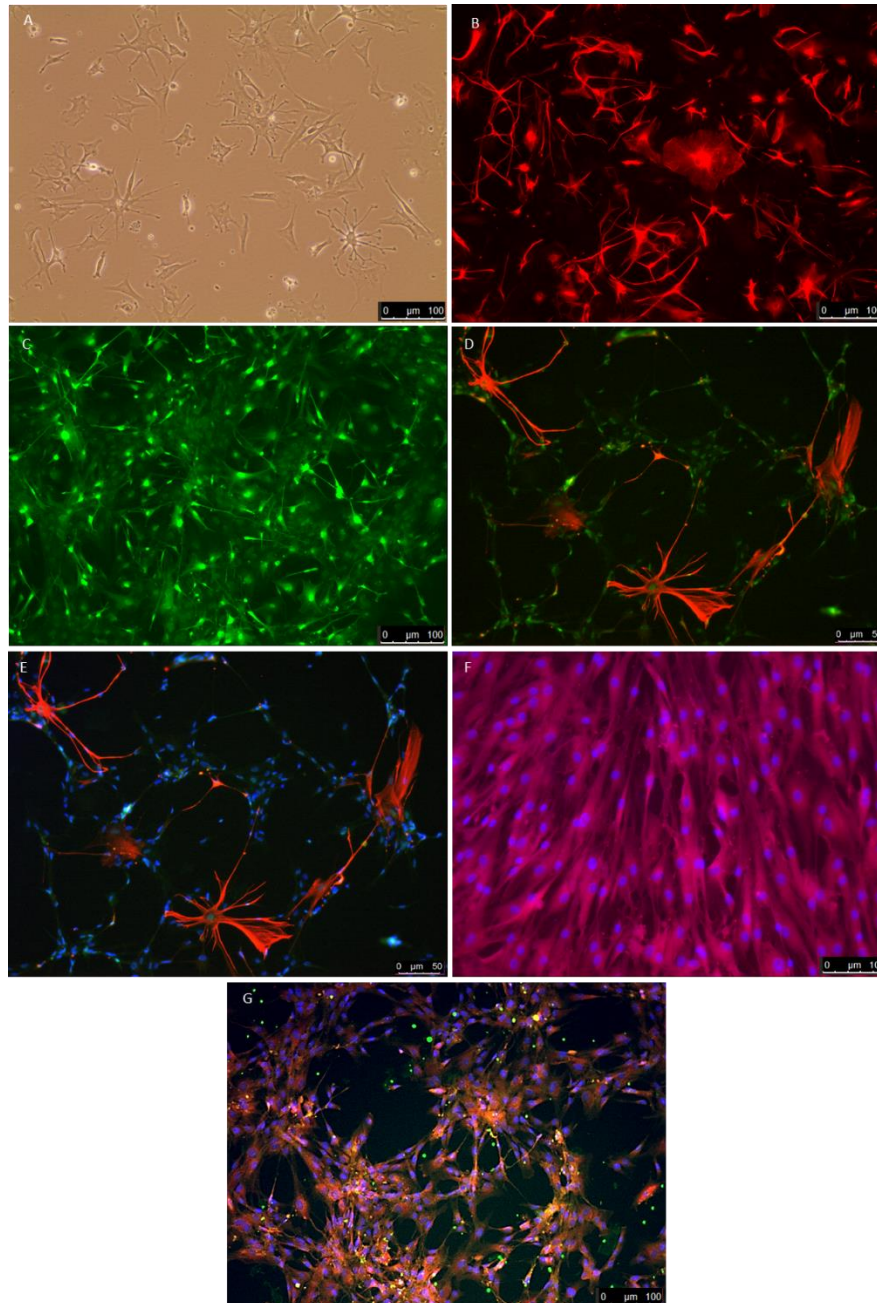


Figure 2.14: Representative images of HA cells using ICC staining. Phase contrast image illustrating the typical star-shaped appearance of the HA cells morphology (A). The cells were stained with ICC staining for common astrocytic markers: GFAP+ (red, B) and S100β+ (green, C). Merged image showing expression of both GFAP+ and S100β+ (D). Cells were counterstained with DAPI+ (blue, E). Astrocytic cells also stained for glycogen using the PAS staining (red, F), and cells were counterstained with DAPI+ (blue). Merged image showing expression of co-staining: S100β+, PAS staining and DAPI+ (G). The cells were stained at passage number 3–5, n=3. Scale bars: 100μm and 50μm (D and E).

2.3.3 Determination of Glycogen Content Levels

To definitively identify glycogen in human primary astrocytic cells; a glycogen assay (section 2.2.6) was used to quantitatively assess the presence of glycogen stores in hiPSC-derived astrocytic cells from ax0018 cell line was compared to C2C12 myoblast cell line as a positive control and SH-SY5Y neuroblastoma cell line as a negative control. The ax0018-derived astrocytes (27.31 μ g/mg) had similar glycogen content level to HA (30.41 μ g/mg) (Fig. 2.15).

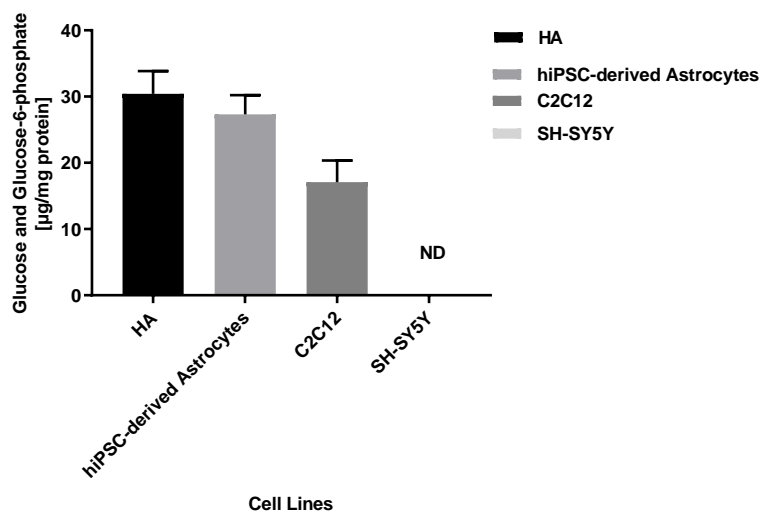


Figure 2.15: Determination of glycogen content levels of different cell lines. The cellular glycogen content was measured using a glycogen assay. Data is expressed as glucose and glucose-6-phosphate μ g/mg total cellular protein, \pm SEM, n=3 (triplicate wells pooled for each run). The statistical analysis was done using One-way ANOVA, Tukey's multiple comparisons test.

2.3.4 Glycogen Breakdown Assays

Having established the storage of glycogen in astrocytic cells (section 2.3.3), HA cells and hiPSC-derived astrocytic cells from ax0018 cell line were investigated for glycogen breakdown under various conditions, including hypoglycaemia and in response to known inducers and inhibitors of glycogen breakdown in neural cells.

2.3.4.1 Hypoglycaemic Conditions Assay

HA cells (Fig. 2.16A) and hiPSC-derived astrocytic cells from line ax0018 (Fig. 2.16B) were cultured under starvation conditions and their glycogen contents measured. Glycogen breakdown in the astrocytic cells was blocked by treating cells with 10 μ M DAB. DAB is an inhibitor of glycogen phosphorylase and α -1,6-glucosidases. The glycogen content of astrocyte cultures post treatment with DAB was compared to astrocytes cultures without DAB treatment over a range of time points. Breakdown of glycogen within astrocytic cells was fully blocked by DAB at 60 minutes and 180 minutes in comparison to control cultures at the zero time point and without DAB treatment at similar time in comparison to control (cell culture without DAB treatment) (HA; at 60min: 31.63 \pm 0.5128 μ g/mg, $P < 0.001$; 180min: 31.55 \pm 0.4376 μ g/mg, $P < 0.001$; ax0018-astrocytes: at 60min: 21.64 \pm 0.6057 μ g/mg, $P < 0.01$; 180min: 20.78 \pm 0.4407 μ g/mg, $P < 0.001$).

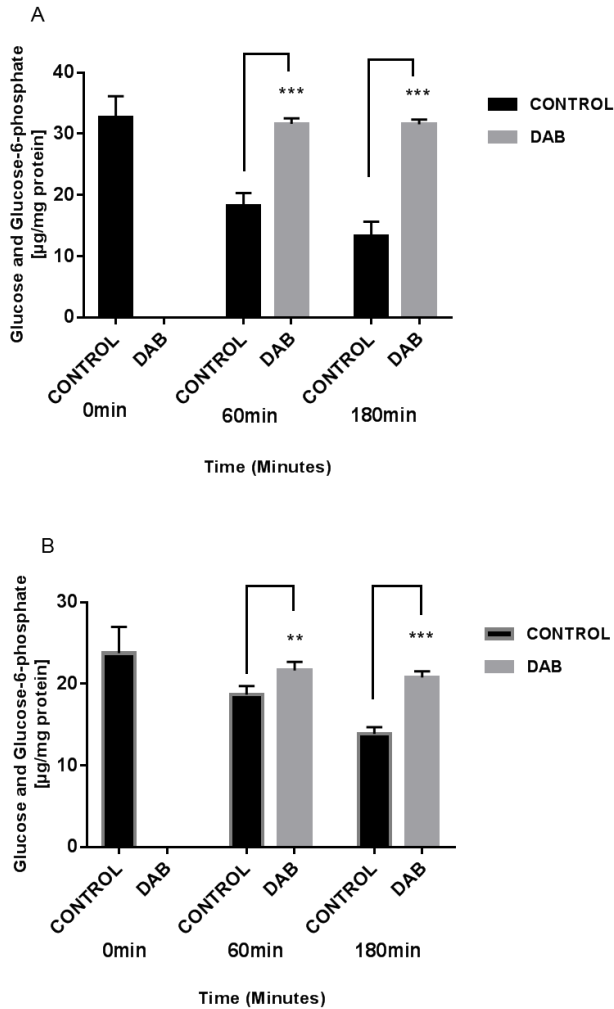


Figure 2.16: Analysis and comparison of glycogen breakdown in HA cells (A) and hiPSC-derived astrocyte from cell line ax0018 (B) using a glycogen assay. Astrocytic cells were cultured without glucose, and with or without 10µM DAB. The cellular glycogen content was measured using a glycogen assay. Data is expressed as glucose and glucose-6-phosphate µg/mg total cellular protein, ± SEM, n=3 (triplicate wells pooled for each run), $P < 0.001$ (***), $P < 0.01$ (**). The statistical analysis was done using Two-way ANOVA, Dunnett's multiple comparisons test.

2.3.4.2 Pharmacological Treatment

HA cells and hiPSC-derived astrocytic cells from line ax0018 in culture were exposed to known neuromodulators: Isoproterenol (a β 1 and β 2 adrenergic agonist) and dbcAMP (an inducer of glycogen phosphorylase) and glycogen levels assessed after 180 minutes. Both modulators induced a significant increase in glycogen breakdown induced by the HA cells (dbcAMP: $1.762 \pm 7.92\mu\text{g}/\text{mg}$, $P < 0.01$; Isoproterenol: $1.762 \pm 6.984\mu\text{g}/\text{mg}$, $P < 0.05$) (Fig. 2.17A). Similarly, dbcAMP induced a significant reduction in glycogen levels in hiPSC-derived astrocytic cells (dbcAMP: $1.758 \pm 14\mu\text{g}/\text{mg}$, $P < 0.001$) while there was no significant difference in glycogen breakdown induced by Isoproterenol in these cells (Fig. 2.17B).

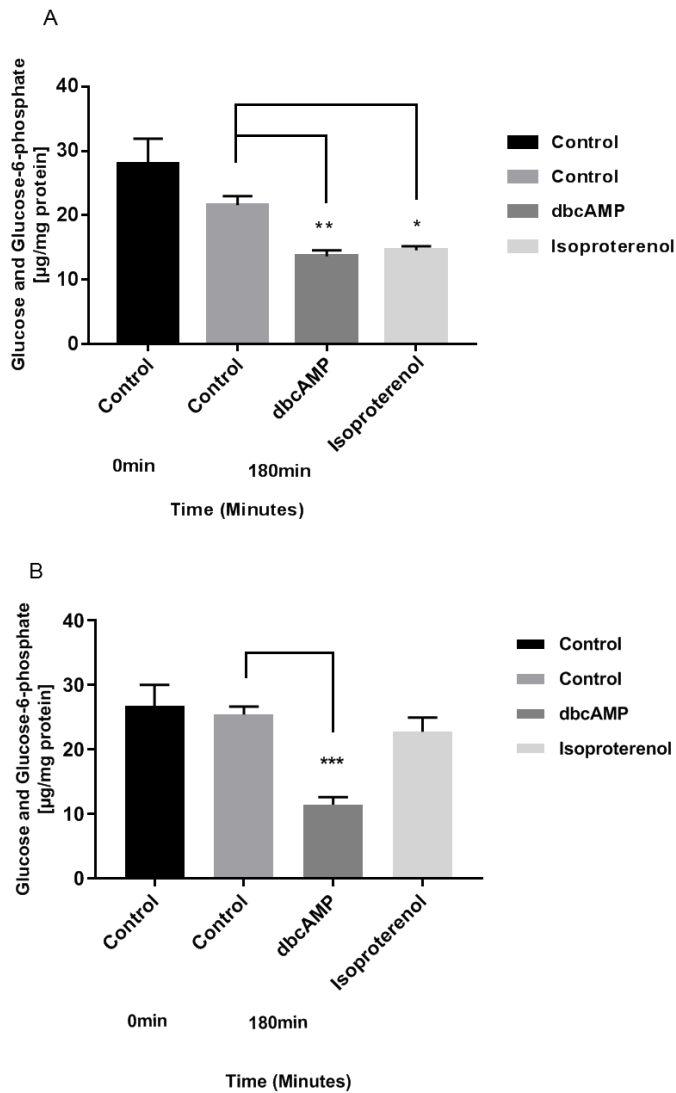


Figure 2.17: Analysis and comparison of glycogen breakdown in human primary astrocyte cells (A) and hiPSC-derived astrocytes from line ax0018 (B) in response to dbcAMP and Isoproterenol. Astrocytic cells were treated with 1mM dbcAMP or 100 μM Isoproterenol versus untreated control; glycogen levels were measured after 180 minutes. The cellular glycogen content was measured using a glycogen assay. Data is expressed as glucose and glucose-6-phosphate $\mu\text{g}/\text{mg}$ total cellular protein, \pm SEM, $n=3$ (triplicate wells pooled for each run), $P<0.001$ (***), $P<0.01$ (**), $P<0.05$ (*). The statistical analysis was done using One-way ANOVA, Dunnett's multiple comparisons test.

2.3.4.3 Glutamate Treatment

HA cells and hiPSC-derived astrocytic cells from line ax0018 in culture were exposed to neurotransmitter glutamate in order to assess the activation of the Na⁺/K⁺ ATPase, which would normally stimulate glycogen breakdown (DiNuzzo *et al.*, 2013). The cells were treated with glutamate with and without Ouabain (an inhibitor of Na⁺/K⁺ ATPase) and TBOA (glutamate transporters inhibitor). Intracellular glycogen levels were measured at 60, 180 and 360 minutes. Glutamate treatment induced significant reduction in glycogen levels in the hiPSC-derived astrocytes (Glutamate at 60min: $0.3001 \pm 3.244\mu\text{g}/\text{mg}$, $P<0.0001$; 180min: $0.7602 \pm 7.31\mu\text{g}/\text{mg}$, $P<0.0001$; 360min: $1.016 \pm 6.877\mu\text{g}/\text{mg}$, $P<0.001$) (Fig. 2.18B), (Glutamate at 180min: $0.4461 \pm 1.52\mu\text{g}/\text{mg}$, $P<0.05$; 360min: $0.3435 \pm 2.102\mu\text{g}/\text{mg}$, $P<0.001$) (Fig. 2.19B). Treatment of HA with either Ouabain or TBOA alone or glutamate and Ouabain or TBOA had no significant effect on glycogen storage (Fig. 2.18A and 2.19A).

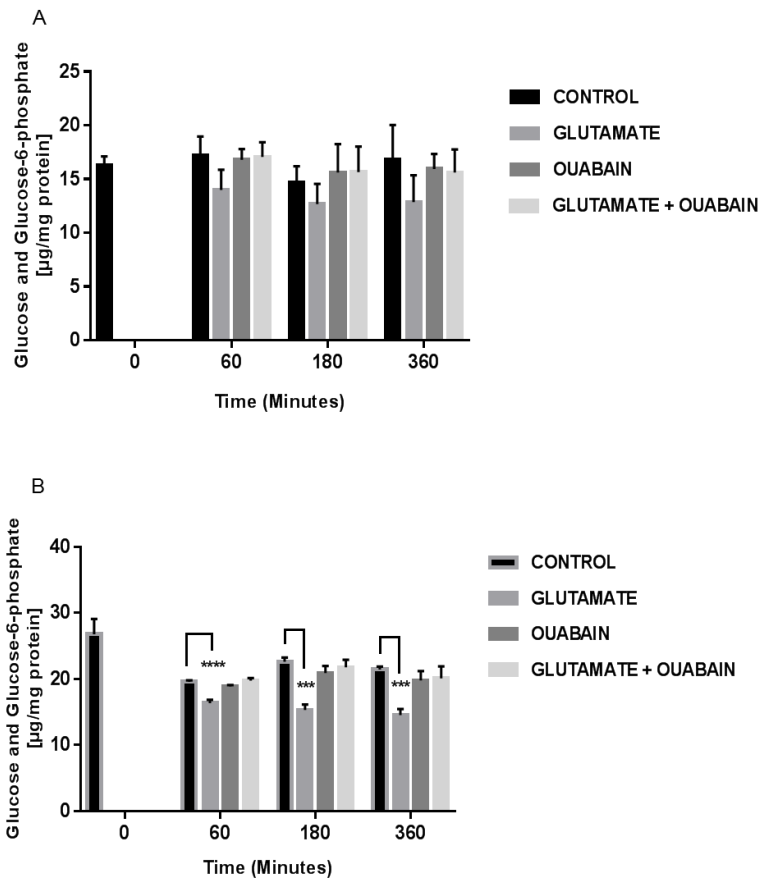


Figure 2.18: Analysis and comparison of glycogen breakdown in HA cells (A) and hiPSC-derived astrocytes from line ax0018 (B) in response to 1mM glutamate in the presence and absence of 100 μM Ouabain. Astrocytic cells were treated with 1mM glutamate in the presence or absence of 100 μM Ouabain in comparison to the untreated control. Glycogen levels were measured after 60, 180 and 360 minutes. The cellular glycogen content was measured using a glycogen assay. Data is expressed as glucose and glucose-6-phosphate $\mu\text{g}/\text{mg}$ total cellular protein, \pm SEM, $n=3$ (triplicate wells pooled for each run), $P < 0.0001$ (****), $P < 0.001$ (***). The statistical analysis was done using One-way ANOVA, Dunnett's multiple comparisons test.

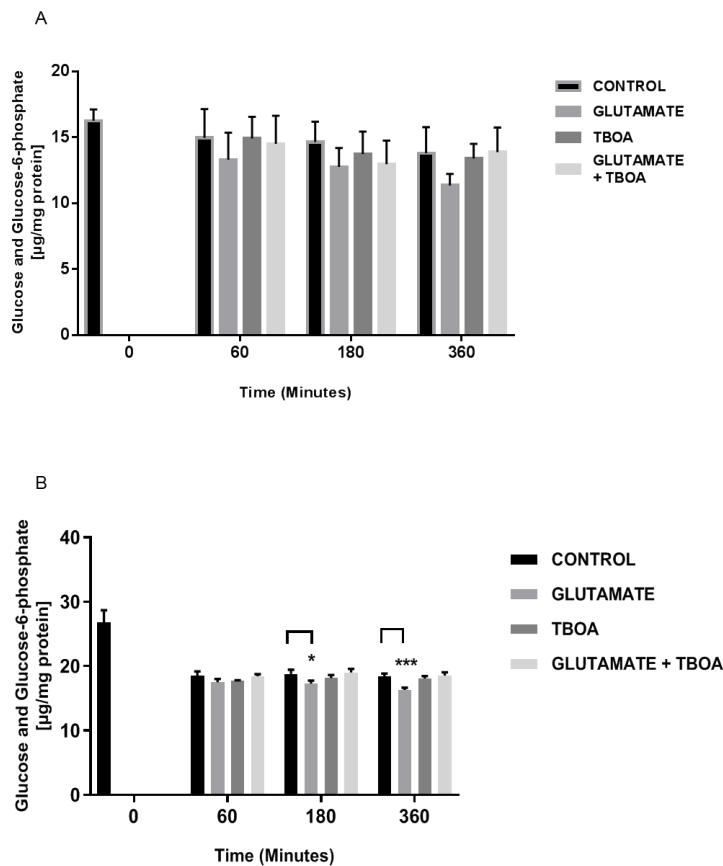


Figure 2.19: Analysis and comparison of glycogen levels in HA cells and hiPSC-derived astrocytes from line ax0018 treated with 1mM glutamate in the presence or absence of 100µM TBOA. Glycogen levels in primary astrocytic cells (A) and hiPSC-derived astrocytes (B) were measured using a glycogen assay. Astrocytic cells were treated with 1mM glutamate in the presence or absence of 100µM TBOA and compared to the untreated control; measurements were taken after 60, 180 and 360 minutes of treatment. The cellular glycogen content was measured using a glycogen assay. Data is expressed as glucose and glucose-6-phosphate µg/mg total cellular protein, ± SEM, n=3 (triplicate wells pooled for each run), $P < 0.001$ (***), $P < 0.05$ (*). The statistical analysis was done using One-way ANOVA, Dunnett's multiple comparisons test.

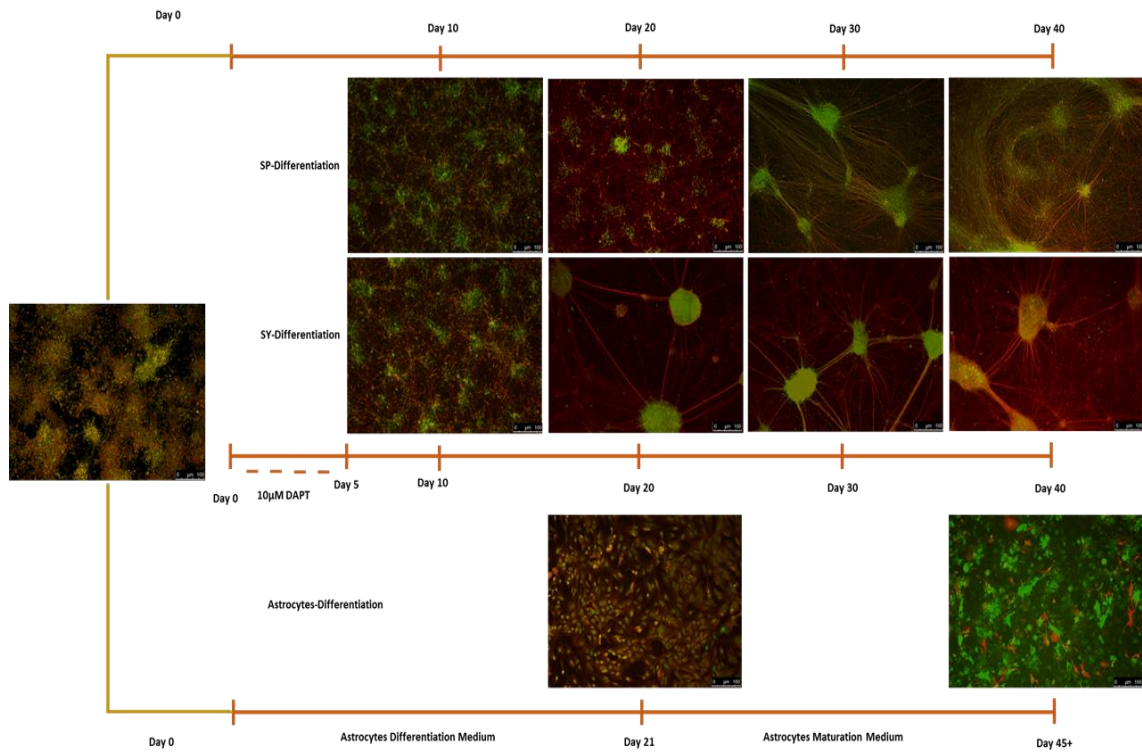


Figure 2.20: Diagram illustrating a summary of the development of cerebral cortical neurons and astrocytes and mixed population from line ax0018 of ‘healthy’ hiPSC-derived NPCs. Neural cells cultured using spontaneous and synchronous differentiation methods over 40 days period, and astrocytes differentiation and maturation protocols over 45+ days.

2.4 Discussion

Understanding the early preclinical metabolic mechanisms of AD has previously been problematic, as a definite diagnosis can only be made post-mortem, and animal models have largely been unable to fully recapitulate the disease process. The use of patient-derived neural cells is an alternative approach for studying the underlying pathophysiological events of AD. These cells can provide important information on possible exploitable diagnostic and therapeutic targets before the appearance of overt clinical features of AD. The development of hiPSC has made it possible to generate pluripotent cells from which neurons and astrocytes can be derived. In addition, recent advances in differentiation procedures have allowed scientists to produce brain cells from regions affected by AD such as the cortex (Shi *et al.*, 2012a, Shi *et al.*, 2012b).

In order to be able to utilise hiPSC-derived cells in studying the early metabolic changes in AD, it will be necessary to first ensure that the hiPSC-derived cells are similar to their naturally derived counterparts. This chapter was focussed on characterising 'healthy' hiPSC-derived astrocytes and neurons, to confirm that the structural and biochemical features of these artificially differentiated cells mirror those of healthy, naturally-derived cells.

Human iPSCs were differentiated into neural precursor cells, which are the progenitors that will eventually become neurons and astrocytes at the completion of the differentiation process. The cells in culture showed similar morphological and immunochemical characteristics to those differentiated by Shi *et al.* (2012a), with positive identification at day 0 of the NPCs markers *sox2* (a marker of pluripotency), *pax6* (neuronal fate determinant and NPCs proliferation) and *nestin* (an intermediate filament protein and NPCs marker), and the formation of cortical rosettes as shown in figure 2.1 for the ax0018 cell line.

The hiPSC-derived NPCs after spontaneous differentiation method yielded a mixed population of neuronal and glial cells, demonstrating neurite networks by day 10 of culture in similitude to the findings by Shi *et al.* (2012a). Astrocyte differentiation occurred later than neuronal differentiation as also observed by Shi *et al.* (2012b), the astrocytic marker S100 β was detectable at day 10. Cortical neurons derived from the hiPSC-derived NPCs were differentiated using the spontaneous and synchronous differentiation methods, showing extensive neurite networks by day 10 for both methods. The differentiated neuronal cells

expressed the neuronal marker (TUJ1) but showed no evidence of synaptic maturation until day 30, when the synaptic markers synaptophysin and PSD-95 were detectable (Fig. 2.9 and 2.10). The synaptic staining was however non-specific and the image quality was suboptimal. This may need further optimisation, and could theoretically be improved for better clarity with the use of negative controls using primary antibodies such as the isotype control antibodies, and the specificity improved with the use of secondary antibodies. However, when the SH-SY5Y cell line was used as control, as well as secondary only controls using goat anti rabbit FITC and donkey anti mouse rhodamine was unsuccessful, as there was no uptake of the markers with completely dark images. This thus indicates that optimisation would also involve re-examining relevant aspects of the process utilised. These include the blocking reagents use and the use of alternate antibodies like the vGlut2 and synapsin as alternate presynaptic markers, and Shank3 and Homer1 as alternative postsynaptic markers. Furthermore, the age of the cells requires further consideration, as the cells may possibly not mature enough at this stage the markers to be localised to the synaptic ends.

When observed morphologically, the neural cells in culture at day 10 appeared almost identical for both the spontaneous and synchronous differentiation methods, but from day 20, the nature of the neurite networks show striking contrasts in culture; there appeared to be more numerous, haphazard and uncoordinated neurite proliferation in the spontaneous cultures, while the networks in the synchronous cultures appeared to be fewer, more direct and better coordinated. This difference is likely due to the addition of DAPT into the synchronous differentiation cultures. DAPT is a γ -secretase inhibitor; it speeds up the neuronal differentiation process by inhibiting Notch signalling in NPCs (Shi *et al.*, 2012b). However, these findings may be influenced by the numbers of passages these cells had gone through prior purchase from the manufacturers to the culture at the time.

As the neurons in the neurite networks were physically difficult to delineate for counting, quantification was unlikely to be precise, hence the results were excluded from the statistical analysis, but have been included in the Appendices for reference and posterity.

The neuronal networks were assessed from day 30 for synaptic maturation. It has been previously reported by Shi *et al.* (2012a) that significant synaptic activity takes several weeks to develop. Indeed, they reported that functional glutamatergic synapses were only common after 50 days of culture. The neurons differentiated via the spontaneous and synchronous differentiation methods demonstrated punctate staining of synaptic markers from day 30,

similar to findings by Shi *et al.* (2012a). The neuronal networks were not assessed for synaptic firing in this project. However, work within our group (Mr James Crowe and Mr Alistair Grainger personal communication) have demonstrated the emergence of early neuronal activity for both SP and SY differentiation methods around this time.

Astrocytes were also differentiated from the 'healthy' hiPSCs and compared with healthy human primary astrocytes. The hiPSC-derived astrocytes showed the typical stellate morphology, and expressed the astrocyte markers S100 β and GFAP. The differentiation process resulted in the production of almost exclusive astrocytic cell populations (Fig. 2.12). When compared with the human astrocytes, the hiPSC-derived astrocytes showed no notable morphological or immunohistochemical differences. The differentiated cells showed very little expression of TUJ1 after 35 days of culture immediately after maturation stage (Fig. 2.12). This is similar to the findings by Shaltouki *et al.* (2013) that the astrocytic cells on differentiated were almost purely of the astrocytic lineage, after the cells underwent passages and cryopreservation. (Fig. 2.12 and 2.13).

Glycogen stores in the HA and hiPSC-derived astrocytes were assessed using PAS staining, and quantitatively assessed by the glycogen assay (section 2.3.3). The C2C12 myoblast cell line was used as positive control, and the SH-SY5Y neuroblastoma cell line was used as negative control. When assessed for glycogen stores, there was no significant difference between the content for the ax0018 hiPSC-derived astrocytes and the HA (Fig. 2.15). However, there was a significant reduction in the glycogen stores in the ax0016 (see Appendices) compared to the HA and ax0018.

Astrocytes increase glycogen breakdown under starvation conditions in order to maintain survival of neurons, protect axons, and ensure synaptic activity is maintained (Brown and Ransom, 2007, Tarczyluk *et al.*, 2013). The hiPSC-derived and primary astrocytes, when cultured under hypoglycaemic conditions, exhibited increased glycogen breakdown, manifested as a significant reduction in their glycogen stores when cultured under hypoglycaemic conditions without the blocking effect of DAB (an inhibitor of glycogenolytic enzymes).

The cultured astrocytes produced mixed responses to exposure to known neuromodulators, with the HA showing a significant increase in glycogen breakdown in response to both dbcAMP and Isoproterenol, while the hiPSC-derived astrocytic cells recorded a significant

increase in response to dbcAMP, but not to the β 1 and β 2 adrenergic agonist. Conversely, the hiPSC-derived astrocytes exhibited significant increase in glycogen breakdown in response to glutamate and the Na⁺/K⁺ ATPase inhibitor, TBOA, while there no significant changes to glycogen turnover in the HA in response to these neuromodulators. Tarczyluk *et al.* (2013) reported consistent increase in glycogen breakdown when astrocytes in co-culture with neurons were exposed to similar neuromodulators. Walls *et al.* (2008), reported similar increase in glycogenolytic activity in response to norepinephrine and glutamate. However, Swanson *et al.* (1990), reported a dynamic response of glycogen turnover to glutamate which was dependent on the availability of alternate substrates and the amount of free glucose available. These mixed responses may be explained by the fact that our experiment was in single culture, as opposed to mixed neuron-astrocyte co-cultures.

The importance of astrocytes to neuronal survival and function is well known, but recent research has shown that their roles may be larger and more central than previously thought. Tarczyluk *et al.* (2013) was able to show that astrocytes participate in the spatial and neurochemical components of synaptic transmission by increasing glycogen turnover, increasing glucose uptake and glycolysis. The complex interactions that make up this so-called functional ANLS was first described by Pellerin and Magistretti (1994), and has been investigated thoroughly since (Ransom and Fern, 1997, Wender *et al.*, 2000, Zwingmann *et al.*, 2003, Amaral *et al.*, 2011). However, this interaction has not been demonstrated using hiPSC-derived astrocytes and neurons.

2.5 Conclusion

In conclusion, this chapter has demonstrated that astrocytes and neurons can be successfully differentiated into mature neurons and astrocytes from hiPSC-derived NPCs. These differentiated neurons and astrocytes bear striking similarities to their naturally derived counterparts in terms of structure and to a large extent for astrocytes, their neurometabolic functions. Neurons can be differentiated using the SP or SY differentiation methods, with the SY producing more mature and better defined neuronal networks than the SP. The differentiated neurons also exhibited the expression of synaptic markers. Astrocytes were differentiated in a two-step process from hiPSC-derived NPCs, and the hiPSC-derived astrocytes were morphologically and metabolically, with some differences from human primary astrocytes in their response to pharmacological treatments. This is the first time to the best of our knowledge, mature astrocytes and neurons have been differentiated from hiPSCs and tested for astrocytic metabolic function in terms of glycogenolysis. Future experiments in the lab will characterise metabolic functions further in terms of electrolyte, carbohydrate, protein metabolism and assessment of the complex astrocyte-neuron synaptic complex structurally and functionality.

The next chapter of this project explores the metabolic response of the differentiated astrocytes and neurons to exogenous A β (chapter 3).

Chapter 3: Treatment of Healthy Human iPSC-derived Neurons and Astrocytes and Primary Astrocytes with Synthetic A β 1-42 Oligomers

3.1 Introduction

It is now well recognised that hypometabolism is an important preclinical event in AD, which likely precedes overt clinical symptoms and signs by decades (Mosconi *et al.*, 2008a and 2008b). The mechanism regulating this hypometabolism in the early disease stages before obvious loss of brain tissue is yet to be fully explained, but is believed to be closely related to toxicity of A β molecules and aggregates to brain cells, with links to dysfunction in insulin signalling (Holscher, 2011). Previous studies have attempted to utilise non-human models to explain the mechanism of early hypometabolism in AD, but have yielded mixed results (Nicolakakis *et al.*, 2008, Nicholson *et al.*, 2010, Allaman *et al.*, 2010, Poisnel *et al.*, 2012, Luo *et al.*, 2012, Uemura and Greenlee, 2001.). The inconsistencies in these results are likely due to the differences in structural and biochemical complexity between the human and non-human species. This may explain why some species do not develop AD naturally, and possible differences between the *in vitro* and *in vivo* systems. Human iPSC-derived neural cells from 'healthy or affected human neurons and astrocytes may enabling early changes in cellular metabolism to be studied in response to exogenous or endogenously produced A β . This chapter, explores the metabolic response of 'healthy' hiPSC-derived neurons and astrocytes to exogenous A β . This work builds on previous efforts in our lab regarding the effects of exogenous A β on human neurons and astrocytes (Tarczyluk *et al.*, 2015).

3.1.1 Astrocytes

The role astrocytes play in acute and chronic disease states has been the focus of much research (Yong *et al.*, 1991, Hu *et al.*, 1998, Zamanian *et al.*, 2012, Pekny and Pekna, 2014, Okada *et al.*, 2006, Martin *et al.*, 2006, Wilhelmsson *et al.*, 2006). Astrocytes are the most abundant glial cells in the brain. They play very important roles in brain metabolism, neuroprotection and in the mechanism of dealing with metabolic stress (Reviewed in Michelle *et al.*, 2018). The neuroprotective functions of astrocytes include protection against glutamate toxicity (Chamoun *et al.*, 2010, Soria *et al.*, 2014), and prevention of oxidative stress. This is particularly important in disease states, which result in excessive production of ROS that is beyond the capacity of usual cellular measures to protect against oxidative damage.

Astrocytes are also able to generate higher quantities than neurons, of glutathione, one of the most important natural antioxidants (Iwata-Ichikawa *et al.*, 1999, Eftekharpour *et al.*, 2000).

The role of mitochondrial dysfunction and hypometabolism in AD is has typically focussed on neurons, however the role of astrocytes is yet to be fully explained. Astrocytes have been shown to engage in transfer of healthy mitochondria into neurons to replace dysfunctional neuronal mitochondria that produce increased ROS (Hayakawa *et al.*, 2016), and also take up damaged mitochondria released from neurons (Davis *et al.*, 2014). This protection against dysfunctional mitochondria may be very important in the prolonged pathogenetic course of AD, as A β is known to induce mitochondrial dysfunction and increase the release of ROS.

Activation of astrocytes to the reactive state can occur via several mechanisms, including exposure to A β oligomers, inflammatory cytokines, neurodegeneration or acute traumatic cellular injury or inflammation (Yong *et al.*, 1991, Hu *et al.*, 1998). When activated, astrocytes are believed to alter their immediate environment to facilitate a return to normal homeostasis and repair in the short term by reducing inflammation and reducing white blood cell infiltration (Bush *et al.*, 1999, Myer *et al.*, 2006). However, with prolonged or continuous damage, reactive astrocytes create a glial scar and are unable to maintain long term neuronal survival and function, and indeed inhibit axonal outgrowth from neurons (Pekny and Pekna, 2014, Sun *et al.*, 2012, Yong *et al.*, 1991, Hu *et al.*, 1998).

While the pathogenic role of activated astrocytes in AD are yet to be completely explained, reactive astrocytes have been shown to be localised around amyloid plaques in post-mortem tissue of AD patients (Serrano-Pozo *et al.*, 2013, Davis *et al.*, 1992, Yan *et al.*, 1996, El Khoury *et al.*, 1996, Le Y Gong *et al.*, 2001). A number of studies have now shown that astrocytes demonstrate altered glucose metabolism, insulin signalling and response to oxidative stress in AD. Similarly, astrocytes derived from human post-mortem tissue demonstrate down regulation of a number of genes associated with phosphatidylinositol-3-kinase and protein kinase B (PI3K-AKT) and mitogen-activated protein kinase (MAPK) signalling-associated transcripts, which may reflect the impact of impaired insulin signalling on subsequent downstream processes (Hansson *et al.*, 1986, Cheng *et al.*, 2003).

3.1.2 Astrocyte-Neuron Metabolic Coupling

The synaptic functions, metabolic needs, as well as the survival and protection of neurons against oxidative stress are closely related, and sometimes dependent on supportive roles

offered by astrocytes. It is therefore important to examine the complex metabolic and spatial relationships between the astrocytes and neurons that could play a crucial role in the early pathogenic course of AD. One crucial component of this relationship is the ANLS (Pellerin and Magistretti, 1994). It was shown that glutamate released during synaptic activity is taken up by astrocytes, with a resultant cascade of metabolic changes in the astrocytes including increased glucose uptake, increased glycolysis and lactate production, which is then released back to the neurons for utilisation via oxidative decarboxylation, a mechanism that has also been demonstrated in stem cell derived neurons and astrocytes (Tarczyluk *et al.*, 2013).

3.1.3 Effects of A β on Metabolism

The amyloid hypothesis of AD aetiology is based on the idea that the AD pathogenesis is determined by the excessive production, accumulation and toxicity of A β , which then creates a chain of events leading to chronic inflammation, neuronal metabolism dysfunction, and eventual cell death (Hardy and Allsop, 1991). Further refinements of the hypothesis have suggested that specific isoforms of A β are likely to be responsible for the pathogenetic events leading up to clinically evident features of AD. The soluble forms of A β , especially the A β 1-40 and A β 1-42 oligomers have now been shown to be more toxic and responsible for ultimate cellular damage, rather than the insoluble accumulations of A β which are seen as amyloid plaque deposits in the brain (Reviewed in Selkoe and Hardy, 2016). Several other isoforms of A β also exist, which may also contribute to the disease process in varying degrees (Mawuenyega *et al.*, 2013).

It is known that A β induces metabolic dysfunction in neuronal cells and astrocytes, and several studies have revealed possible mechanisms of this action (Mattson *et al.*, 1995, Butterfield *et al.*, 1994, Oddo *et al.*, 2003, Knobloch *et al.*, 2007). One mechanism that has been proposed is induction of oxidative stress by excessive release of ROS (Mattson *et al.*, 1995, Butterfield *et al.*, 1994). This is likely because A β induces mitochondrial dysfunction by accumulating in the mitochondrial membranes and at synaptic sites where there is a huge presence of mitochondria (Oddo *et al.*, 2003, Knobloch *et al.*, 2007). A β accumulation in the mitochondrial results in increased mitochondrial permeability (Canevari *et al.*, 1999, Parks *et al.*, 2001, Shevtzova *et al.*, 2001, Kim *et al.*, 2002, Moreira *et al.*, 2002). It has also been shown to cause impaired calcium signalling, especially in astrocytes, leading to calcium influx into astrocytes (Abramov *et al.*, 2003). In addition, A β alters the function of several important enzymes of the Krebs's cycle and the respiratory chain, with α -ketoglutarate dehydrogenase,

and aconitase showing greater susceptibility to A β toxicity, as well as generating ROS (Figure 1.4) (Casley *et al.*, 2002, Longo *et al.*, 2000).

It has been previously demonstrated in our laboratory that exogenous amyloid induces metabolic dysfunction in human neurons and astrocytes derived from the NT2.D1 embryocarcinoma cell line (Tarczyluk *et al.*, 2015). It was shown that there were reductions in uptake of glucose, lactate, glutamate as well as an increase in glycogen content level, with significant impairments to the protective mechanisms against oxidative stress.

3.1.4 Aims and Objectives of the Study

Our hypothesis was that treatment of neurons and astrocytes derived from 'healthy' hiPSCs with synthetic A β 1-42 oligomers would induce changes in glucose uptake and glycogen metabolism as previously reported in NT2.D1 derived neurons and astrocytes (Tarczyluk *et al.*, 2015). The specific aim of this chapter of the project was to explore the occurrence of metabolic dysfunction in response to A β .

The objectives of this study were to:

- Assess the effects of synthetic A β 1-42 oligomers on cell viability in primary human and hiPSC-derived astrocytes and neurons using the MTT and cell count assays.
- Determine the effect of synthetic A β 1-42 oligomers on neuronal glucose uptake (using glucose assay) and astrocytic glycogen content (using glycogen assay) in hiPSC-derived neural cells and primary astrocytes.

3.2 Materials and Methods

3.2.1 Preparation of Synthetic A β 1-42 Oligomers

Synthetic A β 1-42 oligomers were prepared as previously reported (Tarczyluk *et al.*, 2015). Amyloid oligomers were prepared by dissolving synthetic Hexafluoroisopropanol (HFIP)-treated amyloid- β 1-42 (A β 1-42) (AnaSpec, Belgium) in 200mM HEPES buffer (pH 8.5) to generate a stock solution concentration of 100 μ M. The stock solution was then aliquoted into sterile microcentrifuge tubes and stored at -80°C.

3.2.2 Electrophoresis Studies

3.2.2.1 SDS-PAGE Gel Electrophoresis

The presence of synthetic A β 1-42 oligomers (section 3.2.1) was assessed using sodium dodecyl sulfate polyacrylamide gel electrophoresis (SDS-PAGE). The Mini Protean® 3 Cell (Biorad, UK) system was used according to the manufacturer's guidelines. An 8% resolving gel was prepared using 30% Bis-Acrylamide (Geneflow, UK) with a 4% stacking gel. The synthetic A β 1-42 was then serially diluted from a concentration of 100 μ M to 0.39 μ M in sample buffer (sample buffer: 25% glycerol, 62.5mM Tris-HCl pH 6.8, 2% SDS, 0.01% bromophenol blue and 5% β -Mercaptoethanol). 10 μ l of Page Ruler Plus Prestained Protein Ladder (Thermofisher, UK) and 20 μ l of sample buffer and samples were loaded onto the gel. Electrophoresis was carried out at 200V (max) for 35 - 45 minutes until the bromophenol blue reached the bottom of the resolving gel. The plates were then carefully separated, and the gel removed. Gels were prepared for western blotting (section 3.2.2.2) or incubated overnight in Coomassie Brilliant blue stain (0.1% Coomassie, 50% methanol with 7% acetic acid) on slowly rotating using gyro-rocker (Stuart®, UK). Gels were then destained using (50% methanol and 7% acetic acid). Picture images were taken using GeneSys image acquisition software and GBOX-Chemi-XRQ gel documentation system (Syngene, UK).

3.2.2.2 Western Blotting

SDS-PAGE gel followed by Western blotting was performed on the serially diluted synthetic A β 1-42 oligomers samples. Following separation by SDS-PAGE (section 3.2.2.1), the gels were incubated in transfer buffer (25mM Tris, 192mM Glycine, 10% Methanol in deionised water) for 15 minutes. Afterwards, the SDS gels and Nitrocellulose Hybond ECL membranes (Amersham, GE Healthcare, Buckinghamshire, UK), nitrocellulose membranes were then sandwiched between four pieces of Whattmann cellulose chromatography paper and two pieces of sponge, pre-soaked in transfer buffer. Transfers were performed using the mini trans-blot electrophoretic transfer cell (Bio-Rad Laboratories Ltd., Hemel Hempsted, UK) at 30V, 90mA for 16 hours on ice. Next day, the Nitrocellulose membranes were transferred and blocked in TBS-Tween (TBS: 138mM NaCl, 2.68mM KCl, 24.8mM Tris-base in deionized water, pH 8.0), (0.1% (v/v) Tween) and 5% (w/v) powdered milk (Marvel) for 2 hours on gyro-rocker at room temperature. After 2 hours, 10 μ l of a primary antibody Beta Amyloid 1-16 (6E10) (1:1000) (Covance, USA) was diluted in 10ml of 3% (w/v) dried milk powder in TBS 0.1% (v/v) Tween, and then the membranes placed inside 50ml conical tubes on a rolling platform and incubated overnight at 4°C.

On the following day, the membranes were washed six times (5 minutes for each wash) with TBS-0.1%Tween on gyro-rocker at room temperature to eliminate the excess unbound antibody. After this washing step, the membranes were incubated and diluted in 10ml of 3% (w/v) dried milk powder in TBS 0.1% (v/v) Tween with secondary antibody (Anti-mouse IgG HRP-linked antibody (1:2000) (Cell Signalling Technology, UK) to visualise bound primary, which was diluted in 10ml of 3% (w/v) dried milk powder in TBS 0.1% (v/v) and Tween, and then the membranes placed inside 50ml conical tubes. The membranes were incubated for one hour on a rolling platform at room temperature. After incubation with secondary antibody, the blot were washed six times 5 minutes for each wash with TBS-0.1% Tween on gyro-rocker at room temperature to eliminate the excess unbound antibody.

Next, the blot was incubated with Pierce™ ECL Western blotting substrate (Thermo Fisher Scientific, USA) for one minute at room temperature. Subsequently, the membranes were placed in an autoradiography cassette (Hypercassette, Amersham, GE Healthcare, Buckinghamshire, UK) between two pieces of acetate. In a dark room, the blot was exposed to X-ray film (CL-XPosure Film, ThermoFisher Scientific, UK) for 5 minute to 1 hour. After exposure, the X-ray film was placed in developer solution developer (Kodak, Sigma-Aldrich,

Dorset, UK) for 30 second to 1 minute, and then washed thoroughly in water for 30 second, and then the blot transferred in fixer solution (Kodak, Sigma-Aldrich, Dorset, UK) for 1 minute and then washed thoroughly in water 30 second. The blot films were then left to dry, and then picture images were captured using GeneSys image acquisition software and GBOX-Chemi-XRQ gel documentation system (Syngene, UK).

3.2.3 Treatment of Human Primary Astrocytes and iPSC-derived Neurons and Astrocytic Cells with Synthetic A β 1-42 Oligomers

To determine the possible toxic effects of synthetic A β 1-42 oligomers on the metabolism of HA, astrocytic cells derived from 'healthy' hiPSCs (ax0018), and neuronal cells derived from SP and SY differentiation methods from ax0018 'healthy' cell line. All cells were exposed to synthetic oligomeric A β 1-42 over a range of concentrations based on the findings from Tarczyluk *et al.* (2015). The HA (section 2.2.3.1) and astrocytes derived from hiPSCs (section 2.2.2.3) were plated at a density of 5×10^5 cells/cm² in 12-well plates in triplicate and left in culture for 2 - 3 days. The hiPSC-derived were plated at a density of 25×10^3 cells/cm² in 12-well plates in triplicate. Then, the neuronal cells were spontaneously and synchronously differentiated (section 2.2.2.1 and 2.2.2.2, respectively) for 30 days in culture. All the cells were treated with synthetic A β 1-42 oligomers (section 3.2.1) diluted in 1ml of appropriate cell culture medium to working concentration range of 2 μ M, 1 μ M and 0.2 μ M, and were compared to untreated cells. The cells were incubated for 48 hours at 37°C in a humidified atmosphere of 5% CO₂. Subsequently, the conditioned media (CM) were collected and centrifuged at speed of 200 x g for 5 minutes, and then the supernatants were transferred into 1.5ml sterile microcentrifuge and stored at -20°C for analysing glucose uptake using Hexokinase assay (section 3.2.6.1). Homogenised samples of astrocytic cells were collected for analysis using the glycogen assay (section 2.2.6) and protein determination assay (section 2.2.8).

3.2.4 Cell Viability and Cytotoxicity Studies

The viability of cells treated with synthetic A β 1-42 oligomers in comparison with untreated cells was determined using MTT assay (3.2.4.1) (Mosmann, 1983) and cell nucleus count assay (section 3.2.4.2).

3.2.4.1 MTT Assay

The MTT assay is a colorimetric assay that was used to assess cell viability by measuring the reduction of yellow tetrazolium dye to purple formazan in active metabolic living cells. The HA and astrocytes derived from hiPSCs were plated at a density of 3×10^4 cells/cm² in 96-well plates in triplicate, and left in culture for 2 - 3 days prior to treatment with synthetic A β 1-42 oligomers. The cells were treated with serially diluted synthetic A β 1-42 oligomers over a concentration range of 2 - 0.001953 μ M, and were compared to an untreated cells as a control, over 48 hours. Cell culture media was removed by gently inverting the 100 μ l of 2.5 μ g/ml MTT stock in the appropriate cell culture medium was added to the cells. Additionally, neuronal cells were spontaneously and synchronously differentiated (sections 2.2.2.1 and 2.2.2.2, respectively) for 30 days in 96-well plates prior to treatment, which hiPSCs-derived NPCs of ax0018 cell line were plated in triplicate at a density of 10×10^3 - 20×10^3 cells/cm². Next, 100 μ l of 1.25 μ g/ml MTT stock in the appropriate cell culture medium was added to the cells. All the cells were covered with foil and incubated for 3 hours at 37°C. After incubation, MTT solution was aspirated and 50 μ l of DMSO (Sigma-Aldrich, UK) was added to each well and mixed on shaker for 30 second. Plates were then incubated for 10 minutes at 37°C. Absorbance was measured at a wavelength 590nm using a Thermo multiscan EX 96-well plate reader.

3.2.4.2 Cell Nucleus Count Assay

To confirm results obtained from the MTT assay (section 3.2.4.1) the viability of cells was also assessed using NucleoCounters® system (Chemometec, Denmark). The astrocytes derived from hiPSCs of ax0018 cell line (section 2.2.2.3) were plated at a density of 20×10^5 cells/cm² in 6-well plates and left in culture for 2 - 3 days. Afterwards, astrocytic cells were exposed to synthetic oligomeric A β 1-42 that diluted in 2ml AM to working concentration of 2 μ M, 1 μ M, and untreated cells. The treated cells were incubated for 48 hours at 37°C in a humidified atmosphere of 5% CO₂. After incubation, the CM were collected and spun at speed of 200 x g for 5 minutes, and then supernatant was discarded and re-suspended with 1ml AM. The astrocytic cells were detached by washing the cells once with D-PBS, and then adding 1ml of Accutase and incubated for 5 minutes at 37°C in a humidified atmosphere of 5% CO₂. 4ml of AM was added to each well and transferred into a 15ml sterile conical tube and centrifuged for 5 minutes at speed of 200 x g. The supernatant was discarded, and pellet was re-suspended in 1ml of AM. Subsequently, the CM and cell pellet were vortexed for 30 second before assessment using Via1-Cassette™ (Chemometec, Denmark). The cell viability and cell

counting was measured using ChemoMetecNucleoView NC-3000 software (Chemometec, Denmark). Due to issues with producing a single cell suspension of neurons, it was not possible to repeat this experiment using neuronal cultures.

3.2.5 Determination the Effects on Carbohydrate Levels

3.2.5.1 Determination the Effects on Glucose Uptake Levels

The CM samples collected from cells treated with synthetic A β 1-42 oligomers in comparison with untreated cells as a control (section 3.2.3) were assessed for glucose uptake level over time using glucose assay kit. The experiment was carried out according to the manufacturer's instructions (modified for a 96-well plate). Briefly, the standard and samples were serially diluted (1:2) to generate a standards curve giving concentration range between 500 - 3.9 μ g/ml. 30 μ l of standard and samples were mixed with 200 μ l of HK reagent and incubated for 15 minutes at room temperature. The absorbance was read at 370nm Thermo multiscan EX 96-well plate reader (Thermofisher, UK). All readings were corrected for background and total protein levels (section 2.2.8).

3.2.5.2 Determination the Effects on Glycogen Content Levels

The homogenised samples from the HA and hiPSCs-derived astrocytes (ax0018) treated with synthetic A β 1-42 oligomers in comparison with untreated cells (section 3.2.4) were measured for glycogen content levels according to glycogen assay method described in section 2.2.6. All readings were corrected for background, free glucose in homogenised samples and protein levels (section 2.2.8).

3.2.6 Cell Lysis

Human iPSC- derived Neuronal cells from SP and SY neuronal differentiation methods were washed with ice-cold D-PBS, and then 300 μ l of 1X Radioimmunoprecipitation assay (RIPA) lysis buffer (Millipore) containing complete tablets mini EDTA-free, Easypack protease cocktail inhibitors (Roche, USA) was added and incubated for 10 minutes on ice. The cells were then

scraped and the lysate transferred to a 1.5ml sterile microcentrifuge tube, and centrifuged at 12,000rpm at 4°C for 20 minutes. The supernatant was collected and stored at -20°C for protein quantification. Preparation of cell lysate from astrocytic cells for protein quantification was described in section 2.2.6.1.

3.2.7 Determination of Protein Levels

All the protein concentration of cells samples were measured according to protocol described in section 2.2.8.

3.2.8 Quantification and Statistical Analysis

All quantification and statistical analyses were done according to the methods described in section 2.2.9.

3.3 Results

3.3.1 Synthetic A β 1-42 Oligomers Examination

Synthetic A β 1-42 was prepared and then aliquoted at a concentration of 100 μ M using the method described in (section 3.2.1). The synthetic A β 1-42 was then serially diluted from a concentration of 100 μ M to 0.39 μ M in sample buffer, and the presence of monomers and oligomers in the preparation were assessed using SDS-PAGE (section 3.2.2.1) and western blotting (section 3.2.2.2).

3.3.2 Electrophoresis Studies

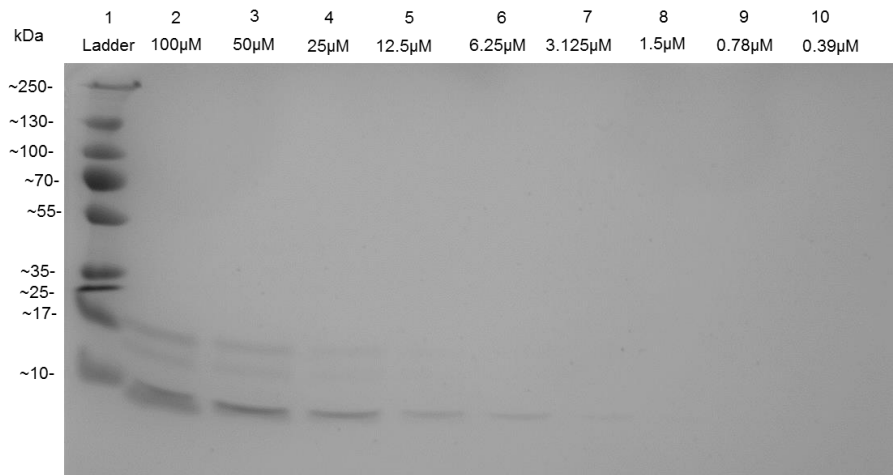
3.3.2.1 SDS-PAGE Gel

To determine the presence of SDS-stable A β oligomers, synthetic A β 1-42 was separated on a SDS-PAGE gel and then stained with Coomassie brilliant blue stain (section 3.2.2.1). Under denaturing and reducing conditions; the gel shows that the majority of synthetic A β 1-42 as monomeric bands from lane 2 - 7 (~4kDa) (Fig. 3.1A). SDS stable oligomers were also visible from lane 2 - 5. These oligomers can be estimated at ~10 - 17kDa and represent SDS stable tetramers and trimers. The lowest level of synthetic A β 1-42 detected using Coomassie staining was 3.125 μ M.

3.3.2.2 Western Blotting

Western blotting was carried out to sensitively monitor the existence of further synthetic A β 1-42 species not detected using Coomassie brilliant blue stain, as well as assess the presence of the various levels of synthetic A β 1-42, which was recognised with 6E10 antibody against A β . Synthetic A β 1-42 was serially diluted from a concentration of 100 μ M to 0.39 μ M and loaded in 8% SDS-PAGE gel followed by western blotting analysis. Western blotting detected synthetic A β 1-42 between concentrations of 100 μ M to 1.5 μ M (lanes 1 - 9, respectively) (Fig. 3.1B), with the largest molecular weights being around ~130kDa.

A



B

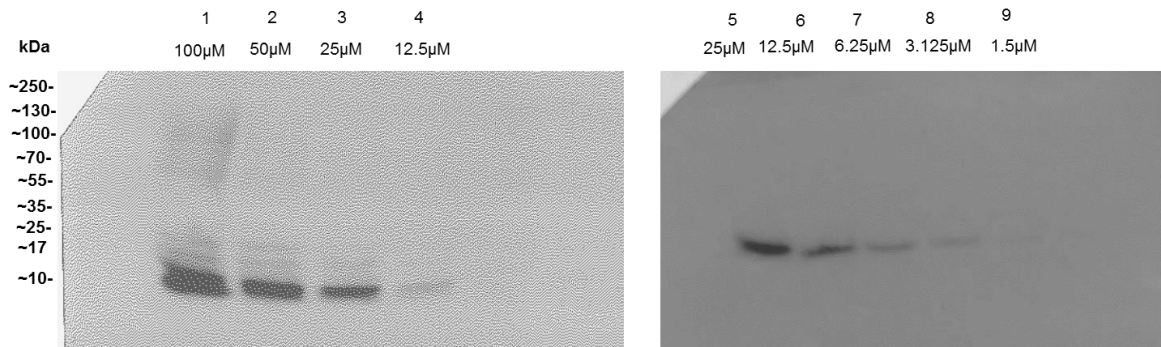


Figure 3.1: Representative 8% SDS-PAGE gel (A) confirming the presence of synthetic Aβ1-42 monomers and oligomers; serially diluted from a concentration of 100 μM to 0.39 μM. Proteins were stained with Coomassie brilliant blue stain. Lane 1 illustrates the pre-stained protein ladder molecular weight markers. Lanes: 2 - 7 show 100 μM to 3.125 μM of synthetic Aβ1-42 concentrations. Representative western blotting analysis (B) of synthetic Aβ1-42 using 6E10 antibody: lane 1 - 9 indicate concentrations of synthetic Aβ1-42 between 100 - 1.5 μM, respectively. (B) Generated from 2 independent blots.

3.3.3 Cell Viability and Cytotoxicity Studies

3.3.3.1 MTT Assay

The MTT cell viability assay was used to determine the possible toxic effects of synthetic A β 1-42 oligomers on HA, hiPSC-derived astrocytes (45+ days old) from ax0018 cell line plus neural cells derived from spontaneous and synchronous differentiation methods (30 days old) (sections 3.2.4).

The cells were treated with synthetic A β 1-42 oligomers over concentration range of 2 - 0.001 μ M, and were compared to an untreated loading control. The concentration range was used based on the findings from Tarczyluk *et al.* (2015). There was a significant reduction in cell viability at concentration 2 - 0.003 μ M as a result of exposure of HA to synthetic A β 1-42 for 48 hours (2 μ M: 77.73 \pm 3.6%, $P < 0.0001$; 1 μ M: 80.85 \pm 3.4%, $P < 0.0001$, 0.5 μ M: 84.23 \pm 2.12%, $P < 0.0001$; 0.25 μ M: 86.16 \pm 2.24%, $P < 0.0001$; 0.125 μ M: 87.90 \pm 2.71%, $P < 0.0001$; 0.0625 μ M: 89.15 \pm 2.42%, $P < 0.001$; 0.03125 μ M: 89.91 \pm 2.39%, $P < 0.01$; 0.015625 μ M: 90.70 \pm 1.76%, $P < 0.01$; 0.007813 μ M: 91.23 \pm 2.66%, $P < 0.01$; 0.003906 μ M: 92.31% \pm 2.62%, $P < 0.01$) (Fig. 3.2A). Similarly, exposure of hiPSC-derived astrocytes to synthetic A β 1-42 for 48 hours yielded a significant difference in the cell viability at concentration 2 - 0.015 μ M (2 μ M: 71.12 \pm 2.90%, $P < 0.0001$; 1 μ M: 76.90 \pm 3.92%, $P < 0.0001$, 0.5 μ M: 79.29 \pm 2.32%, $P < 0.0001$; 0.25 μ M: 83.92 \pm 2.25%, $P < 0.0001$; 0.125 μ M: 86.51 \pm 3.02%, $P < 0.0001$; 0.0625 μ M: 88.69 \pm 1.97%, $P < 0.001$; 0.03125 μ M: 91.19 \pm 2.75%, $P < 0.01$; 0.015625 μ M: 93.42 \pm 2.10%, $P < 0.05$) (Fig. 3.2B).

The viability of 'healthy' hiPSC-derived neuronal cells (ax0018) from spontaneous and synchronous differentiation methods following treatment with synthetic A β 1-42 demonstrated mixed results depending on the differentiation method used. Following neural induction using the spontaneous differentiation method; a significant reduction in cell viability was only observed with the highest concentration of synthetic A β 1-42 oligomers (2 μ M, 1 μ M and 0.5 μ M) (2 μ M: 40.72 \pm 5.48%, $P < 0.001$; 1 μ M: 60.18 \pm 10.14%; $P < 0.01$ and 0.5 μ M: 63.49 \pm 11.18%, $P < 0.05$) (Fig 3.3A), whilst cells differentiated using the synchronous differentiation method a significant reduction in cell viability when treated with synthetic A β 1-42 concentrations as low as 0.001 μ M was observed (2 μ M: 44.64 \pm 13.23%, $P < 0.0001$; 1 μ M: 69.31 \pm 14.14%, $P < 0.05$; 0.5 μ M: 58.75 \pm 15.43%, $P < 0.01$; 0.0625 μ M: 71.88 \pm 11.40%, $P < 0.05$; 0.03125 μ M: 68.44 \pm

15.51%, $P < 0.05$; 0.007813 μ M: $67.68 \pm 13.03\%$, $P < 0.0$; 0.001953 μ M: $70.70 \pm 10.57\%$, $P < 0.05$) (Fig. 3.3B).

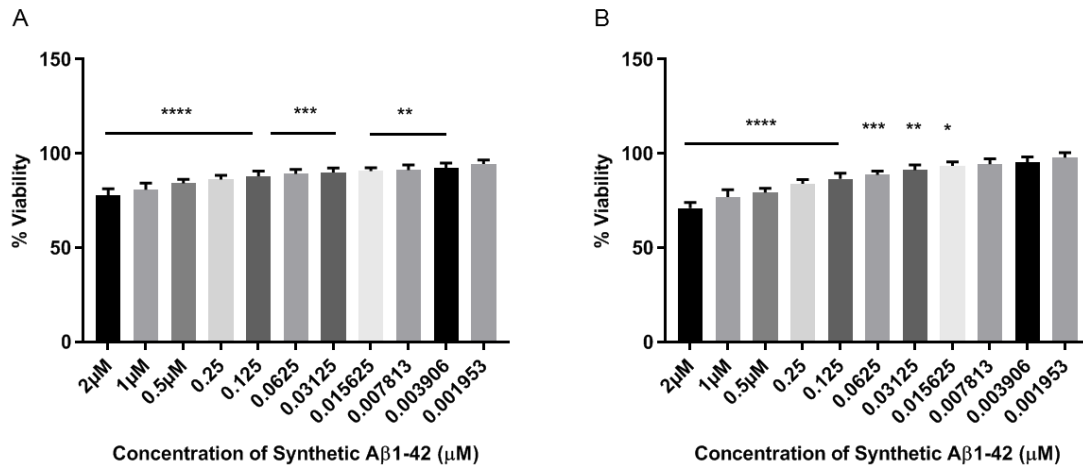


Figure 3.2: Determination of cell viability of astrocytes treated with synthetic Aβ1-42 oligomers. HA (A), hiPSC-derived astrocytes (line ax0018) (B). Cells were exposed to 2 - 0.001μM of synthetic Aβ1-42 for 48 hours. Cell viability was measured using MTT assay. The values are expressed as percentage of untreated cells as a control (100%), ± SEM, n=3, $P < 0.0001$ (****), $P < 0.001$ (***), $P < 0.01$ (**), $P < 0.05$ (*). Comparisons between treatments were performed using statistical analysis of One-way ANOVA, Dunnett's post-test.

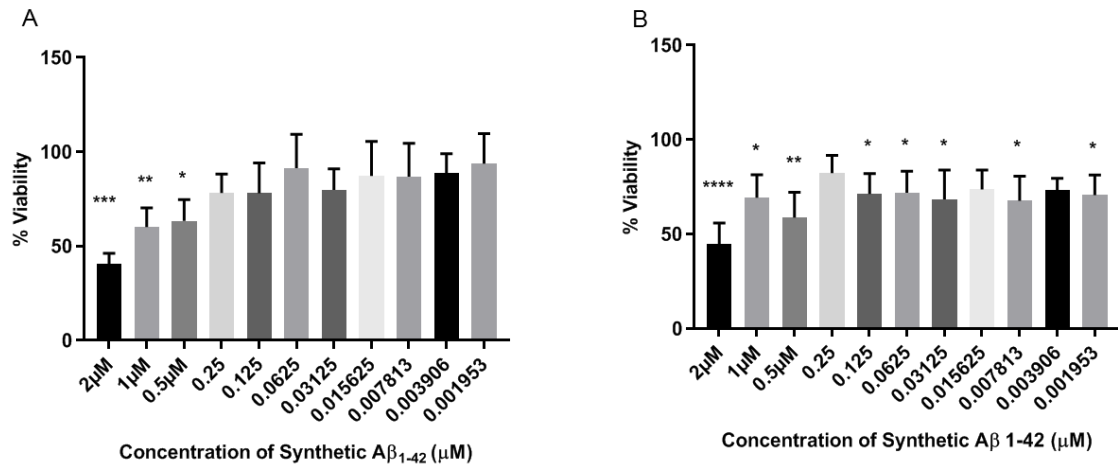


Figure 3.3: Determination of cell viability of neural cells treated with synthetic Aβ 1-42 oligomers. Cells were exposed to 2 - 0.001 μM of synthetic Aβ₁₋₄₂ for 48 hours. Neuronal cells (ax0018) derived from SP (A) and SY differentiation (B) methods at day 30. Cell viability was measured using the MTT assay. Values are expressed as percentage of untreated cells as a control (100%), ± SEM, n=3 (triplicate wells for each run), $P < 0.0001$ (****), $P < 0.001$ (***), $P < 0.01$ (**), $P < 0.05$ (*). Comparisons between treatments were performed using statistical analysis of One-way ANOVA, Dunnett's post-test.

3.3.3.2 Cell Nucleus Count Assay

To confirm the toxicity of synthetic A β 1-42 oligomers (Fig. 3.2B) to neural cell types. Cell viability was measured using the NucleoCounters® machine (section 3.2.4.2). Exposure to synthetic A β 1-42 oligomers (2 μ M and 1 μ M versus control) on hiPSC-derived astrocytes from cell line ax0018 for 48 hours; did not induce significant cell death (Fig. 3.4). Due to difficulties in passaging neuronal cells into a single cell suspension analysis of spontaneous and synchronously differentiated cells was not possible (data not shown).

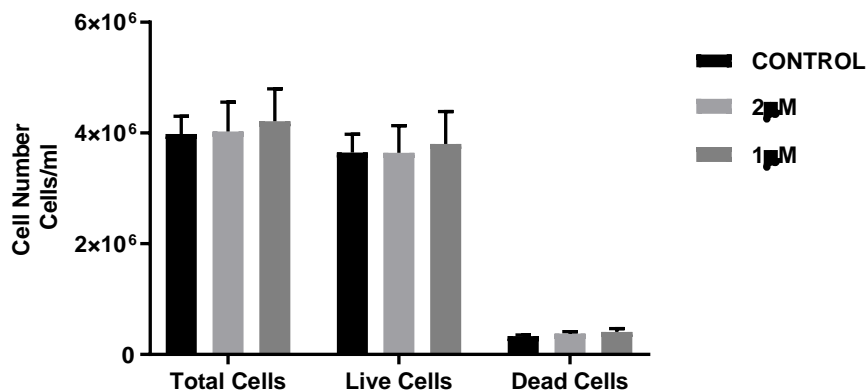


Figure 3.4: Quantitation of cell number of live and dead cells using NucleoCounter. Graph shows the treatment of hiPSC-derived astrocytes from cell line ax0018 at 45+ days old cells with synthetic A β 1-42 oligomers doses; 2 μ M and 1 μ M versus untreated cells as a control for 48 hours \pm SEM, n=3.

3.3.4 Synthetic A β 1-42 Oligomers Treatment and the Effects on Carbohydrate Levels

3.3.4.1 Determination the Effects on Glucose Uptake Levels

To determine the effect of synthetic A β 1-42 oligomers on the uptake of glucose by astrocytes and neurons the concentration of glucose remaining in the CM was used to indirectly monitor glucose uptake over 48 hours using the glucose assay. To control for potential differences in cell number results were corrected for cellular protein concentration. Results are expressed as μg (glucose)/mg (total cellular protein). Following treatment with 2 μM and 1 μM of synthetic A β 1-42 there was significant reduction in glucose uptake by HA and hiPSC-derived astrocytes from cell line ax0018 (HA: 2 μM : 722.20 \pm 43.26 $\mu\text{g}/\text{mg}$, $P < 0.05$; 1 μM : 688.22 \pm 24.38 $\mu\text{g}/\text{mg}$, $P < 0.05$ and ax0018-astrocytes: 2 μM : 297.60 \pm 40.64 $\mu\text{g}/\text{mg}$, $P < 0.05$; 1 μM : 280.71 \pm 42.05 $\mu\text{g}/\text{mg}$ $P < 0.05$, respectively), but no significant change was observed with 0.2 μM concentration of synthetic A β 1-42 (Fig. 3.5A and B, respectively).

Following exposure of hiPSC-derived neurons from cell line ax0018 to synthetic A β 1-42 oligomers for 48 hours, only 2 μM of synthetic A β 1-42 demonstrated a significant reduction in glucose uptake for neurons derived from the synchronous differentiation method (2 μM : 393.69 \pm 10.72 $\mu\text{g}/\text{mg}$, $P < 0.05$) (Fig. 3.6B), while neurons derived from the spontaneous differentiation method showed no significant changes in glucose uptake (Fig. 3.6A).

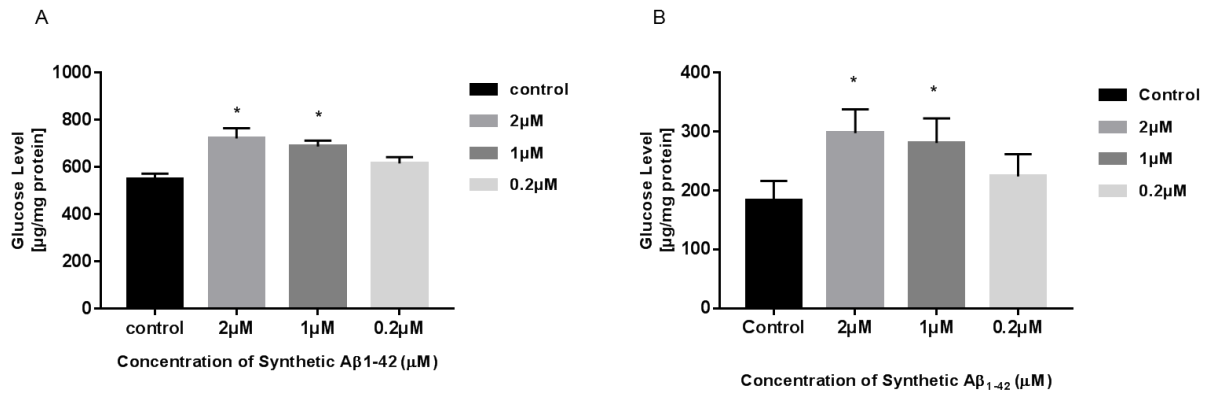


Figure 3.5: Determination of glucose levels remaining in the media following treatment of astrocytes to synthetic Aβ₁₋₄₂ oligomers. Treatment of HA (A), hiPSC-derived astrocytes from cell line ax0018 (B) at 45+ days old cells with synthetic Aβ₁₋₄₂ in the media (2 μM, 1 μM and 0.2 μM) versus untreated cells (control) for 48 hours. The amount of glucose remaining in the conditioned media following treatments were measured using glucose assay. Data is expressed as glucose μg/mg total cellular protein, ± SEM, n=3 (triplicate wells pooled for each run), $P < 0.05$ (*). The statistical analysis was done using One-way ANOVA, Dunnett's post-test.

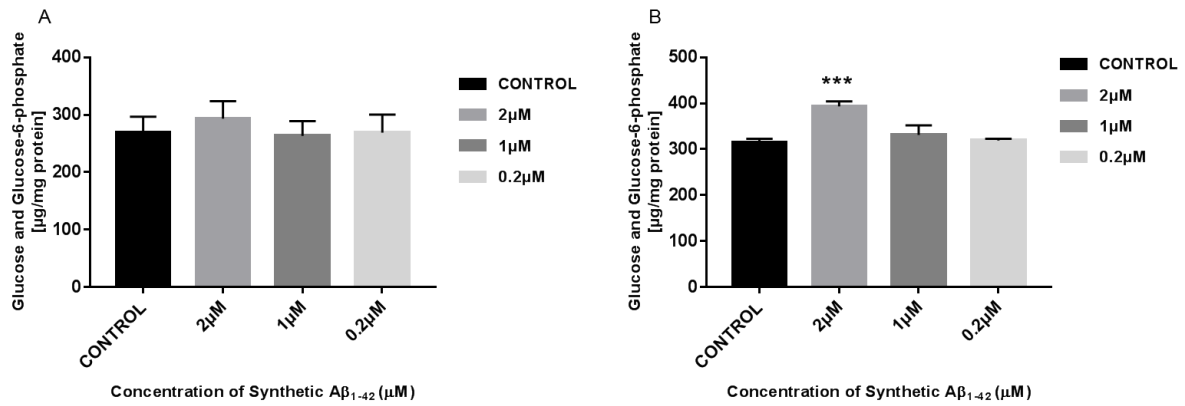


Figure 3.6: Determination of glucose levels remaining in the media following treatment of neuronal cells to synthetic A β_{1-42} oligomers. Treatment of the neuronal cells derived from: SP (A) and SY differentiation (B) methods from cell line ax0018 at day 30 with synthetic A β_{1-42} in the media (2 μM , 1 μM and 0.2 μM) versus untreated cells (control) for 48 hours. The amount of glucose remaining in the conditioned media following treatments were measured using glucose assay. Data is expressed as glucose $\mu\text{g}/\text{mg}$ total cellular protein, \pm SEM, n=3 (triplicate wells pooled for each run), $P < 0.001$ (***) . The statistical analysis was done using One-way ANOVA, Dunnett's post-test.

3.3.4.2 Determination the Effects on Glycogen Content Levels

Astrocytic glycogen content levels following treatment with synthetic A β 1-42 was measured using a glycogen assay to quantitatively assess the effects of glycogen content in HA and hiPSC-derived astrocytic cells from cell line ax0018. A significant reduction in glycogen content was only seen with the ax0018-derived astrocytes following exposure with 2 μ M concentration of synthetic A β 1-42 oligomers ($12.36 \pm 3.35\mu\text{g}/\text{mg}$, $P < 0.01$) (Fig. 3.7B), whilst no significant difference in glycogen content was seen in HA (Fig. 3.7A).

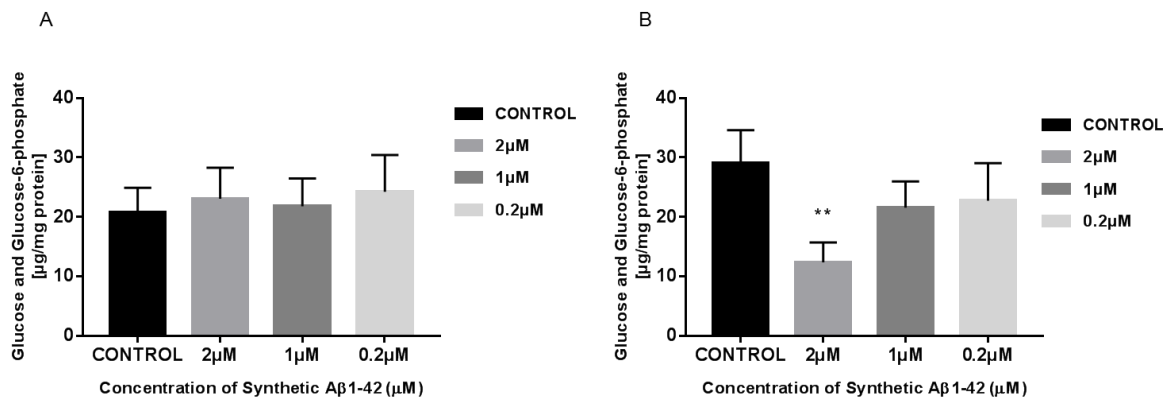


Figure 3.7: Determination the effect of synthetic A β 1-42 oligomers treatment on astrocytic glycogen stores. Treatment of HA (A), hiPSC-derived astrocytes from cell line ax0018 (B) at 45+ days old cells with synthetic A β 1-42 in the media (2 μM , 1 μM and 0.2 μM) and compared to untreated cells as a control for 48 hours. The cellular glycogen content was measured using a glycogen assay. Results are expressed as glucose and glucose-6-phosphate $\mu\text{g}/\text{mg}$ total cellular protein, \pm SEM, $n=3$ (triplicate wells pooled for each run), $P < 0.01$ (**). The statistical analysis was done using One-way ANOVA, Dunnett's post-test.

3.4 Discussion

This chapter was focussed on confirming the metabolic changes induced by A β prior to the clinically evident onset of AD. The previous chapter demonstrated that neural cells differentiated from 'healthy' hiPSC-derived NPCs are similar to their natural counterparts in their morphology and in metabolic function using glycogen breakdown experiments. This chapter is also a follow-up to earlier studies in our lab, which demonstrated that human stem cell derived neural cells exhibit metabolic dysfunction following exposure to synthetic A β 1-42 oligomers (Tarczyluk *et al.*, 2015). This was done using the NT2.D1 embryocarcinoma cell line. This chapter goes further to examine whether similar effects could be derived on exposure of hiPSC-derived neurons and astrocytes and human primary astrocytes to synthetic A β 1-42 oligomers. It is important to note that results shown in chapter 2 suggested that hiPSC-derived NPC from line ax0018 produced 'healthy' populations of neurons and astrocytes depending on the differentiation methods, and yielded more consistent results than the ax0016 cell line. As such, the ax0018 cell line was used for the rest of the thesis. Data produced using hiPSC-derived NPC from line ax0016 cultures, images and results have been excluded from the study (see Appendices).

The synthetic A β 1-42 was prepared as previously described (Tarczyluk *et al.*, 2015). The presence of synthetic A β 1-42 was confirmed using SDS-PAGE gel and by western blotting to show the different sizes of the amyloid oligomers (section 3.3.2).

The MTT assay was used to determine the toxicity of the synthetic A β 1-42 oligomers to HA and the hiPSC-derived neuronal and astrocytic cells. HA and hiPSC-derived astrocytic cells from ax0018 cell line showed a reduction in cell viability following a 48 hours exposure to synthetic A β 1-42 oligomers at day 45+ in culture. This is similar to results by Tarczyluk *et al.* (2015).

However, the viability assays for the neuronal cells in culture was a lot more challenging to achieve, and yielded mixed results. In order to ensure consistency and representativeness of the results, the MTT assay for neuronal cells was done at day 30 of culture for the differentiated neuronal cells. Human iPSC-derived neuronal cells displayed a high degree of susceptibility to the MTT, which resulted in cell lifting independent of exposure to synthetic A β 1-42 oligomers. As a result, half the concentration of 1.25 μ g/ml MTT stock used for astrocytes

assays was used for the neuronal assays. The difference in the susceptibility of the hiPSC-derived cells and NT2 cells to MTT may be as a result of the difference in cellular origins and culture conditions.

Human iPSC-derived neuronal cells from the spontaneous differentiation method only exhibited reduction in viability to the highest concentration of synthetic A β 1-42 oligomers (2 μ M), while a dose-response pattern was seen with neuronal cells cultured via the synchronous differentiation method. Despite this difference, the result still appear is similar to the findings of reported by Tarczyluk *et al.* (2015) on the embryocarcinoma cell line, in which there was a significant reduction in viability to the highest concentration of synthetic A β 1-42 oligomers used for neuronal/astrocyte co-cultures. This similarity for the SP differentiation method is likely due to the fact that the NT2.D1 cell line used was essentially spontaneously differentiated to produce mixed neuron-astrocyte populations (Tarczyluk *et al.*, 2015, Woehrling *et al.*, 2010).

A cellular count was performed to confirm the validity of cellular toxicity results from the MTT assay, and if exposure to synthetic A β 1-42 oligomers resulted in cell death. The results showed that there was no significant cell death in the astrocytes as a result of synthetic A β 1-42 exposure (Fig. 3.4). This may indicate that the toxicity of A β oligomers resulted in cellular metabolic damage but not immediate cell death since the MTT assay itself assesses cell metabolic activity. This appears to be in concert with the natural history of AD in which atrophy and brain tissue loss is not seen until advanced disease is well established. It would have been interesting to assess neuronal cell death following exposure to synthetic A β 1-42 oligomers, as they are the primary cells involved in important brain functions like memory and behaviour, which are the most commonly affected brain functions in AD. However, a similar cell count could not be done for neurons because the neuronal networks make it difficult to separate the neuronal cells into discrete entities for counting, and it was impossible to passage them. However, the validity of the results of cellular counts post A β exposure may be affected by the method of cell counting used. The NucleoCounters® machine counts cells by examining the number of fluorescent nuclei using DAPI versus inflorescent nucleus, and is this unable to differentiate between living cells and those undergoing apoptotic cell death. Other viability assays like the lactate dehydrogenase (LDH) cytotoxicity assay may provide more robust results on assessment of neuronal viability following A β oligomers exposure. This is because it utilises bioluminescent quantification of LDH leakage from cells, which is more accurate than DAPI detection.

To confirm one of the main hypotheses of this project, and determine that amyloid oligomers induced metabolic dysfunction, the HA and hiPSC-derived astrocytes and neurons cultures were exposed to synthetic A β 1-42 oligomers. As this was essentially a repetition of the efforts by Tarczyluk *et al.* on the NT2 embryocarcinoma cell line in 2015, but now on hiPSC-derived astrocytes and neurons. As such the synthetic A β 1-42 was prepared using the same protocol. The concentration range of 0.2 μ M, 1 μ M and 2 μ M A β 1-42 was also used, as this was the range that had previously been reported to induce metabolic dysfunction *in vitro*. The results showed that both HA cells and hiPSC-derived astrocytic cells showed a concentration-dependent pattern of reduction in glucose uptake. Similar amyloid-induced reductions in glucose uptake have been reported previously (Abeti *et al.*, 2011, Tarczyluk *et al.*, 2015).

Neuronal cells have been shown to exhibit metabolic dysfunction in response to A β 1-42 oligomers as evidenced by a reduction in glucose uptake (Praong *et al.*, 2002) while the hiPSC-derived neuronal cells exhibited reduction in glucose uptake in response to the highest concentration of synthetic A β 1-42 oligomers (2 μ M), but with significant results only for the neurons cultured by synchronous differentiation. These mixed results may have occurred as a result of the differences in the nature of the neuronal networks formed as a result of the different differentiation methods, with the synchronous differentiation showing what appear to be better directed and coordinated inter-neuronal connections. Furthermore, the astrocyte populations produced in the differentiation process may also account for this difference in glucose uptake in response to amyloid exposure; since neurons *in vivo* depend on cues from astrocytes in their networks. This may explain why the previous efforts in our lab showed a reduction in glucose uptake to a greater extent in co-cultures than in primary neuronal or astrocytic cultures (Tarczyluk *et al.*, 2015). However, it was impossible to definitively assess the effect of synthetic A β 1-42 oligomers on neuronal populations using this NPC line because it was not possible to produce pure neuronal cultures.

The pathogenesis of amyloid-induced reduction in glucose uptake remains a focus of research, and several mechanisms have been demonstrated as possible pathways for glucose uptake reduction. For example, Praong *et al.* (2002) showed that A β reduces glucose uptake by preventing expression of GLUT3 on the plasma membrane. Impaired lipid peroxidation has also been demonstrated as a mechanism for impaired glucose uptake in AD (Mark *et al.*, 1997). However, it has been reported that endogenous amyloid exhibits more stability *in vitro* than the synthetic amyloid (Moore *et al.*, 2009), and has also been shown to be at least 30 times more neurotoxic than the synthetic form (Muller-Schiffmann *et al.*, 2016).

The second hallmark of metabolic dysfunction assessed in this project was glycogen turnover, which was assessed by glycogen assays in HA and hiPSC-derived astrocytic cells (ax0018) post exposure to synthetic A β 1-42 oligomers. The hiPSC-derived astrocytes in this study displayed significant reduction in glycogen content. The complex mechanisms behind amyloid-induced reduction in glycogen turnover remain to be explained. Future application of Seahorse Bioanalyser (Agilent) and nuclear magnetic resonance (NMR) analysis may provide better explanations of pathways involved. The NMR analysis involves the use of radiolabelled metabolic substrates (glucose, lactate, etc) to examine the metabolic processing of these substrates. It may also provide key information on the function of key enzymes such as pyruvate dehydrogenase and hexokinase in response to treatment with A β .

3.5 Conclusion

Hypometabolism is an established pathogenetic process which precedes the clinical onset of AD by several years. This chapter has confirmed our hypothesis that exposure to synthetic A β 1-42 oligomers induces metabolic dysfunction in 'healthy' hiPSC-derived astrocytes and neurons, as demonstrated by reduction in glucose uptake, and impairment of glycogen turnover in these cells. This provides another step forward towards providing a complex functional *in vitro* system for studying the early preclinical changes in AD where potential novel therapeutic targets can be directed. It will also be important to determine if endogenously produced A β exerts similar effects on metabolism in AD patient-derived astrocytes and neurons. The next chapter aims to determine A β production from fAD patient hiPSC-derived neural cells, as well as to assess metabolic dysfunction induced by the endogenously produced amyloid (Chapter 4).

Chapter 4: Characteristic of Human Familial AD Patient Cell Line and A β Release

4.1 Introduction

The previous chapters of this project have been focussed on the generation of neurons and astrocytes from 'healthy' control hiPSC-derived NPCs (chapter 2), and assessment of the effects of exogenous amyloid on metabolism in these cells (chapter 3). This chapter focuses on the generation of neurons and astrocytes from fAD patient hiPSC-derived neural cells and establishing the occurrence of early metabolic dysfunction in these cells. This will serve as foundation level efforts towards identifying temporal and mechanistic targets for therapeutic intervention in the journey of AD from the preclinical stages to obvious clinical onset.

4.1.1 Familial AD

Familial AD is a rare form of AD which accounts for about 4% of all cases of AD (Prince *et al.*, 2014). It is inherited in an autosomal dominant fashion and is caused by mutations in genes coding for three proteins important in amyloid processing; APP, PSEN1 and PSEN2. Familial AD occurs earlier than the more common sporadic form of AD, having clinical onset from around 50 years of age. Although fAD is a rare form of AD, it is a very useful model to study the pathology and pathogenesis of AD because of the large evidence available with respect to increased A β generation or abnormal A β processing on the aetiology and course of AD.

4.1.2 Genetic Mutations in fAD

The PSEN1 and PSEN2 mutations are most common forms of fAD, and represent the most aggressive form of the disease. For the APP complex, there are at least 30 reported mutations (Cruts *et al.*, 2012, De Jonghe *et al.*, 2001), the most common of which is the London mutation which is a Val-Leu missense mutation at the 717 position of the APP transcript (Cruts *et al.*, 2012). This mutation increases A β 1-42 and A β 1-38 levels in response to increased β -site amyloid precursor protein cleaving enzyme 1 (BACE1) activity as well as reduced γ -secretase activity due to alterations in its active site (Muratore *et al.*, 2014). All three major classes of fAD mutations (PSEN1, PSEN2 and APP) are characterised by altered A β metabolism, and

increased A β production (Ferris *et al.*, 1980). The ax0012 cell line used as the fAD sample in this project has the PSEN1 (L286V) mutation (Table 4.1).

The PSEN1 gene is located on the long arm of Chromosome 14 (position 24.3) (Sherrington *et al.*, 1995), while the PSEN2 gene is located on the long arm of chromosome 1 (position 42.13) (Takano *et al.*, 1997). Mutations of the PSEN1 gene are the most common genetic cause of fAD, accounting for up to 30% of cases of fAD. The PSEN1 gene contains 13 exons, 10 of which contain protein coding sequences (Sherrington *et al.*, 1995). There are at least 211 PSEN1 and 33 PSEN2 gene mutations which have been reported, most of which are missense mutations (Cruts *et al.*, 2012). Different mutations in the presenilin genes produce A β peptides of varying lengths and structure, but most mutations tend to result in a C-terminal or an N-terminal truncation of the A β peptide. The BACE1 and γ -secretase enzymes have multiple potential cleavage sites at the APP sequence, thus resulting in A β peptides of varying lengths. Different mutations in the presenilin genes produce varying effects on the A β species produced, and a resultant variability in the onset and severity of the AD variant, the most severe forms having an onset before the age of 30. However, most variants have an average onset at 40 years of age (Mann and Esiri, 1989).

The fAD patient-derived hiPSCs used in the current project contained the PSEN1 gene mutation L286V, which was isolated from a 38 years old female Caucasian (Table, 4.1). The L286V mutation occurs at exon 8 of the genomic sequence and has an average onset at the age of 47 years old (Ikeuchi *et al.*, 2008). Exon 8 is believed to code for the sixth transmembrane domain and the largest loop on the cytoplasmic surface of PSEN1. The L286V mutation along with another PSEN1 mutation (M146L), and three other APP mutations (human Swedish APP(695), Florida (I716V), and London (V717I) mutations, have been reported to induce an aggressive form of AD characterised by early A β accumulation, reduced glucose utilisation in the brain and cognitive impairment in transgenic 5XFAD mice (Macdonald *et al.*, 2014).

4.1.3 Presenilin Proteins

The PSEN1 and PSEN2 genes code for presenilin 1 and presenilin 2, which are part of the presenilin complex, a group of transmembrane proteins which are important in the regulation of several cellular enzymes. They are both aspartyl proteases, and are made up of six to nine

transmembrane loops, the largest of which is the transmembrane domain 2 (TM-2). TM-2 is the hottest focus for presenilin mutations, accounting for about half of reported mutations in the PSEN1 gene.

PSEN1 is the proteolytic subunit of the γ -secretase enzyme. The sequential proteolytic cleavage of APP by the BACE1, then γ -secretase results in A β production. This process involves intramembrane proteolysis, which occurs at multiple cleavage sites on the APP molecules, and thus results in the production of A β species of varying sizes (Chavez-Gutierrez *et al.*, 2012, Fernandez *et al.*, 2014). This proteolytic cleavage produces A β species which end in an N-terminal (most abundant) or a C-terminal peptide form of A β , if the APP is cleaved by β -secretase at the Asp1 and the Glu11 position of the A β domain respectively. This is then followed by cleavage at Leu49 or Thr48 position of the A β domain by γ -secretase, leading to shorter fragments. Mutations resulting in N-terminal deletion enhance A β aggregation and neurotoxicity, and these have been shown to be highly abundant in post-mortem brain samples of patients with AD (Bayer and Wirths, 2014, Dunys *et al.*, 2018).

4.1.4 A β

The accumulation of toxic amyloid species is the central pathological trigger of the mechanistic cascade of metabolic events that occur in AD. It is believed to induce inflammation, metabolic cellular injury, gliosis and eventually neuronal cell death, which manifests clinically as cognitive impairment (Selkoe and Hardy, 2016). A β occurs in different forms based on size, and the degree of damage induced by A β is believed to be dependent on the species of A β accumulated, as well as the quantity of amyloid accumulated. A β can also be soluble or insoluble. Thus, the A β species can occur as soluble monomers, oligomers, insoluble fibrils or plaques depending on the degree of complexity (Selkoe and Hardy, 2016). The various isoforms of A β have been described in sections 1.7.2.1 and 3.1.3.

A β is produced as a result of APP processing (Fig. 1.2), and in normal individuals, and the amount of A β produced in healthy individuals is tightly regulated normally, as accumulation of A β would normally induce uptake and clearance by glial cells in the brain (Jekabsone *et al.*, 2006, Morgan, 2006). The amyloidogenic and non-amyloidogenic pathways of APP processing have been discussed in section 1.7.2 of this project. A β production mainly occurs in neurons in the brain, but has also been reported at other sites in the body (Puig and Combs, 2013). Indeed, abnormal amyloid accumulation is a characteristic of a series of disorders

called amyloidosis, in which amyloid accumulation is present in several tissues of the body, including the kidneys, heart, skeletal muscles, adipose tissue and the skin (Kazmi, 2013).

A β is known to be one of the potent activators of the proinflammatory reactive state of astrocytes, and continued production of excessive amounts of A β in AD patients causes the persistence of reactive astrocytes, and continued neuroinflammation and astrogliosis with deleterious effects in the form of neuronal cell death (Pekny and Pekna, 2014, Sun *et al.*, 2012).

4.1.5 The Role of Astrocytes in A β Release

There was an initial perception that A β production was an exclusive preserve of neurons in the brain, while astrocytes served to imbibe and remove excess A β produced from APP degradation. This is because neurons express high levels of the BACE1 enzyme complex which is responsible for initial processing of APP. However, astrocytes have also been shown to express this enzyme, albeit in lower quantities by individual cells (Rossner *et al.*, 2005, Jin *et al.*, 2012), but more likely in significant amounts when considering the fact that astrocytes vastly outnumber neurons in the brain. Furthermore, astrocytes are pleomorphic and can alter their metabolism in response to stress and have been shown to increase BACE1 expression in response to stress (Blasko *et al.*, 2000), lending support to the possibility of a significant role of astrocytes in A β generation. The fact that astrocytes play a significant role in A β generation, clearance and the protection against amyloid-induced damage may have important implications in the struggle for a definitive therapeutic management strategy for AD.

4.1.6 Aims and Objectives

The hypothesis for this portion of the project was that fAD patient-derived astrocytes and neurons have a higher A β release profile, and will exhibit metabolic dysfunction as a result of the excess A β production.

The specific objectives were to:

- Differentiate NPCs derived from fAD patient hiPSCs, and then differentiate them to produce neurons and astrocytes.
- Characterise the astrocytes and neurons morphologically and immunohistochemically.
- Assess the production of A β peptides in both fAD patient and 'healthy' control-derived neurons and astrocytes at defined time points during the differentiation process and comparing the A β production using ELISA.
- Determine metabolic dysfunction in fAD patient-derived neurons and astrocytes by assessing glucose uptake in neurons and astrocytes, as well as astrocytic glycogen content level in comparison with 'healthy' control neurons and astrocytes.

4.2 Materials and Methods

4.2.1 Generation and Characterisation of Human fAD Patient iPSC-derived NPCs

4.2.1.1 Neural Cells Differentiation Methods

The human hiPSC-derived NPCs from familial AD patient (fAD, ax0112) was obtained from Axol Bioscience, UK (Table 4.1). The patient cells were differentiated to produce cerebral cortical neuronal cells over 10, 20, 30 and 40 days using spontaneous and synchronous neural differentiation protocols (sections 2.2.2.1 and 2.2.2.2, respectively). Additionally, fAD-derived NPCs were differentiated into astrocytic cells for 45+ days using astrocytes differentiation methods (section 2.2.2.3).

Cell Name	ax0112
Cell Type	hiPSC-derived NPCs Alzheimer's patient line
Starting material	Dermal fibroblast
Mutation	Presenilin1 (PSEN1 L286V)
Donor Age	38 years old
Donor Gender	Female (Caucasian)

Table 4.1: Description of human iPSC-derived neural stem cells from familial AD patient donor.

4.2.2 ICC Staining

The differentiated neural cells from fAD line were assessed using immunohistochemistry staining as described in section 2.2.4.

4.2.3 Microscopes, Images Capture and Slides Storage

Cell images were captured according to the methods described in section 2.2.5.

4.2.4 Characterisation of Amyloid Release Profile

4.2.4.1 Sample Preparation

The fAD patient cells (ax0112) and healthy control cell line (ax0018) were differentiated into neuronal cells and astrocytic cells using the protocols described previously (section 2.2.2).

4.2.4.2 Collection of Conditioned Medium

Cell conditioned medium was collected from each cell lines that was differentiated using neural spontaneous and synchronous differentiation methods and astrocytic cells differentiation methods. Human iPSC-derived NPCs were differentiated to neuronal cells on 12-well plate in triplicate for each day (days: 0, 30 and 40) (sections 2.2.2.1 and 2.2.2.2). On days 29 and 39, the medium was completely replaced with 1ml of fresh medium according to differentiation methods. Likewise, astrocytic cells at 45+ days (section 2.2.2.3) were plated on 12-well plate (triplicate) for 2 - 3 days in culture, and then replaced with 1ml of fresh AM. After 48 hours, the conditioned medium was collected (3 wells pooled) and centrifuged at 200 x g for 5 minutes. Afterwards, 1ml of the supernatant was transferred into 1.5ml sterile microcentrifuge tubes and stored at -20°C for further analysis of A β 1-40 and A β -42 using ELISA (section 4.2.4.3) and Immunodepletion assay (section 5.2.2). The cells were lysed to determine the protein levels (section 2.2.8).

4.2.4.3 Enzyme-Linked Immunoabsorbant Assay (ELISA)

The A β 1-40 and A β -42 ELISA assay was used to quantify the A β 1-40 and A β 1-42 separately (A β 40 kit and A β 42 kit) according to the manufacturer's instructions (ThermoFisher Scientific, UK). Briefly, standards and samples were diluted with standard diluent according to the manufacturer's protocol. 50 μ l of standards (duplicated) and samples (duplicated) were added to the plate. 50 μ l of Human A β 40 and A β 42 detection antibody solution was then added to each well. The plate was then sealed and incubated at room temperature for three hours on a plate shaker. After incubation, the contents were aspirated and the wells were washed 4 times with wash buffer. 100 μ l anti-Rabbit IgG HRP solution was then added to each well and incubated at room temperature for 30 minutes. After incubation, the wells were aspirated and washed 4 times with wash buffer. 100 μ l of stabilized chromogen was added to each well and incubated at room temperature for 30 minutes in the dark. After incubation, 100 μ l of stop solution was added to each well and gently tapped side of the plate to mix. The absorbance was read within 30 minutes after adding the stop solution at 450nm using Thermo multiscan EX 96-well plate reader.

4.2.5 Determination of Carbohydrate Levels

4.2.5.1 Determination of Glucose Uptake Levels

The cells from hiPSC-derived astrocytes, and neuronal cells derived from SP and SY differentiation methods from fAD cell line (ax0112) and 'healthy' control cell line (ax0018) were cultured according to methods described in sections 4.2.1.1 and 3.2.4. CM samples were collected after 48 hours in culture and measured for glucose uptake using glucose assay (section 3.2.5.1). All readings were corrected for background and total cellular protein levels (section 2.2.8).

4.2.5.2 Determination of Glycogen Content Levels

The homogenised samples from hiPSCs-derived astrocytes of fAD cell line and 'healthy' control cell line were measured for glycogen content levels according to glycogen assay

method described in section 2.2.6. All readings were corrected for background, free glucose in homogenised samples and total cellular protein levels (section 2.2.8).

4.2.6 Cell Lysis

Cells were lysed using cell lysis procedure described in section 3.2.6.

4.2.7 Determination of Protein Levels

Protein levels were measured according to protocol described in section 2.2.8.

4.2.8 Quantification and Statistical Analysis

All quantification and statistical analyses were carried out according to the methods described in section 2.2.9.

4.3 Results

4.3.1 Generation and Differentiation of Human Brain Neural Lineage Cells from fAD Patient iPSC-derived NPCs

To characterise the hiPSC-derived NPCs from human fAD patient (PSEN1 L286V) ax0112 cell line (Axol Biosciences) differentiated cells were identified visually by their characteristic morphology and by ICC staining (Fig. 4.2). Quantification of the A β 1-42 and A β 1-40 release from spontaneous and synchronous differentiation methods over 40 days. At days 0, 30 and 40, the A β profile release was compared between fAD patient and 'healthy' control (ax0018) cell lines using ELISA (section 4.2.4).

The ax0112 cells were defrosted and passaged twice before differentiation. Cells were then characterised at time zero using ICC staining for the neural precursor cell markers sox2, pax6 and Nestin after passaging (Fig. 4.1C, D and B, respectively). Cortical neural rosettes can be observed as morphologically identifiable structures in cultures under phase contrast microscopy at day 0 (Fig.4.1A). Human fAD-derived NPCs were differentiated into cortical neurons using spontaneous and synchronous differentiation methods over a period of time 40 days (section 4.2.1.1). Additionally, the NPCs were differentiated into astrocytes using differentiation and maturation methods and cultured for up to 5 weeks prior to use (section 4.2.1).

NPCs derived from fAD patient cell line ax0112 was cultured using the spontaneous and synchronous differentiation methods to produce cerebral cortical neuronal cell populations within 40 days. The phase contrast images of neuronal cells in both differentiation methods revealed the typical morphology of developing neurons in culture, with extensive neurite outgrowths by day 10 (Fig. 4.2A and B), and extensive neural networks by days 20, 30 and 40 (Fig. 4.3A and B, 4.5A and B, 4.5A and B, respectively).

NPCs differentiated into TUJ1-positive expressing cortical neuronal networks and the networks became denser over time from day 10 to 40 of culture (Fig. 4.2C and D, 4.3C and D, 4.4C and D, 4.5C and D, respectively). These neuronal networks are more obvious morphologically earlier (at day 20) with synchronous differentiation (Fig. 4.3H), but only show similar morphological clarity from day 30 with spontaneous differentiation (Fig. 4.4G). The

presence of DAPT in the synchronous differentiation method resulted in subjectively higher number of neurons in the cultures, but the presence of dense interneuronal networks precluded the possibility of quantifying the cell produced for this comparison. Similarly, the proportions of mature neurons produced in the cultures could not be determined.

Both spontaneous and synchronous differentiation methods produced S100 β positive cells are visible at days 10, 20, 30 and 40 (Fig. 4.2E and F, 4.3E and F, 4.4E and F, 4.5E and F, respectively). Synaptophysin and PSD-95 expression was not detected at days 10 and 20 (data not shown). However, positive expression of synaptophysin-positive (Fig. 4.6A, D, G and J) and PSD-95-positive (Fig. 4.6B and E, H and K) was detected at days 30 and 40, respectively.

Human iPSC-derived astrocytes from fAD cell line ax0112 were characterised and stained using ICC staining for astrocytic markers at day 45+. The morphology of the astrocytic cells was assessed via phase-contrast image (Fig. 4.8A). The astrocytes displayed the typical stellate form and followed a similar morphological course as was shown for the 'healthy' hiPSC-derived astrocytic cells (Chapter 2). The astrocytes positively stained for GFAP and S100 β (Fig. 4.7B and C, respectively). Quantification of the stained cells was also difficult, due to the density of the staining and heterogeneous nature of the cultures.

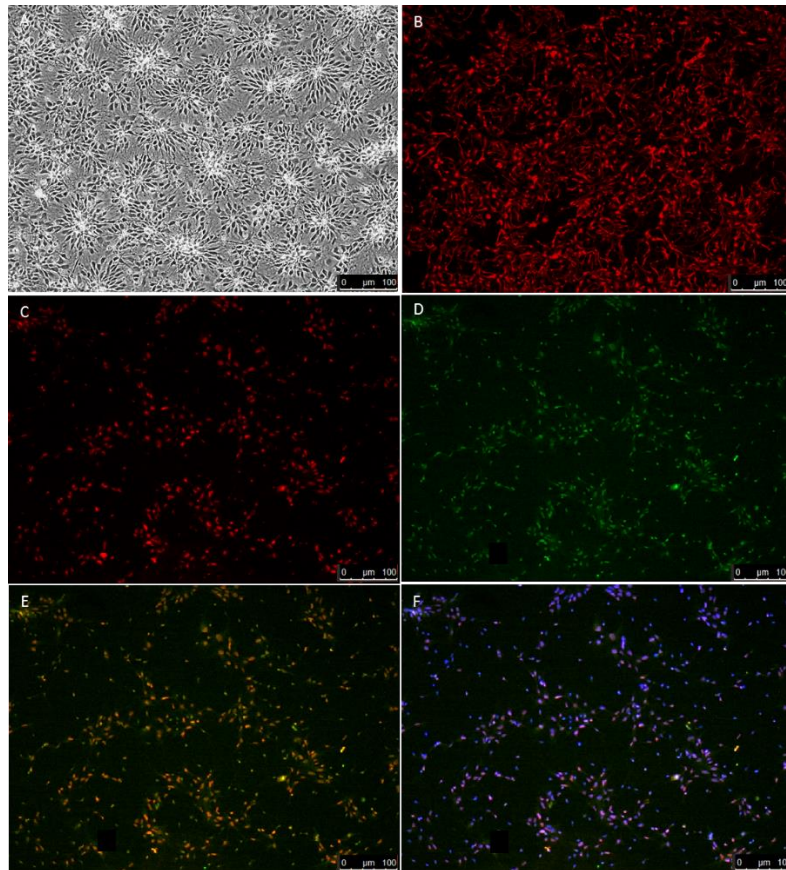


Figure 4.1: Representative images of hiPSC-derived NPCs from fAD patient cell line using ICC staining. Phase contrast image showing the development of neural rosettes in human 'healthy' control NPCs (A). The NPCs were stained for neural precursor cells using antibodies against Nestin (red, B), sox2+ (red, C) and pax6+ (green, D). Merged image showing co-expression of both pax6+ and sox2+ (E). Cells were counterstained with DAPI+ (blue, F). The cells were stained at passage number 2, n=3. Scale bars: 100μM.

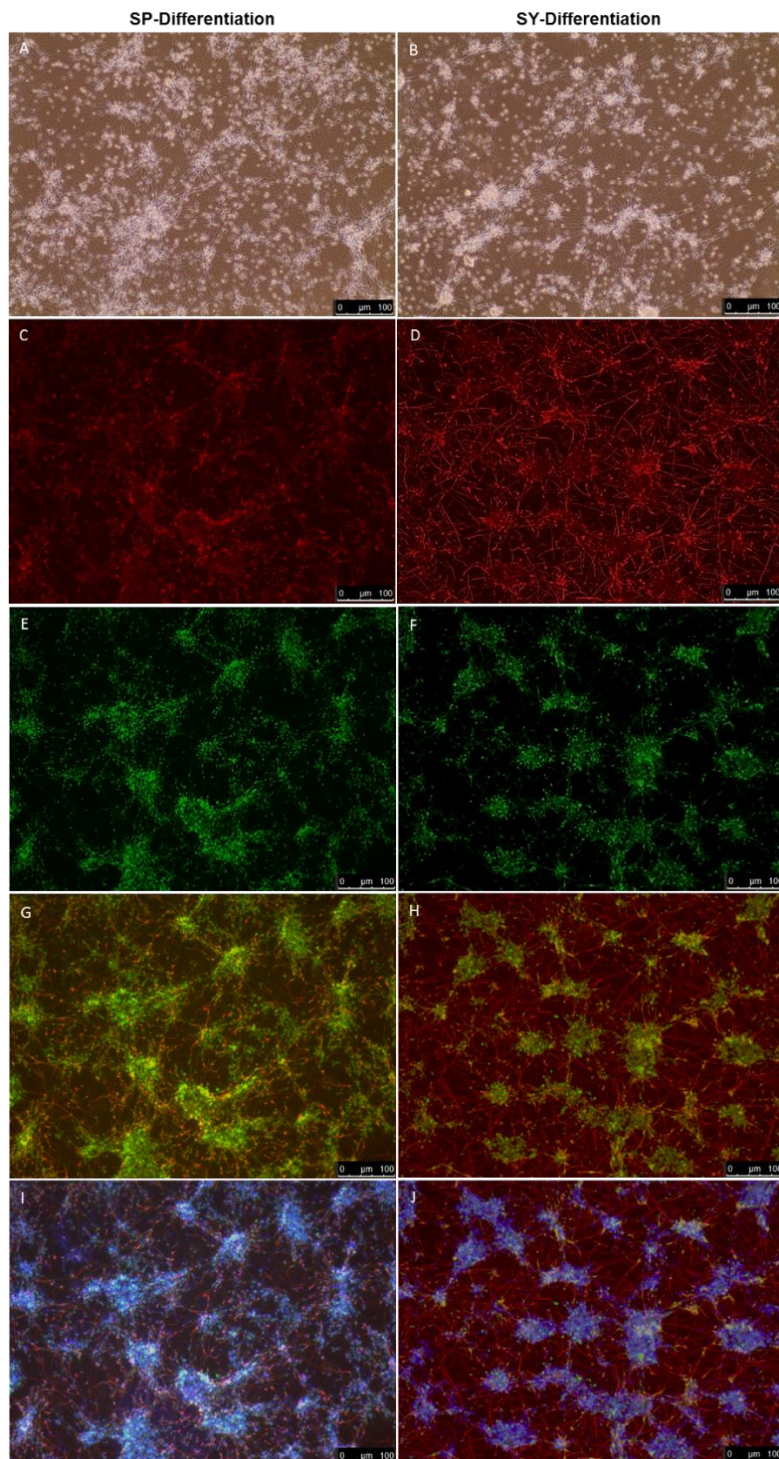


Figure 4.2: Representative images of neural cells differentiated from hiPSC-derived NPCs of fAD patient cell line using spontaneous and synchronous differentiation methods at day 10. Phase contrast images of spontaneous (A) and synchronously (B) differentiated cells. Immunofluorescent images showing TUJ1+ neuronal cells (red) (C and D), and S100 β + astrocytic cells (green) (E and F). Merged image showing expression of both TUJ1+ and S100 β + (G and H). Nuclei were counter stained with DAPI+ (blue) (I and J). n=3. Scale bars: 100 μ M.

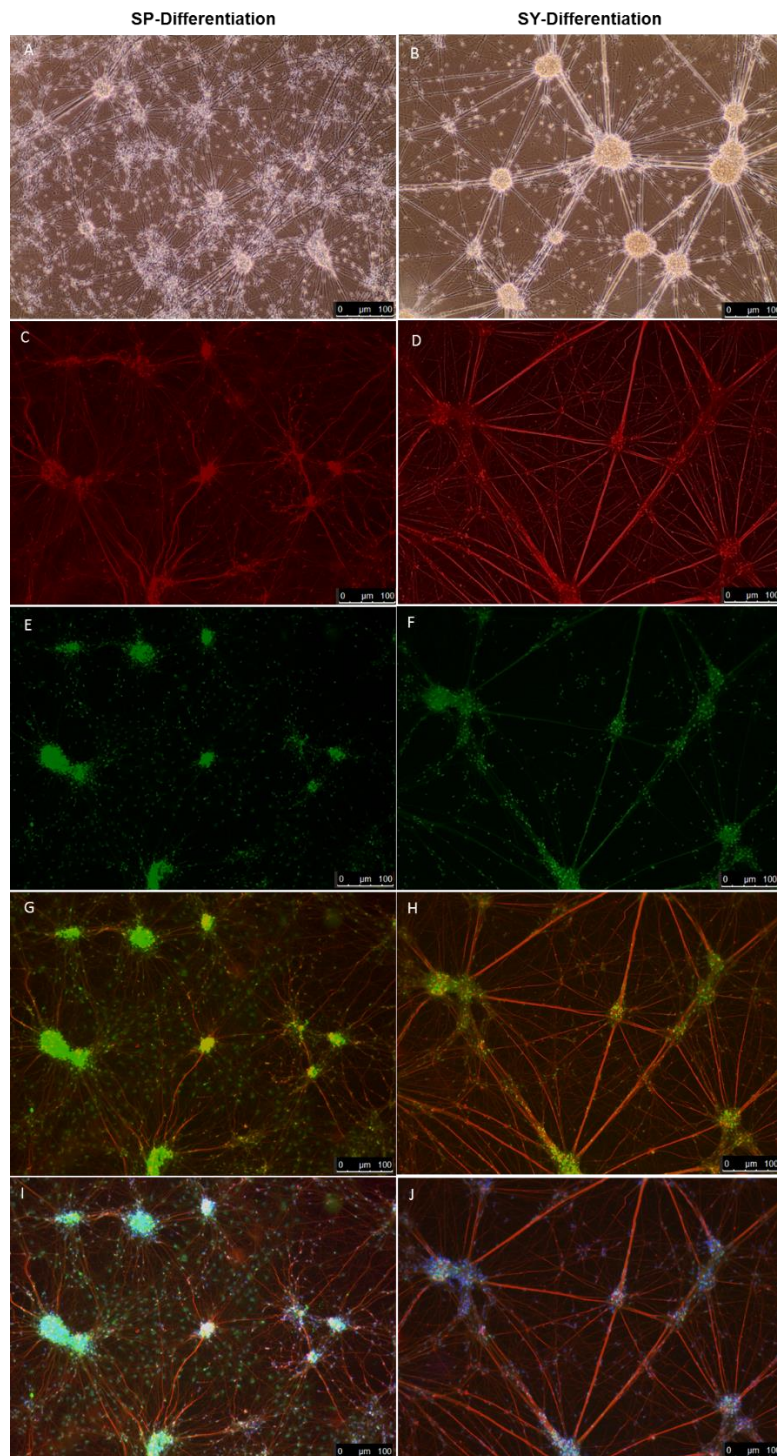


Figure 4.3: Representative images of neural cells differentiated from hiPSC-derived NPCs of fAD patient cell line using spontaneous and synchronous differentiation methods at day 20. Phase contrast images of spontaneous (A) and synchronously (B) differentiated cells. Immunofluorescent images showing TUJ1+ neuronal cells (red) (C and D), and S100 β + astrocytic cells (green) (E and F). Merged image showing expression of both TUJ1+ and S100 β + (G and H). Nuclei were counter stained with DAPI+ (blue) (I and J). n=3. Scale bars: 100 μ M.

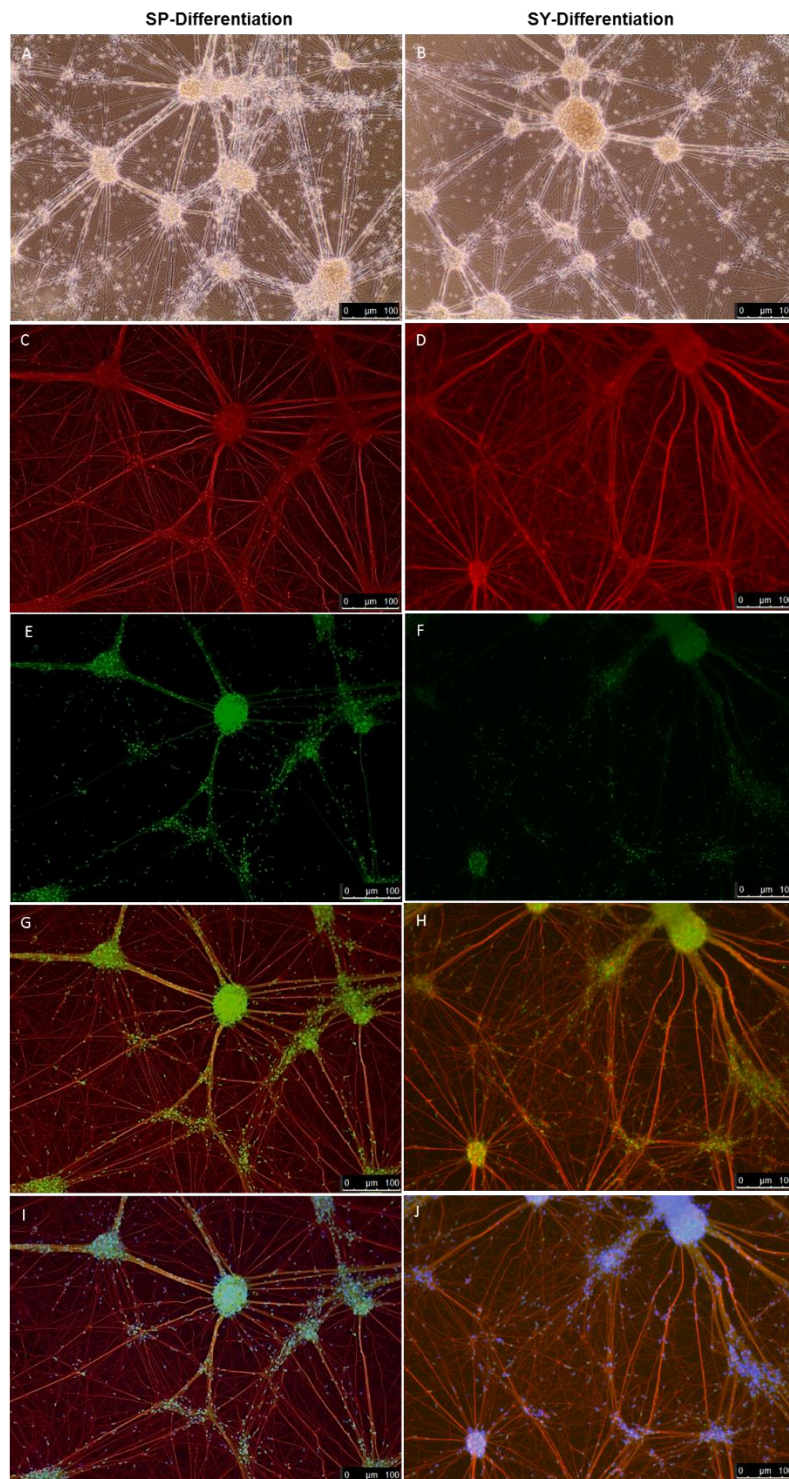


Figure 4.4: Representative images of neural cells differentiated from hiPSC-derived NPCs of fAD patient cell line using spontaneous and synchronous differentiation methods at day 30. Phase contrast images of spontaneous (A) and synchronously (B) differentiated cells. Immunofluorescent images showing TUJ1+ neuronal cells (red) (C and D), and S100 β + astrocytic cells (green) (E and F). Merged image showing expression of both TUJ1+ and S100 β + (G and H). Nuclei were counter stained with DAPI+ (blue) (I and J). n=3. Scale bars: 100 μ M.

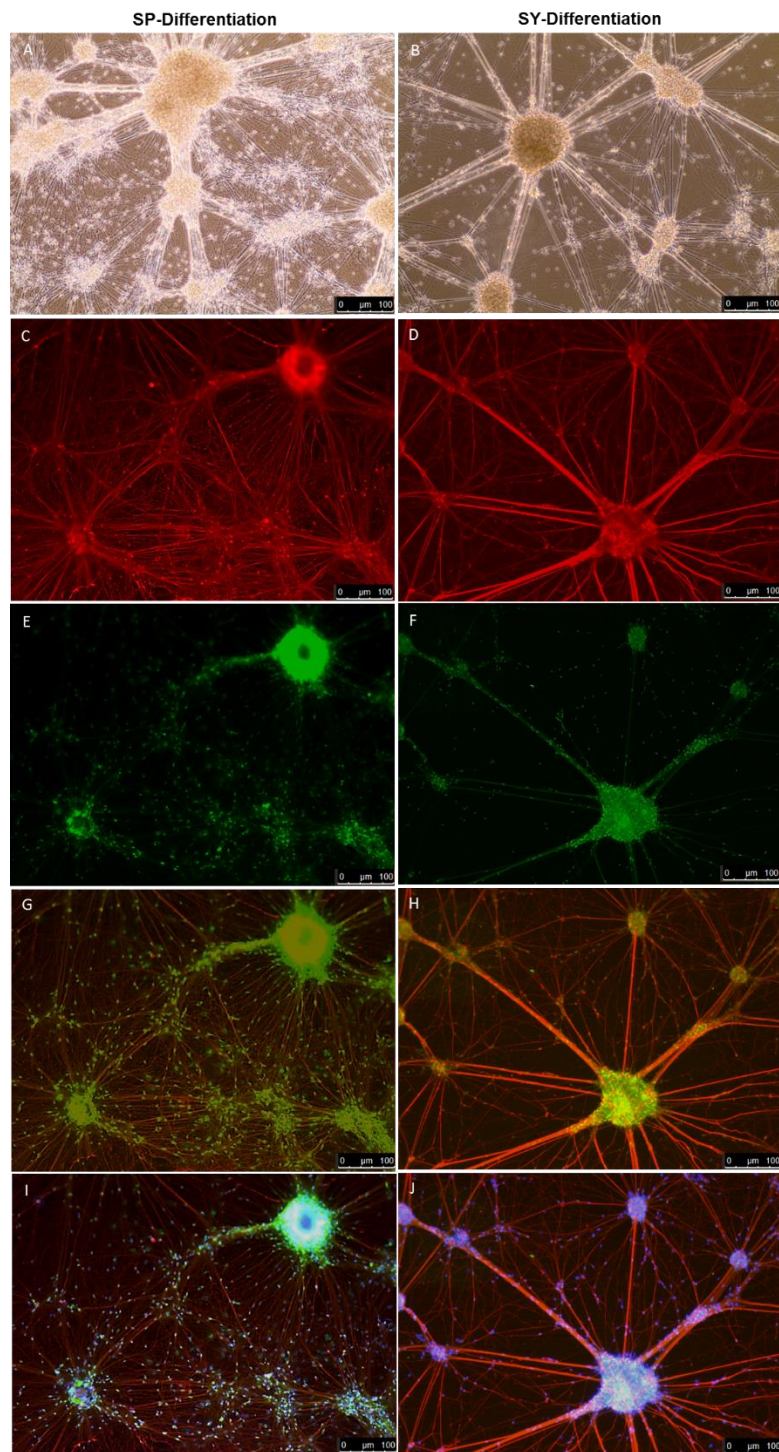


Figure 4.5: Representative images of neural cells differentiated from hiPSC-derived NPCs of fAD patient cell line using spontaneous and synchronous differentiation methods at day 40. Phase contrast images of spontaneous (A) and synchronously (B) differentiated cells. Immunofluorescent images showing TUJ1+ neuronal cells (red) (C and D), and S100 β + astrocytic cells (green) (E and F). Merged image showing expression of both TUJ1+ and S100 β + (G and H). Nuclei were counter stained with DAPI+ (blue) (I and J). n=3. Scale bars: 100 μ M.

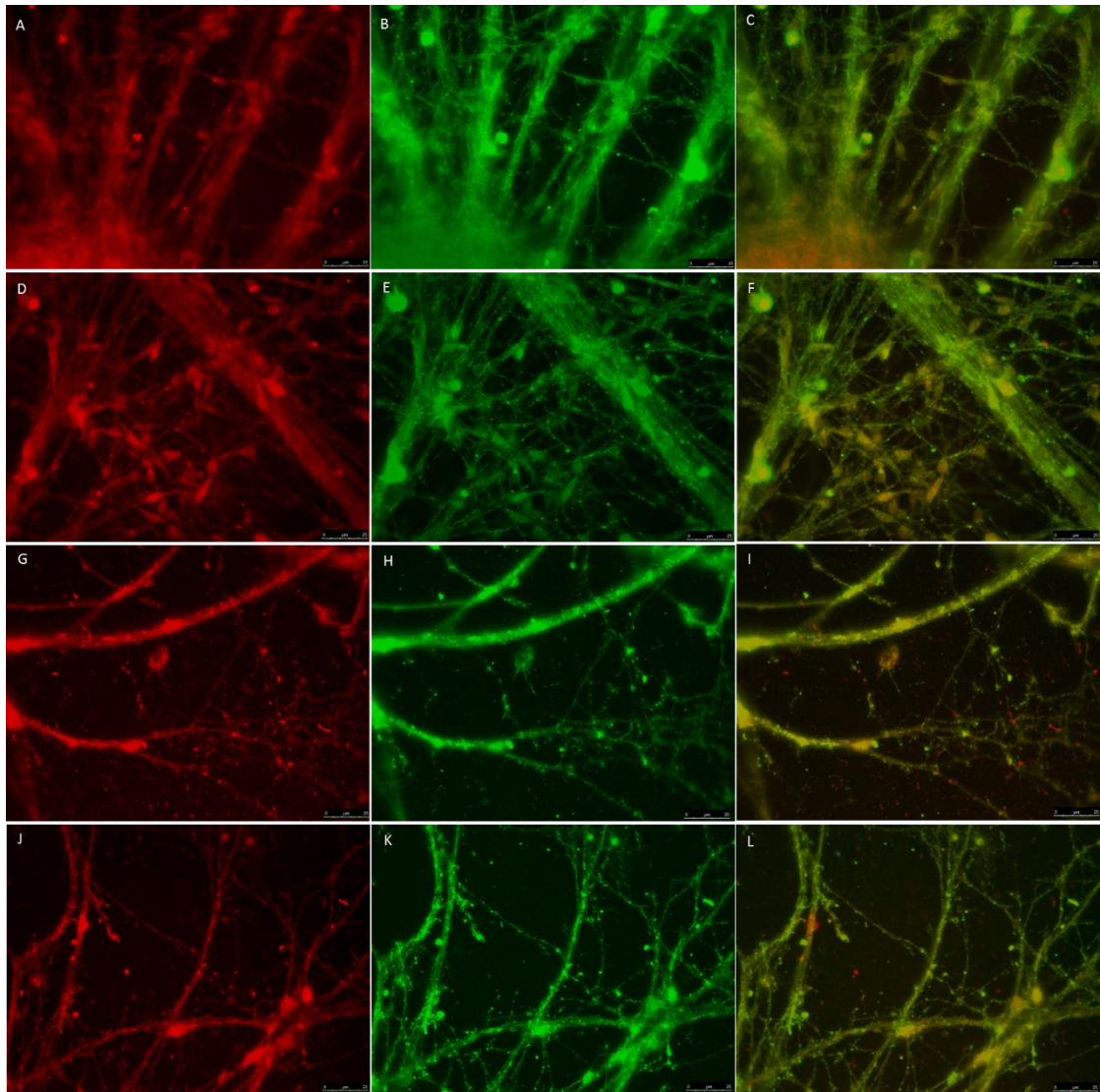


Figure 4.6: Representative immunofluorescent images of synaptic markers expression in neural cells derived from hiPSC-derived NPCs of fAD patient cell line using SP-differentiation (A-F) and SY-differentiation (G-L) at days: 30 (A-C and G-I) and 40 (D-F and J-L). Images showing synaptophysin+ (red) (A, D, G, and L) and PSD95+ (green) (B, E, H and K). Merged images showing expression of both synaptic markers (C, F, I and L). n=3. Scale bars: 25 μ M.

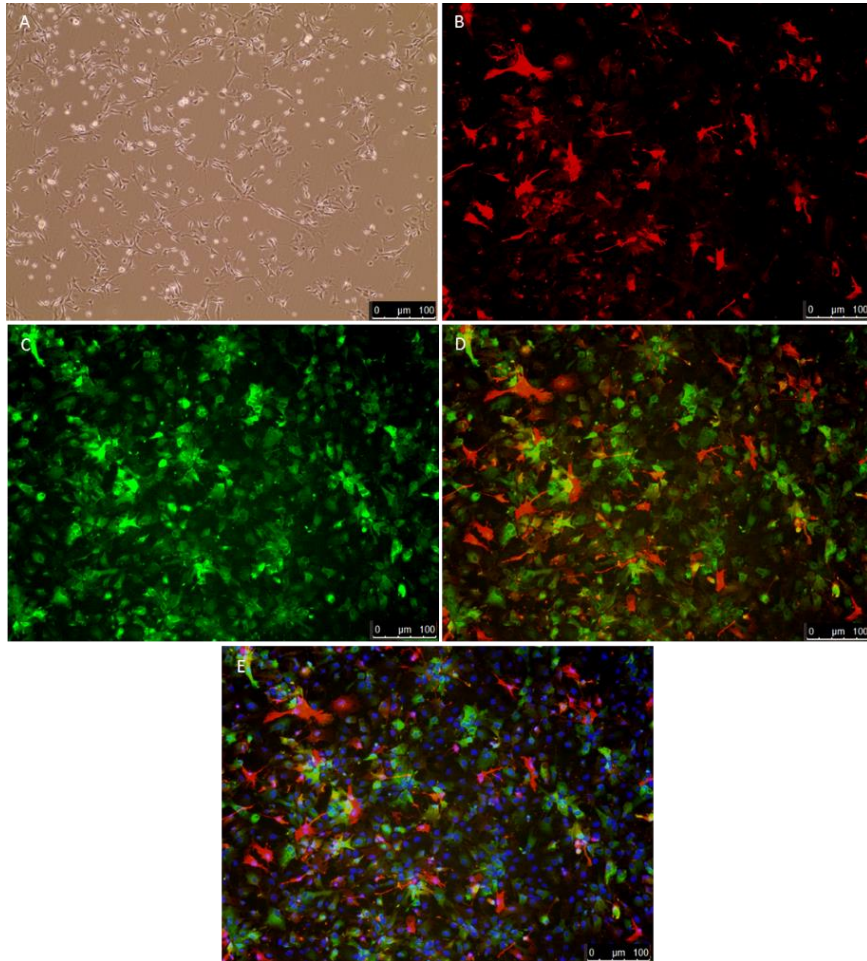


Figure 4.7: Representative images of hiPSC-derived astrocytic cells from fAD patient cell line ax0112 at day 45+. Astrocytic cells were cultured using the astrocytes differentiation and maturation protocols. Phase contrast image showing astrocytic cells (A). Immunofluorescent images of astrocytic markers GFAP+ (red, B) and S100β+ (green, C). Merged image showing expression of both GFAP+ and S100β+ (D). Nuclei were counter stained with DAPI+ (blue, E). n=3. Scale bars: 100μM.

4.3.2 Characterisation of A β Profile Release from fAD Patient-derived iPSCs Using ELISA Analysis

Results shown in sections 2.3.1 and 4.3.1 demonstrate that both neuronal and astrocytic cells can be produced from both control (ax0018) and fAD patient cells (ax0112). To determine if cells are phenotypically distinct the release of A β peptides was determined.

A β production is a core pathogenic component of AD (Hardy and Allsop, 1991). The neural cells derived from fAD patient hiPSCs were assessed for endogenous A β peptides production by assessing the CM from the cells after differentiation.

CM was collected for quantification of A β peptide production after cells were differentiated using spontaneous and synchronous differentiation methods from both fAD patient cell line (ax0112) and the 'healthy' control cell line (ax0018) using an ELISA assay. Media was fully replaced 48 hours before collection of CM. A β 1-40 and A β 1-42 release was measured at days 0, 30 and 40 (section 4.2.4).

Figure 4.9 shows a comparison of A β peptide normalised to total cellular protein production by fAD patient cell line (ax0112) and healthy control cell line (ax0018) at days zero, 30 and 40. There was a significantly higher level of A β 1-42 production in the fAD patient cell line at each assessment point of cell culture by both differentiation methods, reaching a peak of 122.49 ± 12.93 pg/mg, ($P < 0.0001$) and 142.37 ± 9.12 pg/mg, ($P < 0.0001$) at day 40 when the cells were cultured by the spontaneous and synchronous differentiation methods, respectively (Fig. 4.9A and B). However, when the cultured cells of both cell lines were assessed for A β 1-40 production, the concentration of A β 1-40 was very similar at initial assessment at day 0 for SP and SY differentiation methods (Control: 19.67 ± 6.56 pg/mg and fAD patient: 19.89 ± 8.87 pg/mg), and a significant rise in A β 1-40 production of fAD patient cell line was seen from day 30 (SP: 155.57 ± 51.43 pg/mg, $P < 0.05$ and SY: 188.04 ± 20.98 pg/mg, $P < 0.001$) by the spontaneous and synchronous differentiation cultures, respectively (Fig. 4.9C and D). The delay in production of A β 1-40 compared to A β 1-42 however appears to result in higher peaks of 213.88 ± 45.38 pg/mg, ($P < 0.001$) and 256.79 ± 72.42 pg/mg, ($P < 0.0001$) at day 40 when fAD patient cell cultured by the spontaneous and synchronous differentiation cultures, respectively (Fig. 4.9C and D). This significantly higher values of A β 1-40 appear to exert a significant effect when the combined total of A β 1-42 and A β 1-40 production by the fAD patient cell line was assessed for the spontaneous and synchronous differentiation methods; with the

higher total A β peptides levels only significantly higher at days 30 and 40 (SP-D30: 270.05 \pm 63.62pg/mg, $P<0.05$, SP-D40: 336.38 \pm 58.32pg/mg, $P<0.01$, SY-D30: 319.65 \pm 23.50pg/mg, $P<0.01$, SY-D40: 399.17 \pm 61.55pg/mg, $P<0.0001$) (Fig. 4.8A). There was no significant rise in total A β production in the control cells as shown in figure 4.8B.

When the ratios of A β 1-40:A β 1-42 peptides in the CM from both neuronal cell differentiation methods from fAD patient cell line was assessed over 40 days differentiation, the quantity of A β 1-40 was greater than that of the A β 1-42 at days 30 and 40 of assessment, with the greatest difference at day 40 for both the synchronous and spontaneous differentiation methods (Fig. 4.9E). The concentration of A β 1-42 was higher at initial assessment for both the SP and SY differentiation methods. In comparison, when the A β 1-42:A β 1-40 ratio was assessed for the healthy control line, although the A β 1-42 was higher at initial assessment as seen with the patient-derived cells for both the SP and SY differentiation methods, the concentration of A β 1-42 remained slightly higher than A β 1-40 at days 30 and 40 for the SY differentiation method, and a slight reversal at day 40 for the SP-differentiation method (Fig. 4.9F).

As astrocytes have been previously shown to produce and process APP (Busciglio *et al.*, 1993, Shoji *et al.*, 1992), the A β release profile of the hiPSC-derived astrocytic culture was assessed for the fAD patient cell line (ax0112) and 'healthy' control cell line (ax0018) over 48 hours period. There was a significantly higher quantity of both A β 1-42 and A β 1-40 produced by the fAD astrocytic cells at 45+ days (A β 1-42: 113.87 \pm 11.19pg/mg, $P<0.01$ and A β 1-40: 76.67 \pm 7.20pg/mg, $P<0.001$) (Fig. 4.10A). However, the A β 42/40 ratio was higher for the control astrocytes than in the patient derived cultures (Fig. 4.10B), despite the lower A β quantities in the control astrocytes when observed grossly as seen in figure 4.10A.

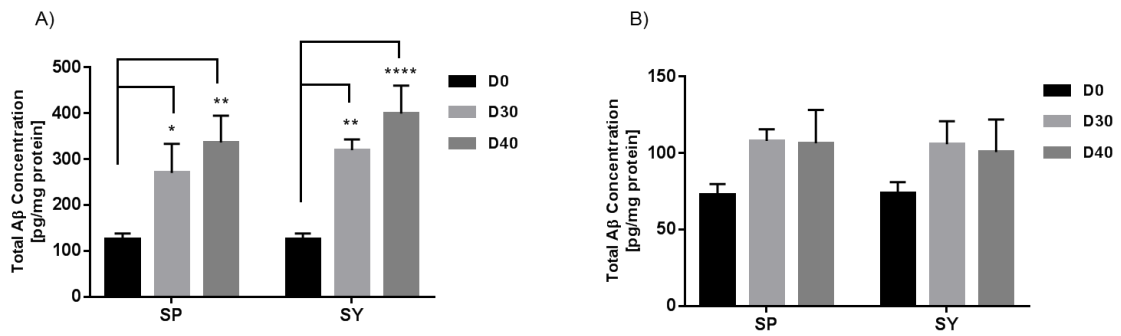


Figure 4.8: Quantification of total Aβ peptides secretion from neuronal cells following spontaneous and synchronous differentiation methods. Release of Aβ₁₋₄₂ and Aβ₁₋₄₀ from fAD patient cell line ax0112 (A) and 'healthy' control cell line ax0018 (B) was detected by ELISA. The CM was assayed after a 48 hours on days 0, 30 and 40. Data is expressed as Aβ concentration pg/mg total cellular protein, ± SEM, n=3 (triplicate wells pooled for each run), $P < 0.0001$ (****), $P < 0.001$, $P < 0.01$ (**), $P < 0.05$ (*). The statistical analysis was done using Two-way ANOVA, Tukey's multiple comparisons test.

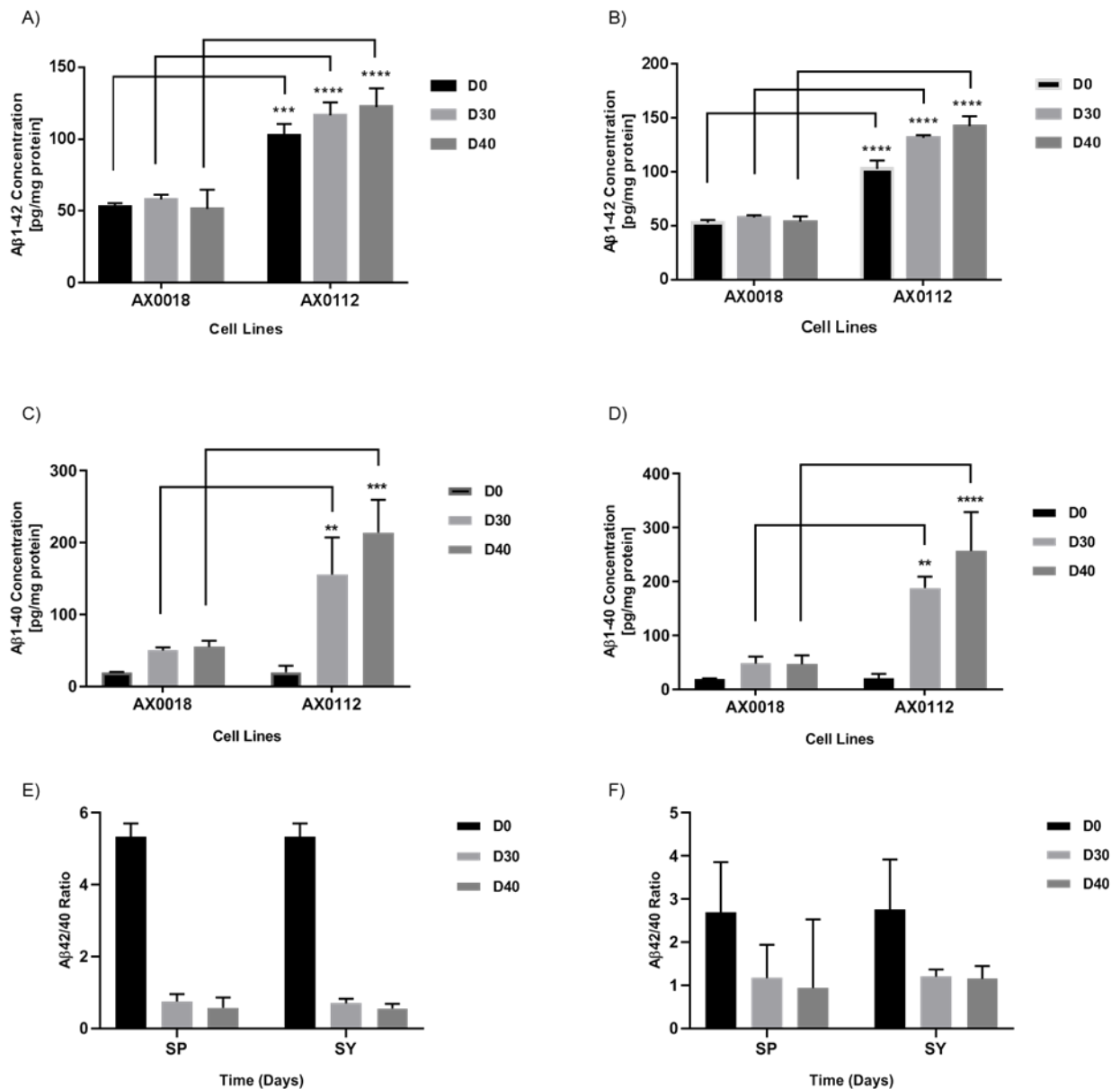


Figure 4.9: Quantification of Aβ peptides secretion from neuronal cells following spontaneous (A and C) and synchronous (B and D) differentiation methods of fAD patient cell line ax0112 versus 'healthy' control cell line ax0018 from neural cells over 40 days. Aβ peptide was detected by ELISA: Aβ1-42 (A and B) and Aβ1-40 (C and D). Ratios of Aβ1-42:Aβ1-40 released from fAD patient cell line (E) and healthy control cell line (F). The CM was assayed by ELISA at different developmental days 0, 30 and 40 over a 48 hours period. Data is expressed as Aβ concentration pg/mg total cellular protein, ± SEM, n=3 (triplicate wells pooled for each run), $P < 0.0001$ (****), $P < 0.001$ (***), $P < 0.01$ (**). The statistical analysis was done using Two-way ANOVA, Sidak's multiple comparisons test.

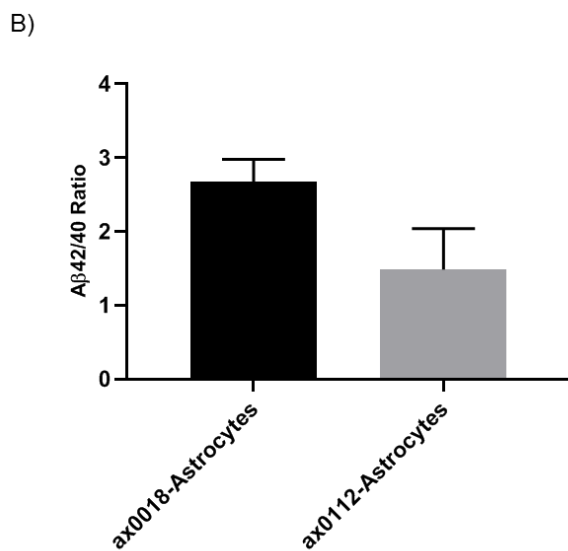
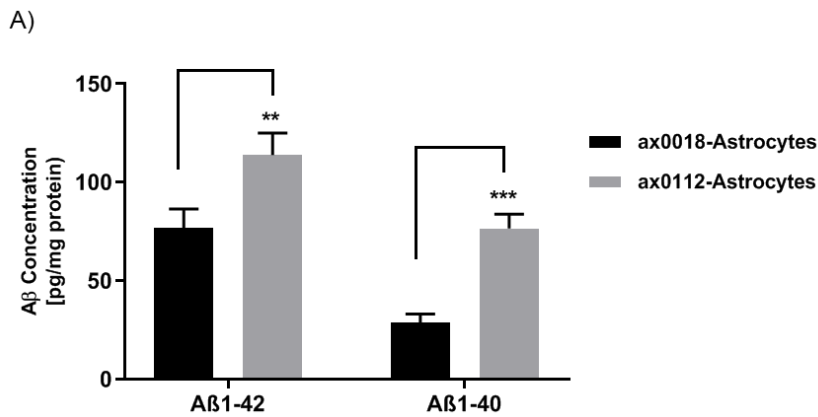


Figure 4.10: Quantification of A β peptide profile released from astrocytic cells following astrocytes differentiation methods of cell lines: fAD patient cell line (ax0112) versus 'healthy' control cell line (ax0018) (A). Ratio of A β 1-42:A β 1-40 released from fAD patient cell line and healthy control cell line (B). The CM was assayed at 45+ days old over a 48 hours period using ELISA test: A β 1-42 and A β 1-40. Data is expressed as A β concentration pg/mg total cellular protein, \pm SEM, n=3 (triplicate wells pooled for each run), $P < 0.001$ (***), $P < 0.01$ (**). The statistical analysis was done using Two-way ANOVA, Tukey's multiple comparisons test.

4.3.3 Determination of Carbohydrate Levels

To determine if metabolic function differs in fAD patient-derived hiPSCs, metabolite utilisation was determined. The glucose uptake and glycogen content levels from the cultured cells were assessed as a measure of metabolic activity in the fAD patient and 'healthy' control cells.

4.3.3.1 Determination of Glucose Uptake Levels

The CM from both spontaneous and synchronous differentiation methods at day 30 from fAD patient and ax0018 cell lines over a 48 hours period were tested for glucose levels using the glucose assay as an indirect measure of glucose uptake by the cells. The utilisation of glucose in the ax0112 cells was significantly reduced compared to the ax0018 cells at day 30 of culture by the synchronous differentiation method ($2591.7 \pm 211.72\mu\text{g}/\text{mg}$, $P < 0.01$) (Fig. 4.11). There was also a higher amount of glucose in the CM for the fAD patient-derived astrocytes compared to the control, indicating a significant reduction in glucose uptake ($219.4 \pm 18.19\mu\text{g}/\text{mg}$, $P < 0.05$) (Fig. 4.12).

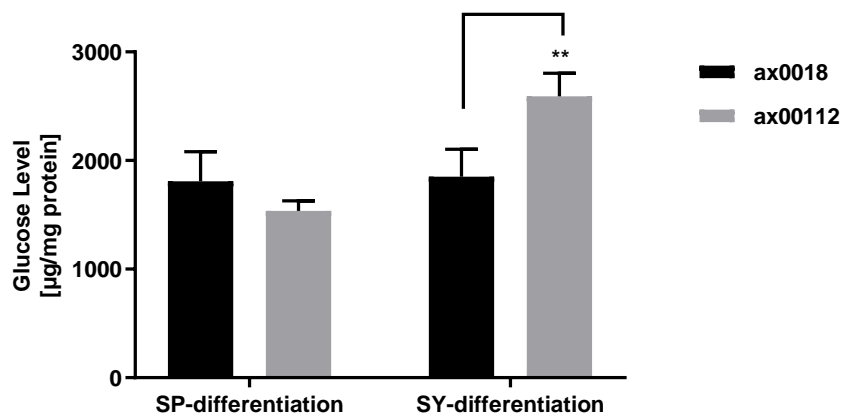


Figure 4.11: Comparison of glucose uptake by hiPSC-derived neural cells from fAD patient and ‘healthy’ control neural cells using SP-differentiation and SY-differentiation methods. The amount of glucose remaining in the conditioned media were measured using glucose assay at day 30 after 48 hours. Data is expressed as glucose $\mu\text{g}/\text{mg}$ total cellular protein, \pm SEM, $n=3$ (triplicate wells pooled for each run), $P<0.01$ (**). The statistical analysis was done using One-way ANOVA, Sidak's multiple comparisons test.

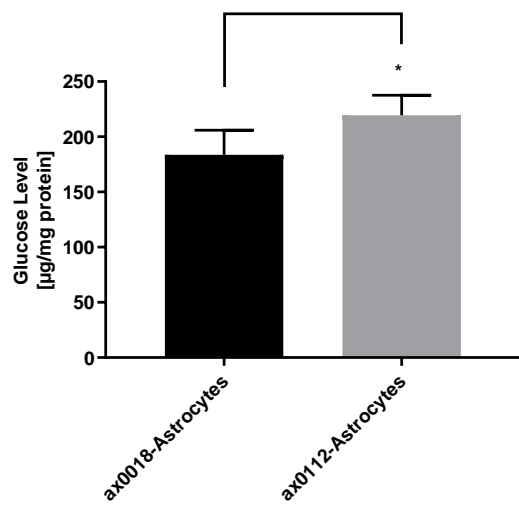


Figure 4.12: Comparison of glucose uptake by hiPSC-derived astrocytic cells from fAD patient ax0112 cell line and 'healthy' control ax0018 cell line at day 45+. The amount of glucose remaining in the conditioned media were measured using glucose assay after 48 hours. Data is expressed as glucose $\mu\text{g}/\text{mg}$ total cellular protein, \pm SEM, $n=3$ (triplicate wells pooled for each run), $P<0.05$ (*). The statistical analysis was done using Unpaired t test post-test.

4.3.3.2 Determination of Glycogen Content Levels

Analysis of glycogen content levels did not demonstrate any significant changes to glycogen storage levels between the fAD patient-derived astrocytes and 'healthy' control-derived astrocytes as measured at 45+ days of culture (Fig. 4.13).

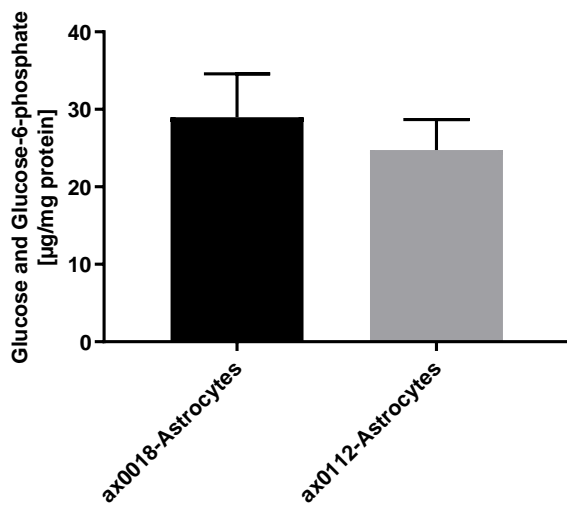


Figure 4.13: Determinations of glycogen content level of hiPSC-derived astrocytic cells from fAD patient cell line and 'healthy' control cell line. Astrocytic glycogen content was measured at 45+ days old over a 48 hours period using a glycogen assay. Results are expressed as glucose and glucose-6-phosphate µg/mg total cellular protein, ± SEM, n=3 (triplicate wells pooled for each run). The statistical analysis was done using Unpaired t test post- test.

4.4 Discussion

This project has successfully differentiated astrocytes and neurons from 'healthy' hiPSC-derived NPCs, and then characterised them in comparison with their naturally derived counterparts. The effects of synthetic A β oligomers have also been examined on these cells to demonstrate that A β is indeed responsible for hypometabolism as an early pathogenic event in AD. This chapter was aimed at differentiating astrocytes and neurons from fAD patient hiPSC-derived NPCs, to observe the natural history of fAD at the cellular level, with particular focus on the early hypometabolism that characterises the disease before onset of gross AD features. This is the first time endogenous A β production from human AD patient iPSC-derived astrocyte cells have been assessed for endogenous A β production and assessed for metabolic dysfunction. This chapter also reproduces the results of other studies by Kondo *et al.* (2013) and Arber *et al.* (2019) in amyloid production from fAD-derived neurons.

4.4.1 Differentiation of fAD Patient-derived hiPSCs to Neurons and Astrocytes

The fAD patient-derived hiPSCs were successfully differentiated from the NPC stage to astrocytes and neurons, and showed the typical morphological features of the healthy counterparts. The morphological and immunohistochemical features of the cells through the course of differentiation showed very similar patterns to those of 'healthy' human-derived counterparts, both from hiPSCs or from human pluripotent stem cells. The NPCs showed the typical rosette formation initially and expressed positivity to the NPC markers (Fig. 4.1). Using the spontaneous and synchronous differentiation methods, the differentiation course was similar from NPC to neurons at day 40 of differentiation as was seen in chapter 2 for the 'healthy' cell line ax0018 (Fig. 2.4 - 2.8).

The neurons showed a similar course of neurite formation and neuronal connections of increasing density with time as well as expression of the TUJ1 neuronal marker. Synaptic connections were obvious morphologically and by positive expression of the synaptic markers: synaptophysin and PSD95. As noted in section 2.4, the synaptic staining was non-specific and would have benefitted from further optimisation and the use of controls. The advantage of the use of DAPT in the synchronous differentiation method was the potential to generate enriched and mature neuronal populations, since it is a γ -secretase inhibitor which would block astrocytic differentiation by inhibiting Notch signalling in the NPCs (Shi *et al.*, 2012b).

However, this aim was not achieved, and the synchronous differentiation cell cultures still contained astrocytes. Future experiments would aim to optimise production of more pure neurons.

Astrocytes were also differentiated from the fAD patient hiPSC-derived NPCs, over 45+ days of differentiation using the differentiation and maturation protocols. They showed the typical stellate appearance of their 'healthy' human iPSC- and non-iPSC-derived counterparts (HA). They expressed positivity for GFAP and S100 β , known astrocytic markers (Fig. 4.7). Similar to our findings as reported in chapter 2 for the 'healthy' hiPSC cell line (Fig. 2.12), the astrocyte differentiation protocol resulted in almost exclusively astrocytic populations from the fAD patient-derived cells.

4.4.2. A β Production by fAD Patient hiPSC-derived Neurons and Astrocytes

The amyloid hypothesis is currently the most explored of all the pathogenetic mechanisms for the occurrence of AD, and the hallmark of this hypothesis is the excessive production of toxic A β species in patients affected by the disease. It was thus important to assess fAD patient-derived neurons and astrocytes for A β production. In line with the proposals of the amyloid hypothesis, the fAD patient-derived neurons showed significantly higher total A β release profiles compared to their 'healthy' human counterparts. Increased A β production in hiPSC-derived neurons from patients with fAD have been reported by other researchers previously (Yagi *et al.*, 2011, Israel *et al.*, 2012, Shi *et al.*, 2012b). Yagi *et al.* (2011) recorded an increased A β _{42/40} ratio in fAD cell lines compared to controls, while Israel *et al.* (2012) recorded increased A β ₄₀ production in two fAD cell lines (patients with duplication of the A β precursor protein gene (APP^{Dp}), and in one out of two sAD cell lines (sAD2)). Shi *et al.* (2012b), recorded increased A β production in hiPSCs derived from patients with Down syndrome.

In comparison, Kondo *et al.* (2013) reported a decrease in A β ₄₀ and A β ₄₂ in neurons differentiated from hiPSCs derived from fAD patients carrying the E693 Δ APP gene mutation. This is interesting because the E693 Δ mutation is known to cause a very rare form of familial early-onset AD without A β deposition or accumulation (Tomiya *et al.*, 2008, Shimada *et al.*, 2011, Arber *et al.*, 2019).

However, when Kondo *et al.* (2013) differentiated astrocytes from hiPSCs derived from patients carrying the E693 Δ APP gene mutation, the authors noted the reverse, as they recorded intracellular accumulation of A β . Accumulation of A β in these astrocytes may have occurred because astrocytes produce and process APP (Busciglio *et al.*, 1993, Shoji *et al.*, 1992). This also lends credibility to the possibility that astrocytes not only play a huge role in mitigating A β toxicity, they may actually play reverse roles, being the source of toxic amyloid species. The astrocytes in this current project had increased A β production profiles for the fAD patient-derived astrocytes as compared to astrocytes derived from 'healthy' patient control. However, we did not assess intracellular production or uptake in this project.

4.4.3 Metabolic Dysfunction in fAD Patient hiPSC-derived Neurons and Astrocytes

The metabolic dysfunction in fAD patient-derived astrocytes and neurons is the main focus of this project. This was assessed by checking the glucose uptake and glycogen content in these cells. Glucose uptake was significantly reduced in the fAD patient-derived astrocytes compared to their healthy counterparts. Familial AD patient-derived neurons differentiated using the SY differentiation method showed a significant reduction in glucose uptake, while the cells cultured by the SP differentiation method did not show this difference. This difference may be as a result of the differentiation mechanisms, with the SY differentiation method potentially being more mature, and this may affect the production of amyloid by these cells. This is supported by the fact that AD occurs usually in adulthood after a high degree of maturity has been established. The differences between the SP, SY as well as the differences between the fAD patient-derived cells and the controls may be due to amyloid production. This may be supported by the higher total A β release profiles of the fAD patient-derived neurons cultured using the SY differentiation method in comparison to the SP differentiation method (Fig. 4.8). Results shown in chapter three, demonstrate a reduction in glucose uptake in response to exogenous amyloid. As such the reduction in glucose uptake in fAD is likely due to the increased presence of endogenously produced toxic amyloid species.

Furthermore, the fact that there are differences in glucose uptake in the neurons based solely on the differentiation method, while there was a significant reduction in glucose uptake by the fAD patient hiPSC-derived astrocytes also suggests that other factors may also be involved in the overall direction of metabolic dysfunction in neurons. Similarly, there was no significant difference in the glycogen content of the fAD patient hiPSC-derived astrocytes as compared to the controls. This is likely to be related to the complex spatial and metabolic interactions

with astrocytes *in vivo* and the astrocyte-neuron lactate shuttle. This is very relevant for the astrocyte glycogen turnover, as the astrocyte metabolism changes significantly when they become activated, a state which can be induced by A β (Hu *et al.*, 1998). The fact these neurons were largely cultured alone, and the short timeframe of the cultures, as well as the high glucose concentration in the media may also be responsible for these differences. A co-culture system which enables controlled interactions between the neurons and astrocytes may provide more representative results.

4.5 Conclusion

This chapter demonstrates that fAD patient hiPSC-derived NPCs can be successfully differentiated into neurons and astrocytes, which bear the morphological and immunochemical characteristics of their naturally occurring counterparts. The chapter also demonstrates for the first time that these fAD patient hiPSC-derived astrocytes demonstrate hypometabolism in the form of reduced glucose uptake, with neurons showing similar reductions when cultured by SY differentiation method. There was no significant difference in glycogen stores of the fAD patient hiPSC-derived astrocytes. These results give credence to our overarching hypothesis that metabolic dysfunction occurs early in AD, and is likely directly related to increased A β release profiles in astrocytes and neurons of these patients.

Chapter 5: Optimising Production of Human A β Derived from fAD Patient iPSCs

5.1 Introduction

The endogenous production of A β by the fAD patient-derived hiPSCs has been shown in chapter 4 of this project. However, it is pertinent to explore if these endogenously produced A β species can induce metabolic dysfunction in a cell autonomous fashion in both fAD patient and 'healthy' hiPSC-derived brain cells. This could be done by exposing healthy brain cells to the CM derived from fAD patient-derived neuronal cell cultures derived from synchronous differentiation method, because this method produced the greatest amount of total amyloid production (Fig. 4.8). This could then be compared with 'healthy' cells exposed to the same CM, but from which the amyloid species have been removed via immunodepletion (Hu *et al.*, 2018) reported the inhibition of long term potentiation (LTP) in rat hippocampal neurons *in vivo* by secretomes derived from human fAD patient-derived neuronal cultures. They also confirmed that the inhibition of LTP was induced by A β released from the fAD patient-derived neurons.

However, shortage of time and requisite funding prevented the completion of these experiments in this project. The preliminary results of exposure of the 'healthy' patient-derived hiPSCs to the concentrated CM derived from fAD patient-derived neuronal cells in culture is presented in this chapter as a supplement.

The hypothesis being tested in this portion of the project was that A β isolated from fAD patient-derived neuronal cell cultures (secretomes) would induce metabolic dysfunction in otherwise 'healthy' hiPSC-derived astrocytes. The aims and objectives were to test this hypothesis by first retrieving the concentrated secretomes from cultures of neuronal cells differentiated using the SY differentiation method, and then to carry out an immunodepletion process to remove A β species from the concentrated secretomes. Healthy patient hiPSC-derived astrocytes would then be exposed to the secretomes to observe if the non-immunodepleted secretomes would induce metabolic dysfunction in the form of impaired glucose uptake and altered glycogen metabolism.

5.2 Materials and Methods

5.2.1 Preparation of Concentrated Secretomes (Amicon®-Concentration)

CM (secretome) of cortical neuronal cells cultures that were differentiated using synchronous neural differentiation method was collected from hiPSC-derived NPCs of fAD patient cell line (ax0112) in cultures for 40 days at 48 hours intervals. Briefly, the secretome was pooled from 12 wells of 12-well plates (three independent cultures), and then centrifuged at 200 x g for 5 minutes to remove dead cells and debris. After centrifugation, the supernatant was transferred into 15ml sterile conical tubes and stored at -80°C for concentration of collected secretome samples. 12ml of secretome samples were added in a sterile Amicon® Ultra-15 (3kDa) centrifugal filter device (Millipore, Ireland). The Amicon devices were spun at 4000 x g maximum for approximately 60 - 90 minutes at 4°C. After centrifugation, secretome samples were concentrated 12-fold to 1ml, and then 100µl aliquots were transferred into 1.5ml sterile microcentrifuge tubes (Fig. 5.1A) and stored at -80°C for further analysis of amyloid immunoprecipitation assay, SDS-PAGE gel, western blotting and ELISA analysis.

5.2.2 Immunodepletion Assay

Immunoprecipitation technique (IP) was used to deplete the A β from the concentrated secretome of neurons cultured in using synchronous differentiation method (section 4.2.4) from fAD patient cell line. The IP assay was performed according to the manufacturer's instructions of Dynabeads® Protein A (Novex® Life Technologies, Norway). 50µl (1.5mg) of Dynabeads® Protein A were added to a 1.5ml Protein LoBind microfuge tube (Eppendorf, USA) and dynabeads were separated from the solution using magnet rack (DynaMag™-2) (Thermo Fisher Scientific, UK). The dynabeads were washed once with D-PBS with 0.02% Tween®-20 (Sigma-Aldrich, UK). To prepare antibody coated dynabeads with 10µg of purified anti- β -Amyloid 17-24 (BioLegend, USA) was diluted in 200µl D-PBS with Tween®-20, and then added to the dynabeads and incubated with rotation for one hour at 4°C. After incubation, microfuge tubes containing dynabeads were placed on DynaMag and the supernatant aspirated, and then gently washed 3 times with D-PBS with Tween®-20. Next, targeting the antigen (Ag) was done by adding 100µl of concentrated secretome samples and incubating with Ab-conjugated-beads overnight with rotation at 4°C. After incubation, the dynabeads were separated on DynaMag and the supernatant sample (secretome) transferred to a microfuge tube (Fig. 5.1B), and then stored at -80°C for ELISA, SDS-PAGE gel and western blotting

analysis. The dynabeads Ab-Ag complex were gently washed 3 times with D-PBS with Tween[®]-20, and then stored at -80°C for SDS-PAGE gel and western blot analysis.

5.2.3 ELISA Analysis

To quantify the A β 1-40 and A β 1-42 in concentrated secretome samples and immunodepleted samples of fAD patient cell (section 4.2.4) was carried out with A β 1-40 and A β 1-42 of ELISA assay (section 4.2.4.3)

5.2.4 Electrophoresis Studies

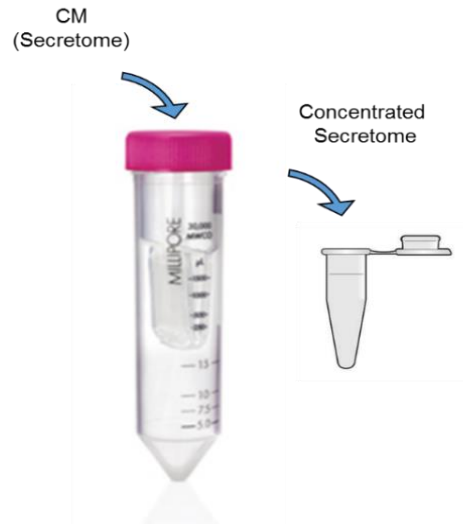
5.2.4.1 SDS-PAGE Gel

The presence of amyloid in the concentrated secretome samples in section 5.2.1 and the immunodepleted A β samples in section 5.2.2 were assessed and analysed using SDS-PAGE gel according to protocol described in section 3.2.2.1. The dynabeads Ab-Ag complex samples were eluted by re-suspended in 100 μ l of sample buffer, and then heated at 95°C for 10 minutes. Next, the supernatant was collected after separating the dynabeads using DynaMag 20 μ l of the supernatant was loaded onto the gel.

5.2.4.2 Western Blotting Analysis

The presence of amyloid in the concentrated secretome samples and immunodepleted of synthetic A β 1-42 samples were performed and analysed using SDS-PAGE gel followed by western blotting according to method described in section 3.2.2.2.

A) Preparation of Concentrated CM (Secretome)



B) Immunodepletion of Concentrated CM (Secretome)

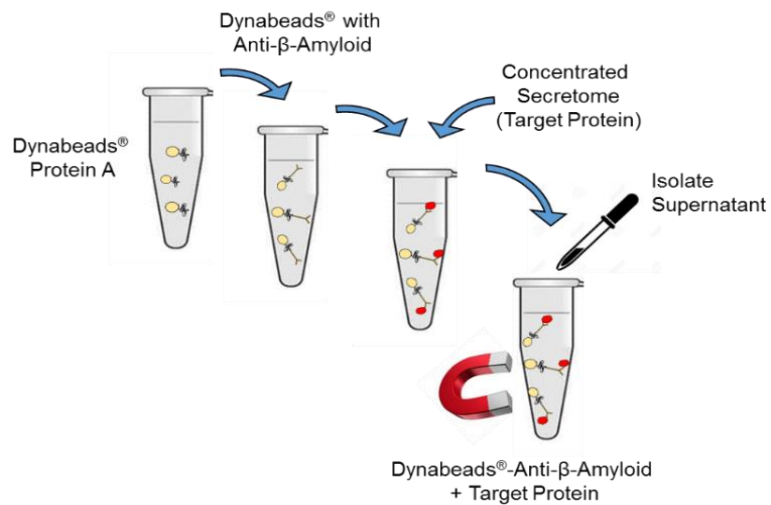


Figure 5.1: Diagrammatic overview of concentrated CM preparation from cortical neuronal cell cultures using Amicon® (A). Immunodepletion assay to deplete the A β from the concentrated CM using IP technique (B).

5.2.5 Treatment with Human fAD Patient-derived A β and Determination the Effects on Carbohydrate Levels

5.2.5.1 Preparation of Treatment

To determine the possible toxic effects of human fAD patient derived A β on metabolism of 'healthy' control hiPSC-derived astrocytic cells (ax0018). Astrocytic cells were plated according to section 3.2.5, and exposed to 1ml of 1:10 dilution of concentrated fAD-secretome (100 μ l) with AM (900 μ l) in comparison with untreated astrocytic cells (control) over 48 hours. CM samples were collected for analysing glucose uptake using glucose assay and homogenised samples were collected for analysing glycogen content level using the glycogen assay and protein determination assay.

5.2.5.2 Determination the Effects on Glucose Uptake Levels

The CM samples collected from astrocytic cells treated with concentrated fAD-secretome in comparison with untreated cells as a control were assessed for glucose uptake level over time using glucose assay (section 3.2.5.1). All readings were corrected for background and protein levels (section 2.2.8).

5.2.5.3 Determination the Effects on Glycogen Content Levels

The homogenised samples of hiPSC-derived astrocytic cells treated with concentrated fAD-secretome in comparison with untreated cells (control) were measured for glycogen content levels according to glycogen assay (section 3.2.4). All readings were corrected for background, free glucose and glucose-6-phosphate values in homogenised samples and protein levels (section 2.2.8).

5.2.6 Determination of Protein Levels

Protein levels were measured according to protocol described in section 2.2.8.

5.2.7 Quantification and Statistical Analysis

All quantification and statistical analyses were carried out according to the methods described in section 2.2.9.

5.3 Results

5.3.1 Immunodepletion Experiment

The CM of control (ax0018) and fAD patient (ax0112) derived from neuronal cells differentiated using the synchronous differentiation method at day 40 was selected for concentration (Fig. 4.8A) to increase the concentration of A β . Subsequently, IP assay was performed to deplete the A β from the concentrated secretomes of fAD patient (ax0012) and 'healthy' control (ax0018) to generate a non-amyloid control. CM was analysed by SDS-PAGE gel, western blotting and quantitatively with ELISA.

5.3.2 SDS-PAGE Gel Electrophoresis

SDS-PAGE gel (8%) was performed to determine the success of media concentration from both fAD patient (ax0112) and control cells (ax0018). (Fig. 5.2).

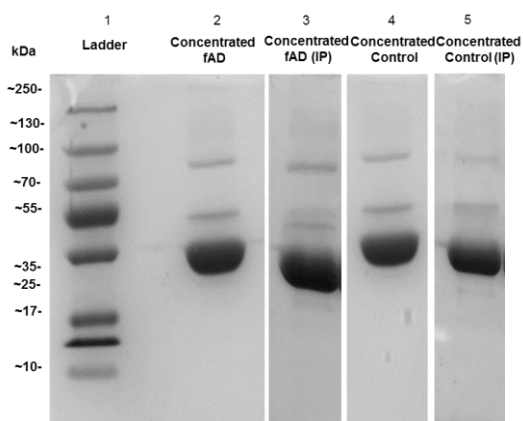


Figure 5.2: Representative SDS-PAGE gel (8%) showing the concentrated secretomes from CM of neuronal cells derived from SY differentiation method at day 40 of both cell lines: (lane 2) fAD patient cell line (ax0112) and (lane 4) 'healthy' control cell line (ax0018). Immunodepleted samples from concentrated secretomes of (lane 3) fAD patient cell line and (lane 5) 'healthy' control cell line. Proteins were stained with Coomassie brilliant blue stain. Lane 1 illustrates the pre-stained protein ladder molecular weight markers. n=3.

5.3.3 Western Blotting Analysis

Western blotting analysis carried out to detect the A β in the concentrated secretome and immunodepleted samples in both cell lines of fAD patient and ax0018 'healthy' control. All the samples were loaded in 8% SDS-PAGE gel followed by western blotting using the 6E10 antibody. This 6E10 antibody is reactive to amino acid residue 1 - 16 of A β and to APP; reacts to the abnormally processed isoforms, as well as precursor forms (AlzForum, USA). Western blotting demonstrated the presence of ~250 - 130kDa species in fAD patient cell line concentrated secretomes (Lane 3) (Fig. 5.3). The smaller A β species were not detectable in the concentrated secretome and immunodepleted samples for both cell lines (Lanes 2 - 5); in comparison 25 μ M synthetic A β 1-42 (Lane 1) (Fig. 5.3).

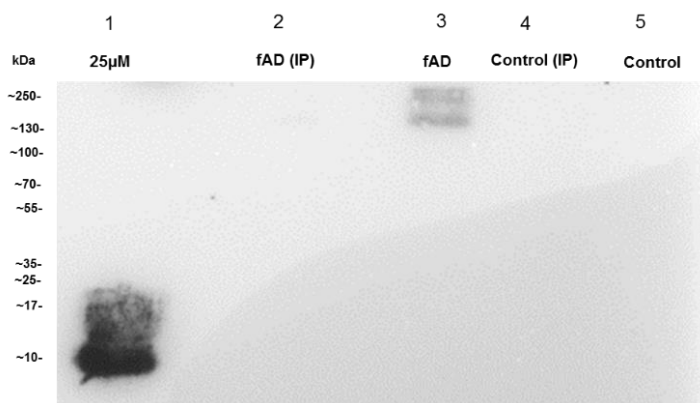


Figure 5.3: Representative western blotting analysis of A β in concentrated CM. 25 μ M of synthetic A β 1-42 was used as a positive control (lane 1) comparison with concentrated CM of neuronal cells derived from SY differentiation method at day 40 of fAD patient cell line (lane 3) and concentrated CM of 'healthy' control cell line (lane 5). Immunodepleted samples from concentrated CM of fAD patient cell line (lane 2) and healthy control cell line (lane 4). The samples were loaded in 8% SDS-PAGE gel followed by western blotting analysis using 6E10 antibody. n=3.

5.3.4 ELISA Analysis

To further confirm the presence/absence of the A β in concentrated secretome and immunodepleted samples from fAD patient cell line, samples were analysed using the A β 1-42 and A β 1-40 ELISA. The total A β 1-42 and A β 1-40 peptides in concentrated secretomes (Fig. 5.4) was 2243.11pg/ml and 1914.10pg/ml, respectively for the A β 1-42 and A β 1-40. Immunodepletion reduced the amount of A β peptides from the concentrated secretomes; 565.05pg/ml and 602.12pg/ml, respectively. This was repeated over three runs of the experiment.

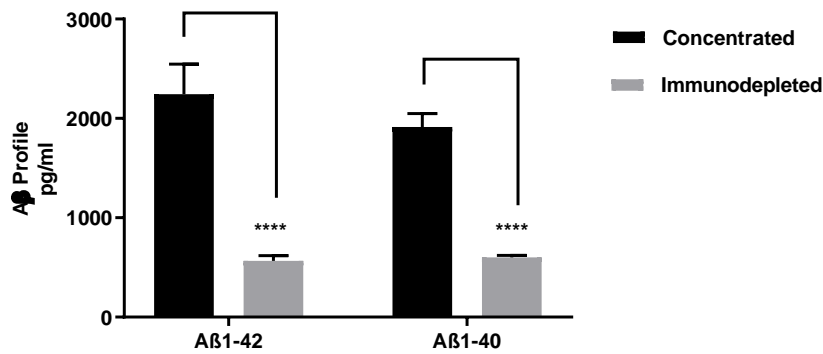


Figure 5.4: Quantification of A β prolife (A β 1-42 and A β 1-40) in the concentrated secretome and immunodepleted samples from fAD patient cell line using ELISA. Data is expressed as A β (pg/ml), \pm SEM, n=3 (triplicate wells pooled for each run), $P < 0.0001$ (****). The statistical analysis was done using One-way ANOVA, Dunnett's multiple comparisons post-test.

5.3.5 Treatment of Healthy hiPSC-derived Astrocytic Cells with fAD Patient-derived Secretome and Effects on Carbohydrate Levels

To determine if treatment with concentrated secretome derived from synchronously differentiated fAD patient neuronal cells could induce changes in glucose uptake and glycogen content levels. The 'healthy' control hiPSC-derived astrocytes from cell line ax0018 were treated with the concentrated secretome derived from synchronously differentiated fAD patient neuronal cells versus treated cells with AM only as a control over 48 hours. The glucose uptake and the glycogen content levels of astrocytes was investigated to detect the effects of concentrated secretomes (human fAD patient-derived A β) on 'healthy' astrocytic cells.

5.3.5.1 Determination the Effects on Glucose Uptake Levels

Astrocytic cells derived from the ax0018 cell line were then treated with the concentrated fAD-secretome at a 1:10 dilution with AM in comparison with astrocytic cells in AM only as control and the effect on glucose uptake observed over 48 hours. The concentrated secretome did not induce a significant reduction in the glucose uptake by the astrocytic cells (Fig. 5.5).

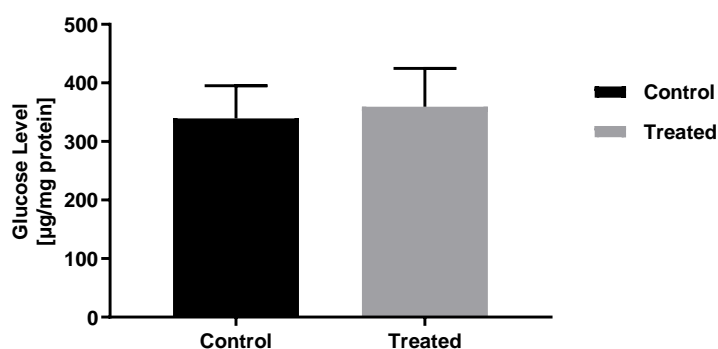


Figure 5.5: Determination of glucose levels remaining in the conditioned media following treatment of astrocytes with fAD patient-derived concentrated secretome. Treatment of hiPSC-derived astrocytes from cell line ax0018 at 45+ days old cells to fAD-derived concentrated secretome in the media versus astrocytic cells in AM as control for 48 hours. The amount of glucose remaining in the conditioned media following treatments were measured using glucose assay. Data is expressed as glucose $\mu\text{g}/\text{mg}$ total cellular protein, \pm SEM, $n=3$ (triplicate wells pooled for each run). The statistical analysis was done using Unpaired t test post-test.

5.3.5.2 Determination the Effects on Glycogen Content Levels

Similarly, when 'healthy' hiPSC-derived astrocytic cells (ax0018) were exposed to the concentrated fAD-secretome at a 1:10 dilution with AM in comparison with astrocytic cells in AM only as control. There was no significant difference in glycogen content level by the astrocytic cells after 48 hours (Fig. 5.6).

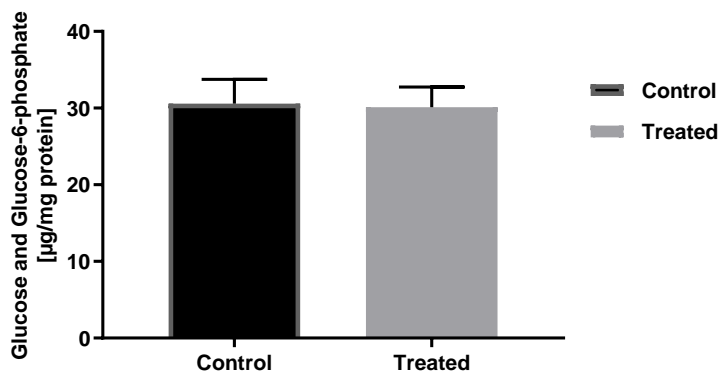


Figure 5.6: Determination of glycogen content of fAD-derived secretome treatment on astrocytic glycogen stores. Treatment of 'healthy' hiPSC-derived astrocytes from cell line ax0018 at 45+ days old cells with fAD patient-derived secretome and compared to astrocytic cells in AM as control for 48 hours. The cellular glycogen content was measured using a glycogen assay. Results are expressed as glucose and glucose-6-phosphate µg/mg total cellular protein, \pm SEM, n=3 (triplicate wells pooled for each run). The statistical analysis was done using Unpaired t test post-test.

5.4 Discussion

It has been shown in chapter 4 of this project that astrocytes and neurons derived from hiPSCs produced from the ax0112 fAD patient cell line produced higher amounts of A β 1-40 and A β 1-42, and exhibited dysregulate energy metabolism in the form of reduced glucose uptake. This portion of the project sought to examine if the secretome of cultured fAD patient-derived neuronal cells could induce metabolic dysfunction in otherwise 'healthy' cells as a result of these amyloid species produced by these fAD patient-derived neural cells. This chapter represents a first attempt at examining the effect of endogenously produced A β on energy metabolism on 'healthy' human cells. The synchronous differentiation method was utilised because it resulted in the greatest production of A β (Fig. 4.8A), and it likely presented the production of more mature neurons compared to the spontaneous differentiation method.

The results showed no significant difference in glucose uptake and glycogen metabolism (Fig. 5.5 and 5.6). These results cannot be taken to face value because an arbitrary dilution ratio of 10% for the concentrated secretome was used to ensure supply of glucose to prevent cell starvation and death. This does not provide a representative concentration of the A β in the secretome. Moreover, the results as shown in section 3.3.4 (Fig. 3.5) demonstrated a significant reduction in glucose uptake in a dose-dependent fashion from concentrations of 2 μ M and 1 μ M of synthetic A β 1-42 oligomers. This indicates that the experiment on endogenously produced A β requires optimisation, and it would be more reliable to purify and isolate the A β species and then conduct a dose-response assessment to identify appropriate concentrations to be used. Similar experiments also need to be conducted using different fAD patient models, as well as different controls to assess reproducibility of these experiments.

The immunodepletion experiment confirmed the reduction of the endogenously produced A β from the concentrated secretome, to be used in control experiments on the induction of metabolic dysfunction by A β in the secretome. However, the control experiment involving exposure of ax0018 'healthy' control cells could not be conducted due to shortage of time and resources. However, the use of pooled CM from different cell cultures could help provide higher quantities of A β . Moreover, a higher concentration of A β could be produced from older cells if they remain in culture for longer periods. In addition, other experiments from our lab on the same cell line (ax0112) confirmed the induction of oxidative stress on ax0018 cells by unconcentrated CM from cellular co-cultures of astrocytes and neurons derived from the ax0012 cells (Richard Elsworthy personal communication, awaiting publication).

Chapter 6: Final Conclusions and Future Directions

6.1 Final Conclusions

The search for a mechanistic understanding of the pathogenic events leading to the occurrence of AD has gained significant progress over the last decade. Since the discovery of the iPSC by Yamanaka *et al.* in 2006, it is now possible to generate patient-specific neurons and astrocytes from AD patients in order to examine the natural history of cellular dysfunction. As metabolic dysfunction has been shown to precede the clinical onset of the disease by decades (Mosconi *et al.*, 2008a and 2008b) hiPSC derived neuronal models enable the researchers to study processing of APP and metabolic dysfunction at the cellular level, prior to the clinically obvious onset of AD.

Previous efforts in our lab have established the occurrence of early metabolic dysfunction in embryocarcinoma models of human neurons and astrocytes in response to synthetic A β peptides (Tarczyluk *et al.*, 2015). However, there is a shortage of available research on the occurrence of metabolic dysfunction in patient-derived models of AD. This project is a follow up effort on these previous research endeavours in our lab, by examining the effects of A β in neurons and astrocytes derived from 'healthy' control hiPSCs and a fAD specific model of the disease.

This project involved the generation of fAD patient-derived neurons and astrocytes and comparison them with their foetal-derived human primary astrocytes and 'healthy' patient hiPSC-derived counterparts for morphological and immunohistochemical conformity. The project also, for the first time, examined metabolic dysfunction as it occurs in these fAD patient-derived astrocytes and neurons to provide an understanding of a temporal pattern of metabolic dysfunction as it occurs spontaneously in these cells.

We generated mature astrocytes from 'healthy' control hiPSCs using the differentiation and maturation protocols, and neurons using the spontaneous and synchronous differentiation methods. Similar protocols were used to generate astrocytes and neurons from fAD patient-derived hiPSCs. The results showed morphological and immunohistochemical concordance between the fAD patient-derived neurons and astrocytes, and their healthy HA and 'healthy' patient-derived hiPSC counterparts. We also recorded the occurrence of metabolic dysfunction, as recorded by reduced glucose uptake induced by synthetic A β 1-42 oligomers on 'healthy' hiPSC-derived astrocytes and neurons derived from synchronous differentiation

method, as well as healthy human primary astrocytes. However, significant reduction in glycogen stores was only recorded for the 'healthy' donor hiPSC-derived astrocytes, but not for human primary astrocytes in response to synthetic A β 1-42 oligomers.

Furthermore, the project also examined the fAD patient-derived astrocytes and neurons for A β production and recorded increased A β production profile as well as alterations in A β 42/40 ratio when compared with their 'healthy' donor hiPSC-derived counterparts. The occurrence of de novo metabolic dysfunction as recorded by reduction in glucose uptake in the fAD patient-derived neurons in comparison to their 'healthy' counterparts was recorded only for neurons differentiated using the synchronous differentiation method. However, there was a significant reduction in glucose uptake in the patient-derived astrocytes as compared to the control. Furthermore, there was no significant alteration in the glycogen content level of the cells in response to endogenous A β .

The fact that fAD patient-derived neurons and astrocytes exhibited increased A β production and displayed evidence of metabolic dysfunction indicates that the induction pathway of metabolic dysfunction by endogenous A β may be an exploitable therapeutic target for the management of AD. This may provide an alternative to current therapeutic strategies being proposed, which involve preventing the production of toxic amyloid species by blocking the key enzymes involved in the production of toxic amyloid species (Panza *et al.*, 2019). Similarly, while most strategies being proposed for a definitive management from AD are focussed on the neurons, and preventing A β -induced neuronal damage, the increasing roles of the astrocytes in A β production and degradation, as well as the pathogenesis of AD are becoming more obvious from recent studies (Blasko *et al.*, 2000, Rossner *et al.*, 2005, Zhao *et al.*, 2011, Jin *et al.*, 2012).

This project also provides a similar perspective from the results showing increased A β generation from the astrocytes, as well metabolic dysfunction in the form of reduced glucose uptake. Furthermore, the important effect of astrocytes on neuronal energy metabolism, through the maintenance of lactate supplies for neuronal oxidative decarboxylation (Magistretti and Pellerin, 2000). This may also indicate that astrocytic carbohydrate metabolism may be an additional or alternative target that could potentially be exploited for future therapeutic options for AD.

As expected with novel research approaches, a number of issues encountered during the project, and some have been discussed in the relevant chapters. Others are highlighted below,

such as issues with culture, differentiation, maturity of the differentiated cells, amongst others. Some of these issues may require addressing before the next steps in the determination of metabolic dysfunction induced by A β in AD using hiPSC-derived models can be comfortably achieved.

6.2 Future Directions

Several issues were encountered during this project regarding the use of commercially obtained hiPSC-derived NPCs. These issues limit the power of the study as we were unable to compare effects in multiple control and patient cell lines.

Human 'healthy' control and fAD patient iPSC-derived NPC cell lines were obtained from Axol Biosciences. Three 'healthy' patient-derived cell lines, ax0016, ax0018 and ax0019 were initially used in the project. Frequent contamination of non-neuronal cells was observed with the ax0019 cell line (see Appendices: Fig. A20), as such these results were excluded from the study. The ax0016 cell line was also used as an alternative but also showed very stark inconsistencies in proliferation in culture and differentiation. As such only ax0018 was used as a 'healthy' control cell line.

Ongoing work in the laboratory have begun to generate NPC lines 'in house' using 'control' hiPSC lines from cell repositories including HiPSci, Coriell and EBISC.

The results of this project are also limited to one fAD patient model. These results will require further validation using additional AD patient-derived cell lines to determine the reproducibility of results. Ongoing work in the laboratory is currently generating a bank of fAD patient-derived hiPSCs for neural induction and use in future experiments. Furthermore, the question of whether the results of these experiments on fAD models will be representative of the vast majority of cases of AD, which are of the sporadic type. These may require further investigations. The use of isogenic lines may also be an alternative approach worth considering. Isogenic controls can also be produced from hiPSCs to show differences in the same cell based on specific genetic mutations or defects that have been removed or altered; diseases such as fAD, Parkinson's disease, Rett's syndrome and Amyotrophic Lateral Sclerosis (Soldner *et al.*, 2011, Sproul *et al.*, 2014, Ananiev *et al.*, 2011)

6.2.1 Neural Induction Method

Neurons used in this study were generated using both synchronous and spontaneous differentiation methods. The initial aim of using synchronous induction was to generate enriched mature neuronal cultures containing minimal astrocyte contamination in a shorter

amount of time (Shi *et al.*, 2012b). However, cultures contaminated with significant numbers of astrocytes. As such further optimisation of DAPT treatment is required for each cell line. Furthermore, the use of a mitotic inhibitor could significantly reduce the number of astrocytes generated in these cultures (James Crowe, personal communication). However, neuronal cells are likely to exhibit cellular stress in monoculture without the support of astrocytes. The use of conditioned media from astrocyte cultures may be able to provide this support without the need for the physical presence of astrocytes in future experiments.

Moreover, the contribution of cellular aging over multiple passages as well as contamination (from source) was a time consuming and procedural hindrance encountered during the project. In addition, the control (ax0018) and fAD patient (ax0012) cells were not sex or age-matched, as the ax0012 cells were retrieved from a 38 year old female, and the ax0018 cells were from a 72-year old male. It is unclear how much influence these differences may have exerted on the results of the experiments.

This project investigated the production of A β 1-40 and A β 1-42 by the fAD patient-derived astrocytes and neurons. The effects of other amyloid species which may have significant impact on the results may have been overlooked (Chavez-Gutierrez *et al.*, 2012, Slemmon *et al.*, 2015). However, A β 1-40 and A β 1-42 are known to be the most abundant and significant A β species isolated in AD patients (Slemmon *et al.*, 2015). Further experiments may examine the effects of other amyloid species, soluble and non-soluble amyloid species, as well as the aggregation of amyloid peptides using ELISA. There are also other aspects of APP processing that may exert significant relevance on the pathogenesis of AD. Unlike PSEN1 and PSEN2 mutations which are more likely to generate longer A β fragments, APP mutations are more likely to generate shorter A β fragments (Szaruga *et al.*, 2003, Chavez-Gutierrez *et al.*, 2012).

Moreover, as stated in the chapter 5 (preliminary results) of the immunodepletion experiment, future experiments should also determine if dysfunction correlates with the release of A β peptides using both pharmacological blockade of amyloid processing and immunodepletion studies.

Furthermore, this project explored the occurrence of metabolic dysfunction using glucose uptake and glycogen metabolism only as markers. Future experiments may explore the occurrence of metabolic dysfunction through the assessment of ATP, NAD⁺/NADH, lactate, pyruvate, glutamine and glutamate levels (Tarczyluk *et al.*, 2015). Further analysis using the Seahorse Bioanalyser Agilent would also enable, assessment of glycolysis and oxidative

phosphorylation in live cells by measuring the rate of mitochondrial activity as measured by their oxygen utilisation rate as well as extracellular acidification rate as a measure of glycolysis. It also examines fatty acid oxidation amongst other determinants of metabolic activity and stress.

Whilst Tarczyluk *et al.* (2015) utilised plate based kits to measure release of metabolite more sensitive methods could be utilised to monitor cell metabolism analysis using labelled glucose, lactate and other metabolites may also be carried to provide documented mechanistic effects on metabolic pathways of various substrates as explained in section 3.4. This analysis can also provide important insights into the mechanisms involved in degradation and recycling of important substrates such as glutamate as well as trafficking of substrates between the neurons and astrocytes.

Further experiments also need to explore the nuances of gene expression involved in metabolic dysfunction as a result of amyloid exposure. Ongoing work in our laboratory is currently using RNA-seq to determine gene expression changes following treatment of 'healthy' hiPSC-derived astrocytes with synthetic A β 1-42 oligomers. This study may identify pathways that are dysregulated, that lead to alterations in glucose uptake and glycogen content levels. The reduction in expression of important enzymes such as hexokinase and pyruvate dehydrogenase can be measured using this method, as they have been shown to exhibit reduced activity in AD patients (Gibson *et al.*, 1998).

6.2.2 2D vs 3D Culture

In addition, although this project provides a novel assessment of metabolic dysfunction induced by endogenously produced A β , the *in vitro* setting of the project may not be very representative of the metabolic events as they occur *in vivo* in the human brain. Experiments using 3D models may provide a more reliable representation of these occurrences *in vivo*, as these may be able to reproduce complex intercellular interactions including those of the astrocyte-neuron lactate shunt. As it has been shown in this projects that astrocytes have a significant role to play in the AD pathogenic process, the role of other cell types in the aetiology and progression of the disease is slowly being realised (De Strooper and Karran, 2016), and may need 3D modelling to be properly investigated. Indeed, 3D culture models using isogenic APOE3 and APOE4 iPSCs have demonstrated astrocyte-dependent temporal increases in A β and phosphorylated Tau production (Lin *et al.*, 2018). These models can also provide an

insight into the mechanism of A β aggregation and accumulation to the development of amyloid plaques and neurofibrillary tangles by reproducing these processes real time. Indeed, efforts at 3D modelling of AD have gained good momentum since the development of cerebral organoids, which involves the incorporation of iPSCs into matrigel, allowing the developing neural precursors to self-organise and form different layers specific to different brain parts (Hattori, 2014, Raja *et al.*, 2016). These organoids, when grown from iPSCs derived from AD patients have also been shown to demonstrate increased A β production and aggregation as well as tau phosphorylation (Gonzalez *et al.*, 2018).

Other 3D models have also been produced from NPCs carrying amyloid-generating mutations of fAD, and these have been shown to develop amyloid plaques and neurofibrillary tangles (Gonzalez *et al.*, 2018).

Overall, these models when fully developed, represent the most reliable means of demonstrating mechanistic changes during the pathogenic courses of several diseases like AD and other neurodegenerative conditions. They also represent the most reliable means for drug screening and understanding of the mechanisms of therapeutic changes induced by newer therapies during treatment.

List of References

- AARSLAND, D., CUMMINGS, J. L., YENNER, G., & MILLER, B. 1996. Relationship of aggressive behavior to other neuropsychiatric symptoms in patients with Alzheimer's disease. *American Journal of Psychiatry*, 153, 243-247.
- ABETI, R., ABRAMOV, A. Y. & DUCHEN, M. R. 2011. Beta-amyloid activates PARP causing astrocytic metabolic failure and neuronal death. *Brain*, 134, 1658-72.
- ABRAMOV, A. Y., CANEVARI, L. & DUCHEN, M. R. 2004. Beta-amyloid peptides induce mitochondrial dysfunction and oxidative stress in astrocytes and death of neurons through activation of NADPH oxidase. *J Neurosci*, 24, 565-75.
- AGING, N. I. O. Alzheimer's Disease Fact Sheet.
- AKSENOV, M. Y., TUCKER, H. M., NAIR, P., AKSENOVA, M. V., BUTTERFIELD, D. A., ESTUS, S. & MARKESBERY, W. R. 1999. The expression of several mitochondrial and nuclear genes encoding the subunits of electron transport chain enzyme complexes, cytochrome c oxidase, and NADH dehydrogenase, in different brain regions in Alzheimer's disease. *Neurochem Res*, 24, 767-74.
- ALBERT, M. S., DEKOSKY, S. T., DICKSON, D., DUBOIS, B., FELDMAN, H. H., FOX, N. C., GAMST, A., HOLTZMAN, D. M., JAGUST, W. J., PETERSEN, R. C., SNYDER, P. J., CARRILLO, M. C., THIES, B. & PHELPS, C. H. 2011. The diagnosis of mild cognitive impairment due to Alzheimer's disease: recommendations from the National Institute on Aging-Alzheimer's Association workgroups on diagnostic guidelines for Alzheimer's disease. *Alzheimers Dement*, 7, 270-9.
- ALIPOUR, M., NABAVI, S. M., ARAB, L., VOSOUGH, M., PAKDAMAN, H., EHSANI, E. & SHAHPASAND, K. 2019. Stem cell therapy in Alzheimer's disease: possible benefits and limiting drawbacks. *Mol Biol Rep*, 46, 1425-1446.
- ALLAMAN, I., GAVILLET, M., BELANGER, M., LAROCHE, T., VIERTL, D., LASHUEL, H. A. & MAGISTRETTI, P. J. 2010. Amyloid-beta aggregates cause alterations of astrocytic metabolic phenotype: impact on neuronal viability. *J Neurosci*, 30, 3326-38.
- ALZHEIMER, A. 1907. Über eine eigenartige Erkrankung der Hirnrinde. *Allgemeine Zeitschrift für Psychiatrie und psychisch-Gerichtliche Medizin (Berlin)*.
- ALZHEIMER, A., STELZMANN, R. A., SCHNITZLEIN, H. N. & MURTAGH, F. R. 1995. An English translation of Alzheimer's 1907 paper, "Über eine eigenartige Erkrankung der Hirnrinde". *Clin Anat*, 8, 429-31.
- AMARAL, A. I., TEIXEIRA, A. P., HAKONSEN, B. I., SONNEWALD, U. & ALVES, P. M. 2011. A comprehensive metabolic profile of cultured astrocytes using isotopic transient metabolic flux analysis and C-labeled glucose. *Front Neuroenergetics*, 3, 5.

- ANANIEV, G., WILLIAMS, E. C., LI, H. & CHANG, Q. 2011. Isogenic pairs of wild type and mutant induced pluripotent stem cell (iPSC) lines from Rett syndrome patients as in vitro disease model. *PLoS One*, 6, e25255.
- ANDERSON, G. W., DEANS, P. J. M., TAYLOR, R. D. T., RAVAL, P., CHEN, D., LOWDER, H., MURKERJI, S., ANDREAE, L. C., WILLIAMS, B. P. & SRIVASTAVA, D. P. 2015. Characterisation of neurons derived from a cortical human neural stem cell line CTX0E16. *Stem cell research & therapy*, 6, 149-149.
- ANTHONY, J. C., BREITNER, J. C., ZANDI, P. P., MEYER, M. R., JURASOVA, I., NORTON, M. C. & STONE, S. V. 2000. Reduced prevalence of AD in users of NSAIDs and H2 receptor antagonists: the Cache County study. *Neurology*, 54, 2066-71.
- ARBER, C., TOOMBS, J., LOVEJOY, C., RYAN, N. S., PATERSON, R. W., WILLUMSEN, N., GKANATSIU, E., PORTELIUS, E., BLENNOW, K., HESLEGRAVE, A., SCHOTT, J. M., HARDY, J., LASHLEY, T., FOX, N. C., ZETTERBERG, H. & WRAY, S. 2019. Familial Alzheimer's disease patient-derived neurons reveal distinct mutation-specific effects on amyloid beta. *Molecular Psychiatry*.
- ASSOCIATION., A. S. Alzheimer's Disease Facts and Figures.
- ATWOOD, C. S., MOIR, R. D., HUANG, X., SCARPA, R. C., BACCARRA, N. M. E., ROMANO, D. M., HARTSHORN, M. A., TANZI, R. E. & BUSH, A. I. 1998. Dramatic Aggregation of Alzheimer A β by Cu(II) Is Induced by Conditions Representing Physiological Acidosis. *Journal of Biological Chemistry*, 273, 12817-12826.
- BALLATORE, C., LEE, V. M. Y. & TROJANOWSKI, J. Q. 2007. Tau-mediated neurodegeneration in Alzheimer's disease and related disorders. *Nature Reviews Neuroscience*, 8, 663.
- BARKER, A. J., KOCH, S. M., REED, J., BARRES, B. A. & ULLIAN, E. M. 2008. Developmental control of synaptic receptivity. *J Neurosci*, 28, 8150-60.
- BARSOUM, M. J., YUAN, H., GERENCSEK, A. A., LIOT, G., KUSHNAREVA, Y., GRABER, S., KOVACS, I., LEE, W. D., WAGGONER, J., CUI, J., WHITE, A. D., BOSSY, B., MARTINOU, J. C., YOULE, R. J., LIPTON, S. A., ELLISMAN, M. H., PERKINS, G. A. & BOSSY-WETZEL, E. 2006. Nitric oxide-induced mitochondrial fission is regulated by dynamin-related GTPases in neurons. *Embo j*, 25, 3900-11.
- BASSIL, F., FERNAGUT, P. O., BEZARD, E. & MEISSNER, W. G. 2014. Insulin, IGF-1 and GLP-1 signaling in neurodegenerative disorders: targets for disease modification? *Prog Neurobiol*, 118, 1-18.
- BAYER, T. A. & WIRTHS, O. 2014. Focusing the amyloid cascade hypothesis on N-truncated Abeta peptides as drug targets against Alzheimer's disease. *Acta Neuropathol*, 127, 787-801.

- BELL, S. M., BARNES, K., CLEMMENS, H., AL-RAFIAH, A. R., AL-OFI, E. A., LEECH, V., BANDMANN, O., SHAW, P. J., BLACKBURN, D. J., FERRAIUOLO, L. & MORTIBOYS, H. 2018. Ursodeoxycholic Acid Improves Mitochondrial Function and Redistributes Drp1 in Fibroblasts from Patients with Either Sporadic or Familial Alzheimer's Disease. *Journal of Molecular Biology*, 430, 3942-3953.
- BENITEZ, B. A. & CRUCHAGA, C. 2013. TREM2 and neurodegenerative disease. *N Engl J Med*, 369, 1567-8.
- BERMEJO-PAREJA, F., BENITO-LEÓN, J., VEGA, S., MEDRANO, M. J. & ROMÁN, G. C. 2008. Incidence and subtypes of dementia in three elderly populations of central Spain. *Journal of the Neurological Sciences*, 264, 63-72.
- BERTRAM, L. & TANZI, R. E. 2008. Thirty years of Alzheimer's disease genetics: the implications of systematic meta-analyses. *Nature Reviews Neuroscience*, 9, 768.
- BLASKO, I., VEERHUIS, R., STAMPFER-KOUNTCHEV, M., SAURWEIN-TEISSEL, M., EIKELBOOM, P. & GRUBECK-LOEBENSTEIN, B. 2000. Costimulatory effects of interferon-gamma and interleukin-1beta or tumor necrosis factor alpha on the synthesis of Abeta1-40 and Abeta1-42 by human astrocytes. *Neurobiol Dis*, 7, 682-9.
- BLENNOW, K., DE LEON, M. J. & ZETTERBERG, H. 2006. Alzheimer's disease. *Lancet*, 368, 387-403.
- BLESSED, G., TOMLINSON, B. E. & ROTH, M. 1968. The Association Between Quantitative Measures of Dementia and of Senile Change in the Cerebral Grey Matter of Elderly Subjects. *British Journal of Psychiatry*, 114, 797-811.
- BOMFIM, T. R., FORNY-GERMANO, L., SATHLER, L. B., BRITO-MOREIRA, J., HOUZEL, J. C., DECKER, H., SILVERMAN, M. A., KAZI, H., MELO, H. M., MCCLEAN, P. L., HOLSCHER, C., ARNOLD, S. E., TALBOT, K., KLEIN, W. L., MUNOZ, D. P., FERREIRA, S. T. & DE FELICE, F. G. 2012. An anti-diabetes agent protects the mouse brain from defective insulin signaling caused by Alzheimer's disease-associated Abeta oligomers. *J Clin Invest*, 122, 1339-53.
- BONNI, A., SUN, Y., NADAL-VICENS, M., BHATT, A., FRANK, D. A., ROZOVSKY, I., STAHL, N., YANCOPOULOS, G. D. & GREENBERG, M. E. 1997. Regulation of gliogenesis in the central nervous system by the JAK-STAT signaling pathway. *Science*, 278, 477-83.
- BRAAK, H., ALAFUZOFF, I., ARZBERGER, T., KRETZSCHMAR, H. & DEL TREDICI, K. 2006. Staging of Alzheimer disease-associated neurofibrillary pathology using paraffin sections and immunocytochemistry. *Acta neuropathologica*, 112, 389-404.
- BRAAK, H. & BRAAK, E. 1991. Neuropathological staging of Alzheimer-related changes. *Acta Neuropathol*, 82, 239-59.

- BROWN, A. M. & RANSOM, B. R. 2007. Astrocyte glycogen and brain energy metabolism. *Glia*, 55, 1263-1271.
- BROWN, A. M., SICKMANN, H. M., FOSGERAU, K., LUND, T. M., SCHOUSBOE, A., WAAGEPETERSEN, H. S. & RANSOM, B. R. 2005. Astrocyte glycogen metabolism is required for neural activity during aglycemia or intense stimulation in mouse white matter. *J Neurosci Res*, 79, 74-80.
- BUBBER, P., HAROUTUNIAN, V., FISCH, G., BLASS, J. P. & GIBSON, G. E. 2005. Mitochondrial abnormalities in Alzheimer brain: mechanistic implications. *Ann Neurol*, 57, 695-703.
- BURNS, A. & ILIFFE, S. 2009. Alzheimer's disease. *BMJ*, 338, b158.
- BURNS, A. & ILIFFE, S. 2009. Dementia. *BMJ*, 338, b75.
- BUSCIGLIO, J., GABUZDA, D. H., MATSUDAIRA, P. & YANKNER, B. A. 1993. Generation of beta-amyloid in the secretory pathway in neuronal and nonneuronal cells. *Proceedings of the National Academy of Sciences*, 90, 2092-2096.
- BUSH, T. G., PUVANACHANDRA, N., HORNER, C. H., POLITO, A., OSTENFELD, T., SVENDSEN, C. N., MUCKE, L., JOHNSON, M. H. & SOFRONIEW, M. V. 1999. Leukocyte infiltration, neuronal degeneration, and neurite outgrowth after ablation of scar-forming, reactive astrocytes in adult transgenic mice. *Neuron*, 23, 297-308.
- BUTTERFIELD, D. A., HENSLEY, K., HARRIS, M., MATTSON, M. & CARNEY, J. 1994. beta-Amyloid peptide free radical fragments initiate synaptosomal lipoperoxidation in a sequence-specific fashion: implications to Alzheimer's disease. *Biochem Biophys Res Commun*, 200, 710-5.
- BYLICKY, M. A., MUELLER, G. P. & DAY, R. M. 2018. Mechanisms of Endogenous Neuroprotective Effects of Astrocytes in Brain Injury. *Oxid Med Cell Longev*, 2018, 6501031.
- CAILLE, I., ALLINQUANT, B., DUPONT, E., BOUILLOT, C., LANGER, A., MULLER, U. & PROCHIANTZ, A. 2004. Soluble form of amyloid precursor protein regulates proliferation of progenitors in the adult subventricular zone. *Development*, 131, 2173-81.
- CARMIGNOTO, G. 2000. Reciprocal communication systems between astrocytes and neurones. *Prog Neurobiol*, 62, 561-81.
- CARROLL, C. M. & LI, Y.-M. 2016. Physiological and pathological roles of the γ -secretase complex. *Brain research bulletin*, 126, 199-206.
- CASLEY, C. S., LAND, J. M., SHARPE, M. A., CLARK, J. B., DUCHEN, M. R. & CANEVARI, L. 2002. Beta-amyloid fragment 25-35 causes mitochondrial dysfunction in primary cortical neurons. *Neurobiol Dis*, 10, 258-67.

- CASPERSEN, C., WANG, N., YAO, J., SOSUNOV, A., CHEN, X., LUSTBADER, J. W., XU, H. W., STERN, D., MCKHANN, G. & YAN, S. D. 2005. Mitochondrial Abeta: a potential focal point for neuronal metabolic dysfunction in Alzheimer's disease. *Faseb j*, 19, 2040-1.
- CHAMBERS, S. M., FASANO, C. A., PAPAPETROU, E. P., TOMISHIMA, M., SADELAIN, M. & STUDER, L. 2009. Highly efficient neural conversion of human ES and iPS cells by dual inhibition of SMAD signaling. *Nat Biotechnol*, 27, 275-80.
- CHAMOUN, R., SUKI, D., GOPINATH, S. P., GOODMAN, J. C. & ROBERTSON, C. 2010. Role of extracellular glutamate measured by cerebral microdialysis in severe traumatic brain injury. *J Neurosurg*, 113, 564-70.
- CHAVEZ-GUTIERREZ, L., BAMMENS, L., BENILOVA, I., VANDERSTEEN, A., BENURWAR, M., BORGERS, M., LISMONT, S., ZHOU, L., VAN CLEYNENBREUGEL, S., ESSELMANN, H., WILTFANG, J., SERNEELS, L., KARRAN, E., GIJSEN, H., SCHYMKOWITZ, J., ROUSSEAU, F., BROERSEN, K. & DE STROOPER, B. 2012. The mechanism of gamma-Secretase dysfunction in familial Alzheimer disease. *Embo j*, 31, 2261-74.
- CHEN, X. & YAN, S. D. 2006. Mitochondrial Abeta: a potential cause of metabolic dysfunction in Alzheimer's disease. *IUBMB Life*, 58, 686-94.
- CHEN, Y. F., WANG, H., CHU, Y., HUANG, Y. C. & SU, M. Y. 2006. Regional quantification of white matter hyperintensity in normal aging, mild cognitive impairment, and Alzheimer's disease. *Dement Geriatr Cogn Disord*, 22, 177-84.
- CHENG, Y., KATO, N., WANG, W., LI, J. & CHEN, X. 2003. Two RNA binding proteins, HEN4 and HUA1, act in the processing of AGAMOUS pre-mRNA in Arabidopsis thaliana. *Developmental cell*, 4, 53-66.
- CHIANG, P. M., FORTNA, R. R., PRICE, D. L., LI, T. & WONG, P. C. 2012. Specific domains in anterior pharynx-defective 1 determine its intramembrane interactions with nicastrin and presenilin. *Neurobiol Aging*, 33, 277-85.
- CHOI, S. H., KIM, Y. H., HEBISCH, M., SLIWINSKI, C., LEE, S., D'AVANZO, C., CHEN, H., HOOLI, B., ASSELIN, C., MUFFAT, J., KLEE, J. B., ZHANG, C., WAINGER, B. J., PEITZ, M., KOVACS, D. M., WOOLF, C. J., WAGNER, S. L., TANZI, R. E. & KIM, D. Y. 2014. A three-dimensional human neural cell culture model of Alzheimer's disease. *Nature*, 515, 274-8.
- CIRRITO, J. R., MAY, P. C., O'DELL, M. A., TAYLOR, J. W., PARSADANIAN, M., CRAMER, J. W., AUDIA, J. E., NISSEN, J. S., BALES, K. R., PAUL, S. M., DEMATTOS, R. B. & HOLTZMAN, D. M. 2003. *In Vivo* Assessment of Brain Interstitial Fluid with Microdialysis Reveals Plaque-Associated Changes in Amyloid- β Metabolism and Half-Life. *The Journal of Neuroscience*, 23, 8844-8853.

- CLARKE, L. E. & BARRES, B. A. 2013. Emerging roles of astrocytes in neural circuit development. *Nat Rev Neurosci*, 14, 311-21.
- CLEARY, J. P., WALSH, D. M., HOFMEISTER, J. J., SHANKAR, G. M., KUSKOWSKI, M. A., SELKOE, D. J. & ASHE, K. H. 2005. Natural oligomers of the amyloid- β protein specifically disrupt cognitive function. *Nature Neuroscience*, 8, 79-84.
- CORIC, V., SALLOWAY, S., VAN DYCK, C. H., DUBOIS, B., ANDREASEN, N., BRODY, M., CURTIS, C., SOININEN, H., THEIN, S., SHIOVITZ, T., PILCHER, G., FERRIS, S., COLBY, S., KERSELAERS, W., DOCKENS, R., SOARES, H., KAPLITA, S., LUO, F., PACHAI, C., BRACOD, L., MINTUN, M., GRILL, J. D., MAREK, K., SEIBYL, J., CEDARBAUM, J. M., ALBRIGHT, C., FELDMAN, H. H. & BERMAN, R. M. 2015. Targeting Prodromal Alzheimer Disease With Avagacestat: A Randomized Clinical Trial. *JAMA Neurol*, 72, 1324-33.
- CORIC, V., VAN DYCK, C. H., SALLOWAY, S., ANDREASEN, N., BRODY, M., RICHTER, R. W., SOININEN, H., THEIN, S., SHIOVITZ, T., PILCHER, G., COLBY, S., ROLLIN, L., DOCKENS, R., PACHAI, C., PORTELIUS, E., ANDREASSON, U., BLENNOW, K., SOARES, H., ALBRIGHT, C., FELDMAN, H. H. & BERMAN, R. M. 2012. Safety and tolerability of the gamma-secretase inhibitor avagacestat in a phase 2 study of mild to moderate Alzheimer disease. *Arch Neurol*, 69, 1430-40.
- CRAFT, S., ASTHANA, S., SCHELLENBERG, G., BAKER, L., CHERRIER, M., BOYT, A. A., MARTINS, R. N., RASKIND, M., PESKIND, E. & PLYMATE, S. 2000. Insulin effects on glucose metabolism, memory, and plasma amyloid precursor protein in Alzheimer's disease differ according to apolipoprotein-E genotype. *Ann N Y Acad Sci*, 903, 222-8.
- CRUTS, M., THEUNS, J. & VAN BROECKHOVEN, C. 2012. Locus-specific mutation databases for neurodegenerative brain diseases. *Hum Mutat*, 33, 1340-4.
- CRYSTAL, A. S., MORAIS, V. A., PIERSON, T. C., PIJAK, D. S., CARLIN, D., LEE, V. M. & DOMS, R. W. 2003. Membrane topology of gamma-secretase component PEN-2. *J Biol Chem*, 278, 20117-23.
- DAVIS, C. H., KIM, K. Y., BUSHONG, E. A., MILLS, E. A., BOASSA, D., SHIH, T., KINEBUCHI, M., PHAN, S., ZHOU, Y., BIHLMAYER, N. A., NGUYEN, J. V., JIN, Y., ELLISMAN, M. H. & MARSH-ARMSTRONG, N. 2014. Transcellular degradation of axonal mitochondria. *Proc Natl Acad Sci U S A*, 111, 9633-8.
- DAVIS, J. B., MCMURRAY, H. F. & SCHUBERT, D. 1992. The amyloid beta-protein of Alzheimer's disease is chemotactic for mononuclear phagocytes. *Biochem Biophys Res Commun*, 189, 1096-100.
- DE FELICE, F. G., WU, D., LAMBERT, M. P., FERNANDEZ, S. J., VELASCO, P. T., LACOR, P. N., BIGIO, E. H., JERECIC, J., ACTON, P. J., SHUGHRUE, P. J., CHEN-DODSON,

- E., KINNEY, G. G. & KLEIN, W. L. 2008. Alzheimer's disease-type neuronal tau hyperphosphorylation induced by A beta oligomers. *Neurobiol Aging*, 29, 1334-47.
- DE JONGHE, C., ESSELENS, C., KUMAR-SINGH, S., CRAESSAERTS, K., SERNEELS, S., CHECLER, F., ANNAERT, W., VAN BROECKHOVEN, C. & DE STROOPER, B. 2001. Pathogenic APP mutations near the gamma-secretase cleavage site differentially affect Abeta secretion and APP C-terminal fragment stability. *Hum Mol Genet*, 10, 1665-71.
- DE STROOPER, B. & KARRAN, E. 2016. The Cellular Phase of Alzheimer's Disease. *Cell*, 164, 603-15.
- DE STROOPER, B., VASSAR, R. & GOLDE, T. 2010. The secretases: enzymes with therapeutic potential in Alzheimer disease. *Nat Rev Neurol*, 6, 99-107.
- DENHAM, M. & DOTTORI, M. 2011. Neural differentiation of induced pluripotent stem cells. *Methods Mol Biol*, 793, 99-110.
- DI CARLO, A., BALDERESCHI, M., AMADUCCI, L., LEPORE, V., BRACCO, L., MAGGI, S., BONAIUTO, S., PERISSINOTTO, E., SCARLATO, G., FARCHI, G., INZITARI, D. & GROUP, F. T. I. W. 2002. Incidence of Dementia, Alzheimer's Disease, and Vascular Dementia in Italy. The ILSA Study. *Journal of the American Geriatrics Society*, 50, 41-48.
- DI LULLO, E. & KRIEGSTEIN, A. R. 2017. The use of brain organoids to investigate neural development and disease. *Nature reviews. Neuroscience*, 18, 573-584.
- DIENEL, G. A. & HERTZ, L. 2001. Glucose and lactate metabolism during brain activation. *J Neurosci Res*, 66, 824-38.
- DINUZZO, M., MANGIA, S., MARAVIGLIA, B. & GIOVE, F. 2013. Regulatory mechanisms for glycogenolysis and K⁺ uptake in brain astrocytes. *Neurochemistry international*, 63, 458-464.
- DITARANTO, K., TEKIRIAN, T. L. & YANG, A. J. 2001. Lysosomal Membrane Damage in Soluble A β -Mediated Cell Death in Alzheimer's Disease. *Neurobiology of Disease*, 8, 19-31.
- DODEL, R. C., DU, Y., DEPBOYLU, C., HAMPEL, H., FROLICH, L., HAAG, A., HEMMETER, U., PAULSEN, S., TEIPEL, S. J., BRETTSCHEIDER, S., SPOTTKE, A., NOLKER, C., MOLLER, H. J., WEI, X., FARLOW, M., SOMMER, N. & OERTEL, W. H. 2004. Intravenous immunoglobulins containing antibodies against beta-amyloid for the treatment of Alzheimer's disease. *J Neurol Neurosurg Psychiatry*, 75, 1472-4.
- DOODY, R. S., RAMAN, R., FARLOW, M., IWATSUBO, T., VELLAS, B., JOFFE, S., KIEBURTZ, K., HE, F., SUN, X., THOMAS, R. G., AISEN, P. S., SIEMERS, E., SETHURAMAN, G. & MOHS, R. 2013. A phase 3 trial of semagacestat for treatment of Alzheimer's disease. *N Engl J Med*, 369, 341-50.

- DOS SANTOS, L. R., PIMASSONI, L. H. S., SENA, G. G. S., CAMPOREZ, D., BELCAVELLO, L., TRANCOZO, M., MORELATO, R. L., ERRERA, F. I. V., BUENO, M. R. P. & DE PAULA, F. 2017. Validating GWAS Variants from Microglial Genes Implicated in Alzheimer's Disease. *J Mol Neurosci*, 62, 215-221.
- DR KAJ BLENNOW, MONY J DE LEON & HENRIK ZETTERBERG 2006. Alzheimer's disease. *Elsevier Ltd.*, 368, 387-403.
- DUNYS, J., VALVERDE, A. & CHECLER, F. 2018. Are N- and C-terminally truncated Abeta species key pathological triggers in Alzheimer's disease? *J Biol Chem*, 293, 15419-15428.
- EDBAUER, D., WINKLER, E., REGULA, J. T., PESOLD, B., STEINER, H. & HAASS, C. 2003. Reconstitution of gamma-secretase activity. *Nat Cell Biol*, 5, 486-8.
- EFTEKHARPOUR, E., HOLMGREN, A. & JUURLINK, B. H. 2000. Thioredoxin reductase and glutathione synthesis is upregulated by t-butylhydroquinone in cortical astrocytes but not in cortical neurons. *Glia*, 31, 241-8.
- EFTHYMIU, A. G. & GOATE, A. M. 2017. Late onset Alzheimer's disease genetics implicates microglial pathways in disease risk. *Molecular neurodegeneration*, 12, 43-43.
- EL KHOURY, J., HICKMAN, S. E., THOMAS, C. A., CAO, L., SILVERSTEIN, S. C. & LOIKE, J. D. 1996. Scavenger receptor-mediated adhesion of microglia to beta-amyloid fibrils. *Nature*, 382, 716-9.
- ELMARIAH, S. B., OH, E. J., HUGHES, E. G. & BALICE-GORDON, R. J. 2005. Astrocytes regulate inhibitory synapse formation via Trk-mediated modulation of postsynaptic GABAA receptors. *J Neurosci*, 25, 3638-50.
- ESTERHAZY, D., STUTZER, I., WANG, H., RECHSTEINER, M. P., BEAUCHAMP, J., DOBELI, H., HILPERT, H., MATILE, H., PRUMMER, M., SCHMIDT, A., LIESKE, N., BOEHM, B., MARSELLI, L., BOSCO, D., KERR-CONTE, J., AEBERSOLD, R., SPINAS, G. A., MOCH, H., MIGLIORINI, C. & STOFFEL, M. 2011. Bace2 is a beta cell-enriched protease that regulates pancreatic beta cell function and mass. *Cell Metab*, 14, 365-77.
- FANG, Y., GAO, T., ZHANG, B. & PU, J. 2018. Recent Advances: Decoding Alzheimer's Disease With Stem Cells. *Frontiers in aging neuroscience*, 10, 77-77.
- FERNANDEZ, M. A., BIETTE, K. M., DOLIOS, G., SETH, D., WANG, R. & WOLFE, M. S. 2016. Transmembrane Substrate Determinants for gamma-Secretase Processing of APP CTFbeta. *Biochemistry*, 55, 5675-5688.
- FERNANDEZ, M. A., KLUTKOWSKI, J. A., FRERET, T. & WOLFE, M. S. 2014. Alzheimer presenilin-1 mutations dramatically reduce trimming of long amyloid beta-peptides (Abeta) by gamma-secretase to increase 42-to-40-residue Abeta. *J Biol Chem*, 289, 31043-52.

- FERRI, C. P., PRINCE, M., BRAYNE, C., BRODATY, H., FRATIGLIONI, L. & GANGULI, M. 2010. Global prevalence of dementia: a Delphi consensus study. *Lancet (London, England)*, 366, 2112–2117.
- FERRI, C. P., PRINCE, M., BRAYNE, C., BRODATY, H., FRATIGLIONI, L., GANGULI, M., HALL, K., HASEGAWA, K., HENDRIE, H., HUANG, Y., JORM, A., MATHERS, C., MENEZES, P. R., RIMMER, E. & SCAZUFCA, M. 2005. Global prevalence of dementia: a Delphi consensus study. *Lancet*, 366, 2112-7.
- FERRIS, S. H., DE LEON, M. J., WOLF, A. P., FARKAS, T., CHRISTMAN, D. R., REISBERG, B., FOWLER, J. S., MACGREGOR, R., GOLDMAN, A., GEORGE, A. E. & RAMPAL, S. 1980. Positron emission tomography in the study of aging and senile dementia. *Neurobiol Aging*, 1, 127-31.
- FILSER, S., OVSEPIAN, S. V., MASANA, M., BLAZQUEZ-LLORCA, L., BRANDT ELVANG, A., VOLBRACHT, C., MULLER, M. B., JUNG, C. K. & HERMS, J. 2015. Pharmacological inhibition of BACE1 impairs synaptic plasticity and cognitive functions. *Biol Psychiatry*, 77, 729-39.
- FRÖLICH, L., BLUM-DEGEN, D., BERNSTEIN, H.-G., ENGELSBERGER, S., HUMRICH, J., LAUFER, S., MUSCHNER, D., THALHEIMER, A., TÜRK, A., HOYER, S., ZÖCHLING, R., BOISSEL, K. W., JELLINGER, K. & RIEDERER, P. 1998. Brain insulin and insulin receptors in aging and sporadic Alzheimer's disease. *Journal of Neural Transmission*, 105, 423-438.
- FUNAMOTO, S., MORISHIMA-KAWASHIMA, M., TANIMURA, Y., HIROTANI, N., SAIDO, T. C. & IHARA, Y. 2004. Truncated carboxyl-terminal fragments of beta-amyloid precursor protein are processed to amyloid beta-proteins 40 and 42. *Biochemistry*, 43, 13532-40.
- FURUKAWA, K., SOPHER, B. L., RYDEL, R. E., BEGLEY, J. G., PHAM, D. G., MARTIN, G. M., FOX, M. & MATTSON, M. P. 1996. Increased Activity-Regulating and Neuroprotective Efficacy of α -Secretase-Derived Secreted Amyloid Precursor Protein Conferred by a C-Terminal Heparin-Binding Domain. *Journal of Neurochemistry*, 67, 1882-1896.
- GALEFFI, F., FOSTER, K. A., SADGROVE, M. P., BEAVER, C. J. & TURNER, D. A. 2007. Lactate uptake contributes to the NAD(P)H biphasic response and tissue oxygen response during synaptic stimulation in area CA1 of rat hippocampal slices. *J Neurochem*, 103, 2449-61.
- GALLAGHER, C. N., CARPENTER, K. L., GRICE, P., HOWE, D. J., MASON, A., TIMOFEEV, I., MENON, D. K., KIRKPATRICK, P. J., PICKARD, J. D., SUTHERLAND, G. R. & HUTCHINSON, P. J. 2009. The human brain utilizes lactate via the tricarboxylic acid

- cycle: a ¹³C-labelled microdialysis and high-resolution nuclear magnetic resonance study. *Brain*, 132, 2839-49.
- GARCIA-OSTA, A. & ALBERINI, C. M. 2009. Amyloid beta mediates memory formation. *Learn Mem*, 16, 267-72.
- GIAUME, C., KOULAKOFF, A., ROUX, L., HOLCMAN, D. & ROUACH, N. 2010. Astroglial networks: a step further in neuroglial and gliovascular interactions. *Nat Rev Neurosci*, 11, 87-99.
- GIBSON, G. E. & BLASS, J. P. 1976. Inhibition of acetylcholine synthesis and of carbohydrate utilization by maple-syrup-urine disease metabolites. *J Neurochem*, 26, 1073-8.
- GIBSON, G. E., HAROUTUNIAN, V., ZHANG, H., PARK, L. C., SHI, Q., LESSER, M., MOHS, R. C., SHEU, R. K. & BLASS, J. P. 2000. Mitochondrial damage in Alzheimer's disease varies with apolipoprotein E genotype. *Ann Neurol*, 48, 297-303.
- GIBSON, G. E., SHEU, K. F. & BLASS, J. P. 1998. Abnormalities of mitochondrial enzymes in Alzheimer disease. *J Neural Transm (Vienna)*, 105, 855-70.
- GILMAN, S., KOLLER, M., BLACK, R. S., JENKINS, L., GRIFFITH, S. G., FOX, N. C., EISNER, L., KIRBY, L., ROVIRA, M. B., FORETTE, F. & ORGOGOZO, J. M. 2005. Clinical effects of Abeta immunization (AN1792) in patients with AD in an interrupted trial. *Neurology*, 64, 1553-62.
- GLENNER, G. & WONG, C. 1984. Alzheimer's disease: Initial report of the purification and characterization of a novel cerebrovascular amyloid protein. 120, 885-890.
- GONZALEZ, C., ARMIJO, E., BRAVO-ALEGRIA, J., BECERRA-CALIXTO, A., MAYS, C. E. & SOTO, C. 2018. Modeling amyloid beta and tau pathology in human cerebral organoids. *Mol Psychiatry*, 23, 2363-2374.
- GOURAS, G. K., TSAI, J., NASLUND, J., VINCENT, B., EDGAR, M., CHECLER, F., GREENFIELD, J. P., HAROUTUNIAN, V., BUXBAUM, J. D., XU, H., GREENGARD, P. & RELKIN, N. R. 2000. Intraneuronal Abeta42 accumulation in human brain. *The American journal of pathology*, 156, 15-20.
- GRUETTER, R. 2003. Glycogen: the forgotten cerebral energy store. *J Neurosci Res*, 74, 179-83.
- GUERREIRO, R. & HARDY, J. 2013. TREM2 and neurodegenerative disease. *N Engl J Med*, 369, 1569-70.
- HAHN, S., BRUNING, T., NESS, J., CZIRR, E., BACHES, S., GIJSEN, H., KORTH, C., PIETRZIK, C. U., BULIC, B. & WEGGEN, S. 2011. Presenilin-1 but not amyloid precursor protein mutations present in mouse models of Alzheimer's disease attenuate the response of cultured cells to gamma-secretase modulators regardless of their potency and structure. *J Neurochem*, 116, 385-95.

- HALL, A. C., MIRA, H., WAGNER, J. & ARENAS, E. 2003. Region-specific effects of glia on neuronal induction and differentiation with a focus on dopaminergic neurons. *Glia*, 43, 47-51.
- HAMA, H., HARA, C., YAMAGUCHI, K. & MIYAWAKI, A. 2004. PKC signaling mediates global enhancement of excitatory synaptogenesis in neurons triggered by local contact with astrocytes. *Neuron*, 41, 405-15.
- HAMPEL, H., TOSCHI, N., BABILONI, C., BALDACCI, F., BLACK, K. L., BOKDE, A. L. W., BUN, R. S., CACCIOLA, F., CAVEDO, E., CHIESA, P. A., COLLIOT, O., COMAN, C.-M., DUBOIS, B., DUGGENTO, A., DURRLEMAN, S., FERRETTI, M.-T., GEORGE, N., GENTHON, R., HABERT, M.-O., HERHOLZ, K., KORONYO, Y., KORONYO-HAMAOU, M., LAMARI, F., LANGEVIN, T., LEHÉRICY, S., LORENCEAU, J., NERI, C., NISTICÒ, R., NYASSE-MESSENE, F., RITCHIE, C., ROSSI, S., SANTARNECCHI, E., SPORNS, O., VERDOONER, S. R., VERGALLO, A., VILLAIN, N., YOUNESI, E., GARACI, F., LISTA, S. & ALZHEIMER PRECISION MEDICINE, I. 2018. Revolution of Alzheimer Precision Neurology. Passageway of Systems Biology and Neurophysiology. *Journal of Alzheimer's disease : JAD*, 64, S47-S105.
- HARDY, J. & ALLSOP, D. 1991. Amyloid deposition as the central event in the aetiology of Alzheimer's disease. *Trends in Pharmacological Sciences*, 12, 383-388.
- HARTLEY, R. S., MARGULIS, M., FISHMAN, P. S., LEE, V. M. & TANG, C. M. 1999. Functional synapses are formed between human NTera2 (NT2N, hNT) neurons grown on astrocytes. *J Comp Neurol*, 407, 1-10.
- HATTORI, N. 2014. Cerebral organoids model human brain development and microcephaly. *Mov Disord*, 29, 185.
- HAYAKAWA, K., ESPOSITO, E., WANG, X., TERASAKI, Y., LIU, Y., XING, C., JI, X. & LO, E. H. 2016. Transfer of mitochondria from astrocytes to neurons after stroke. *Nature*, 535, 551-5.
- HEAD, E., SILVERMAN, W., PATTERSON, D. & LOTT, I. T. 2012. Aging and down syndrome. *Curr Gerontol Geriatr Res*, 2012, 412536.
- HENSLEY, K., CARNEY, J. M., MATTSON, M. P., AKSENOVA, M., HARRIS, M., WU, J. F., FLOYD, R. A. & BUTTERFIELD, D. A. 1994. A model for beta-amyloid aggregation and neurotoxicity based on free radical generation by the peptide: relevance to Alzheimer disease. *Proceedings of the National Academy of Sciences of the United States of America*, 91, 3270-3274.
- HERCULANO-HOUZEL, S. 2009. The human brain in numbers: a linearly scaled-up primate brain. *Front Hum Neurosci*, 3, 31.

- HERTZ, L., PENG, L. & DIENEL, G. A. 2007. Energy metabolism in astrocytes: high rate of oxidative metabolism and spatiotemporal dependence on glycolysis/glycogenolysis. *J Cereb Blood Flow Metab*, 27, 219-49.
- HILL, E. J., JIMENEZ-GONZALEZ, C., TARCZYLUK, M., NAGEL, D. A., COLEMAN, M. D. & PARRI, H. R. 2012. NT2 derived neuronal and astrocytic network signalling. *PLoS One*, 7, e36098.
- HIRAI, K., ALIEV, G., NUNOMURA, A., FUJIOKA, H., RUSSELL, R. L., ATWOOD, C. S., JOHNSON, A. B., KRESS, Y., VINTERS, H. V., TABATON, M., SHIMOHAMA, S., CASH, A. D., SIEDLAK, S. L., HARRIS, P. L., JONES, P. K., PETERSEN, R. B., PERRY, G. & SMITH, M. A. 2001. Mitochondrial abnormalities in Alzheimer's disease. *J Neurosci*, 21, 3017-23.
- HOCHSTIM, C., DENEEN, B., LUKASZEWICZ, A., ZHOU, Q. & ANDERSON, D. J. 2008. Identification of positionally distinct astrocyte subtypes whose identities are specified by a homeodomain code. *Cell*, 133, 510-22.
- HOFF, P. & HIPPIUS, H. 1989. [Alois Alzheimer 1864-1915. An overview of his life and work on the occasion of his 125th birthday]. *Nervenarzt*, 60(6).
- HOLMES, B. B. & DIAMOND, M. I. 2014. Prion-like properties of Tau protein: the importance of extracellular Tau as a therapeutic target. *J Biol Chem*, 289, 19855-61.
- HOLMES, B. B., FURMAN, J. L., MAHAN, T. E., YAMASAKI, T. R., MIRBAHA, H., EADES, W. C., BELAYGOROD, L., CAIRNS, N. J., HOLTZMAN, D. M. & DIAMOND, M. I. 2014. Proteopathic tau seeding predicts tauopathy in vivo. *Proc Natl Acad Sci U S A*, 111, E4376-85.
- HOLSCHER, C. 2011. Diabetes as a risk factor for Alzheimer's disease: insulin signalling impairment in the brain as an alternative model of Alzheimer's disease. *Biochem Soc Trans*, 39, 891-7.
- HOLTZMAN, D. M., BALES, K. R., TENKOVA, T., FAGAN, A. M., PARSADANIAN, M., SARTORIUS, L. J., MACKAY, B., OLNEY, J., MCKEEL, D., WOZNIAK, D. & PAUL, S. M. 2000. Apolipoprotein E isoform-dependent amyloid deposition and neuritic degeneration in a mouse model of Alzheimer's disease. *Proceedings of the National Academy of Sciences of the United States of America*, 97, 2892-2897.
- HOULDEN, H., BAKER, M., ADAMSON, J., GROVER, A., WARING, S., DICKSON, D., LYNCH, T., BOEVE, B., PETERSEN, R. C., PICKERING-BROWN, S., OWEN, F., NEARY, D., CRAUFURD, D., SNOWDEN, J., MANN, D. & HUTTON, M. 1999. Frequency of tau mutations in three series of non-Alzheimer's degenerative dementia. *Ann Neurol*, 46, 243-8.
- HOULDEN, H., JOHNSON, J., GARDNER-THORPE, C., LASHLEY, T., HERNANDEZ, D., WORTH, P., SINGLETON, A. B., HILTON, D. A., HOLTON, J., REVESZ, T., DAVIS,

- M. B., GIUNTI, P. & WOOD, N. W. 2007. Mutations in TTBK2, encoding a kinase implicated in tau phosphorylation, segregate with spinocerebellar ataxia type 11. *Nat Genet*, 39, 1434-6.
- HU, J., AKAMA, K. T., KRAFFT, G. A., CHROMY, B. A. & VAN ELDIK, L. J. 1998. Amyloid-beta peptide activates cultured astrocytes: morphological alterations, cytokine induction and nitric oxide release. *Brain Res*, 785, 195-206.
- HU, N. W., CORBETT, G. T., MOORE, S., KLYUBIN, I., O'MALLEY, T. T., WALSH, D. M., LIVESEY, F. J. & ROWAN, M. J. 2018. Extracellular Forms of Abeta and Tau from iPSC Models of Alzheimer's Disease Disrupt Synaptic Plasticity. *Cell Rep*, 23, 1932-1938.
- HU, Y. & WILSON, G. S. 1997. A temporary local energy pool coupled to neuronal activity: fluctuations of extracellular lactate levels in rat brain monitored with rapid-response enzyme-based sensor. *J Neurochem*, 69, 1484-90.
- HUANG, H. M., ZHANG, H., XU, H. & GIBSON, G. E. 2003. Inhibition of the alpha-ketoglutarate dehydrogenase complex alters mitochondrial function and cellular calcium regulation. *Biochim Biophys Acta*, 1637, 119-26.
- IKEUCHI, T., KANEKO, H., MIYASHITA, A., NOZAKI, H., KASUGA, K., TSUKIE, T., TSUCHIYA, M., IMAMURA, T., ISHIZU, H., AOKI, K., ISHIKAWA, A., ONODERA, O., KUWANO, R. & NISHIZAWA, M. 2008. Mutational analysis in early-onset familial dementia in the Japanese population. The role of PSEN1 and MAPT R406W mutations. *Dement Geriatr Cogn Disord*, 26, 43-9.
- ISRAEL, M. A., YUAN, S. H., BARDY, C., REYNA, S. M., MU, Y., HERRERA, C., HEFFERAN, M. P., VAN GORP, S., NAZOR, K. L., BOSCOLO, F. S., CARSON, C. T., LAURENT, L. C., MARSALA, M., GAGE, F. H., REMES, A. M., KOO, E. H. & GOLDSTEIN, L. S. B. 2012. Probing sporadic and familial Alzheimer's disease using induced pluripotent stem cells. *Nature*, 482, 216.
- IWATA-ICHIKAWA, E., KONDO, Y., MIYAZAKI, I., ASANUMA, M. & OGAWA, N. 1999. Glial cells protect neurons against oxidative stress via transcriptional up-regulation of the glutathione synthesis. *J Neurochem*, 72, 2334-44.
- JEKABSONE, A., MANDER, P. K., TICKLER, A., SHARPE, M. & BROWN, G. C. 2006. Fibrillar beta-amyloid peptide Abeta1-40 activates microglial proliferation via stimulating TNF-alpha release and H2O2 derived from NADPH oxidase: a cell culture study. *J Neuroinflammation*, 3, 24.
- JIN, S. M., CHO, H. J., KIM, Y. W., HWANG, J. Y. & MOOK-JUNG, I. 2012. Abeta-induced Ca(2+) influx regulates astrocytic BACE1 expression via calcineurin/NFAT4 signals. *Biochem Biophys Res Commun*, 425, 649-55.

- JONSSON, T., ATWAL, J. K., STEINBERG, S., SNAEDAL, J., JONSSON, P. V., BJORNSSON, S., STEFANSSON, H., SULEM, P., GUDBJARTSSON, D., MALONEY, J., HOYTE, K., GUSTAFSON, A., LIU, Y., LU, Y., BHANGALE, T., GRAHAM, R. R., HUTTENLOCHER, J., BJORNSDOTTIR, G., ANDREASSEN, O. A., JONSSON, E. G., PALOTIE, A., BEHRENS, T. W., MAGNUSSON, O. T., KONG, A., THORSTEINSDOTTIR, U., WATTS, R. J. & STEFANSSON, K. 2012. A mutation in APP protects against Alzheimer's disease and age-related cognitive decline. *Nature*, 488, 96-9.
- JORFI, M., D'AVANZO, C., TANZI, R. E., KIM, D. Y. & IRIMIA, D. 2018. Human Neurospheroid Arrays for In Vitro Studies of Alzheimer's Disease. *Sci Rep*, 8, 2450.
- KARUMBAYARAM, S., NOVITCH, B. G., PATTERSON, M., UMBACH, J. A., RICHTER, L., LINDGREN, A., CONWAY, A. E., CLARK, A. T., GOLDMAN, S. A., PLATH, K., WIEDAU-PAZOS, M., KORNBLUM, H. I. & LOWRY, W. E. 2009. Directed differentiation of human-induced pluripotent stem cells generates active motor neurons. *Stem Cells*, 27, 806-11.
- KAZMI, M. 2013. AL amyloidosis. *Medicine*, 41, 299-301.
- KIM, D. S., LEE, J. S., LEEM, J. W., HUH, Y. J., KIM, J. Y., KIM, H. S., PARK, I. H., DALEY, G. Q., HWANG, D. Y. & KIM, D. W. 2010. Robust enhancement of neural differentiation from human ES and iPS cells regardless of their innate difference in differentiation propensity. *Stem Cell Rev*, 6, 270-81.
- KIM, W. & HECHT, M. H. 2006. Generic hydrophobic residues are sufficient to promote aggregation of the Alzheimer's A β 42 peptide. *Proceedings of the National Academy of Sciences*, 103, 15824-15829.
- KIMBERLY, W. T., LAVOIE, M. J., OSTASZEWSKI, B. L., YE, W., WOLFE, M. S. & SELKOE, D. J. 2003. Gamma-secretase is a membrane protein complex comprised of presenilin, nicastrin, Aph-1, and Pen-2. *Proceedings of the National Academy of Sciences of the United States of America*, 100, 6382-6387.
- KLIVENYI, P., STARKOV, A. A., CALINGASAN, N. Y., GARDIAN, G., BROWNE, S. E., YANG, L., BUBBER, P., GIBSON, G. E., PATEL, M. S. & BEAL, M. F. 2004. Mice deficient in dihydrolipoamide dehydrogenase show increased vulnerability to MPTP, malonate and 3-nitropropionic acid neurotoxicity. *J Neurochem*, 88, 1352-60.
- KNOBLOCH, M., KONIETZKO, U., KREBS, D. C. & NITSCH, R. M. 2007. Intracellular A β and cognitive deficits precede β -amyloid deposition in transgenic arcA β mice. *Neurobiology of Aging*, 28, 1297-1306.
- KONDO, T., ASAI, M., TSUKITA, K., KUTOKU, Y., OHSAWA, Y., SUNADA, Y., IMAMURA, K., EGAWA, N., YAHATA, N., OKITA, K., TAKAHASHI, K., ASAKA, I., AOI, T., WATANABE, A., WATANABE, K., KADOYA, C., NAKANO, R., WATANABE, D.,

- MARUYAMA, K., HORI, O., HIBINO, S., CHOSHI, T., NAKAHATA, T., HIOKI, H., KANEKO, T., NAITOH, M., YOSHIKAWA, K., YAMAWAKI, S., SUZUKI, S., HATA, R., UENO, S., SEKI, T., KOBAYASHI, K., TODA, T., MURAKAMI, K., IRIE, K., KLEIN, W. L., MORI, H., ASADA, T., TAKAHASHI, R., IWATA, N., YAMANAKA, S. & INOUE, H. 2013. Modeling Alzheimer's disease with iPSCs reveals stress phenotypes associated with intracellular Abeta and differential drug responsiveness. *Cell Stem Cell*, 12, 487-96.
- KOO, E. H., SISODIA, S. S., ARCHER, D. R., MARTIN, L. J., WEIDEMANN, A., BEYREUTHER, K., FISCHER, P., MASTERS, C. L. & PRICE, D. L. 1990. Precursor of amyloid protein in Alzheimer disease undergoes fast anterograde axonal transport. *Proc Natl Acad Sci U S A*, 87, 1561-5.
- KORNILOVA, A. Y., BIHEL, F., DAS, C. & WOLFE, M. S. 2005. The initial substrate-binding site of gamma-secretase is located on presenilin near the active site. *Proc Natl Acad Sci U S A*, 102, 3230-5.
- KRENCIK, R., WEICK, J. P., LIU, Y., ZHANG, Z.-J. & ZHANG, S.-C. 2011. Specification of transplantable astroglial subtypes from human pluripotent stem cells. *Nature biotechnology*, 29, 528-534.
- LADRAN, I., TRAN, N., TOPOL, A. & BRENNAND, K. J. 2013. Neural stem and progenitor cells in health and disease. *Wiley Interdisciplinary Reviews: Systems Biology and Medicine*, 5, 701-715.
- LAFERLA, F. M., GREEN, K. N. & ODDO, S. 2007. Intracellular amyloid- β in Alzheimer's disease. *Nature Reviews Neuroscience*, 8, 499.
- LAMBERT, J. C., IBRAHIM-VERBAAS, C. A., HAROLD, D., NAJ, A. C., SIMS, R., BELLENGUEZ, C., DESTAFANO, A. L., BIS, J. C., BEECHAM, G. W., GRENIER-BOLEY, B., RUSSO, G., THORTON-WELLS, T. A., JONES, N., SMITH, A. V., CHOURAKI, V., THOMAS, C., IKRAM, M. A., ZELENKA, D., VARDARAJAN, B. N., KAMATANI, Y., LIN, C. F., GERRISH, A., SCHMIDT, H., KUNKLE, B., DUNSTAN, M. L., RUIZ, A., BIHOREAU, M. T., CHOI, S. H., REITZ, C., PASQUIER, F., CRUCHAGA, C., CRAIG, D., AMIN, N., BERR, C., LOPEZ, O. L., DE JAGER, P. L., DERAMECOURT, V., JOHNSTON, J. A., EVANS, D., LOVESTONE, S., LETENNEUR, L., MORÓN, F. J., RUBINSZTEIN, D. C., EIRIKSDOTTIR, G., SLEEGERS, K., GOATE, A. M., FIÉVET, N., HUENTELMAN, M. W., GILL, M., BROWN, K., KAMBOH, M. I., KELLER, L., BARBERGER-GATEAU, P., MCGUINNESS, B., LARSON, E. B., GREEN, R., MYERS, A. J., DUFOUIL, C., TODD, S., WALLON, D., LOVE, S., ROGAEVA, E., GALLACHER, J., ST GEORGE-HYSLOP, P., CLARIMON, J., LLEO, A., BAYER, A., TSUANG, D. W., YU, L., TSOLAKI, M., BOSSÙ, P., SPALLETTA, G., PROITSI, P., COLLINGE, J., SORBI, S., SANCHEZ-GARCIA, F.,

- FOX, N. C., HARDY, J., DENIZ NARANJO, M. C., BOSCO, P., CLARKE, R., BRAYNE, C., GALIMBERTI, D., MANCUSO, M., MATTHEWS, F., EUROPEAN ALZHEIMER'S DISEASE, I., GENETIC, ENVIRONMENTAL RISK IN ALZHEIMER'S, D., ALZHEIMER'S DISEASE GENETIC, C., COHORTS FOR, H., AGING RESEARCH IN GENOMIC, E., MOEBUS, S., MECOCCI, P., DEL ZOMPO, M., MAIER, W., HAMPEL, H., PILOTTO, A., BULLIDO, M., PANZA, F., CAFFARRA, P., et al. 2013. Meta-analysis of 74,046 individuals identifies 11 new susceptibility loci for Alzheimer's disease. *Nature genetics*, 45, 1452-1458.
- LANOISELÉE, H.-M., NICOLAS, G., WALLON, D., ROVELET-LECRUX, A., LACOUR, M., ROUSSEAU, S., RICHARD, A.-C., PASQUIER, F., ROLLIN-SILLAIRE, A., MARTINAUD, O., QUILLARD-MURAINÉ, M., DE LA SAYETTE, V., BOUTOLEAU-BRETONNIERE, C., ETCHARRY-BOUYX, F., CHAUVIRÉ, V., SARAZIN, M., LE BER, I., EPELBAUM, S., JONVEAUX, T., ROUAUD, O., CECCALDI, M., FÉLICIAN, O., GODEFROY, O., FORMAGLIO, M., CROISILE, B., AURIACOMBE, S., CHAMARD, L., VINCENT, J.-L., SAUVÉE, M., MARELLI-TOSI, C., GABELLE, A., OZSANCAK, C., PARIENTE, J., PAQUET, C., HANNEQUIN, D., CAMPION, D. & COLLABORATORS OF THE, C. N. R. M. A. J. P. 2017. APP, PSEN1, and PSEN2 mutations in early-onset Alzheimer disease: A genetic screening study of familial and sporadic cases. *PLoS medicine*, 14, e1002270-e1002270.
- LE, Y., GONG, W., TIFFANY, H. L., TUMANOV, A., NEDOSPASOV, S., SHEN, W., DUNLOP, N. M., GAO, J. L., MURPHY, P. M., OPPENHEIM, J. J. & WANG, J. M. 2001. Amyloid (beta)42 activates a G-protein-coupled chemoattractant receptor, FPR-like-1. *J Neurosci*, 21, Rc123.
- LESNE, S., KOH, M. T., KOTILINEK, L., KAYED, R., GLABE, C. G., YANG, A., GALLAGHER, M. & ASHE, K. H. 2006. A specific amyloid-beta protein assembly in the brain impairs memory. *Nature*, 440, 352-7.
- LEUCHTENBERGER, S., BEHER, D. & WEGGEN, S. 2006. Selective modulation of Abeta42 production in Alzheimer's disease: non-steroidal anti-inflammatory drugs and beyond. *Curr Pharm Des*, 12, 4337-55.
- LEVERENZ, J. B. & RASKIND, M. A. 1998. Early Amyloid Deposition in the Medial Temporal Lobe of Young Down Syndrome Patients: A Regional Quantitative Analysis. *Experimental Neurology*, 150, 296-304.
- LI, X.-J., ZHANG, X., JOHNSON, M. A., WANG, Z.-B., LAVAUTE, T. & ZHANG, S.-C. 2009. Coordination of sonic hedgehog and Wnt signaling determines ventral and dorsal telencephalic neuron types from human embryonic stem cells. *Development (Cambridge, England)*, 136, 4055-4063.

- LIN, Y. T., SEO, J., GAO, F., FELDMAN, H. M., WEN, H. L., PENNEY, J., CAM, H. P., GJONESKA, E., RAJA, W. K., CHENG, J., RUEDA, R., KRITSKIY, O., ABDURROB, F., PENG, Z., MILO, B., YU, C. J., ELMSAOURI, S., DEY, D., KO, T., YANKNER, B. A. & TSAI, L. H. 2018. APOE4 Causes Widespread Molecular and Cellular Alterations Associated with Alzheimer's Disease Phenotypes in Human iPSC-Derived Brain Cell Types. *Neuron*, 98, 1141-1154.e7.
- LODISH H, B. A., ZIPURSKY SL, 2000. Molecular Cell Biology. 4th edition *New York: W. H. Freeman*, Section 21.1.
- LOTT, I. T. & HEAD, E. 2005. Alzheimer disease and Down syndrome: factors in pathogenesis. *Neurobiol Aging*, 26, 383-9.
- LUO, F., RUSTAY, N. R., EBERT, U., HRADIL, V. P., COLE, T. B., LLANO, D. A., MUDD, S. R., ZHANG, Y., FOX, G. B. & DAY, M. 2012. Characterization of 7- and 19-month-old Tg2576 mice using multimodal in vivo imaging: limitations as a translatable model of Alzheimer's disease. *Neurobiol Aging*, 33, 933-44.
- LUSTBADER, J. W., CIRILLI, M., LIN, C., XU, H. W., TAKUMA, K., WANG, N., CASPERSEN, C., CHEN, X., POLLAK, S., CHANEY, M., TRINCHESE, F., LIU, S., GUNN-MOORE, F., LUE, L. F., WALKER, D. G., KUPPUSAMY, P., ZEWIER, Z. L., ARANCIO, O., STERN, D., YAN, S. S. & WU, H. 2004. ABAD directly links Abeta to mitochondrial toxicity in Alzheimer's disease. *Science*, 304, 448-52.
- MA, Q. L., YANG, F., ROSARIO, E. R., UBEDA, O. J., BEECH, W., GANT, D. J., CHEN, P. P., HUDSPETH, B., CHEN, C., ZHAO, Y., VINTERS, H. V., FRAUTSCHY, S. A. & COLE, G. M. 2009. Beta-amyloid oligomers induce phosphorylation of tau and inactivation of insulin receptor substrate via c-Jun N-terminal kinase signaling: suppression by omega-3 fatty acids and curcumin. *J Neurosci*, 29, 9078-89.
- MACDONALD, I. R., DEBAY, D. R., REID, G. A., O'LEARY, T. P., JOLLYMORE, C. T., MAWKO, G., BURRELL, S., MARTIN, E., BOWEN, C. V., BROWN, R. E. & DARVESH, S. 2014. Early detection of cerebral glucose uptake changes in the 5XFAD mouse. *Curr Alzheimer Res*, 11, 450-60.
- MAEDER, M. L., LINDER, S. J., CASCIO, V. M., FU, Y., HO, Q. H. & JOUNG, J. K. 2013. CRISPR RNA-guided activation of endogenous human genes. *Nat Methods*, 10, 977-9.
- MAGISTRETTI, P. J. 2000. Cellular bases of functional brain imaging: insights from neuron-glia metabolic coupling. *Brain Res*, 886, 108-112.
- MAGISTRETTI, P. J. & PELLERIN, L. 1996. Cellular mechanisms of brain energy metabolism. Relevance to functional brain imaging and to neurodegenerative disorders. *Ann N Y Acad Sci*, 777, 380-7.

- MAGISTRETTI, P. J. & PELLERIN, L. 2000. [Functional brain imaging: role metabolic coupling between astrocytes and neurons]. *Rev Med Suisse Romande*, 120, 739-42.
- MANCZAK, M., ANEKONDA, T. S., HENSON, E., PARK, B. S., QUINN, J. & REDDY, P. H. 2006. Mitochondria are a direct site of A beta accumulation in Alzheimer's disease neurons: implications for free radical generation and oxidative damage in disease progression. *Hum Mol Genet*, 15, 1437-49.
- MANN, D. M. A. & ESIRI, M. M. 1989. The pattern of acquisition of plaques and tangles in the brains of patients under 50 years of age with Down's syndrome. *Journal of the Neurological Sciences*, 89, 169-179.
- MARK, R. J., PANG, Z., GEDDES, J. W., UCHIDA, K. & MATTSON, M. P. 1997. Amyloid beta-peptide impairs glucose transport in hippocampal and cortical neurons: involvement of membrane lipid peroxidation. *J Neurosci*, 17, 1046-54.
- MARTIN, E. D., FERNANDEZ, M., PEREA, G., PASCUAL, O., HAYDON, P. G., ARAQUE, A. & CENA, V. 2007. Adenosine released by astrocytes contributes to hypoxia-induced modulation of synaptic transmission. *Glia*, 55, 36-45.
- MATTSON, M. P. 1997. Cellular actions of beta-amyloid precursor protein and its soluble and fibrillogenic derivatives. *Physiological Reviews*, 77, 1081-1132.
- MATTSON, M. P. 2004. Pathways towards and away from Alzheimer's disease. *Nature*, 430, 631-9.
- MATTSON, M. P., BARGER, S. W., BEGLEY, J. G. & MARK, R. J. 1995. Calcium, free radicals, and excitotoxic neuronal death in primary cell culture. *Methods Cell Biol*, 46, 187-216.
- MAWUENYEGA, K. G., KASTEN, T., SIGURDSON, W. & BATEMAN, R. J. 2013. Amyloid-beta isoform metabolism quantitation by stable isotope-labeled kinetics. *Anal Biochem*, 440, 56-62.
- MCGEER, P. L., SCHULZER, M. & MCGEER, E. G. 1996. Arthritis and anti-inflammatory agents as possible protective factors for Alzheimer's disease: a review of 17 epidemiologic studies. *Neurology*, 47, 425-32.
- MCKENNA, M. C., SONNEWALD, U., HUANG, X., STEVENSON, J. & ZIELKE, H. R. 1996. Exogenous Glutamate Concentration Regulates the Metabolic Fate of Glutamate in Astrocytes. *Journal of Neurochemistry*, 66, 386-393.
- MING, G. L. & SONG, H. 2011. Adult neurogenesis in the mammalian brain: significant answers and significant questions. *Neuron*, 70, 687-702.
- MOORE, B. D., RANGACHARI, V., TAY, W. M., MILKOVIC, N. M. & ROSENBERY, T. L. 2009. Biophysical Analyses of Synthetic Amyloid- β (1-42) Aggregates before and after Covalent Cross-Linking. Implications for Deducing the Structure of Endogenous Amyloid- β Oligomers. *Biochemistry*, 48, 11796-11806.

- MOREIRA, P. I., SANTOS, M. S., MORENO, A. & OLIVEIRA, C. 2001. Amyloid beta-peptide promotes permeability transition pore in brain mitochondria. *Biosci Rep*, 21, 789-800.
- MORGAN, D. 2006. Modulation of microglial activation state following passive immunization in amyloid depositing transgenic mice. *Neurochem Int*, 49, 190-4.
- MOSCONI, L., PUPI, A. & DE LEON, M. J. 2008. Brain glucose hypometabolism and oxidative stress in preclinical Alzheimer's disease. *Ann N Y Acad Sci*, 1147, 180-95.
- MOSCONI, L., TSUI, W. H., HERHOLZ, K., PUPI, A., DRZEZGA, A., LUCIGNANI, G., REIMAN, E. M., HOLTHOFF, V., KALBE, E., SORBI, S., DIEHL-SCHMID, J., PERNECZKY, R., CLERICI, F., CASELLI, R., BEUTHIEN-BAUMANN, B., KURZ, A., MINOSHIMA, S. & DE LEON, M. J. 2008. Multicenter standardized 18F-FDG PET diagnosis of mild cognitive impairment, Alzheimer's disease, and other dementias. *J Nucl Med*, 49, 390-8.
- MOSMANN, T. 1983. Rapid colorimetric assay for cellular growth and survival: application to proliferation and cytotoxicity assays. *J Immunol Methods*, 65, 55-63.
- MUDHER, A. & LOVESTONE, S. 2002. Alzheimer's disease-do tauists and baptists finally shake hands? *Trends Neurosci*, 25, 22-6.
- MUIRHEAD, K. E., BORGER, E., AITKEN, L., CONWAY, S. J. & GUNN-MOORE, F. J. 2010. The consequences of mitochondrial amyloid beta-peptide in Alzheimer's disease. *Biochem J*, 426, 255-70.
- MULLER-SCHIFFMANN, A., HERRING, A., ABDEL-HAFIZ, L., CHEPKOVA, A. N., SCHABLE, S., WEDEL, D., HORN, A. H., STICHT, H., DE SOUZA SILVA, M. A., GOTTMANN, K., SERGEEVA, O. A., HUSTON, J. P., KEYVANI, K. & KORTH, C. 2016. Amyloid-beta dimers in the absence of plaque pathology impair learning and synaptic plasticity. *Brain*, 139, 509-25.
- MURATORE, C. R., RICE, H. C., SRIKANTH, P., CALLAHAN, D. G., SHIN, T., BENJAMIN, L. N., WALSH, D. M., SELKOE, D. J. & YOUNG-PEARSE, T. L. 2014. The familial Alzheimer's disease APPV717I mutation alters APP processing and Tau expression in iPSC-derived neurons. *Hum Mol Genet*, 23, 3523-36.
- MYER, D. J., GURKOFF, G. G., LEE, S. M., HOVDA, D. A. & SOFRONIEW, M. V. 2006. Essential protective roles of reactive astrocytes in traumatic brain injury. *Brain*, 129, 2761-72.
- NEWMAN, L. A., KOROL, D. L. & GOLD, P. E. 2011. Lactate produced by glycogenolysis in astrocytes regulates memory processing. *PLoS One*, 6, e28427.
- NICHOLAS, C. R., CHEN, J., TANG, Y., SOUTHWELL, D. G., CHALMERS, N., VOGT, D., ARNOLD, C. M., CHEN, Y. J., STANLEY, E. G., ELEFANTY, A. G., SASAI, Y., ALVAREZ-BUYLLA, A., RUBENSTEIN, J. L. & KRIEGSTEIN, A. R. 2013. Functional

- maturation of hPSC-derived forebrain interneurons requires an extended timeline and mimics human neural development. *Cell Stem Cell*, 12, 573-86.
- NICHOLSON, R. M., KUSNE, Y., NOWAK, L. A., LAFERLA, F. M., REIMAN, E. M. & VALLA, J. 2010. Regional cerebral glucose uptake in the 3xTG model of Alzheimer's disease highlights common regional vulnerability across AD mouse models. *Brain Res*, 1347, 179-85.
- NICOLAKAKIS, N., ABOULKASSIM, T., ONGALI, B., LECRUX, C., FERNANDES, P., ROSA-NETO, P., TONG, X. K. & HAMEL, E. 2008. Complete rescue of cerebrovascular function in aged Alzheimer's disease transgenic mice by antioxidants and pioglitazone, a peroxisome proliferator-activated receptor gamma agonist. *J Neurosci*, 28, 9287-96.
- NOWAKOWSKI, R. S. 2006. Stable neuron numbers from cradle to grave. *Proc Natl Acad Sci U S A*, 103, 12219-20.
- O'BRIEN, R. J. & WONG, P. C. 2011. Amyloid precursor protein processing and Alzheimer's disease. *Annu Rev Neurosci*, 34, 185-204.
- ODDO, S., CACCAMO, A., KITAZAWA, M., TSENG, B. P. & LAFERLA, F. M. 2003. Amyloid deposition precedes tangle formation in a triple transgenic model of Alzheimer's disease. *Neurobiology of Aging*, 24, 1063-1070.
- OHSAWA, I., TAKAMURA, C., MORIMOTO, T., ISHIGURO, M. & KOHSAKA, S. 1999. Amino-terminal region of secreted form of amyloid precursor protein stimulates proliferation of neural stem cells. *Eur J Neurosci*, 11, 1907-13.
- OKADA, S., NAKAMURA, M., KATOH, H., MIYAO, T., SHIMAZAKI, T., ISHII, K., YAMANE, J., YOSHIMURA, A., IWAMOTO, Y., TOYAMA, Y. & OKANO, H. 2006. Conditional ablation of STAT3 or SOCS3 discloses a dual role for reactive astrocytes after spinal cord injury. *Nature medicine*, 12, 829-34.
- OKOCHI, M., FUKUMORI, A., JIANG, J., ITOH, N., KIMURA, R., STEINER, H., HAASS, C., TAGAMI, S. & TAKEDA, M. 2006. Secretion of the Notch-1 Abeta-like peptide during Notch signaling. *J Biol Chem*, 281, 7890-8.
- ORGANISATION, W. H. 2015. International Statistical Classification of Diseases and Related Health Problems 10th Revision (ICD-10) Mental and behavioural disorders.
- ORGOGOZO, J.-M., GILMAN, S., DARTIGUES, J.-F., LAURENT, B., PUEL, M., KIRBY, L. C., JOUANNY, P., DUBOIS, B., EISNER, L., FLITMAN, S., MICHEL, B. F., BOADA, M., FRANK, A. & HOCK, C. 2003. Subacute meningoencephalitis in a subset of patients with AD after A β 42 immunization. *Neurology*, 61, 46-54.
- OTT, A., STOLK, R. P., VAN HARKAMP, F., POLS, H. A., HOFMAN, A. & BRETELER, M. M. 1999. Diabetes mellitus and the risk of dementia: The Rotterdam Study. *Neurology*, 53, 1937-42.

- OZES, O. N., AKCA, H., MAYO, L. D., GUSTIN, J. A., MAEHAMA, T., DIXON, J. E. & DONNER, D. B. 2001. A phosphatidylinositol 3-kinase/Akt/mTOR pathway mediates and PTEN antagonizes tumor necrosis factor inhibition of insulin signaling through insulin receptor substrate-1. *Proceedings of the National Academy of Sciences of the United States of America*, 98, 4640-4645.
- PANZA, F., LOZUPONE, M., LOGROSCINO, G. & IMBIMBO, B. P. 2019. A critical appraisal of amyloid-beta-targeting therapies for Alzheimer disease. *Nat Rev Neurol*, 15, 73-88.
- PAQUET, D., KWART, D., CHEN, A., SPROUL, A., JACOB, S., TEO, S., OLSEN, K. M., GREGG, A., NOGGLE, S. & TESSIER-LAVIGNE, M. 2016. Efficient introduction of specific homozygous and heterozygous mutations using CRISPR/Cas9. *Nature*, 533, 125-9.
- PEKNY, M. & PEKNA, M. 2014. Astrocyte Reactivity and Reactive Astrogliosis: Costs and Benefits. *Physiological reviews*, 94, 1077-1098.
- PELLERIN, L. & MAGISTRETTI, P. J. 1994. Glutamate uptake into astrocytes stimulates aerobic glycolysis: a mechanism coupling neuronal activity to glucose utilization. *Proc Natl Acad Sci U S A*, 91, 10625-9.
- PERRY, E. K., PERRY, R. H., TOMLINSON, B. E., BLESSED, G. & GIBSON, P. H. 1980. Coenzyme A-acetylating enzymes in Alzheimer's disease: possible cholinergic 'compartment' of pyruvate dehydrogenase. *Neurosci Lett*, 18, 105-10.
- PETERS, A., VERONESI, B., CALDERON-GARCIDUENAS, L., GEHR, P., CHEN, L. C., GEISER, M., REED, W., ROTHEN-RUTISHAUSER, B., SCHURCH, S. & SCHULZ, H. 2006. Translocation and potential neurological effects of fine and ultrafine particles a critical update. *Part Fibre Toxicol*, 3, 13.
- PIRTTIMAKI, T. M., CODADU, N. K., AWNI, A., PRATIK, P., NAGEL, D. A., HILL, E. J., DINELEY, K. T. & PARRI, H. R. 2013. alpha7 Nicotinic receptor-mediated astrocytic gliotransmitter release: Abeta effects in a preclinical Alzheimer's mouse model. *PLoS One*, 8, e81828.
- PLANT, L. D., BOYLE, J. P., SMITH, I. F., PEERS, C. & PEARSON, H. A. 2003. The production of amyloid beta peptide is a critical requirement for the viability of central neurons. *J Neurosci*, 23, 5531-5.
- POISNEL, G., HERARD, A. S., EL TANNIR EL TAYARA, N., BOURRIN, E., VOLK, A., KOBER, F., DELATOUR, B., DELZESCAUX, T., DEBEIR, T., ROONEY, T., BENAVIDES, J., HANTRAYE, P. & DHENAIN, M. 2012. Increased regional cerebral glucose uptake in an APP/PS1 model of Alzheimer's disease. *Neurobiol Aging*, 33, 1995-2005.
- PRAPONG, T., BUSS, J., HSU, W. H., HEINE, P., WEST GREENLEE, H. & UEMURA, E. 2002. Amyloid beta-peptide decreases neuronal glucose uptake despite causing

- increase in GLUT3 mRNA transcription and GLUT3 translocation to the plasma membrane. *Exp Neurol*, 174, 253-8.
- PRAPONG, T., UEMURA, E. & HSU, W. H. 2001. G protein and cAMP-dependent protein kinase mediate amyloid beta-peptide inhibition of neuronal glucose uptake. *Exp Neurol*, 167, 59-64.
- PRASHER, V. P. & FILER, A. 1995. Behavioural disturbance in people with Down's syndrome and dementia. *J Intellect Disabil Res*, 39 (Pt 5), 432-6.
- PRINCE, M., KNAPP, M, GUERCHET, M, MCCRONE, P, PRINA, M., COMAS-HERRERA, A., WITTENBERG, R, ADELAJA, B, HU, B, KING, D, & REHILL, A. A. S., D 2014. Dementia UK: Second edition. © *Alzheimer's Society 2014*.
- PUIG, K. L. & COMBS, C. K. 2013. Expression and function of APP and its metabolites outside the central nervous system. *Exp Gerontol*, 48, 608-11.
- QIAN, X., NGUYEN, H. N., SONG, M. M., HADIONO, C., OGDEN, S. C., HAMMACK, C., YAO, B., HAMERSKY, G. R., JACOB, F., ZHONG, C., YOON, K. J., JEANG, W., LIN, L., LI, Y., THAKOR, J., BERG, D. A., ZHANG, C., KANG, E., CHICKERING, M., NAUEN, D., HO, C. Y., WEN, Z., CHRISTIAN, K. M., SHI, P. Y., MAHER, B. J., WU, H., JIN, P., TANG, H., SONG, H. & MING, G. L. 2016. Brain-Region-Specific Organoids Using Mini-bioreactors for Modeling ZIKV Exposure. *Cell*, 165, 1238-1254.
- RAJA, W. K., MUNGENAST, A. E., LIN, Y. T., KO, T., ABDURROB, F., SEO, J. & TSAI, L. H. 2016. Self-Organizing 3D Human Neural Tissue Derived from Induced Pluripotent Stem Cells Recapitulate Alzheimer's Disease Phenotypes. *PLoS One*, 11, e0161969.
- RANSOM, B. R. & FERN, R. 1997. Does astrocytic glycogen benefit axon function and survival in CNS white matter during glucose deprivation? *Glia*, 21, 134-141.
- RATZMANN, K. P. & HAMPEL, R. 1980. Glucose and insulin concentration patterns in cerebrospinal fluid following intravenous glucose injection in humans. *Endokrinologie*, 76, 185-8.
- REDDY, P. H. & BEAL, M. F. 2008. Amyloid beta, mitochondrial dysfunction and synaptic damage: implications for cognitive decline in aging and Alzheimer's disease. *Trends Mol Med*, 14, 45-53.
- RELKIN, N. R., SZABO, P., ADAMIAK, B., BURGUT, T., MONTHE, C., LENT, R. W., YOUNKIN, S., YOUNKIN, L., SCHIFF, R. & WEKSLER, M. E. 2009. 18-Month study of intravenous immunoglobulin for treatment of mild Alzheimer disease. *Neurobiol Aging*, 30, 1728-36.
- REMPE, D. A., LELLI, K. M., VANGEISON, G., JOHNSON, R. S. & FEDEROFF, H. J. 2007. In cultured astrocytes, p53 and MDM2 do not alter hypoxia-inducible factor-1alpha function regardless of the presence of DNA damage. *J Biol Chem*, 282, 16187-201.

- REPORT, W. A. 2015. The global impact of dementia, an analysis of prevalence, incidence, cost and trends. 2015. *Alzheimer's Disease International*.
- RHEIN, V., SONG, X., WIESNER, A., ITTNER, L. M., BAYSANG, G., MEIER, F., OZMEN, L., BLUETHMANN, H., DROSE, S., BRANDT, U., SAVASKAN, E., CZECH, C., GOTZ, J. & ECKERT, A. 2009. Amyloid-beta and tau synergistically impair the oxidative phosphorylation system in triple transgenic Alzheimer's disease mice. *Proc Natl Acad Sci U S A*, 106, 20057-62.
- ROBERSON, E. D., HALABISKY, B., YOO, J. W., YAO, J., CHIN, J., YAN, F., WU, T., HAMTO, P., DEVIDZE, N., YU, G.-Q., PALOP, J. J., NOEBELS, J. L. & MUCKE, L. 2011. Amyloid- β /Fyn-induced synaptic, network, and cognitive impairments depend on tau levels in multiple mouse models of Alzheimer's disease. *The Journal of neuroscience : the official journal of the Society for Neuroscience*, 31, 700-711.
- ROSENBERG, P. A. & DICHTER, M. A. 1985. Glycogen accumulation in rat cerebral cortex in dissociated cell culture. *J Neurosci Methods*, 15, 101-12.
- ROSS, R. A., SPENGLER, B. A. & BIEDLER, J. L. 1983. Coordinate morphological and biochemical interconversion of human neuroblastoma cells. *J Natl Cancer Inst*, 71, 741-7.
- ROSSNER, S., LANGE-DOHNA, C., ZEITSCHER, U. & PEREZ-POLO, J. R. 2005. Alzheimer's disease beta-secretase BACE1 is not a neuron-specific enzyme. *J Neurochem*, 92, 226-34.
- SANTA-MARIA, I., HERNANDEZ, F., DEL RIO, J., MORENO, F. J. & AVILA, J. 2007. Tramiprosate, a drug of potential interest for the treatment of Alzheimer's disease, promotes an abnormal aggregation of tau. *Mol Neurodegener*, 2, 17.
- SANTA-MARIA, I., HERNANDEZ, F., MORENO, F. J. & AVILA, J. 2007. Taurine, an inducer for tau polymerization and a weak inhibitor for amyloid-beta-peptide aggregation. *Neurosci Lett*, 429, 91-4.
- SATO, T., DOHMAE, N., QI, Y., KAKUDA, N., MISONOU, H., MITSUMORI, R., MARUYAMA, H., KOO, E. H., HAASS, C., TAKIO, K., MORISHIMA-KAWASHIMA, M., ISHIURA, S. & IHARA, Y. 2003. Potential link between amyloid beta-protein 42 and C-terminal fragment gamma 49-99 of beta-amyloid precursor protein. *J Biol Chem*, 278, 24294-301.
- SELKOE, D. J. & HARDY, J. 2016. The amyloid hypothesis of Alzheimer's disease at 25 years. *EMBO Mol Med*, 8, 595-608.
- SERRANO-POZO, A., MUZIKANSKY, A., GOMEZ-ISLA, T., GROWDON, J. H., BETENSKY, R. A., FROSCH, M. P. & HYMAN, B. T. 2013. Differential relationships of reactive astrocytes and microglia to fibrillar amyloid deposits in Alzheimer disease. *J Neuropathol Exp Neurol*, 72, 462-71.

- SESHADRI, S., FITZPATRICK, A. L., IKRAM, M. A., DESTEFANO, A. L., GUDNASON, V., BOADA, M., BIS, J. C., SMITH, A. V., CARASSQUILLO, M. M., LAMBERT, J. C., HAROLD, D., SCHRIJVERS, E. M. C., RAMIREZ-LORCA, R., DEBETTE, S., LONGSTRETH, W. T., JR., JANSSENS, A. C. J. W., PANKRATZ, V. S., DARTIGUES, J. F., HOLLINGWORTH, P., ASPELUND, T., HERNANDEZ, I., BEISER, A., KULLER, L. H., KOUDSTAAL, P. J., DICKSON, D. W., TZOURIO, C., ABRAHAM, R., ANTUNEZ, C., DU, Y., ROTTER, J. I., AULCHENKO, Y. S., HARRIS, T. B., PETERSEN, R. C., BERR, C., OWEN, M. J., LOPEZ-ARRIETA, J., VARADARAJAN, B. N., BECKER, J. T., RIVADENEIRA, F., NALLS, M. A., GRAFF-RADFORD, N. R., CAMPION, D., AUERBACH, S., RICE, K., HOFMAN, A., JONSSON, P. V., SCHMIDT, H., LATHROP, M., MOSLEY, T. H., AU, R., PSATY, B. M., UITTERLINDEN, A. G., FARRER, L. A., LUMLEY, T., RUIZ, A., WILLIAMS, J., AMOUYEL, P., YOUNKIN, S. G., WOLF, P. A., LAUNER, L. J., LOPEZ, O. L., VAN DUIJN, C. M., BRETELER, M. M. B., CONSORTIUM, C., CONSORTIUM, G. & CONSORTIUM, E. 2010. Genome-wide analysis of genetic loci associated with Alzheimer disease. *JAMA*, 303, 1832-1840.
- SHALTOUKI, A., PENG, J., LIU, Q., RAO, M. S. & ZENG, X. 2013. Efficient generation of astrocytes from human pluripotent stem cells in defined conditions. *Stem Cells*, 31, 941-52.
- SHERRINGTON, R., ROGAEV, E. I., LIANG, Y., ROGAEVA, E. A., LEVESQUE, G., IKEDA, M., CHI, H., LIN, C., LI, G., HOLMAN, K., TSUDA, T., MAR, L., FONCIN, J. F., BRUNI, A. C., MONTESI, M. P., SORBI, S., RAINERO, I., PINESSI, L., NEE, L., CHUMAKOV, I., POLLEN, D., BROOKES, A., SANSEAU, P., POLINSKY, R. J., WASCO, W., DA SILVA, H. A., HAINES, J. L., PERKICAK-VANCE, M. A., TANZI, R. E., ROSES, A. D., FRASER, P. E., ROMMENS, J. M. & ST GEORGE-HYSLOP, P. H. 1995. Cloning of a gene bearing missense mutations in early-onset familial Alzheimer's disease. *Nature*, 375, 754-60.
- SHI, Y., KIRWAN, P. & LIVESEY, F. J. 2012. Directed differentiation of human pluripotent stem cells to cerebral cortex neurons and neural networks. *Nat Protoc*, 7, 1836-46.
- SHI, Y., KIRWAN, P., SMITH, J., MACLEAN, G., ORKIN, S. H. & LIVESEY, F. J. 2012. A human stem cell model of early Alzheimer's disease pathology in Down syndrome. *Sci Transl Med*, 4, 124ra29.
- SHI, Y., KIRWAN, P., SMITH, J., ROBINSON, H. P. & LIVESEY, F. J. 2012. Human cerebral cortex development from pluripotent stem cells to functional excitatory synapses. *Nat Neurosci*, 15, 477-86, S1.
- SHI, Z. & JIAO, J. 2012. Direct lineage conversion: induced neuronal cells and induced neural stem cells. *Protein Cell*, 3, 826-33.

- SHIMOJO, H., OHTSUKA, T. & KAGEYAMA, R. 2008. Oscillations in notch signaling regulate maintenance of neural progenitors. *Neuron*, 58, 52-64.
- SHIN, W. S., DI, J., CAO, Q., LI, B., SEIDLER, P. M., MURRAY, K. A., BITAN, G. & JIANG, L. 2019. Amyloid β -protein oligomers promote the uptake of tau fibril seeds potentiating intracellular tau aggregation. *Alzheimer's Research & Therapy*, 11, 86.
- SHOJI, M., GOLDE, T., GHISO, J., CHEUNG, T., ESTUS, S., SHAFFER, L., CAI, X., MCKAY, D., TINTNER, R., FRANGIONE, B. & ET, A. 1992. Production of the Alzheimer amyloid beta protein by normal proteolytic processing. *Science*, 258, 126-129.
- SILVERMAN, D. H. & PHELPS, M. E. 2001. Application of positron emission tomography for evaluation of metabolism and blood flow in human brain: normal development, aging, dementia, and stroke. *Mol Genet Metab*, 74, 128-38.
- SIMIAN, M. & BISSELL, M. J. 2017. Organoids: A historical perspective of thinking in three dimensions. *J Cell Biol*, 216, 31-40.
- SIRK, D., ZHU, Z., WADIA, J. S., SHULYAKOVA, N., PHAN, N., FONG, J. & MILLS, L. R. 2007. Chronic exposure to sub-lethal beta-amyloid (Abeta) inhibits the import of nuclear-encoded proteins to mitochondria in differentiated PC12 cells. *J Neurochem*, 103, 1989-2003.
- SLEMMON, J. R., SHAPIRO, A., MERCKEN, M., STREFFER, J., ROMANO, G., ANDREASEN, N., ZETTERBERG, H. & BLENNOW, K. 2015. Impact of cerebrospinal fluid matrix on the detection of Alzheimer's disease with Abeta42 and influence of disease on the total-Abeta42/Abeta40 ratio. *J Neurochem*, 135, 1049-58.
- SMALL, B. J., FRATIGLIONI, L., VIITANEN, M., WINBLAD, B. & BACKMAN, L. 2000. The course of cognitive impairment in preclinical Alzheimer disease: three- and 6-year follow-up of a population-based sample. *Arch Neurol*, 57, 839-44.
- SOFRONIEW, M. V. & VINTERS, H. V. 2010. Astrocytes: biology and pathology. *Acta neuropathologica*, 119, 7-35.
- SOLDNER, F., LAGANIERE, J., CHENG, A. W., HOCKEMEYER, D., GAO, Q., ALAGAPPAN, R., KHURANA, V., GOLBE, L. I., MYERS, R. H., LINDQUIST, S., ZHANG, L., GUSCHIN, D., FONG, L. K., VU, B. J., MENG, X., URNOV, F. D., REBAR, E. J., GREGORY, P. D., ZHANG, H. S. & JAENISCH, R. 2011. Generation of isogenic pluripotent stem cells differing exclusively at two early onset Parkinson point mutations. *Cell*, 146, 318-31.
- SOLODKIN, A., VAN HOESEN, G. W. & INSAUSTI, R. 2014. Entorhinal Cortex. *Reference Module in Biomedical Sciences*. Elsevier.
- SOLTANI, M. H., PICHARDO, R., SONG, Z., SANGHA, N., CAMACHO, F., SATYAMOORTHY, K., SANGUEZA, O. P. & SETALURI, V. 2005. Microtubule-associated protein 2, a marker of neuronal differentiation, induces mitotic defects,

- inhibits growth of melanoma cells, and predicts metastatic potential of cutaneous melanoma. *The American journal of pathology*, 166, 1841-1850.
- SORIA, F. N., PEREZ-SAMARTIN, A., MARTIN, A., GONA, K. B., LLOP, J., SZCZUPAK, B., CHARA, J. C., MATUTE, C. & DOMERCQ, M. 2014. Extrasynaptic glutamate release through cystine/glutamate antiporter contributes to ischemic damage. *J Clin Invest*, 124, 3645-55.
- SPROUL, A., JACOB, S., PAQUET, D., ORTIZ-VIRUMBRALES, M., CAMPOS, B., GANDY, S., TESSIER-LAVIGNE, M. & NOGGLE, S. 2014. USING FAMILIAL ALZHEIMER'S DISEASE AND ISOGENIC CONTROL IPSC-DERIVED BASAL FOREBRAIN NEURONS TO MODEL AD. *Alzheimer's & Dementia*, 10, P643-P644.
- STANCU, I. C., VASCONCELOS, B., TERWEL, D. & DEWACHTER, I. 2014. Models of beta-amyloid induced Tau-pathology: the long and "folded" road to understand the mechanism. *Mol Neurodegener*, 9, 51.
- STEEN, E., TERRY, B. M., RIVERA, E. J., CANNON, J. L., NEELY, T. R., TAVARES, R., XU, X. J., WANDS, J. R. & DE LA MONTE, S. M. 2005. Impaired insulin and insulin-like growth factor expression and signaling mechanisms in Alzheimer's disease--is this type 3 diabetes? *J Alzheimers Dis*, 7, 63-80.
- SUBBARAO, K. V., RICHARDSON, J. S. & ANG, L. C. 1990. Autopsy Samples of Alzheimer's Cortex Show Increased Peroxidation In Vitro. *Journal of Neurochemistry*, 55, 342-345.
- SUN, D. & JAKOBS, T. C. 2012. Structural remodeling of astrocytes in the injured CNS. *Neuroscientist*, 18, 567-88.
- SWANSON, R. A. & CHOI, D. W. 1993. Glial glycogen stores affect neuronal survival during glucose deprivation in vitro. *J Cereb Blood Flow Metab*, 13, 162-9.
- SWANSON, R. A., YU, A. C. H., CHAN, P. H. & SHARP, F. R. 1990. Glutamate Increases Glycogen Content and Reduces Glucose Utilization in Primary Astrocyte Culture. *Journal of Neurochemistry*, 54, 490-496.
- SZARUGA, M., VEUGELEN, S., BENURWAR, M., LISMONT, S., SEPULVEDA-FALLA, D., LLEO, A., RYAN, N. S., LASHLEY, T., FOX, N. C., MURAYAMA, S., GIJSEN, H., DE STROOPER, B. & CHAVEZ-GUTIERREZ, L. 2015. Qualitative changes in human gamma-secretase underlie familial Alzheimer's disease. *J Exp Med*, 212, 2003-13.
- TAKAMI, M., NAGASHIMA, Y., SANO, Y., ISHIHARA, S., MORISHIMA-KAWASHIMA, M., FUNAMOTO, S. & IHARA, Y. 2009. gamma-Secretase: successive tripeptide and tetrapeptide release from the transmembrane domain of beta-carboxyl terminal fragment. *J Neurosci*, 29, 13042-52.
- TAKANO, T., SAHARA, N., YAMANOUCHI, Y. & MORI, H. 1997. Assignment of Alzheimer's presenilin-2 (PS-2) gene to 1q42.1 by fluorescence in situ hybridization. *Neurosci Lett*, 221, 205-7.

- TAKASHIMA, A., NOGUCHI, K., SATO, K., HOSHINO, T. & IMAHORI, K. 1993. Tau protein kinase I is essential for amyloid beta-protein-induced neurotoxicity. *Proceedings of the National Academy of Sciences of the United States of America*, 90, 7789-7793.
- TANG, X., ZHOU, L., WAGNER, A. M., MARCHETTO, M. C., MUOTRI, A. R., GAGE, F. H. & CHEN, G. 2013. Astroglial cells regulate the developmental timeline of human neurons differentiated from induced pluripotent stem cells. *Stem Cell Res*, 11, 743-57.
- TARCZYLUK, M. A., NAGEL, D. A., O'NEIL, J. D., PARRI, H. R., TSE, E. H., COLEMAN, M. D. & HILL, E. J. 2013. Functional astrocyte-neuron lactate shuttle in a human stem cell-derived neuronal network. *J Cereb Blood Flow Metab*, 33, 1386-93.
- TARCZYLUK, M. A., NAGEL, D. A., RHEIN PARRI, H., TSE, E. H., BROWN, J. E., COLEMAN, M. D. & HILL, E. J. 2015. Amyloid beta 1-42 induces hypometabolism in human stem cell-derived neuron and astrocyte networks. *J Cereb Blood Flow Metab*, 35, 1348-57.
- THAL, D. R., RUB, U., ORANTES, M. & BRAAK, H. 2002. Phases of A beta-deposition in the human brain and its relevance for the development of AD. *Neurology*, 58, 1791-800.
- THOMPSON, C. M., MARKESBERY, W. R., EHMANN, W. D., MAO, Y. X. & VANCE, D. E. 1988. Regional brain trace-element studies in Alzheimer's disease. *Neurotoxicology*, 9, 1-7.
- TOWNSEND, M., SHANKAR, G. M., MEHTA, T., WALSH, D. M. & SELKOE, D. J. 2006. Effects of secreted oligomers of amyloid beta-protein on hippocampal synaptic plasticity: a potent role for trimers. *The Journal of physiology*, 572, 477-492.
- TURNER, P. R., O'CONNOR, K., TATE, W. P. & ABRAHAM, W. C. 2003. Roles of amyloid precursor protein and its fragments in regulating neural activity, plasticity and memory. *Prog Neurobiol*, 70, 1-32.
- UEMURA, E. & GREENLEE, H. W. 2001. Amyloid beta-peptide inhibits neuronal glucose uptake by preventing exocytosis. *Exp Neurol*, 170, 270-6.
- VAN DE LEEMPUT, J., BOLES, N. C., KIEHL, T. R., CORNEO, B., LEDERMAN, P., MENON, V., LEE, C., MARTINEZ, R. A., LEVI, B. P., THOMPSON, C. L., YAO, S., KAYKAS, A., TEMPLE, S. & FASANO, C. A. 2014. CORTECON: a temporal transcriptome analysis of in vitro human cerebral cortex development from human embryonic stem cells. *Neuron*, 83, 51-68.
- VANDENBERGHE, R., RIVIERE, M.-E., CAPUTO, A., SOVAGO, J., MAGUIRE, R. P., FARLOW, M., MAROTTA, G., SANCHEZ-VALLE, R., SCHELTENS, P., RYAN, J. M. & GRAF, A. 2016. Active A β immunotherapy CAD106 in Alzheimer's disease: A phase 2b study. *Alzheimer's & dementia (New York, N. Y.)*, 3, 10-22.
- VASSAR, R. 2004. Bace 1. *Journal of Molecular Neuroscience*, 23, 105-113.

- VOLTERRA, A. & MELDOLESI, J. 2005. Astrocytes, from brain glue to communication elements: the revolution continues. *Nat Rev Neurosci*, 6, 626-40.
- WALLS, A. B., HEIMBÜRGER, C. M., BOUMAN, S. D., SCHOUSBOE, A. & WAAGEPETERSEN, H. S. 2009. Robust glycogen shunt activity in astrocytes: Effects of glutamatergic and adrenergic agents. *Neuroscience*, 158, 284-292.
- WANDERLEY, L. F., SOARES, A. M. D. S., SILVA, C. R. E., FIGUEIREDO, I. M. D., FERREIRA, A. T. D. S., PERALES, J., MOTA, H. R. D. O., OLIVEIRA, J. T. A. & COSTA JUNIOR, L. M. 2018. A cysteine protease from the latex of *Ficus benjamina* has in vitro anthelmintic activity against *Haemonchus contortus*. *Revista Brasileira de Parasitologia Veterinária*, 27, 473-480.
- WANG, H. W., PASTERNAK, J. F., KUO, H., RISTIC, H., LAMBERT, M. P., CHROMY, B., VIOLA, K. L., KLEIN, W. L., STINE, W. B., KRAFFT, G. A. & TROMMER, B. L. 2002. Soluble oligomers of beta amyloid (1-42) inhibit long-term potentiation but not long-term depression in rat dentate gyrus. *Brain Res*, 924, 133-40.
- WARD, A., ARRIGHI, H. M., MICHELS, S. & CEDARBAUM, J. M. 2012. Mild cognitive impairment: Disparity of incidence and prevalence estimates. *Alzheimer's & Dementia: The Journal of the Alzheimer's Association*, 8, 14-21.
- WARD, A., CREAN, S., MERCALDI, C. J., COLLINS, J. M., BOYD, D., COOK, M. N. & ARRIGHI, H. M. 2012. Prevalence of apolipoprotein E4 genotype and homozygotes (APOE e4/4) among patients diagnosed with Alzheimer's disease: a systematic review and meta-analysis. *Neuroepidemiology*, 38, 1-17.
- WEGGEN, S., ERIKSEN, J. L., DAS, P., SAGI, S. A., WANG, R., PIETRZIK, C. U., FINDLAY, K. A., SMITH, T. E., MURPHY, M. P., BULTER, T., KANG, D. E., MARQUEZ-STERLING, N., GOLDE, T. E. & KOO, E. H. 2001. A subset of NSAIDs lower amyloidogenic A β 42 independently of cyclooxygenase activity. *Nature*, 414, 212-6.
- WENDER, R., BROWN, A. M., FERN, R., SWANSON, R. A., FARRELL, K. & RANSOM, B. R. 2000. Astrocytic glycogen influences axon function and survival during glucose deprivation in central white matter. *J Neurosci*, 20, 6804-10.
- WILCOCK, D. M. & COLTON, C. A. 2008. Anti-amyloid-beta immunotherapy in Alzheimer's disease: relevance of transgenic mouse studies to clinical trials. *J Alzheimers Dis*, 15, 555-69.
- WILHELMSSON, U., BUSHONG, E. A., PRICE, D. L., SMARR, B. L., PHUNG, V., TERADA, M., ELLISMAN, M. H. & PEKONY, M. 2006. Redefining the concept of reactive astrocytes as cells that remain within their unique domains upon reaction to injury. *Proc Natl Acad Sci U S A*, 103, 17513-8.

- WITTENBERG, R., KNAPP, M., HU, B., COMAS-HERRERA, A., KING, D., REHILL, A., SHI, C., BANERJEE, S., PATEL, A., JAGGER, C. & KINGSTON, A. 2019. The costs of dementia in England. *International journal of geriatric psychiatry*, 34, 1095-1103.
- WOEHLING, E. K., HILL, E. J. & COLEMAN, M. D. 2010. Evaluation of the importance of astrocytes when screening for acute toxicity in neuronal cell systems. *Neurotox Res*, 17, 103-13.
- WOLFE, N., REED, B. R., EBERLING, J. L. & JAGUST, W. J. 1995. Temporal lobe perfusion on single photon emission computed tomography predicts the rate of cognitive decline in Alzheimer's disease. *Arch Neurol*, 52, 257-62.
- YAMANAKA, S. & TAKAHASHI, K. 2006. [Induction of pluripotent stem cells from mouse fibroblast cultures]. *Tanpakushitsu Kakusan Koso*, 51, 2346-51.
- YAN, S. D., CHEN, X., FU, J., CHEN, M., ZHU, H., ROHER, A., SLATTERY, T., ZHAO, L., NAGASHIMA, M., MORSE, J., MIGHELI, A., NAWROTH, P., STERN, D. & SCHMIDT, A. M. 1996. RAGE and amyloid-beta peptide neurotoxicity in Alzheimer's disease. *Nature*, 382, 685-91.
- YAN, S. D., FU, J., SOTO, C., CHEN, X., ZHU, H., AL-MOHANNA, F., COLLISON, K., ZHU, A., STERN, E., SAIDO, T., TOHYAMA, M., OGAWA, S., ROHER, A. & STERN, D. 1997. An intracellular protein that binds amyloid-beta peptide and mediates neurotoxicity in Alzheimer's disease. *Nature*, 389, 689-95.
- YAN, Y., YANG, D., ZARNOVSKA, E. D., DU, Z., WERBEL, B., VALLIERE, C., PEARCE, R. A., THOMSON, J. A. & ZHANG, S. C. 2005. Directed differentiation of dopaminergic neuronal subtypes from human embryonic stem cells. *Stem Cells*, 23, 781-90.
- YAO, J., IRWIN, R. W., ZHAO, L., NILSEN, J., HAMILTON, R. T. & BRINTON, R. D. 2009. Mitochondrial bioenergetic deficit precedes Alzheimer's pathology in female mouse model of Alzheimer's disease. *Proc Natl Acad Sci U S A*, 106, 14670-5.
- YONG, V. W., MOUMDJIAN, R., YONG, F. P., THEODORA, C. G. R., FREEDMAN, M. S., CASHMAN, N. & ANTEL, J. P. 1991. Interferon Promotes Proliferation of Adult Human Astrocytes In vitro and Reactive Gliosis in the Adult Mouse Brain in vivo. *Proceedings of the National Academy of Sciences of the United States of America*, 88, 7016-7020.
- ZAMANIAN, J. L., XU, L., FOO, L. C., NOURI, N., ZHOU, L., GIFFARD, R. G. & BARRES, B. A. 2012. Genomic analysis of reactive astrogliosis. *J Neurosci*, 32, 6391-410.
- ZHAO, C., DENG, W. & GAGE, F. H. 2008. Mechanisms and functional implications of adult neurogenesis. *Cell*, 132, 645-60.
- ZHAO, J., O'CONNOR, T. & VASSAR, R. 2011. The contribution of activated astrocytes to A β production: Implications for Alzheimer's disease pathogenesis. *Journal of Neuroinflammation*, 8, 150.

- ZHENG, H., CHENG, B., LI, Y., LI, X., CHEN, X. & ZHANG, Y.-W. 2018. TREM2 in Alzheimer's Disease: Microglial Survival and Energy Metabolism. *Frontiers in Aging Neuroscience*, 10.
- ZHENG, L., KAGEDAL, K., DEHVARI, N., BENEDIKZ, E., COWBURN, R., MARCUSSON, J. & TERMAN, A. 2009. Oxidative stress induces macroautophagy of amyloid beta-protein and ensuing apoptosis. *Free Radic Biol Med*, 46, 422-9.
- ZHU, K., XIANG, X., FILSER, S., MARINKOVIC, P., DOROSTKAR, M. M., CRUX, S., NEUMANN, U., SHIMSHEK, D. R., RAMMES, G., HAASS, C., LICHTENTHALER, S. F., GUNNERSEN, J. M. & HERMS, J. 2018. Beta-Site Amyloid Precursor Protein Cleaving Enzyme 1 Inhibition Impairs Synaptic Plasticity via Seizure Protein 6. *Biol Psychiatry*, 83, 428-437.
- ZIGMAN, W. B., SCHUPF, N., SERSEN, E. & SILVERMAN, W. 1996. Prevalence of dementia in adults with and without Down syndrome. *Am J Ment Retard*, 100, 403-12.
- ZWINGMANN, C. & LEIBFRITZ, D. 2003. Regulation of glial metabolism studied by ¹³C-NMR. *NMR Biomed*, 16, 370-99.

Appendices

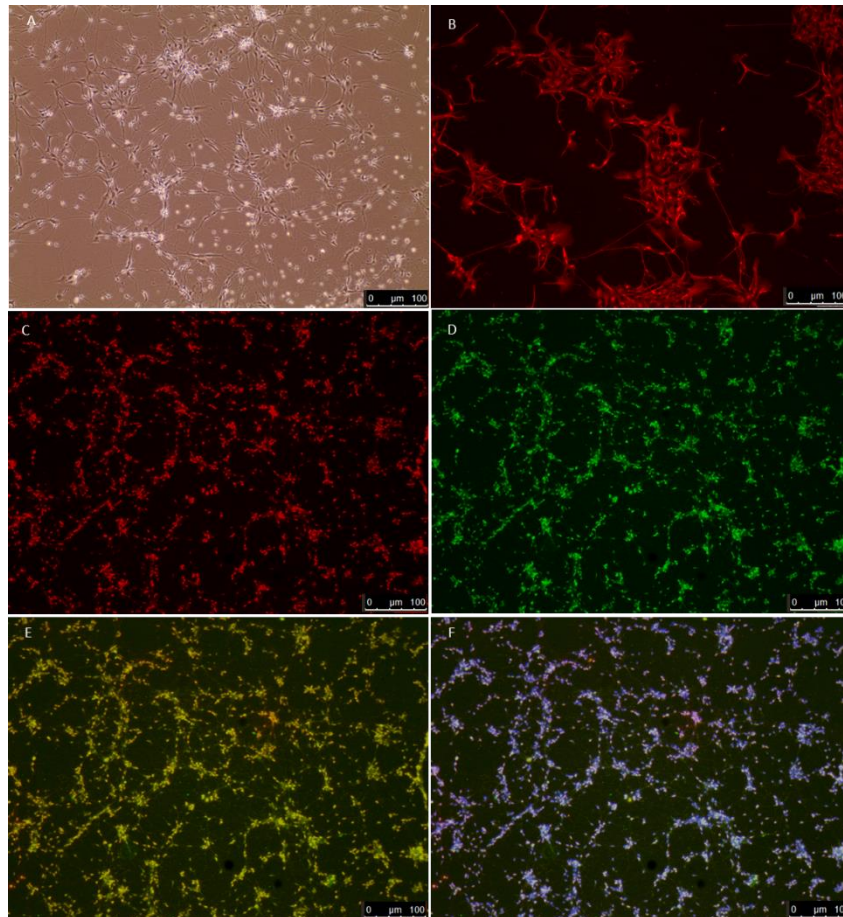


Figure A1: Representative images of hiPSC-Derived NPCs from 'healthy' ax0016 cell line using ICC staining. Phase contrast image of NPCs (A). The NPCs were stained for neural precursor cells antibodies against nestin (red, B), sox2+ (red, C) and pax6+ (green, D). Merged image showing co-expression of both pax6+ and sox2+ (E). Cells were counterstained with DAPI+ (blue, F). Cells were stained at passage number 2, n=2. Scale bars: 100μM.

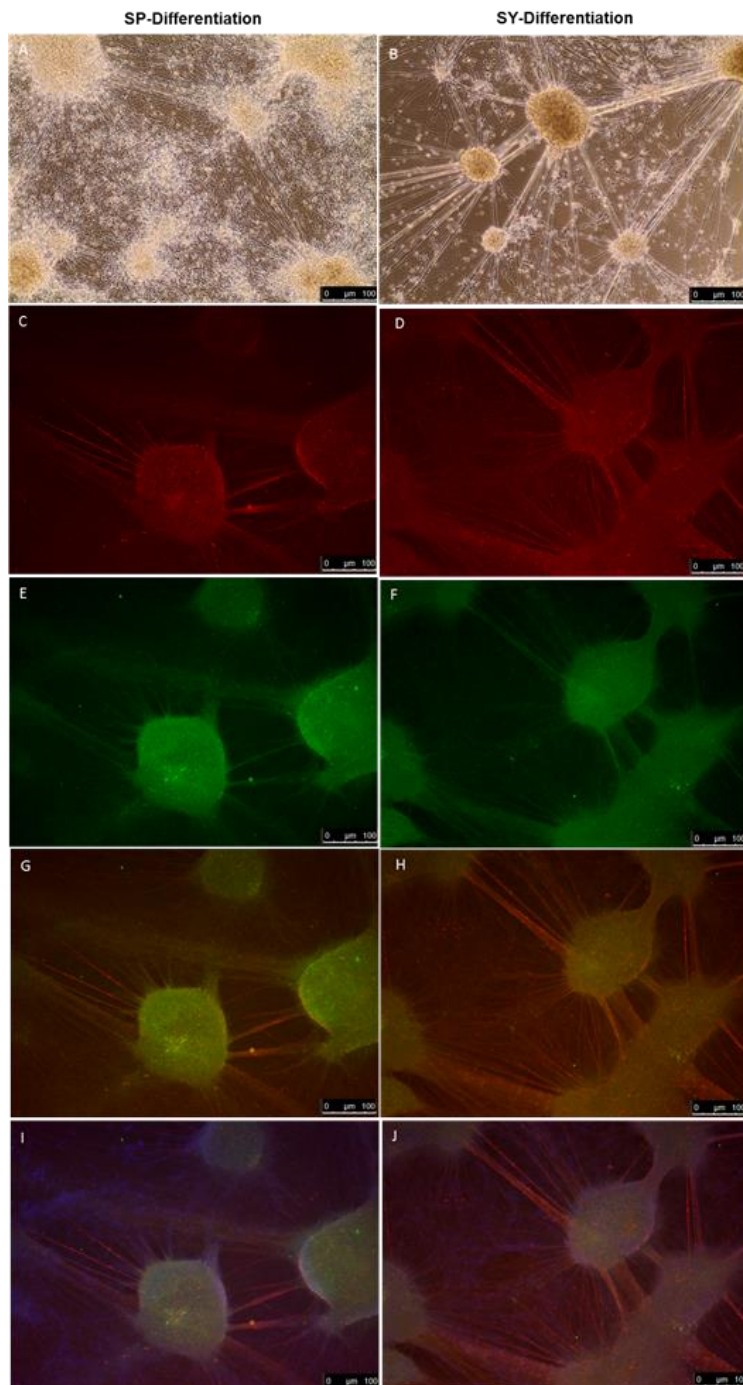


Figure A2: Representative images illustrating the development of neural cells at day 30 in SP and SY differentiation cultures from ax0016 cell line of 'healthy' hiPSC-derived NPCs. A and B showing phase contrast images of neural cells in network of the differentiation cells. Immunofluorescent images showing a network neuronal cells that was confirmed using a TUJ1+ (red, C and D). Astrocytic cells were identified using S100 β + marker (green, E and F). Merged image showing expression of both TUJ1+ and S100 β + (G and H). Nuclei were counter stained with DAPI+ (blue, I and J). n=3. Scale bars: 100 μ M.

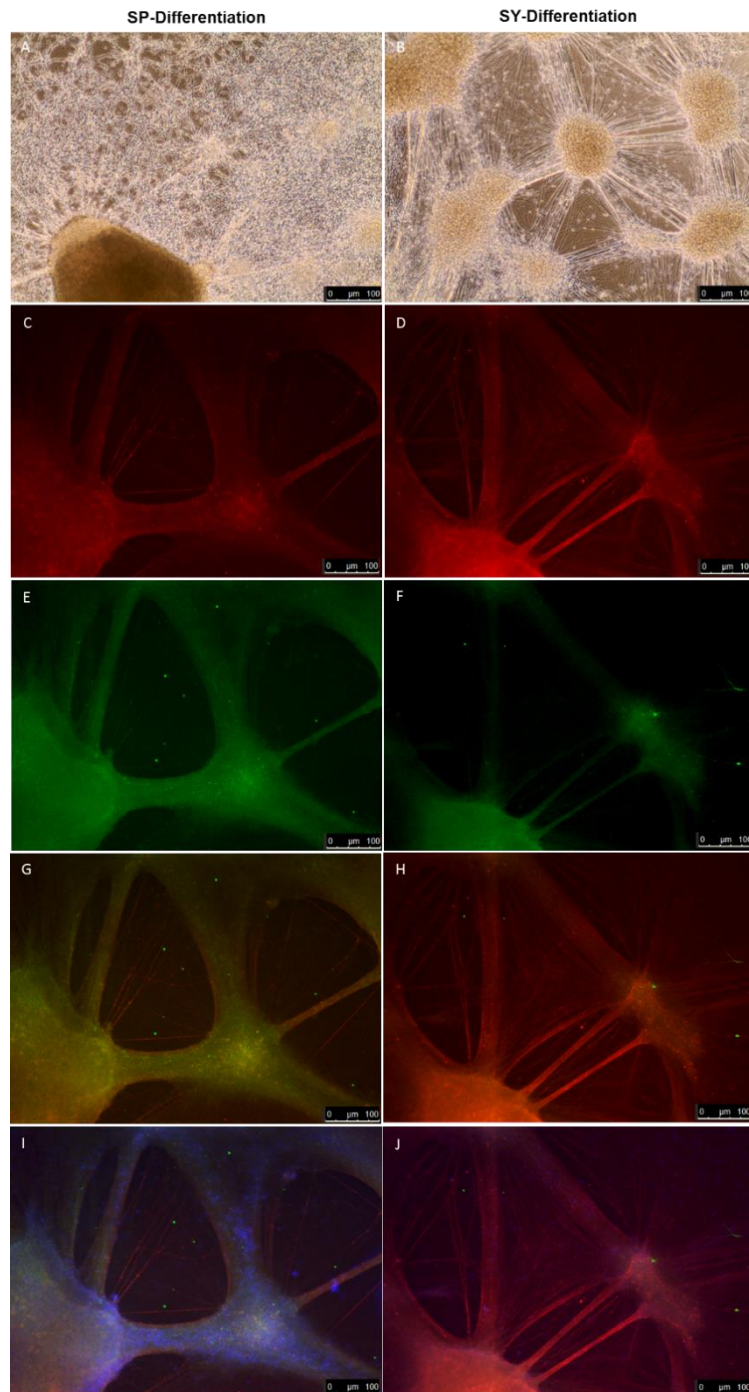


Figure A3: Representative images illustrating the development of neural cells at day 40 in SP and SY differentiation cultures from ax0016 cell line of 'healthy' hiPSC-derived NPCs. A and B showing phase contrast images of neural cells in network of the differentiation cells. Immunofluorescent images showing a network neuronal cells that was confirmed using a TUJ1+ (red, C and D). Astrocytic cells were identified using S100 β + marker (green, E and F). Merged image showing expression of both TUJ1+ and S100 β + (G and H). Nuclei were counter stained with DAPI+ (blue, I and J). n=3. Scale bars: 100 μ M.

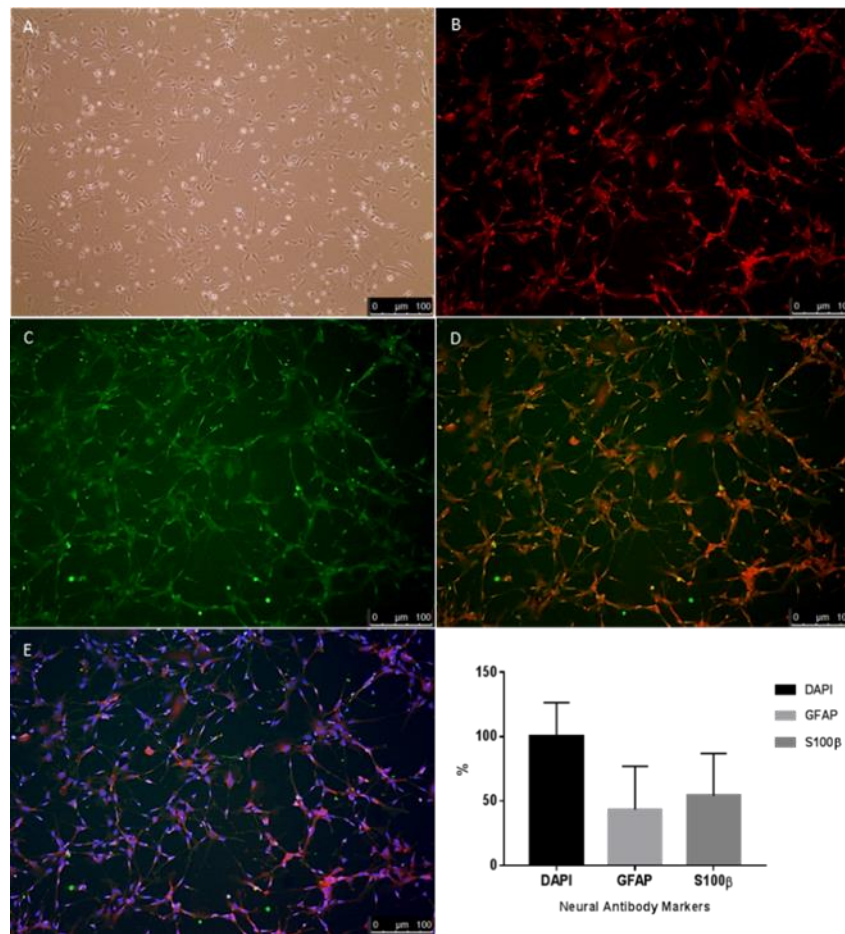


Figure A4: Representative images showing ICC staining of 'healthy' hiPSC-derived astrocytic cells from ax0016 cell line at day 45+. The cells were cultured using the astrocytes differentiation and maturation protocols. (A) shows a phase contrast image of the astrocyte cells. Immunofluorescent images of astrocytic markers GFAP+ (red, B) and S100β+ (green, C). Merged image showing expression of both GFAP+ and S100β+ (D). Nuclei were counter stained with DAPI+ (blue, E). Scale bars: 100μM. The graph shows the quantification of cell-types using ImageJ analysis of neural cell populations produced at this stage of differentiation, n=2. The statistical analysis was done using One-way ANOVA, Dunnett's post-test.

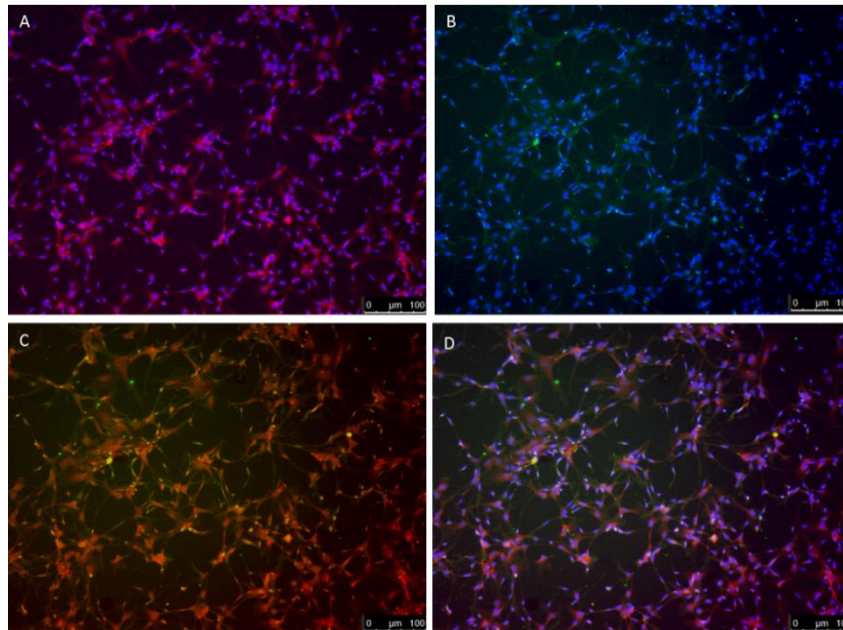


Figure A5: Representative images of 'healthy' hiPSC-derived astrocytic cells from ax0016 cell line at day 45+. PAS staining confirmed the presence of glycogen in astrocytes cells (red, A) and S100 β + (green, B). Cells were counterstained with DAPI+ (blue). Merged image showing expression of co-staining: S100 β + and PAS+ staining (C). Merged image showing expression of S100 β +, PAS+ staining and DAPI+ (D). n=2. Scale bars: 100 μ M.

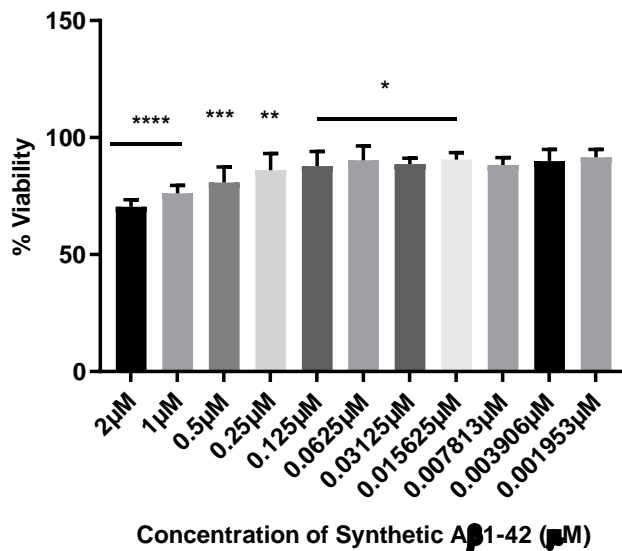


Figure A6: Determination of cell viability of astrocytes treated with synthetic Aβ1-42. Healthy hiPSC-derived astrocytes from ax0016 cell line. Cells were exposed to 2 μM-0.001 μM of synthetic Aβ1-42 oligomers for 48 hours. Cell viability was measured using MTT assay. The values are expressed as percentage of untreated cells as a control (100%), ± SEM, n=3, $P=0.0001$ (****), $P<0.001$ (***), $P<0.01$ (**), $P<0.05$ (*). Comparisons between treatments were performed using statistical analysis of One-way ANOVA, Dunnett's post-test.

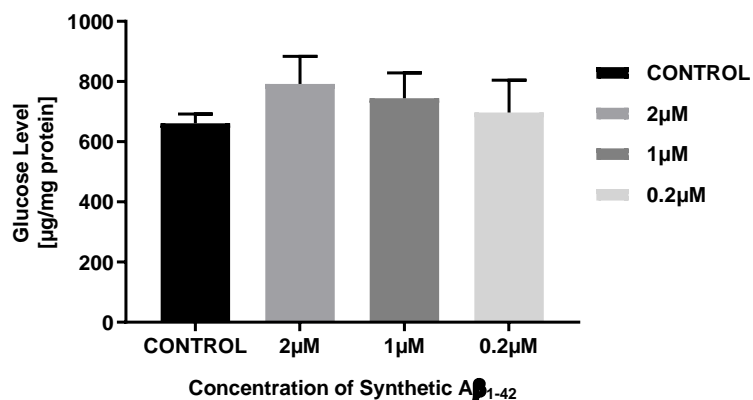


Figure A7: Determination of glucose levels remaining in the media following treatment of astrocytes to synthetic A β 1-42 oligomers. Treatment of 'healthy' hiPSC-derived astrocytes from ax0016 cell line at 45+ days old cells with synthetic A β 1-42 in the media (2 μ M, 1 μ M and 0.2 μ M) versus untreated cells (control) for 48 hours. The amount of glucose remaining in the conditioned media following treatments were measured using glucose assay. Data is expressed as glucose μ g/mg total cellular protein, \pm SEM, n=3 (triplicate wells pooled for each run). The statistical analysis was done using One-way ANOVA, Dunnett's post-test

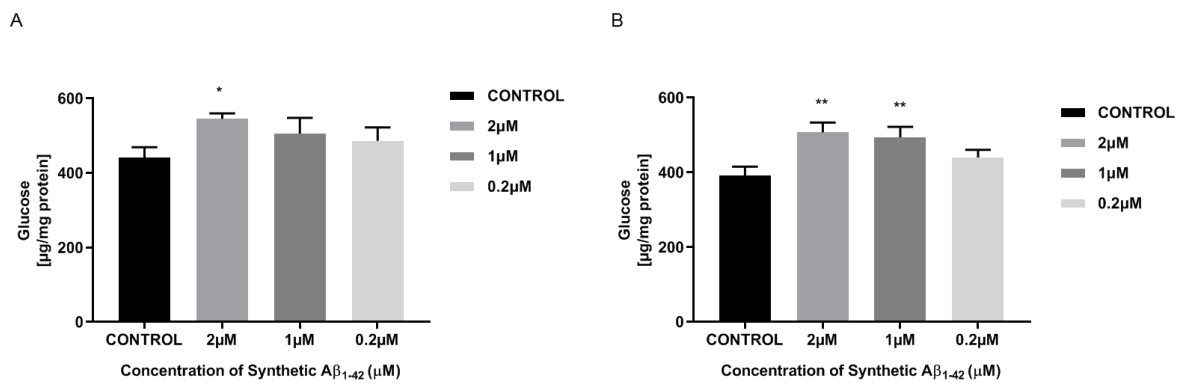


Figure A8: Determination of glucose levels remaining in the media following treatment of neuronal cells to synthetic Aβ₁₋₄₂ oligomers. Treatment of the neuronal cells derived from: SP (A) and SY (B) differentiation methods from ax0016 cell line at day 30 with synthetic Aβ₁₋₄₂ in the media (2μM, 1μM and 0.2μM) versus untreated cells (control) for 48hrs. The amount of glucose remaining in the conditioned media following treatments were measured using glucose assay. Data is expressed as glucose μg/mg total cellular protein, ± SEM, n=3 (triplicate wells pooled for each run), $P < 0.01$ (**), $P < 0.05$ (*). The statistical analysis was done using One-way ANOVA, Dunnett's post-test.

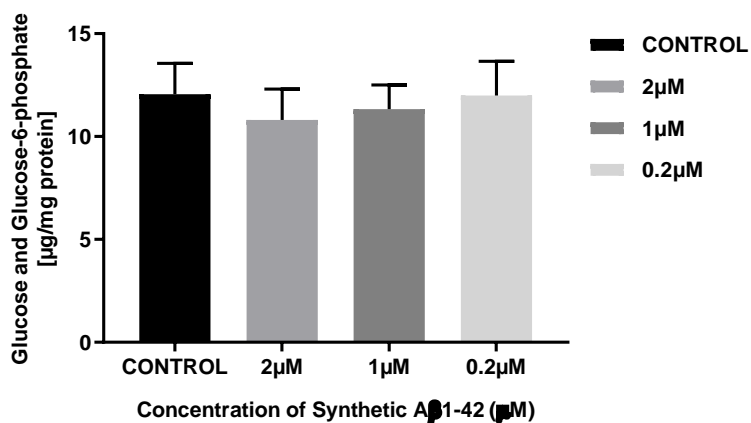


Figure A9: Determination the effect of synthetic A β 1-42 treatment on astrocytic glycogen stores. Treatment of 'healthy' hiPSC-derived astrocytes from ax0016 cell line (A) at 45+ days old cells with synthetic A β 1-42 oligomers in the media (2 μ M, 1 μ M and 0.2 μ M) and compared to untreated cells as a control for 48 hours. The cellular glycogen content was measured using a glycogen assay. Results are expressed as glucose and glucose-6-phosphate μ g/mg total cellular protein, \pm SEM, n=3 (triplicate wells pooled for each run). The statistical analysis was done using One-way ANOVA, Dunnett's post-test.

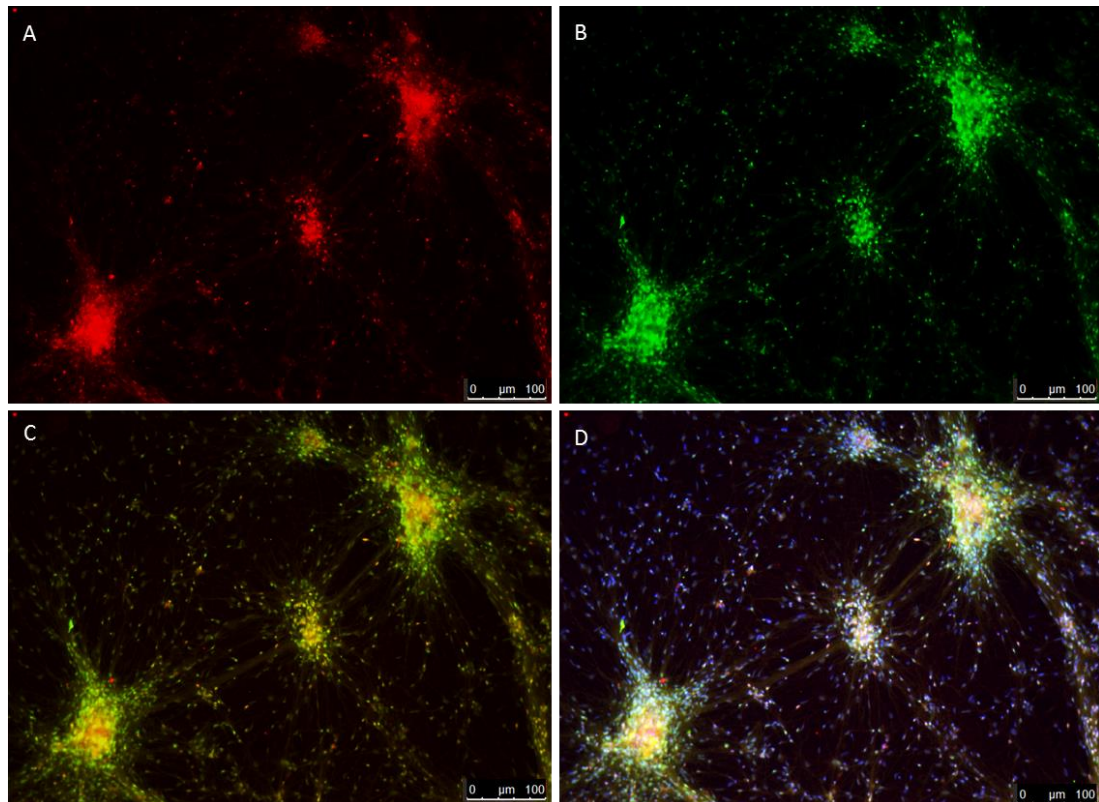


Figure A10: Representative images showing the development of neural cells from fAD patient hiPSC-derived NPCs of ax0112 cell line at day 30 in SP differentiation culture of fAD patient NPCs. Confirming the presence of cortical neuronal cell type using CTIP2+ marker (red, A) and confirming the glutamatergic neuronal cell type using VGLUT1+ marker (green, B). Merged image showing co-expression of both CTIP2+ and VGLUT1+ (C). Nuclei were counter-stained with DAPI+ (blue, D). n=3. Scale bars: 100μM.

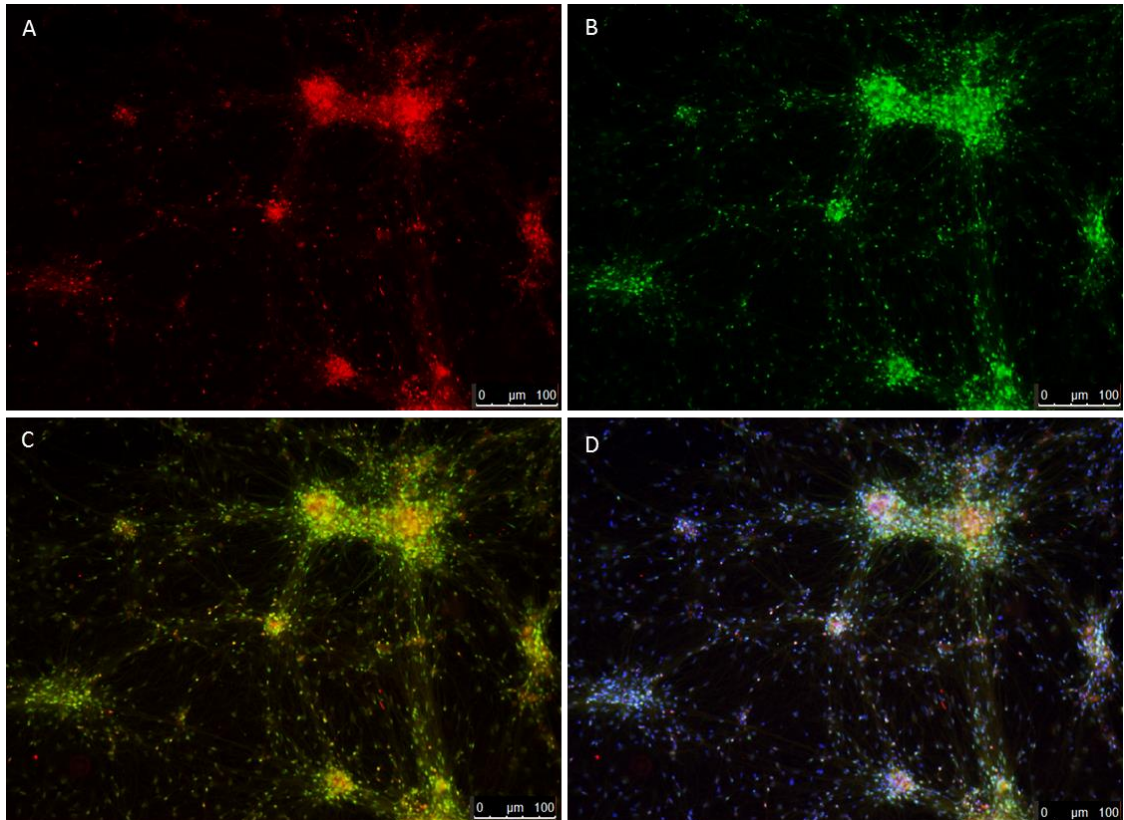


Figure A11: Representative images showing the development of neural cells from fAD patient hiPSC-derived NPCs of ax0112 cell line at day 40 in SP differentiation culture of fAD patient NPCs. Confirming the presence of cortical neuronal cell type using CTIP2+ marker (red, A) and confirming the glutamatergic neuronal cell type using VGLUT1+ marker (green, B). Merged image showing co-expression of both CTIP2+ and VGLUT1+ (C). Nuclei were counter-stained with DAPI+ (blue, D). n=3. Scale bars: 100 μ M.

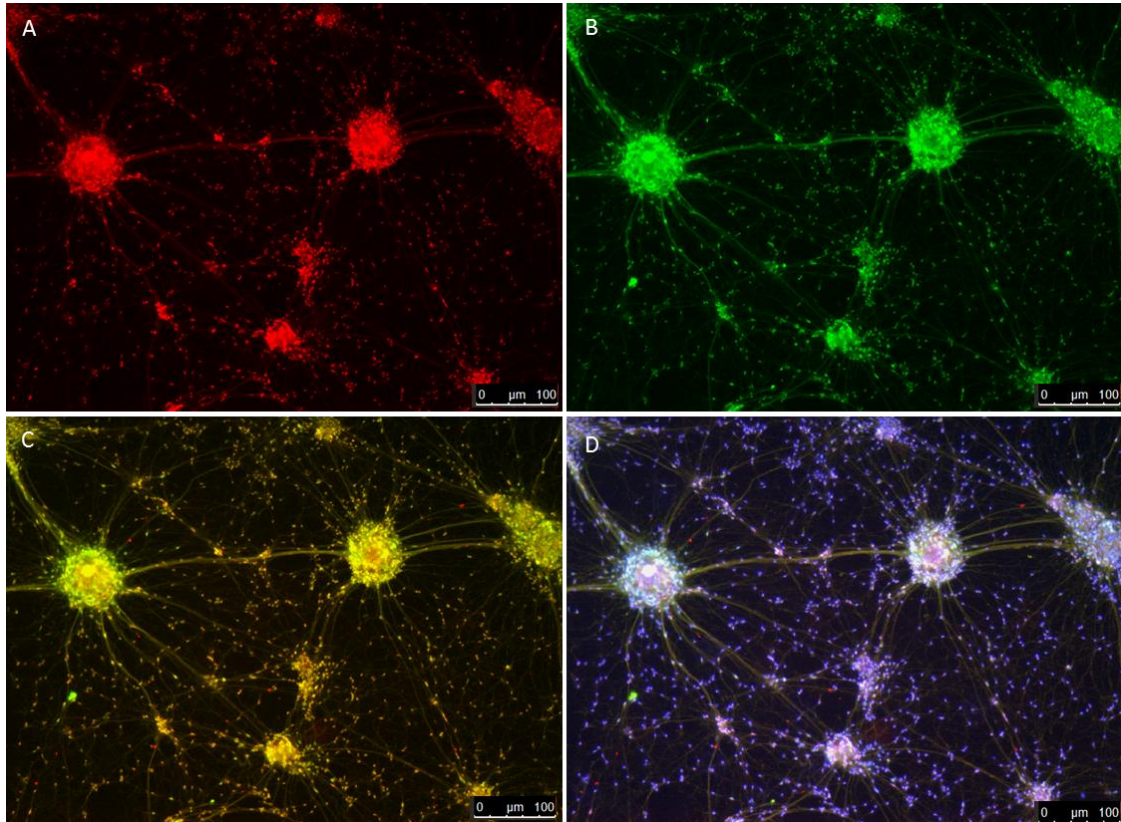


Figure A12: Representative images showing the development of neural cells from Fad patient hiPSC-derived NPCs of ax0112 cell line at day 30 in SY differentiation culture of fAD patient NPCs. Confirming the presence of cortical neuronal cell type using CTIP2+ marker (red, A) and confirming the glutamatergic neuronal cell type using VGLUT1+ marker (green, B). Merged image showing co-expression of both CTIP2+, VGLU1T+ (C) and nuclei were counter-stained with DAPI (blue, D). n=3. Scale bars: 100μM.

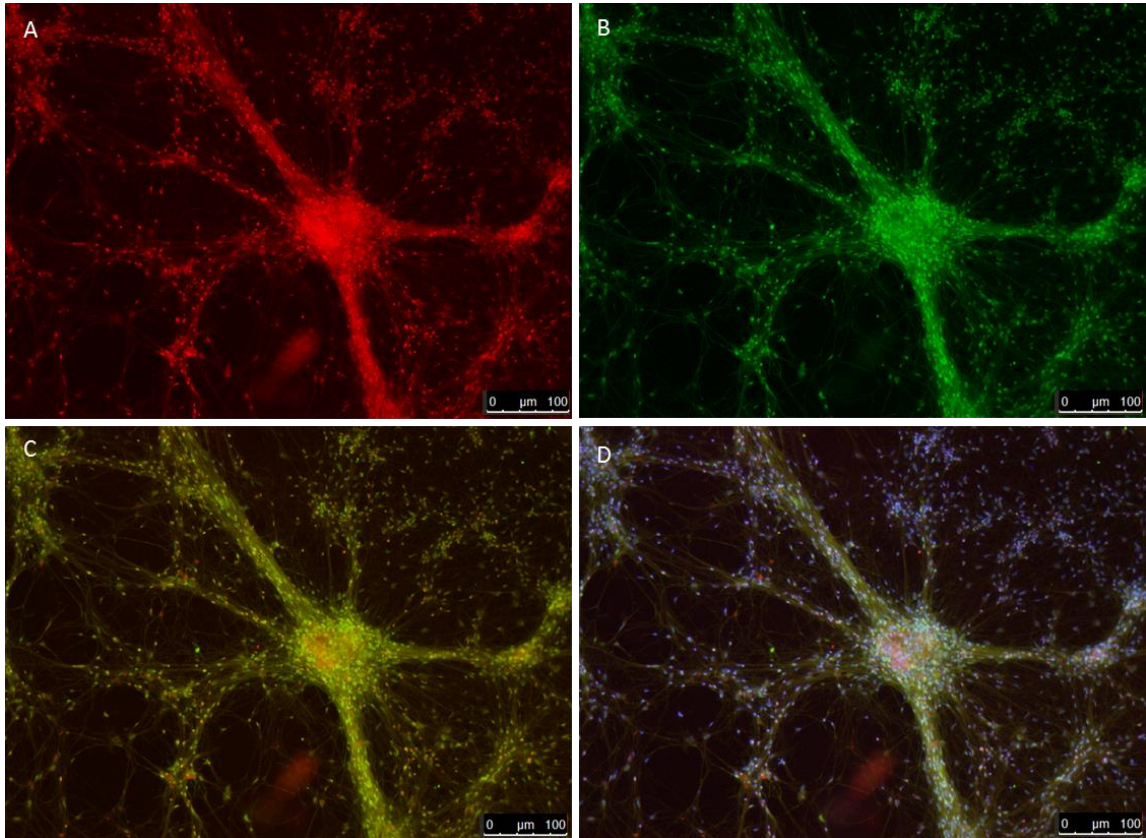


Figure A13: Representative images showing the development of neural cells from fAD patient hiPSC-derived NPCs of ax0112 cell line at day 40 in SY differentiation culture of fAD patient NPCs. Confirming the presence of cortical neuronal cell type using CTIP2+ marker (red, A) and confirming the glutamatergic neuronal cell type using VGLUT1+ marker (green, B). Merged image showing co-expression of both CTIP2+, VGLUT1+ (C) and nuclei were counter-stained with DAPI+ (blue, D). n=3. Scale bars: 100μM.

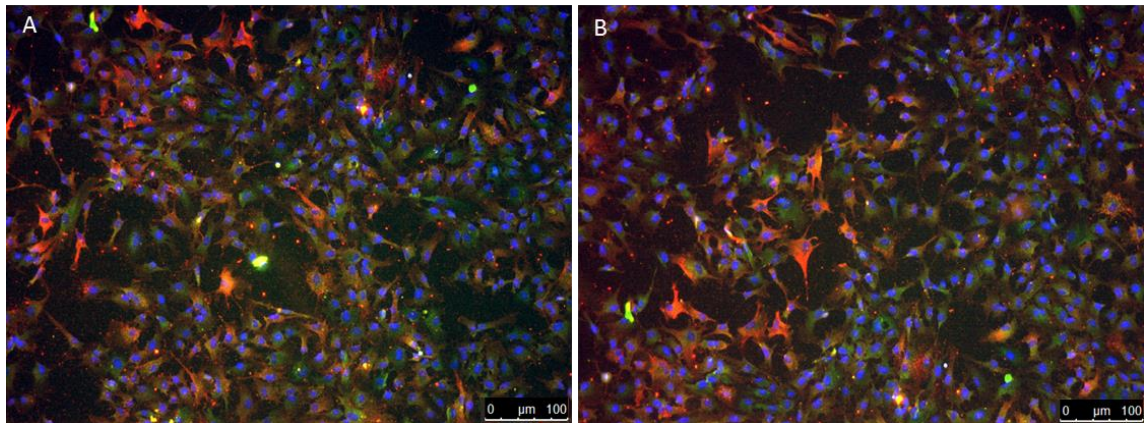


Figure A14: Representative images of 'healthy' hiPSC-derived astrocytic cells from ax0018 (A) and fAD patient hiPSC-derived astrocytic cells from ax0112 (B) cell lines at day 45+. The cells were cultured using the astrocytes differentiation and maturation protocols. Merged images showing expression of both GFAP+ (red) and pax6+ (green). Nuclei were counter stained with DAPI+ (blue). Scale bars: 100 μ M. n=3.

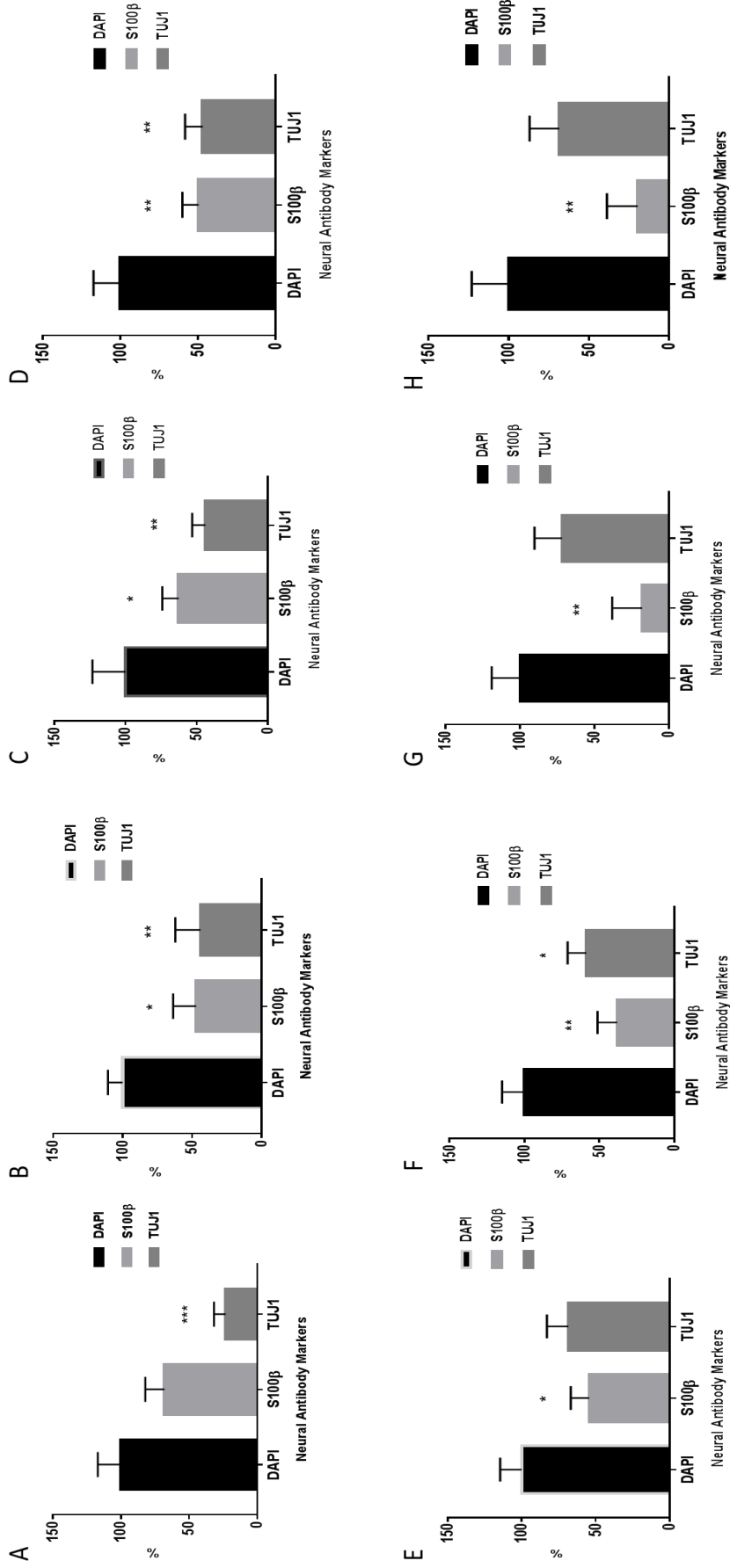


Figure A15: The graph presenting the quantification of neural cell populations from 'healthy' hiPSC-derived NPCs of ax0018 cell line following culture in SP (A-D) and SY (E-H) differentiation methods at days 10, 20, 30 and 40, respectively. Analysis of quantification cells produced by ImageJ showing a percentage number of astrocytes and neurons; counts are presented as percentages with respect to DAPI controls, \pm SEM, $n=3$, $P<0.01$ (**), $P<0.05$ (*), $P<0.001$ (***). The statistical analysis was done using One-way ANOVA, Dunnett's post-test.

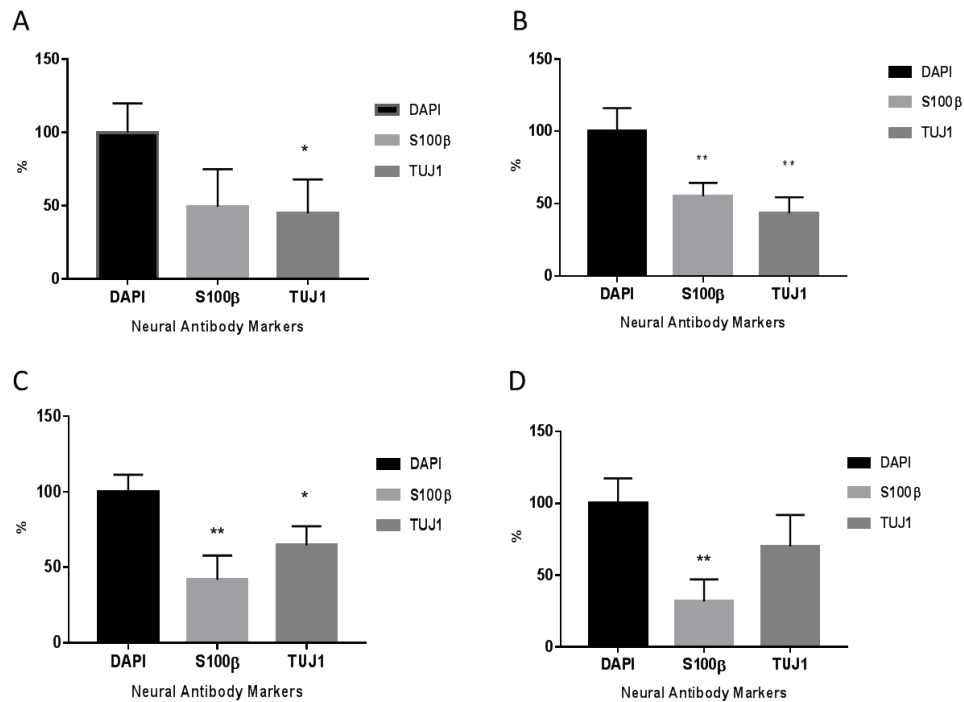


Figure A16: The graph presenting the quantification of neural cell populations from 'healthy' hiPSC-derived NPCs of ax0016 cell line following culture in SP (A and B) and SY (C and D) differentiation methods at days 30 and 40, respectively. Analysis of quantification cells produced by ImageJ showing a percentage number of astrocytes and neurons; counts are presented as percentages with respect to DAPI controls, \pm SEM, $n=3$, $P<0.01$ (**), $P<0.05$ (*). The statistical analysis was done using One-way ANOVA, Dunnett's post-test.

A

Ax0018	S100 β	TUJ1
Day 10	68.09117%	23.36182%
Day 20	47.1464%	44.00331%
Day 30	62.80353%	43.98455%
Day 40	49.65592%	47.04817%

B

Ax0016	S100 β	TUJ1
Day 30	49.4582%	44.96904%
Day 40	55.17319%	43.44578%

Table A17: Quantification by percentages based on ImageJ analysis of neural cell populations produced at different stages of SP differentiation of 'healthy' cell lines: ax0018 (A) and ax0016 (B). Counts are presented as percentages with respect to DAPI controls. n=3.

A

Ax0018	S100 β	TUJ1
Day 10	54.46009%	68.5446%
Day 20	38.21457%	58.80971%
Day 30	18.20913%	71.9351%
Day 40	19.66102%	68.53107%

B

Ax0016	S100 β	TUJ1
Day 30	41.90174%	64.65927%
Day 40	31.69709%	69.8816%

Table A18: Quantification by percentages based on nuclear counts of neural cell populations produced at different stages of SY differentiation of 'healthy' cell lines: ax0018 (A) and ax0016 (B). Counts are presented as percentages with respect to DAPI controls. n=3.

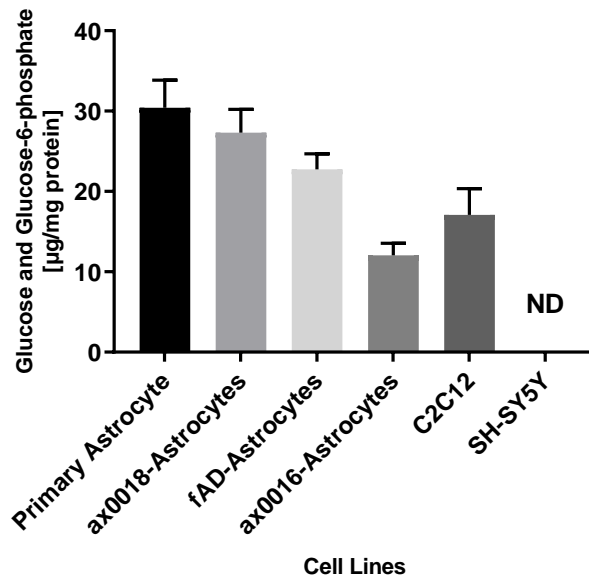


Figure A19: Determination of glycogen content levels of different cell lines. Cellular glycogen content level was measured using a glycogen assay. Data is expressed as glucose and glucose-6-phosphate $\mu\text{g}/\text{mg}$ total cellular protein, \pm SEM, $n=3$ (triplicate wells pooled for each run). The statistical analysis was done using One-way ANOVA, Tukey's multiple comparisons test.

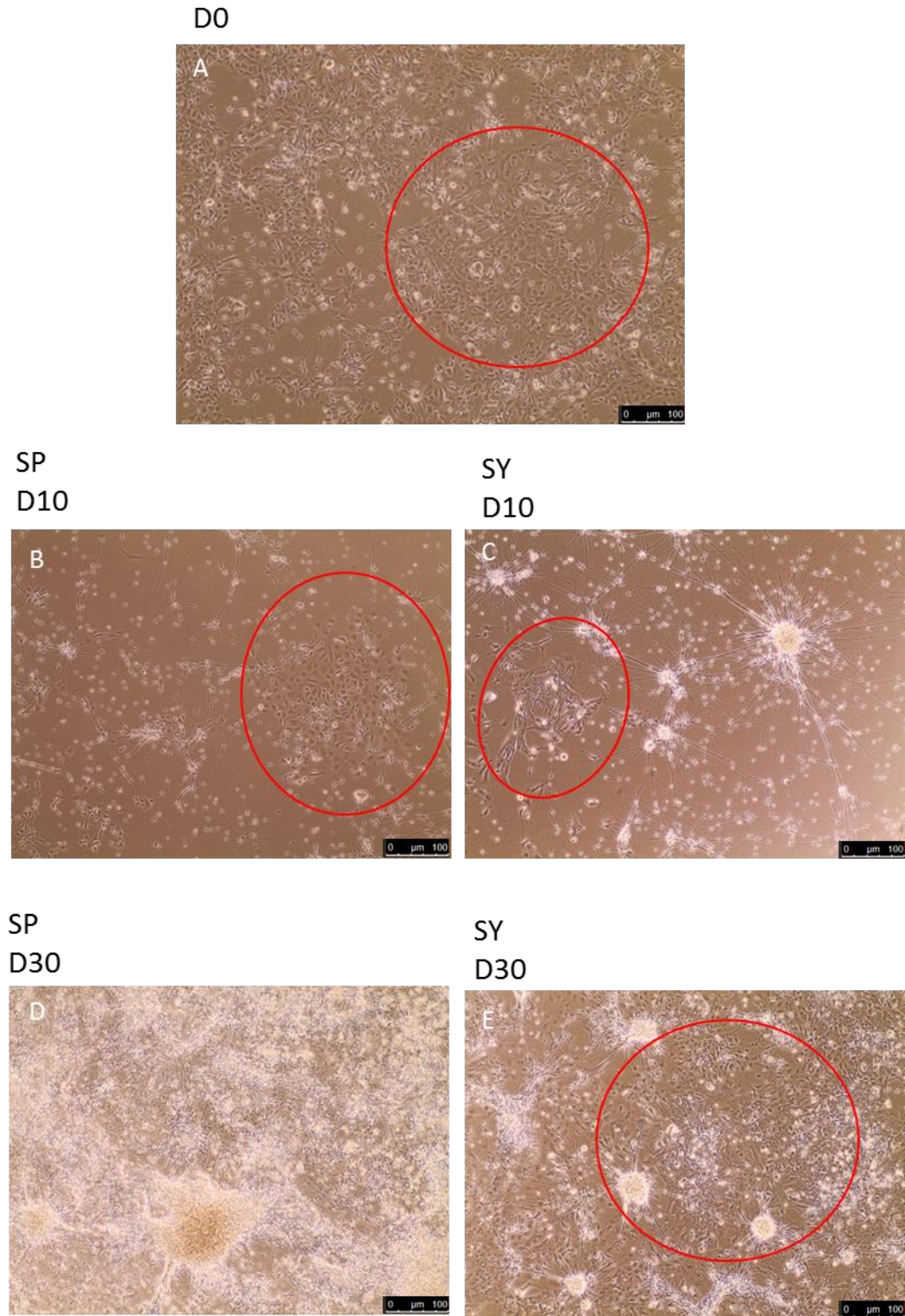


Figure A20: Representative images of hiPSC-Derived NPCs from 'healthy' ax0019 cell line in phase contrast at day zero (A). Representative images illustrating the development of neural cells at days zero, 10 and 30 in spontaneous and synchronous differentiation cultures. Scale bars: 100 μ M.

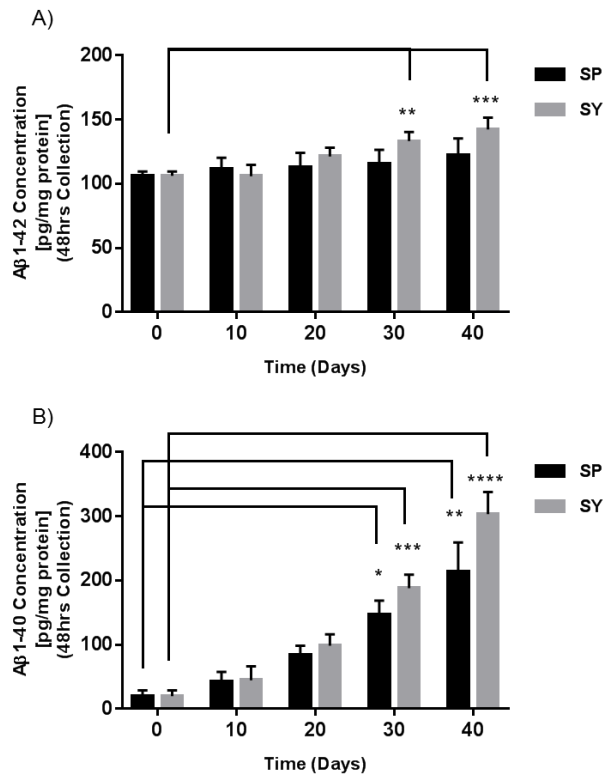


Figure A21: Quantification of A β peptide secretion profile release from neuronal cells following SP and SY differentiation methods of fAD patient cell line was detected using ELISA test: A β 1-42 (A) and A β 1-40 (B). The CM was assayed in different developmental days over a 48hr period. Data is expressed as A β pg/mg total cellular protein, \pm SEM, n=3 (triplicate wells pooled for each run), $P < 0.0001$ (****), $P < 0.001$ (***), $P < 0.01$ (**), $P < 0.05$ (*). The statistical analysis was done using Two-way ANOVA, Dunnett's multiple comparisons test.

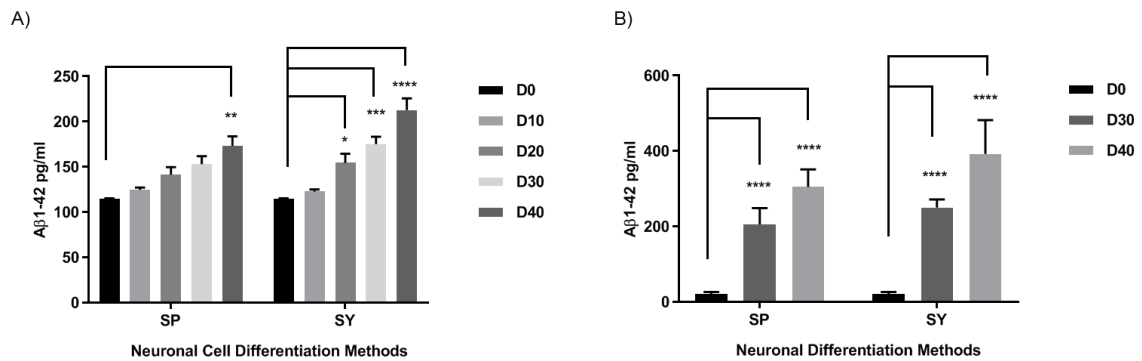


Figure A22: Quantification of Aβ peptide secretion profile release from neuronal cells following SP and SY differentiation methods of fAD patient cell line (ax0112) (A) and 'healthy' control cell line (ax0018) (B) was detected using ELISA test: Aβ1-42. The CM was assayed in different developmental days over a 48 hours period. Data is expressed as Aβ pg/ml in conditioned media, ± SEM, n=3 (triplicate wells pooled for each run), $P < 0.0001$ (****), $P < 0.001$ (***), $P < 0.01$ (**), $P < 0.05$ (*). The statistical analysis was done using Two-way ANOVA, Dunnett's multiple comparisons test.

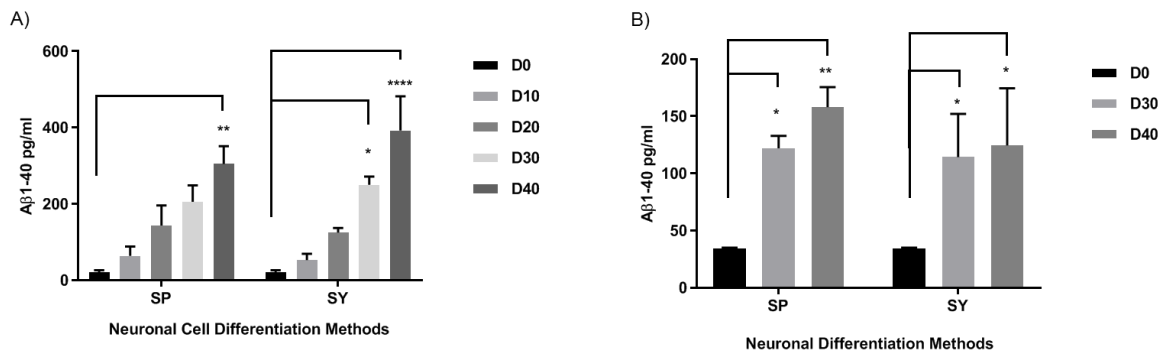


Figure A23: Quantification of Aβ peptide secretion profile release from neuronal cells following SP and SY differentiation methods of fAD patient cell line (ax0112) (A) and 'healthy' control cell line (ax0018) (B) was detected using ELISA test: Aβ₁₋₄₀. The CM was assayed in different developmental days over a 48 hours period. Data is expressed as Aβ pg/ml in conditioned media, ± SEM, n=3 (triplicate wells pooled for each run), $P < 0.0001$ (****), $P < 0.001$ (***), $P < 0.01$ (**), $P < 0.05$ (*). The statistical analysis was done using Two-way ANOVA, Dunnett's multiple comparisons test.

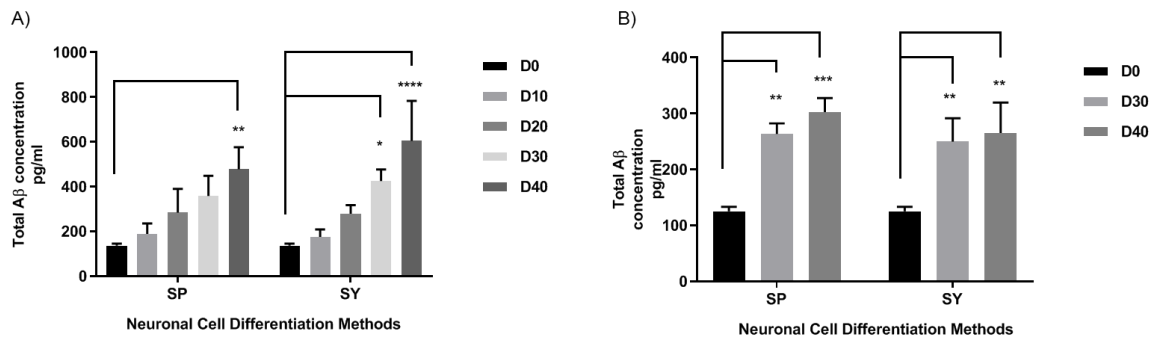


Figure A24: Quantification of total A β peptide secretion profile release from neuronal cells following SP and SY differentiation methods of fAD patient cell line (ax0112) (A) and 'healthy' control cell line (ax0018) (B) was detected using ELISA test. The CM was assayed in different developmental days over a 48 hours period. Data is expressed as A β pg/ml in conditioned media, \pm SEM, n=3 (triplicate wells pooled for each run), $P < 0.0001$ (****), $P < 0.01$ (**), $P < 0.05$ (*). The statistical analysis was done using Two-way ANOVA, Dunnett's multiple comparisons test.

A)

Comparisons	Significant	P Value
SP:D0 vs. SP:D30	**	0.0020
SP:D0 vs. SP:D40	****	<0.0001
SP:D0 vs. SY:D0	ns	>0.9999
SP:D0 vs. SY:D30	***	0.0002
SP:D0 vs. SY:D40	****	<0.0001
SP:D30 vs. SP:D40	ns	0.0953
SP:D30 vs. SY:D0	**	0.0020
SP:D30 vs. SY:D30	ns	0.2008
SP:D30 vs. SY:D40	**	0.0042
SP:D40 vs. SY:D0	****	<0.0001
SP:D40 vs. SY:D30	ns	0.6560
SP:D40 vs. SY:D40	ns	0.1122
SY:D0 vs. SY:D30	***	0.0002
SY:D0 vs. SY:D40	****	<0.0001
SY:D30 vs. SY:D40	ns	0.0507

B)

Comparisons	Significant	P Value
SP:D0 vs. SP:D30	*	0.0126
SP:D0 vs. SP:D40	*	0.0160
SP:D0 vs. SY:D0	ns	0.9171
SP:D0 vs. SY:D30	*	0.0176
SP:D0 vs. SY:D40	*	0.0384
SP:D30 vs. SP:D40	ns	0.9004
SP:D30 vs. SY:D0	*	0.0154
SP:D30 vs. SY:D30	ns	0.8601
SP:D30 vs. SY:D40	ns	0.5565
SP:D40 vs. SY:D0	*	0.0195
SP:D40 vs. SY:D30	ns	0.9592
SP:D40 vs. SY:D40	ns	0.6419
SY:D0 vs. SY:D30	*	0.0214
SY:D0 vs. SY:D40	*	0.0465
SY:D30 vs. SY:D40	ns	0.6784

Figure A25: Comparisons of total A β peptides secretion from neuronal cells following SP and SY differentiation methods (Fig. 4.8). Release of A β 1-42 and A β 1-40 from fAD patient cell line ax0112 (A) and 'healthy' control cell line ax0018 (B) was detected by ELISA. Data is expressed as A β concentration pg/mg total cellular protein, \pm SEM, n=3 (triplicate wells pooled for each run). The statistical analysis was done using Two-way ANOVA, Tukey's multiple comparisons test.

A)

Comparisons	Significant	P Value
ax0018:D0 vs. ax0018:D30	ns	0.9794
ax0018:D0 vs. ax0018:D40	ns	>0.9999
ax0018:D0 vs. ax0112:D0	***	0.0003
ax0018:D0 vs. ax0112:D30	****	<0.0001
ax0018:D0 vs. ax0112:D40	****	<0.0001
ax0018:D30 vs. ax0018:D40	ns	0.9463
ax0018:D30 vs. ax0112:D0	***	0.0008
ax0018:D30 vs. ax0112:D30	****	<0.0001
ax0018:D30 vs. ax0112:D40	****	<0.0001
ax0018:D40 vs. ax0112:D0	***	0.0002
ax0018:D40 vs. ax0112:D30	****	<0.0001
ax0018:D40 vs. ax0112:D40	****	<0.0001
ax0112:D0 vs. ax0112:D30	ns	0.4848
ax0112:D0 vs. ax0112:D40	ns	0.1648
ax0112:D30 vs. ax0112:D40	ns	0.9631

B)

Comparisons	Significant	P Value
ax0018:D0 vs. ax0018:D30	ns	0.3057
ax0018:D0 vs. ax0018:D40	ns	0.8363
ax0018:D0 vs. ax0112:D0	****	<0.0001
ax0018:D0 vs. ax0112:D30	****	<0.0001
ax0018:D0 vs. ax0112:D40	****	<0.0001
ax0018:D30 vs. ax0018:D40	ns	0.4072
ax0018:D30 vs. ax0112:D0	****	<0.0001
ax0018:D30 vs. ax0112:D30	****	<0.0001
ax0018:D30 vs. ax0112:D40	****	<0.0001
ax0018:D40 vs. ax0112:D0	****	<0.0001
ax0018:D40 vs. ax0112:D30	****	<0.0001
ax0018:D40 vs. ax0112:D40	****	<0.0001
ax0112:D0 vs. ax0112:D30	****	<0.0001
ax0112:D0 vs. ax0112:D40	****	<0.0001
ax0112:D30 vs. ax0112:D40	*	0.0356

C)

Comparisons	Significant	P Value
ax0018:D0 vs. ax0018:D30	ns	0.2179
ax0018:D0 vs. ax0018:D40	ns	0.1553
ax0018:D0 vs. ax0112:D0	ns	>0.9999
ax0018:D0 vs. ax0112:D30	****	<0.0001
ax0018:D0 vs. ax0112:D40	****	<0.0001
ax0018:D30 vs. ax0018:D40	ns	0.8325
ax0018:D30 vs. ax0112:D0	ns	0.2179
ax0018:D30 vs. ax0112:D30	***	0.0007
ax0018:D30 vs. ax0112:D40	****	<0.0001
ax0018:D40 vs. ax0112:D0	ns	0.1553
ax0018:D40 vs. ax0112:D30	***	0.0010
ax0018:D40 vs. ax0112:D40	****	<0.0001
ax0112:D0 vs. ax0112:D30	****	<0.0001
ax0112:D0 vs. ax0112:D40	****	<0.0001
ax0112:D30 vs. ax0112:D40	*	0.0277

D)

Comparisons	Significant	P Value
ax0018:D0 vs. ax0018:D30	ns	0.8787
ax0018:D0 vs. ax0018:D40	ns	0.8965
ax0018:D0 vs. ax0112:D0	ns	>0.9999
ax0018:D0 vs. ax0112:D30	***	0.0004
ax0018:D0 vs. ax0112:D40	****	<0.0001
ax0018:D30 vs. ax0018:D40	ns	>0.9999
ax0018:D30 vs. ax0112:D0	ns	0.8817
ax0018:D30 vs. ax0112:D30	**	0.0019
ax0018:D30 vs. ax0112:D40	****	<0.0001
ax0018:D40 vs. ax0112:D0	ns	0.8992
ax0018:D40 vs. ax0112:D30	**	0.0018
ax0018:D40 vs. ax0112:D40	****	<0.0001
ax0112:D0 vs. ax0112:D30	***	0.0004
ax0112:D0 vs. ax0112:D40	****	<0.0001
ax0112:D30 vs. ax0112:D40	ns	0.1655

Figure A26: Comparisons of A β peptides secretion from neuronal cells (Fig. 4.9) following SP (A and C) and SY (B and D) differentiation methods of fAD patient cell line ax0112 versus 'healthy' control cell line ax0018 from neural cells over 40 days. A β peptide was detected by ELISA: A β 1-42 (A and B) and A β 1-40 (C and D). Data is expressed as A β concentration pg/mg total cellular protein, \pm SEM, n=3 (triplicate wells pooled for each run). The statistical analysis was done using Two-way ANOVA, Sidak's multiple comparisons test.

Comparisons	Significant	P Value
A β 1-42:ax0018-Astrocytes vs. A β 1-42:ax0112-Astrocytes	***	0.0007
A β 1-42:ax0018-Astrocytes vs. A β 1-40:ax0018-Astrocytes	****	<0.0001
A β 1-42:ax0018-Astrocytes vs. A β 1-40:ax0112-Astrocytes	ns	0.9871
A β 1-42:ax0112-Astrocytes vs. A β 1-40:ax0018-Astrocytes	****	<0.0001
A β 1-42:ax0112-Astrocytes vs. A β 1-40:ax0112-Astrocytes	***	0.0007
A β 1-40:ax0018-Astrocytes vs. A β 1-40:ax0112-Astrocytes	****	<0.0001

Figure A27: Comparisons of A β peptide profile released from astrocytic cells (Fig. 4.10) following astrocytes differentiation methods of cell lines: fAD patient cell line (ax0112) versus 'healthy' control cell line (ax0018). Data is expressed as A β concentration pg/mg total cellular protein, \pm SEM, n=3 (triplicate wells pooled for each run). The statistical analysis was done using Two-way ANOVA, Tukey's multiple comparisons test.

Comparisons	Significant	P Value
SP-differentiation:ax0018 vs. SP-differentiation:ax00112	ns	0.6532
SP-differentiation:ax0018 vs. SY-differentiation:ax0018	ns	>0.9999
SP-differentiation:ax0018 vs. SY-differentiation:ax00112	*	0.0137
SP-differentiation:ax00112 vs. SY-differentiation:ax0018	ns	0.5130
SP-differentiation:ax00112 vs. SY-differentiation:ax00112	**	0.0021
SY-differentiation:ax0018 vs. SY-differentiation:ax00112	*	0.0189

Figure A28: Comparisons of glucose uptake by hiPSC-derived neural cells from fAD patient and 'healthy' control neural cells using SP and SY differentiation methods (Fig. 4.11). Data is expressed as A β concentration pg/mg total cellular protein, \pm SEM, n=3 (triplicate wells pooled for each run). The statistical analysis was done using One-way ANOVA, Sidak's multiple comparisons test.